Engineering antibodies to study and improve immunomagnetic isolation of tumour cells

Jayati Jain

Department of Biochemistry

Keble College, University of Oxford

Hilary 2013

A thesis submitted in partial fulfillment of the requirements for the degree of Doctor of Philosophy, University of Oxford

This thesis is dedicated to all those who have lost the fight, and to those who won't quit the fight, against cancer…

Abstract

Engineering antibodies to study and improve immunomagnetic isolation of tumour cells

Jayati Jain, Keble College, University of Oxford
DPhil thesis, Hilary 2013

Cell separation based on antibody-targeted magnetic beads has been widely used in a number of applications in immunology, microbiology, oncology and more recently, in the isolation of circulating tumour cells (CTCs) in cancer patients. Although other cell separation techniques such as size-based cell filtration and Fluorescence Activated Cell Sorting have also been in popular use, immunomagnetic cell isolation possesses the advantages of high throughput, good specificity and reduced cell stress. However, certain fundamental features of the cell-bead interface are still unknown.

In this study, some of the key features of the cell-bead synapse were investigated in an effort to improve the efficiency of immunomagnetic cell isolation and reduce its dependence on high-expressing cell surface markers. A clinically relevant antibody fragment (Fab) against tyrosine kinase receptor HER2 was applied to study the immunomagnetic isolation of HER2-expressing cancer cells. First, the minimum number of target proteins required on a cell for it to be isolated was determined. Second, the importance of the primary antibody affinity was investigated, using a series of Fab mutants with known kinetics and it was shown that despite starting with sub-nanomolar affinity, improving Fab affinity increased cell isolation. Third, the influence of the connection between the primary antibody and the bead was studied by comparing Fab bridged to the magnetic bead via a secondary antibody, Protein L or streptavidin; the high affinity biotin-streptavidin linkage increased isolation sensitivity by an order of magnitude. Fourth, the effect of manipulating cytoskeletal polymerization and cell membrane fluidity using small molecules was tested; cholesterol depletion decreased isolation and cholesterol loading increased cell isolation. The insights from these observations were then applied to isolate a panel of cell-lines expressing a wide range of surface HER2. While the standard approach isolated less than 10% of low HER2-expressing cancer cells from spiked rabbit and human blood, our enhanced approach with the optimized cholesterol level, antibody affinity and antibody-bead linkage could specifically isolate more than 80% of such cells. The final part of this work focussed on developing an antibody clamp that could physically restrict the antigen within its binding site on the Fab and prevent antigen dissociation, using the HER2-Fab complex and the anti-myc peptide antibody 9E10.

Work from this thesis provides useful insights into the molecular and cellular parameters guiding immunomagnetic cell isolation and can be used to extend the range of target receptors and biomarkers for tumour cell isolation and other types of cell separation, thereby enhancing the power and capacity of this approach.

Authorship Declaration

The work described in this thesis was carried out in Dr. Mark Howarth's laboratory at the Department of Biochemistry, University of Oxford between October 2009 and September 2012. All the work described in this thesis is entirely my own unless stated otherwise. This thesis has not been submitted for any other degree at the University of Oxford or any other institution. Publications arising from this thesis are detailed below:-

Jain, J., Veggiani, G. and Howarth, M. (2013). Cholesterol Loading and Ultrastable Protein Interactions Determine the Level of Tumor Marker Required for Optimal Isolation of Cancer Cells. Cancer Research, 73: 2310-2321

Jayati Jain

Hilary 2013

Acknowledgements

The process of attaining a DPhil has truly been a life-changing experience for me, and I would like to thank everyone who has helped me through this journey. My first and foremost thanks goes to my supervisor Dr. Mark Howarth, for his patient guidance, enthusiastic encouragement and useful critiques of my work. Under his supervision, I developed from a naïve biology undergraduate to a critically thinking researcher. Dr. Howarth's passion and dedication towards science has been truly inspirational, and I am extremely grateful to him for always being available for advice on the designing of experiments, discussion of my results and inputs from the latest scientific literature. I would also like to express my deepest gratitude to my co-supervisor, Prof. Neil Brockdorff, for his constant feedback and suggestions regarding my work.

I would further like to thank my funding bodies, the Clarendon Fund, DeBreyne scholarships and the Department of Biochemistry for granting me the opportunity and the resources to work at such a world-renowned institution. My three years in Oxford would have been incomplete without the collegiate support from Keble college staff. A special thanks also goes out to the Keble MCR, for making my Oxford experience wholesome and giving me the wonderful opportunity of meeting and interacting with brilliant people from all around the world.

The past four years have been a huge learning curve for me, but getting to the DPhil stage in the first place would not have been possible without the constant support and unconditional love of my family. Thank you Mummy and Papa, for believing in me, and for never holding me back from achieving my dreams. Thank you Niyati and Saksham, for always greeting me with smiles and laughter, and for letting me act like the "smart" one!

During the course of my DPhil, I have realized the importance of having supportive colleagues and friends. My fellow lab members, Apurba, Claire, Bijan, Denis, Mike and Jacob – thank you all so much for always being available to answer my trivial questions regarding protein purifications, mammalian cell cultures, technical support and especially, for making the long hours in the lab more endurable!

Last but definitely not the least, I would like to thank my best friends Arjun, Tania and Ruchi. Arjun, thank you for patiently listening to all my complaining about failed experiments, for supporting me in my troubles, sharing in my joys and constantly pushing me to strive on. Ruchi, thank you for teaching me how just laughing at problems can make them look trivial and for always appreciating my "experiments" in the kitchen. Tania, thank you for always supporting me during my "existential crises" and feeding me the best-ever chocolate chip banana bread when I was having a bad day.

I have learned so much from all of you. Thank you all, for everything.

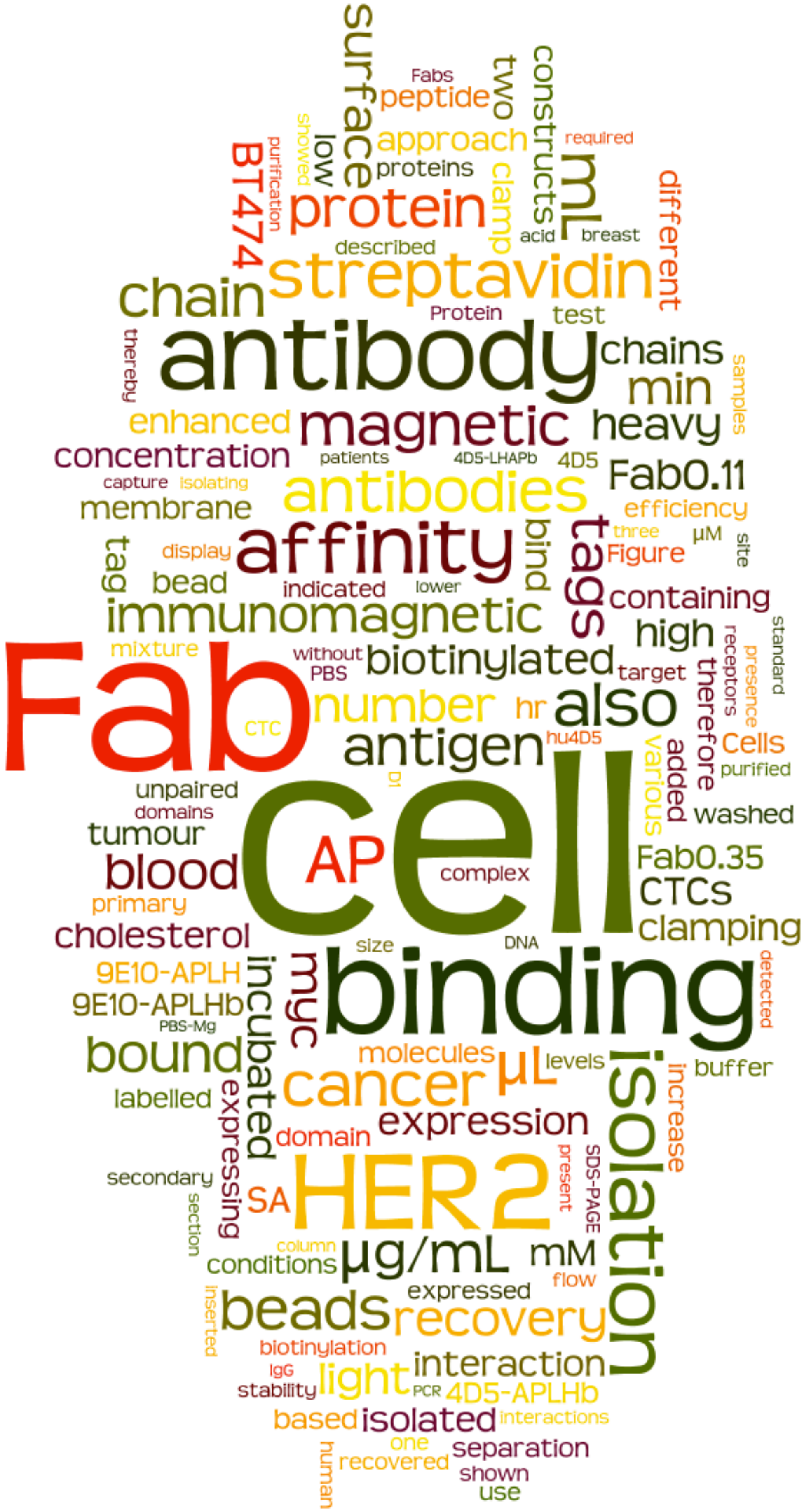

surface
Fabs
two
constructs
peptide
approach
required
showed
purification
low
proteins
BT474
protein
clamp
ml
different
acid
breast
described
chain
streptavidin
Protein
test
thereby
antibody
chains
min
samples
enhanced
magnetic
heavy
concentration
patients
4D5-LHAPb
4D5
Fab0.11
capture
isolating
antibodies
efficiency
membrane
three
µM
site
tag
display
affinity
bind
tags
Figure
bead
indicated
lower
containing
immunomagnetic
standard
high
receptors
presence
mixture
without
biotinylated
Fab
PBS
target
therefore
number
hr
also
CTC
antigen
hu4D5
various
added
Cells
purified
unpaired
D1
domains
cell
washed
tumour
AP
Fab0.35
blood
complex
CTCs
primary
clamping
cholesterol
size
DNA
9E10-APLH
incubated
myc
binding
detected
9E10-APLHb
PBS-Mg
bound
molecules
µL
levels
isolation
buffer
labelled
cancer
increase
expressing
domain
expression
secondary
present
SDS-PAGE
section
SA
HER2
column
conditions
µg/mL
mM
flow
inserted
expressed
beads
recovery
biotinylation
interaction
IgG
stability
light
PCR
4D5-APLHb
based
isolated
interactions
one
human
recovered
separation
shown
use

Abbreviations

A_{280}	Absorbance at 280 nm
Ab	Antibody
AP	Acceptor peptide (for BirA biotinylation)
BirA	Biotin ligase
bp	Base pair
BSA	Bovine Serum Albumin
CFP	Cyan Fluorescent Protein
CTC	Circulating Tumour Cell
DMEM	Dulbecco's Modified Eagle Medium
DNA	Deoxyribonucleic acid
dNTP	Deoxynucleotide triphosphate
dSA	Divalent streptavidin
E. coli	*Escherichia coli*
EGFR	Epidermal Growth Factor Receptor
ELISA	Enzyme-Linked Immunosorbent Assay
EpCAM	Epithelial Cell Adhesion Molecule
ExPASy	Expert Protein Analysis System
Fab	Fragment antigen-binding
FACS	Fluorescence Activated Cell Sorting
Fc	Fragment crystallizable
HER2	Human Epidermal Growth Factor Receptor 2
hr	hour
hu4D5	Humanized 4D5 antibody
IPTG	Isopropyl-β-D-thiogalactopyranoside
kb	kilobases
K_d	Equilibrium dissociation constant; k_{off}/k_{on}
kDa	kilodaltons
k_{off}	Dissociation rate
k_{on}	Association rate
LB	Luria Bertani broth
mAb	Monoclonal antibody
MBP	Maltose Binding Protein
MESF	Molecules of Equivalent Soluble Fluorochrome
mSA	Monovalent streptavidin
Ni-NTA	Nickel-nitrilotriacetic acid
O/N	Overnight
PCR	Polymerase chain reaction
PDB	Protein Data Bank
PBS	Phosphate buffered saline
PBS-Mg	PBS with 5 mM $MgCl_2$
PBST	Phosphate buffered saline with 0.05% Triton X-100
PBS-T	Phosphate buffered saline with 0.05% Tween
PMSF	Phenylmethylsulfonyl Fluoride
RNA	Ribonucleic acid
SA	Streptavidin
scFv	Single-chain Fragment variable
SDS-PAGE	Sodium dodecyl sulfate - polyacrylamide gel electrophoresis
TM	Trans-membrane helix

Table of contents

Chapter 1: Introduction

Chapter 1: Introduction

1.1 Antibody engineering

1.1.1 History of antibodies

The term "antibody" is derived from the German word "antikörper", first coined by scientist and physician Paul Ehrlich in 1891 (Lindenmann, 1984). The initial clues about the existence of antibodies in mammalian systems came from his work on immunization of mice against the plant toxin proteins, ricin and abrin. At the same time, in a landmark discovery by Emil Behring and Shibasabura Kitasato, it was shown that serum from an animal actively immunized against diphtheria toxin could neutralize a fatal dose of the toxin in another animal (Behring and Kitasato, 1890; Hankin, 1890). Thus the idea of passive immunization was first generated, and its potential in humans was immediately investigated.

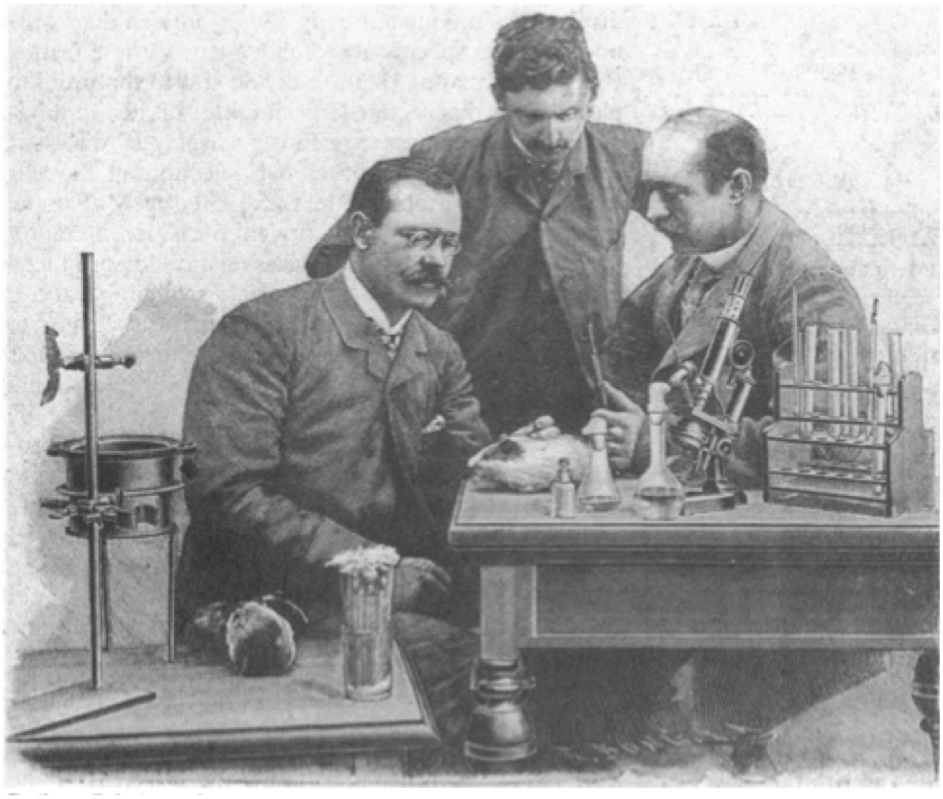

Figure 1.1. Emil von Behring (right) with his colleagues Erich Wernicke (left) and Paul Frosch (centre) immunizing guinea pigs for the development of anti-diphtheria therapeutic serum in Robert Koch's laboratory in Berlin (from Llewelyn et al., 1992. Permission obtained).

In 1894, pharmaceutical company Farbwerke Hoechst launched the first immunobiological therapeutic, an anti-diphtheria serum that could be used to prevent epidemic diphtheria (Yamada, 2011). The introduction of serum therapy, popularly known as the "magic bullet", reduced the mortality rate from diphtheria in Paris from 52% to 25% (Llewelyn et al., 1992). However, as the serum came from non-human sources (horses, rabbits), serum therapy had major side-effects and often led to fever, rashes and joint pain (Llewelyn et al., 1992). Efforts were taken to improve the methods for purification of serum and Paul Ehrlich even developed a standardized procedure for quantification of serum therapeutic effect, including the concept of LD_{50} (Lethal Dose, 50%; a measurement of toxicity, the dose required to kill half of the tested population after a specific test duration) (Yamada, 2011). A decade later, Austrian biologist Karl Landsteiner identified the different blood groups and studied how blood transfusion between two different blood types can lead to agglutination (Merino, 2011). This finding was later used to support the formation of antibodies in blood serum on the introduction of a foreign antigen (Merino, 2011).

Purified human immunoglobulin preparations were finally introduced in 1944 as a treatment for measles and the problems due to serum side-effects were overcome (Llewelyn et al., 1992). The first elegant system for obtaining pure monoclonal antibodies (mAbs) of known specificities in large amounts was described by George Köhler and Cesar Milstein in 1975 (Kohler and Milstein, 1975). Two years later Alan Williams showed that mAbs could be raised against biologically interesting molecules and this triggered the development of a series of mAb-based diagnostic methods. However, the use of murine mAbs for therapeutic use in humans was still problematic, as their circulating half-life was very short, they did not initiate the same effector functions and the human anti-mouse immune response posed difficulties (Llewelyn et al., 1992). Producing human mAbs had its own set of challenges, including the difficulty in sourcing B-cells from the peripheral blood instead of the spleen, bone marrow or lymph nodes. The introduction of chimeric antibodies, containing mouse variable regions and constant human domains partly solved this problem, and the first therapeutic mAb generated was OKT3 by Ortho Biotech in 1984 (Yamada, 2011). Thereafter, a renaissance in the field of immunotherapy took place, with the introduction of complementarity determining region (CDR, see section 1.1.2) grafted humanized monoclonals in 1986, phage display libraries to increase Ab

affinity *in vitro* in 1990, human mAbs produced from transgenic mice expressing human antibody repertoires in 1994 and finally the commercialization of the first human mAb Humira in 2002 (Yamada, 2011). Currently there are more than 25 mAbs in clinical use and ~ 250 mAbs in the pharmaceutical pipeline (Yamada, 2011).

1.1.2 Antibody structure and classes

Each IgG antibody molecule is a glycoprotein made up of four chains – two identical heavy chains and two identical light chains. The four chains are joined together by disulfide bridges, forming a spatial structure similar to the letter "Y" (Fig. 1.2A). Each heavy chain comprises one variable (V_H) and three constant (C_H) immunoglobulin domains. Each light chain comprises one variable (V_L) and one constant (C_L) immunoglobulin domains. From a functional perspective, there are two main features in an antibody: the Fab (Fragment antigen-binding) fragments, which are responsible for recognizing and binding the antigen, and the Fc region (Fragment crystallisable), which is responsible for initiating the host defence mechanism (Fig. 1.2A) (Llewelyn et al., 1992). The two identical Fab regions lie at the amino terminal ends of the chains (constituting Fragment variable, Fv). Each Fab includes one light chain and one variable and one constant region of a single heavy chain. The Fc region includes the two constant domains at the carboxyl ends of the heavy chains. The hinge region between the two Fab fragments in an antibody is flexible and therefore allows the antibody to bind two variably-separated identical antigens (Llewelyn et al., 1992). Each variable domain contains three short loops of amino acids, which are hypervariable and are termed complementarity determining regions (CDRs). At the antigen binding site, all six of these CDRs (three each from heavy and light chains) come together and are therefore responsible for the extraordinary specificity that antibodies can have for their antigens (Al-Lazikani et al., 1997). The Fc region on the Ab binds to the Fc receptors on immune cells and are responsible for initiating the antigen-dependent cellular cytotoxicity responses. Antibodies contain conserved glycosylation sites on their Fc regions and these sites can now be modified to control antibody conformation and subsequently the antibody effector functions (Crispin et al., 2009).

The constant region of the light chain differs depending on the class of light chain: κ or λ chain. Similarly, there are five classes of antibodies depending on the heavy

chain constant regions: IgG, IgM, IgA, IgD and IgE (Merino, 2011). IgG, the prototype antibody, is mainly produced in secondary immune responses. Nearly three quarters of all commercial antibody products currently in development are intact IgG antibodies (Zider and Drakeman, 2010). IgG antibodies can be further divided into four sub-classes: IgG1, IgG2, IgG3 and IgG4, which vary in their ability to activate the host defence mechanisms. IgM antibodies have a pentameric structure and are present in the intravascular space, whereas IgA antibodies have a dimeric structure and are present in secretions such as saliva and breast milk (Llewelyn et al., 1992). IgD antibodies are monomeric and found mainly on B-cell surfaces. IgE antibodies bind to Fcε receptors on the surface of eosinophils, basophils and mast cells, and can cause hypersensitivity reactions in allergic diseases. The Ig class of the antibody determines both the type and the temporal nature of the immune response.

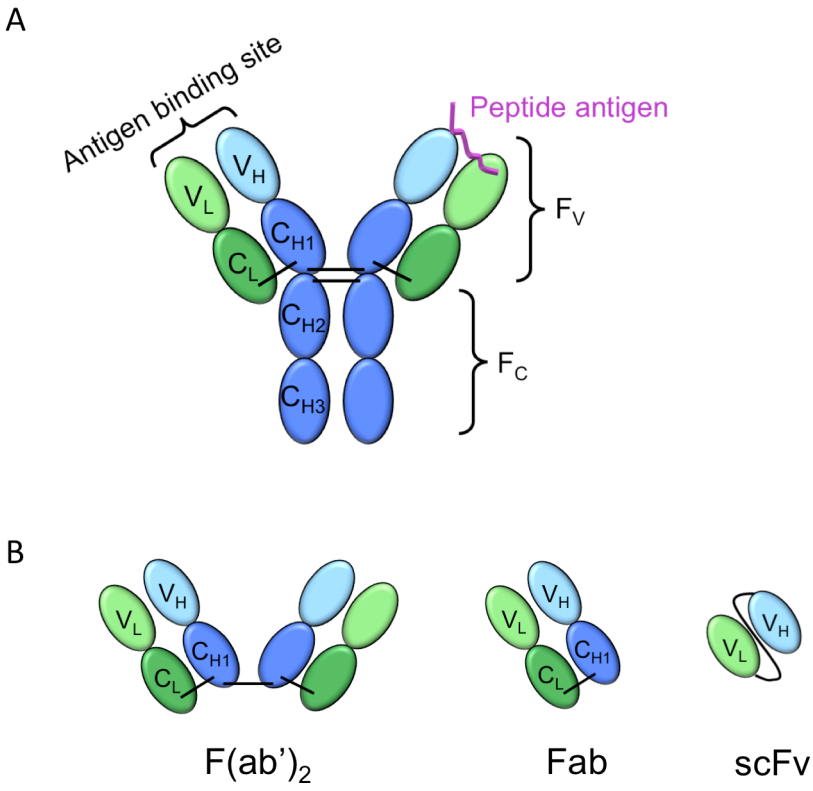

Figure 1.2. Cartoon representation of IgG structure and commonly used Ab fragments. A. Structure of a generic IgG antibody with two heavy chains (blue) and two light chains (green). Each oval represents an immunoglobulin domain; lighter shades represent variable domains (V_L, V_H) and darker shades represent constant domains (C_L, C_H). Disulfide bonds (▬) hold the four chains together. B. Various Ab fragments; divalent Fragment antigen-binding ($F(ab')_2$), Fragment antigen-binding (Fab) and single chain Fragment variable (scFv).

1.1.3 Polyclonal and monoclonal antibodies

Antibodies in the mammalian system are produced by B-lymphocytes that develop in the bone marrow of an individual. When an antigen enters the body, it binds specifically to a few of the B-cell clones, which migrate to the lymph nodes and spleen, where the B-cells proliferate and undergo somatic hypermutation, during which genetic mutations in the CDRs is followed by the selection of antibodies with an even greater affinity for the antigen. This process of affinity maturation leads to the high affinity antibody producing B-cell clones to mature into plasma cells, which go on to secrete large amounts of the antibody displayed on their surface (Llewelyn et al., 1992).

When a foreign antigen is introduced into a mammal, the immune system can produce a polyclonal antibody response. As most antigens are highly complex, they present a number of different sites for many B-lymphocytes to recognize and bind. As each B-lymphocyte produces a different mAb, the resulting antibody response is a mixture of various mAbs and is termed a polyclonal response. Polyclonal antibodies can be purified from the immune serum by isolating the immunoglobulin-containing fractions and can recognize multiple epitopes of the same antigen.

Polyclonal antibodies are cheaper and quicker to produce as compared to monoclonal antibodies. Intravenous IgG, containing pooled IgG purified from the plasma of over a thousand blood donors, is widely used as a treatment in immune deficiency diseases, autoimmune diseases and acute infections (Bayry et al., 2003). Polyclonal antibodies are especially beneficial when the targeted antigen can occur in many forms, such as various protein conformations, phosphorylation, ubiquitinylation, as the polyclonals can still recognize other unmodified epitopes in the antigen (Lipman et al., 2005). However, polyclonal antibodies often have lower specificity for the antigen, as polyclonal Abs can cross-react with other members of the same protein family to which the antigen belongs.

Monoclonal antibodies are antibodies produced by a single B-cell clone. Monoclonal antibodies are produced in the following way: B-cells from an immunized mammal's spleen are extracted and fused to immortal myeloma cells (Kohler and Milstein, 1975). The resulting hybridomas are then screened and the clone producing mAb with

good specificity for the antigen is selected and further cultured to produce large amounts of the required mAb. The principal advantages of mAbs are their homogeneity, consistency and the strong specificity for the target antigen (Lipman et al., 2005). The immortal hybridomas also allow for continuous and standardized production of the same kind of mAb. With the advances in genetic engineering, murine mAbs can easily be transformed into other constructs, such as chimeric (with human Fc region) or humanized (human antibody with mouse CDR regions) antibodies that are more applicable in human treatment. Furthermore, recombinant mAbs have had their glycosylation engineered to enable reduced inhibition by serum IgG of the mAb binding to Fcγ receptors (Baruah et al., 2012); addition of the endoglycosidase S cleaves the complex-glycans found on serum IgG, but is inactive against IgG Fc engineered with oligomannose-type glycans (Baruah et al., 2012). This technique has the potential to mediate better immune effector functions by the administered therapeutic mAb.

However, due to their monospecificity, mAbs can lose their effectiveness against rapidly mutating targets, such as HIV or influenza, which undergo random mutations and thereby evade the immune system. In such cases, polyclonal antibodies offer a better alternative for the treatment of infectious diseases (Haurum, 2006). The production of recombinant polyclonal antibodies is now being explored using platforms such as Symplex™ and Sympress™ technologies. Antibody-producing cells are isolated from the blood of immune donors, antibody mRNA is reverse transcribed, and the heavy and light chain of an antibody are linked together by the Symplex™ PCR, thereby preserving their natural pairing (Haurum, 2006). Antibodies are selected for antigen specificity using high-throughput screening methods such as ELISA. Selected constructs are then stably transfected into mammalian cells, and each clone producing a different antibody is mixed together to form a polyclonal master cell bank, which can then be used for large scale production (Haurum, 2006). Due to their binding of multiple sites on the target, recombinant polyclonals can trigger a range of effector functions such as enhanced phagocytosis of antigens, preventing antibody-coated cells from attaching to host cells, toxin neutralization and agglutination and subsequent clearance of soluble antigens (Haurum, 2006). However, the production of recombinant polyclonal antibodies is still in its initial stages and only a few have reached clinical trials (Symphogen).

1.1.4 Antibody fragments

Recombinant mAbs have been widely used both as IgGs or as antibody fragments when injected systemically to target tumours (Allen, 2002). Antibody fragments used for antigen targeting in research applications include the monovalent antigen binding fragment (Fab), divalent antigen binding fragment ($F(ab')_2$), single chain fragment variables (scFv) and a number of other multivalent fragments derived from a combination of these (Fig. 1.2B) (Maynard and Georgiou, 2000; Miller et al., 2003). The use of antibody fragments may have advantages over intact IgGs for tumour targetting, as antibody fragments can have decreased immunogenicity, increased tumour penetration owing to their smaller size and lower non-specific binding (Carter, 2001; Pavlinkova et al., 2001; Peer et al., 2007). Antibody fragments are also easier to produce in large quantities and their affinity can be modulated using various combinatorial display libraries (Aitken, 2009).

1.1.5 Antibody display technologies

Antibodies produced during mammalian immune response have an affinity ceiling of $\sim K_D=10^{-10}$ M due to the regulated rate of internalization of B-cell receptors during affinity maturation (Foote and Eisen, 1995). Over the last three decades, several *in vitro* systems have been developed to artificially increase the affinity of an antibody against its antigen. The most successful of these is the generation of antibody gene libraries, from which the best affinity clones are selected and further characterized.

To increase the affinity of an antibody or antibody fragment under investigation, its gene sequence is amplified using an error-prone replication mechanism or primer-based introduction of diversity, in order to generate random mutations and assemble a diverse DNA library containing $> 10^7$ clones (Marks et al., 1991). However, as most randomized CDRs give poor specificity and folding, the best libraries now mostly start with the human repertoire, where each clone has a higher probability of yielding a useful result.

In the phage display technology (Fig. 1.3), the gene library is fused to the gene III coat protein (pIII) of filamentous phage, which is used to infect *E. coli* (Barbas et al., 1991). Once inside the bacterial cells, the phage produces the protein sequence of the contained Ab gene and displays the Ab at the tip of the phage fused to pIII (Fig. 1.3).

When the phage is released from the bacterial cell, a selection process based on recognition of immobilized antigen is applied to the phage pool to select strong binding Ab constructs (Gram et al., 1992). As the DNA sequence of the displayed Ab mutant is enclosed within the same phage, the antigen-bound phage clones can be eluted and the corresponding region in the phage genome can be sequenced to determine the gene sequence of the high affinity antibody mutant (Fig. 1.3). This process can be repeated multiple times to optimize the antigen-antibody binding. As a complete IgG contains four chains and it is difficult to correctly fold IgG in *E. coli*, the phage display system is mostly used to engineer high affinity Fab and scFv fragments (Ahmad et al., 2012). The optimized Ab fragment can then be transferred onto an IgG framework as desired.

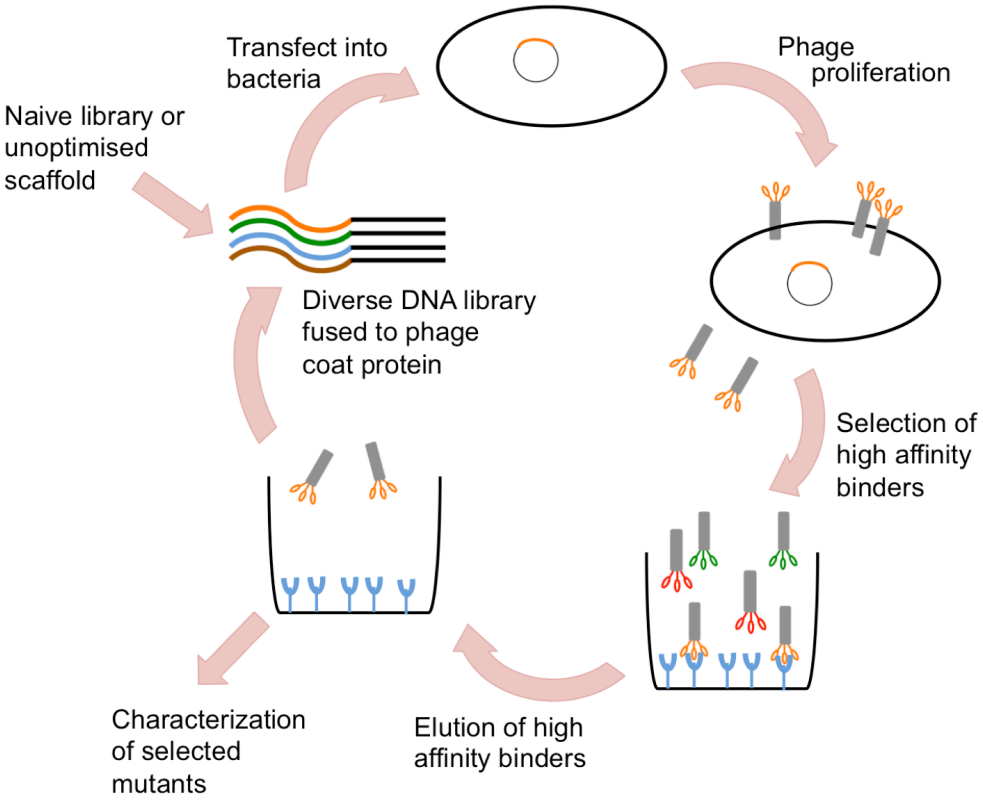

Figure 1.3. Illustration of phage display technology. A diverse gene library (curved lines) generated from error prone PCR, diverse primers or naïve library is fused to pIII phage gene (straight black lines) and transfected into bacteria. Inside the bacterial cell, the phage (grey) displays the protein sequence of the contained Ab gene. Once released from the bacterial cells, phage particles displaying high affinity antibodies can be selected using immobilized antigen (blue). The high affinity binders can then be eluted and subjected to further rounds of phage display or the enclosed DNA could be sequenced to obtain the gene sequence of the high affinity binders.

The robustness, simplicity and stability of the phage particles make phage display a widely-used display technology for protein affinity maturation (Dufner et al., 2006). However, the phage library size is limited by its transformation efficiency in bacterial cells and can therefore reduce library diversity and the probability of selecting the highest affinity binding protein (Dufner et al., 2006). Despite major improvements in phage display, the largest reported libraries contain a maximum of 10^{10}-10^{11} different mutants (Dufner et al., 2006). Furthermore, mutants that are toxic for the host, poorly expressed or folded, susceptible to proteolysis or aggregation can slow down the growth of bacterial cells and be displayed less efficiently. This can favour the dominance of low binding but fast growing clones after a few rounds of selection (Dufner et al., 2006).

Yeast surface display is another technique widely used to engineer high affinity antibodies and antibody fragments (Gai and Wittrup, 2007). The protein of interest is fused to the Aga2 protein and displayed on the surface of *Saccharomyces cerevisiae* (Chao et al., 2006). High affinity clones can be isolated using flow cytometry and magnetic separation (sections 1.2.2 and 1.2.4). Yeast display has the advantage that the displayed proteins are folded in the endoplasmic reticulum of the eukaryotic yeast cells, in the presence of the endoplasmic reticulum chaperones and quality-control machinery and therefore the clones generated are usually well-folded and the library is of high quality (Chao et al., 2006). However, yeast display also faces challenges similar to phage display, such as relatively small library size (10^{7}-10^{9} clones), susceptibility to protein aggregates and the dominance of well-folded but not necessarily high affinity mutants (Gai and Wittrup, 2007).

Some of these problems have been overcome by the development of alternate display technologies like ribosome display and mRNA display, both of which can help construct and screen antibody libraries containing more than 10^{12}-10^{13} clones (Lipovsek and Pluckthun, 2004). For ribosome display, the DNA library encoding the randomly mutagenized polypeptide of interest is fused to a C-terminal tether region that does not contain the stop codon and the library is transcribed *in vitro*. The resulting modified mRNA is translated using ribosomes, which stop after translation but do not release the mRNA. This leads to the formation of a tertiary complex,

containing the folded polypeptide attached via the ribosome to its encoding mRNA. In mRNA display, the mRNA is first translated and then covalently bound to its encoded protein using adaptor molecules such as puromycin (Lipovsek and Pluckthun, 2004). This close coupling of the genotype (mRNA) to its phenotype (protein) allows for the selection of strong binding antibodies using immobilized antigen, and the selected clones can be back translated to obtain the required Ab gene sequence.

As both these methods are best performed on single-chain constructs, such techniques are mostly used for the generation of high affinity scFvs and other synthetic Ab constructs rather than complete IgGs (Lipovsek and Pluckthun, 2004). Although few reports have been published on the application of mRNA display, ribosome display has already been used to produce scFv constructs with dissociation constants in the picomolar range (Hanes et al., 2000). Both these technologies avoid the issues of negative selection seen due to limited transformation efficiency in phage and yeast display. Ribosome display and mRNA display library size is limited mainly by the number of ribosomes and the number of diverse mRNA molecules present in the translation mixture (Lipovsek and Pluckthun, 2004). The non-specific binding due to misfolded proteins can however possess a mechanistic challenge to the success of these technologies. Therefore, although the library size in mRNA/ribosome display is large, the library quality might be low due to the presence of a number of misfolded clones and it is important to keep this in mind when choosing a display technology for engineering antibodies.

1.1.6 Rational design

With the advancement in X-ray crystallography and computational modeling, computer-aided antibody design can provide useful insights into optimizing antigen-antibody interaction sites and creating more stable Ab conformations. *In silico* modeling and Molecular Dynamics simulations have been used to 1.) predict the 3D protein structures of antibodies from their polypeptide sequences when an X-ray crystal structure is unavailable 2.) study antigen docking into its binding site 3.) increase Ab affinity by multiple amino acid substitutions in the CDR regions and 4.) increase the solubility and thermodynamic stability of an antibody by optimizing its heavy chain–light chain interface (Belogurov et al., 2012; Kuroda et al., 2012). The predicted useful mutants can then be produced and tested empirically.

A rational approach can also be conducted by making point mutants of the Ab to create more favourable conformations. Selected stretches of residues can be fine-tuned based on size, charge, hydrophobicity and secondary structure to enhance the antibody's properties or develop novel functionality. Although, this is mostly a trial and error method, can be very laborious and several mutants often need to be screened to get a better clone, the rational approach has been successfully used to modify Fabs (Teerinen et al., 2006) and other binding proteins (Chivers et al., 2010; Zakeri et al., 2012).

1.1.7 Chemical modifications

Several antibodies or antibody fragments have been chemically modified to produce "reactive antibodies" that irreversibly bind their target antigen. Metalloantibodies are antibodies that have been engineered with reactive metal binding sites that can effectively form covalent complexes with unmodified target protein antigen (Trisler et al., 2007). Trisler et al. grafted a metal binding motif in the anti-TNFα scFv (RA7), such that the motif was in close proximity with the antigen but did not affect the antigen's approach and binding. A library was created using a consensus metal binding motif (HEXXH) from metalloproteases and was inserted at the N-terminal of the heavy chain. The library clones were then tested for TNFα binding and selected using phage display. Specific HEXXH-scFv fusion sequences were discovered that formed Co^{2+}-dependent covalent complexes with their target. The scFv-antigen complex showed resistance to boiling, strong reducing conditions, chemical denaturants, excess metal chelator and SDS-PAGE (Trisler et al., 2007). Such metalloantibodies can also be used to inactivate the target, as they irreversibly modify the target. However, the use of such antibodies might be toxic, and therefore needs to be carefully tested *in vivo* before therapeutic use. Also, the specificity of the reaction was not clearly demonstrated and could have been severely affected since the metalloantibody reacted with itself (Trisler et al., 2007).

An alternative method to form reactive antibodies is by synthesizing electrophilic antigens that can induce nucleophilic character in the antibody and promote covalent bond formation, "reactive immunization" (Nishiyama et al., 2007). Nishiyama et al. report the preparation of an electrophilic phosphonate analog of the PDN (Principle Neutralizing Determinant) peptide antigen (belonging to an HIV strain) which, when

introduced into mice, generates antibodies with nucleophilic characteristics. These mice, when infected with HIV, exhibited a strong immune response (~50-fold better than controls), consisting of antibodies that bound to the antigen very strongly to form stable complexes (Nishiyama et al., 2007). However, although enhanced stability of the antigen-antibody interaction was shown, the nature of the covalent reaction between the generated nucleophilic antibodies and the immunogen was uncertain. Also, as this study was based on a polyclonal response, only a small fraction of the antibodies displayed strong nucleophilic characteristics (Nishiyama et al., 2007).

1.1.8 Non-immunoglobulin binding proteins

The biophysical properties, large multidomain assemblage and need for disulfide bonds and glycosylation often limit the production and application of antibodies, making them expensive to manufacture. Smaller antibody fragments such as Fabs and scFvs also often rely on disulfide bonds and have more tendency to aggregate due to exposed hydrophobic surfaces. These problems have driven attempts to create alternative binding proteins, based on non-immunoglobulin scaffolds. In fact complete immune systems based on non-IgG domains have been discovered in jawless sea lampreys, which instead use leucine-rich repeat proteins (Pancer et al., 2004).

Various protein scaffolds such as fibronectin domains, affibodies, lipocalins and designed ankyrin repeat proteins (DARPins) have been investigated (Binz et al., 2005). DARPins contain consecutive copies of small structural units, consisting of a β-turn followed by two anti-parallel α-helices, stacked together to form a continuous protein (Tamaskovic et al., 2012). DARPins with a mass of 14.5 kDa and affinities in the nanomolar to picomolar range have shown efficiency in tumour penetration (Zahnd et al., 2010). High thermodynamic stability, reversible folding, absence of cysteines and low aggregation tendencies also make the use of DARPins favourable for various diagnostic and therapeutic applications (Tamaskovic et al., 2012). As they are repeat proteins, DARPins can be easily generated in multispecific formats with effector functions or used to target multiple receptors (Tamaskovic et al., 2012).

Affibodies, another class of non-immunoglobulin based proteins, are derived from an immunoglobulin-binding domain of *Staphylococcus aureus* protein A (Nilsson et al.,

1987). Affibodies consist of three α-helices with a total of 58 amino acids and display reversible folding. Randomization of 13 surface residues can be used to construct the binding domain, selecting from a phage display library (Orlova et al., 2007). A synthetic affibody conjugate which folds spontaneously and binds Human Epidermal Growth Factor Receptor 2 (HER2) with picomolar affinity has been produced and used for molecular imaging of HER2-expressing malignant tumours (Orlova et al., 2007). In another approach, an electrophilic affibody (modified with acrylamide) that covalently binds its protein target (containing nucleophilic residues like cysteine, histidine and lysine) was developed (Fig. 1.4). (Holm et al., 2009). This ZSPA (Z domain derived from *Staphylococcus auerus* protein A) binding affibody showed more stable protein labelling at the mammalian cell surface and improved the sensitivity of protein detection in immunoassays by two orders of magnitude when compared to the unmodified affibody (Holm et al., 2009).

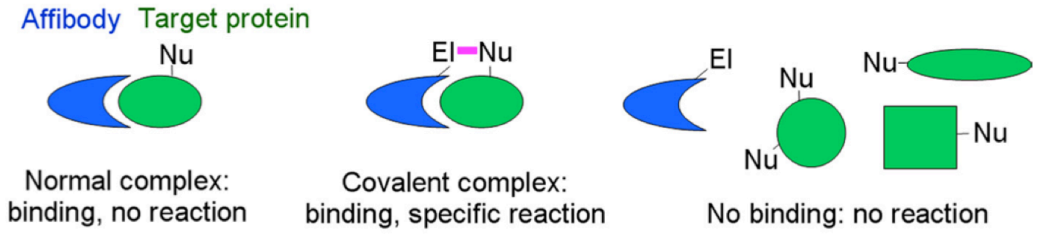

Figure 1.4. Electrophilic affibodies. A normal protein-affibody complex can be modified to bind covalently. A weak electrophile (El) is introduced in the affibody (blue) close to the target (green) binding site such that the electrophile is aligned with a nucleophilic residue on the target protein. The proximity of the reactive groups drives covalent bond formation. If the affibody does not bind a protein, the reaction does not occur (from Holm et al., 2009. Permission obtained).

Alternative scaffolds, such as zinc finger proteins and scorpion toxins, can be as small as 20-30 amino acids and can be engineered with the antigen binding region, using methods based on point mutations, pre-existing consensus binding sequences and generating combinatorial libraries (Binz et al., 2005). The smaller size of these alternative binding proteins can make production easier (compared to antibodies) and the absence of disulfide bonds makes them apt for targeting intracellular antigens and co-crystallization with macromolecular targets (Binz et al., 2005). Their therapeutic

potential as a new class of protein drugs has yet to be demonstrated (Gebauer and Skerra, 2009). However, binding proteins based on alternative scaffolds may be immunogenic, show reduced effect due to lower avidity, and do not have immune effector functions (Allen, 2002). Furthermore, whereas antibodies have been in use for many decades and the crystal structures of many of them are now available, only a few affibodies and DARPins have their structure crystallized and are not easily available for all kinds of antigens. The practical use of engineered protein scaffolds in therapy will only become clear once a number of ongoing clinical trials show successful results (Tamaskovic et al., 2012).

1.2 Cell separation technologies

Cell separation techniques are important in areas including immunology, stem cell research and cancer research. Research involving cell analysis frequently requires the isolation of a certain cell-type from a complex mixture, as a final objective or for further analysis. A number of commercial products are available for separation of different cell sub-populations based on various parameters (Dainiak et al., 2007). Current cell separation techniques can be classified into three main categories. The first class is cell separation based on physical characteristics, such as size, shape and density, and includes filtration and centrifugation techniques. The second class is based on biophysical and cell surface characteristics, such as different amounts of fluorescent antibody binding to cell surface proteins, and includes fluorescence activated cell sorting (FACS). The third class, based on differences in surface protein expression, comprises affinity methods of capturing cells on solid phases such as an affinity column, polyacrylamide/agarose beads, microfluidic chips and more recently, magnetic particles. The main applications of these techniques and their efficiency in terms of yield, purity and scalability are discussed below.

1.2.1 Cell separation based on physical characteristics

Cell separation based on physical characteristics such as size and density of cells is probably the oldest existing method for cell separation. It is primarily done in two

ways: density gradient separation by centrifugation and filtration based on cell size by passing the cells through a synthetic sieve.

Cell separation by centrifugation involves the use of a reagent that can form a density gradient over the desired range. The reagent, which is typically Percoll- or Ficoll-based (Dainiak et al., 2007; He et al., 2008), is added to a centrifugal tube, and the sample containing the mixture of cells (such as blood) is layered on top. After spinning, the lowest-density cells (or plasma) collect at the top and the increasingly heavier cells get arranged in the following layers below. The required cells can be pipetted out from the respective layer. Density gradient separation is mainly used as a pre-enrichment technique when isolating cells from blood, as it can quickly and easily remove the bulk of unwanted cells. After blood fractionation, rare cells can be further purified from the density layer, using affinity-based cell isolation. The relative sedimentation rates of the required cells, conjugated to various other cells or particles, have also been investigated in order to optimize the density differences between various cell-types (Park et al., 2012). Density gradient separation has the advantage of adjustable pH and osmolarity, helping preserve the integrity of the cells.

A novel spiral-shaped microchannel with inherent centrifugal properties for size-based separation has also recently been introduced to isolate Circulating Tumour Cells (CTCs, section 1.3.2) from blood (Hou et al., 2013). The microchannel uses the differences in drag forces and inertia between smaller blood cells and larger CTCs to focus the cells in separate streams in the spiral channel (Hou et al., 2013). The continuous flow and collection of sorted cells ensures short residence time of individual cells within the device (0.1 ms), thereby reducing shear stress on the cells. However, this device has a minimum CTC size cut-off of ~11 μm and smaller CTCs are inevitably lost (Hou et al., 2013). It also takes 20 min to process 1 mL blood (Hou et al., 2013), and therefore isolating from a typical 10 mL blood sample would take more than 3 hr.

For size-based separation, another attractive method is the use of membrane filters such as track-etched polycarbonate membrane filters- multi-layered microfabricated parylene membrane filters or microcavity arrays, comprising pores that allow the passage of unwanted smaller cells, but trap the desired larger cells. A recent ScreenCell® device is a single-use low-cost invention, which has a track-etched

polycarbonate removable filter (pore size – 6.5-7.5 μm) for live or fixed cells (Desitter et al., 2011). Passing blood samples through the filter captures the larger cells onto the filter, which can then be removed and used for immunocytochemistry, fluorescence in situ hybridization assays, isolating genetic material, or for growing the live cells in culture (Desitter et al., 2011).

Physical filtration microdevices based on centrifugation usually require minimal sample preparation, thereby reducing experiment time. They are also cheaper and more easily accessible than other cell separation devices. A growing amount of evidence has now shown that carcinoma cells at a primary tumour can undergo epithelial-mesenchymal transition, downregulating their epithelial markers and invading the bloodstream to form CTCs (Rhim et al., 2012) (sections 1.2.3, 1.2.4, 1.3.2, 1.3.3). Studies in prostate cancer have also shown that lower levels of certain cancer biomarkers are associated with more rapid tumour cell proliferation and poor prognosis (Minner et al., 2010). Therefore, when isolating cancer cells from tissues or blood, using a biomarker-independent method could be valuable, as it does not prejudice isolation based on selected cell surface markers, but gives an impartial recovery of cells that can then be analysed for cell surface markers.

However, physical filtration and high-speed centrifugation can lead to shearing of cell membranes and might therefore be unsuitable for the isolation of rare cells (Autebert et al., 2012). Size-based filtration can be time-consuming, as the lateral flow applied to the filtration device is slow, resulting in slow sample processing and limited sample throughput (Mohamed et al., 2009). Cells trapped in filters may deform at the pores, due to the constant thrust by other cells passing through the filter as the entire cell mix is pumped through (Mohamed et al., 2009). This can also result in clogging of the microfilters by a large number of unwanted cells and cell debris, making cell retrieval difficult and unsuitable for further processing (Autebert et al., 2012). Furthermore, size-based filtration is based on the assumption that a particular cell-type is larger than the others, whereas sometimes cell size ranges are hard to define. For example, CTCs are often separated from leukocytes on the basis of CTCs being larger: the average size of CTCs is ~16-20 μm and that of leukocytes is 10-15 μm (Hou et al., 2011). However, CTCs in prostate cancer patients have been reported to range from 8-16 μm (Stott et al., 2010). Typical filtration devices with pore sizes of 5-10 μm can

capture many unwanted leukocytes and their presence in CTC analysis can lead to false positive enumeration of CTCs, and contamination of CTC-specific molecular analysis. Therefore, size-based filtration methods mostly lead to low cell purity and recovery rates.

1.2.2 Fluorescence Activated Cell Sorting

The FACS instrument, first developed in the 1970s, is an analytical tool that measures the properties of individual cells in a fluid stream via illumination with a laser and separates the cells accordingly (Bonner, 1972; Herzenberg et al., 1976). Cells are first labelled with antibodies (conjugated to fluorescent molecules) against cell surface markers, according to which cell type is required. The labelled cell suspension is inserted into the instrument, where it passes through sheath fluid in the form of a narrow cylindrical stream, orienting cells in a single file (Bonner, 1972). A laser beam is directed towards the stream. Detectors positioned in line with the beam and perpendicular to the beam, pick up forward- and side-scattered light respectively. Fluorescence detectors pick up the fluorescence emitted by the cell. As the stream is broken into a series of small droplets, segregating individual cells, each droplet is interrogated by the laser beam, and depending on the cell properties, is electrostatically charged and deflected into various collection tubes (Bonner, 1972).

FACS analysis generates information about the morphological, structural and functional characteristics of the sorted cells. The development of multiple fluorescence parameters has increased the number of variables for which the cells can be interrogated, thus making the purification criteria extremely specific (Hawley et al., 2004). The advent of novel technology such as imaging flow cytometry, which combines the statistical power of flow cytometry with fluorescence microscopy has further increased the power and scope of this tool (Basiji et al., 2007). FACS has had a number of research and clinical applications. In cancer, FACS has been used for the diagnosis and monitoring of haematolymphoid cancers by isolating cancer cells from the blood and bone marrow of patients (Jaye et al., 2012). In immunology, FACS was key to defining T cell subsets and isolation of T cell subsets by FACS has helped detect HIV/AIDS and other primary immunodeficiencies (Jaye et al., 2012). Multi-parameter FACS analysis has also been used to purify $CD34^+$ cells in order to identify

potent haematopoietic stem cells that can be used for bone marrow transplantation (Will and Steidl, 2010).

Despite its high accuracy, ability to generate large amounts of multidimensional, high-complexity data and sort rare cells, FACS has some major limitations. Firstly, FACS has comparatively low throughput, as it inspects cells serially and therefore intrinsically slowly. FACS can typically analyse around 10^3-10^4 cells/s (BD Aria II, BD FACSJazz), although the latest models can go up to 7×10^4 cells/s (BD Aria III). Taking the current average acquisition rate of 5×10^3 cells/s, for an experiment that requires sorting from at least 10^7 cells, this would take more than half an hour for each sample. Considering that the concentration of rare cells such as circulating tumour cells (CTCs) in blood can be 1 CTC in 10^7 mononuclear cells (Sun et al., 2011), sorting from at least 10^8-10^9 cells would be required, and acquisition by FACS would then take hours per sample. Similarly, to purify high affinity binders from a phage or yeast display library consisting of $>10^8$ clones, and using a 10-fold excess to ensure that each clone is represented at least once, analysis by FACS is impractical and limits the size of the library that can be analysed (Ackerman et al., 2009).

At higher acquisition rates, the biophysical stress on the cells during sheath flow may be more than the cells can sustain, thereby rendering the isolated cell population unusable for further investigation (Ibrahim and van den Engh, 2003). In terms of purity, FACS was shown to be insufficient in complete depletion of malignant cells from a testicular cell suspension that was needed for testicular stem cell transplantation (Geens et al., 2007). Only one of 11 samples showed complete decontamination from malignant cells (Geens et al., 2007). Maintaining a FACS instrument is also expensive, both in terms of initial investment and the continuous requirement of expert professionals (Dainiak et al., 2007). Therefore, although flow cytometry-based technologies are an essential laboratory tool and have had major impacts on the diagnosis and classification of diseases, flow cytometry-based cell isolation is not ideal for sorting very small subsets of cell population and a number of other cell isolation approaches are now being developed and investigated.

1.2.3 Affinity capture on solid phase

Adhesion-based cell separation is similar to affinity chromatography, where a mixture is passed through a column or microdevice capable of binding the cell-type of interest through attached antibodies or other binding agents. Adhesion-based cell separation can be used for positive selection, where target cells bind to the affinity matrix and after washing are released in purified form, or for negative selection where unwanted cells adhere to the column while target cells are collected in the flow-through.

Cryogels are macroporous hydrogels, which are characterized by large interconnected pores, and are coated with antibodies, enabling capture of affinity-bound cells in a chromatography column (Dainiak et al., 2007). Cryogels are designed such that once the target cells are bound to the matrix and unwanted cells have flown through, bound cells can be detached by mechanical compression of the cryogel, avoiding the use of harsh elution conditions, but stressing the cell membrane (Fig. 1.5) (Dainiak et al., 2007).

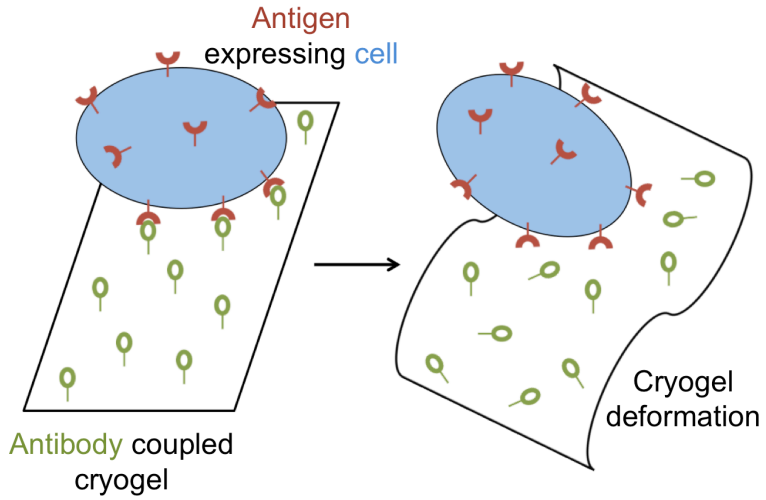

Figure 1.5. Cell separation using cryogels. Schematic representation of antigen (red)-expressing cell (blue) attachment to an antibody (green)-coupled cryogel and detachment of the cell on cryogel deformation (Figure adapted from Dainiak et al., 2007).

Polyacrylamide beads conjugated to avidin can also be used in an immunoaffinity system, to bind cells labelled with biotin-conjugated antibodies (Berenson et al., 1986). This method was first used for the selective enrichment of lymphoid subpopulations from bone marrow and peripheral blood using monoclonal antibody

(Berenson et al., 1986). However, bound cells were released from the beads by mechanical agitation, which led to low overall recovery due to cell shearing. Recent studies have shown the efficiency of pH-mediated release of captured cells from antibody-loaded beads (Bryan et al., 2013). Furthermore, using beads much larger than target cells can also overcome the commonly faced problem of endocytosis of capture beads (Bryan et al., 2013).

Material modification of the solid phase can also be used to enhance the efficiency of cell capture. $-CH_3$ modified surfaces have been shown to initiate the adhesive properties of mesenchymal stem cells, but in addition the length of the alkyl chain can also influence the mesenchymal cells' phenotype and function (Curran et al., 2011). Cell separation based on calcium-dependent reversible binding of calmodulin with calmodulin-binding peptide has also been explored (Colinas and Walsh, 1998). Leukaemia cells labelled with antibodies conjugated to calmodulin-binding peptide were immobilized on solid phase via calmodulin in the presence of Ca^{2+}. After unwanted cells had been washed away, the target leukaemia cells were released by chelating Ca^{2+}, to detach calmodulin from its binding peptide (Colinas and Walsh, 1998).

Several microfluidic devices have also been developed for affinity-based cell separation. In a landmark paper a few years ago, a microfluidic silicon chip was devised with microposts coated with neutravidin (Nagrath et al., 2007). Cancer cells, labelled with biotinylated antibody and spiked into blood, were passed over the chip in a continuous laminar flow, allowing the target cells to collide and attach to the microposts. This technology allowed the detection of CTCs in more than 99% of advanced cancer patients (breast, colon, prostate, pancreatic) in a single step, although the purity of isolated cells was only 50% (Nagrath et al., 2007). This chip was later upgraded to the "herringbone-chip", which uses a herringbone pattern to enhance cell-surface interactions with the chip, and gives a 30% better CTC capture efficiency than the original CTC-chip (Stott et al., 2010). The relationship between cell capture efficiency and laminar flow rate in microchips has also been explored and optimized (Stott et al., 2010; Dickson et al., 2011). In another approach, a 3D nanostructure composed of silicon-nanopillars has been developed to optimize the topology of the solid phase surface used to capture cells (Wang et al., 2009a). Coated with an

antibody, the nanopillars help enhance the interaction with the extracellular membrane extensions, thereby capturing more cells as compared to a flat silicon surface that provides limited interface for interactions with the dynamic cell surface (Wang et al., 2009a).

Apart from enhanced cell capture, these novel affinity based purifications have the advantage of separating cells that have the same size or density, such as sub-populations of human lymphocytes. In cases where the solid phase is directly conjugated with the primary antibody, there is no need for preprocessing the cells and is therefore time efficient. However, multivalent binding between cell surface markers and the ligands/antibodies on the affinity matrix could lead to undesirable cell activation. A major drawback of affinity capture is the difficulty in finding cell-specific proteins that are regularly expressed at high levels on the cell. Many cancer-related antigens are heterogeneously expressed in different cancer cell-lines (McDonagh et al., 2012) and therefore affinity methods may give false negative results. Furthermore, an unoptimized laminar flow rate in microfluidic devices could lead to either non-specific binding of unwanted cells (slow flow rate), or cell shearing (high flow rate). In cases where the cells are irreversibly bound to the solid phase, such as in the CTC-chip, target cells become unviable for certain downstream applications, such as growing cell cultures.

1.2.4 Immunomagnetic cell isolation

Immunomagnetic cell isolation combines the power of affinity capture along with that of magnetophoresis, the movement of magnetic particles relative to a fluid under the influence of a magnetic field. In a typical immunomagnetic cell sorting experiment (Fig. 1.6A), cells are first incubated with a primary antibody against a cell surface antigen and the labelled cells are then mixed with magnetic particles conjugated to detection agents (such as a secondary antibody) that can bind the primary antibody on the cells. Application of a magnetic field allows the magnetic bead-bound cells to separate from the unlabelled cells. Positive selection allows the enrichment of target cells and in cases where specific antibodies for target cells are unavailable, negative selection allows the depletion of unwanted cells from the cell mixture. A number of magnetic particles, differing in composition, shape, size and protein conjugation capacity are now available commercially (Dainiak et al., 2007).

The most widely used commercial system for immunomagnetic cell separation is based on superparamagnetic Magnetic-Activated Cell Sorting (MACS) nanoparticles (Miltenyi Biotech, Germany). MACS beads coated with dextran and can be 20–100 nm in size. Cells bound to antibody-conjugated MACS beads are added to a high gradient magnetic separation column that is filled with a ferromagnetic matrix of stainless steel wool and has a strong external magnet (4 Tesla). The induction of the magnetic field gradient attracts cells bound to magnetic beads and binds the cells to the surface of the matrix (Grützkau and Radbruch, 2010). After the unwanted cells have been washed away, the target cells can be eluted by removing the column from the magnet. MACS beads have been used to isolate a wide array of cells, including leukocytes, stem cells, connective tissue cells and other rare cells (Dainiak et al., 2007; Grützkau and Radbruch, 2010). Cells isolated using MACS can also be used for further analysis by flow cytometry (Thiel et al., 1998). The introduction of MACS-MultiSort has allowed the isolation of cells based on more than one parameter (Thiel et al., 1997). However, due to the small size and polyvalent binding of MACS beads, the beads can be endocytosed by labelled cells, which may lead to artificial activation of the cells (Grützkau and Radbruch, 2010).

Dynabeads (Life Technologies), uniform polystyrene spherical beads, are another class of magnetic particles that are widely used in cell isolation (Fig. 1.6B). The diameter of Dynabeads can be 2.8 μm, 4.5 μm or 5 μm, and their superparamagnetic characteristic ensures that they are magnetic only in a magnetic field, thereby avoiding self-clustering. The larger-sized Dynabeads are also less prone to internalization by bound cells, as compared to MACS beads.

A number of commercial products based on immunomagnetic cell separation such as CellSearch™ (Veridex, LLC) and EasySep™ (Stemcell Technologies) have been developed for the purification of CTCs and immune cell subpopulations from human blood. Apart from human cells, immunomagnetic cell isolation has also been used to isolate microbial organisms from various food, water and soil samples (Safaník and Safaníková, 1999) and as a selection tool for protein engineering by yeast surface display (Ackerman et al., 2009). Immunomagnetic cell isolation has extremely high throughput, as it is performed in batch mode instead of serially and can process 10^{10}-10^{11} cells in less than 30 min, with a more than 10,000 -30,000 enrichment rate (Thiel

et al., 1998; Ackerman et al., 2009; Grützkau and Radbruch, 2010). Unlike FACS, immunomagnetic isolation does not expose cells to high velocity-induced cell stress (McCloskey et al., 2003a).

However, a major drawback of immunomagnetic separation is its strong dependence on antigen expression levels and the affinity of the antibody used (McCloskey et al., 2003a; Antolovic et al., 2010). Using different Epithelial Cell Adhesion Molecule (EpCAM)-specific antibodies gave variable detection of CTCs in patients with colorectal cancer (Antolovic et al., 2010). The purity of immunomagnetically isolated cells can be highly variable and when the target cells are present in low concentrations, depletion methods give extremely impure results (Geens et al., 2007; Sieuwerts et al., 2009). This is probably because, while much research has been done on the optimal size and composition of the magnetic bead (McCloskey et al., 2003a) and automation of the immunomagnetic cell separation protocol, there still exists a need to understand and enhance the cell and magnetic bead interaction at the molecular level. Immunomagnetic cell separation has the potential to become the preferred cell separation tool if these challenges are overcome.

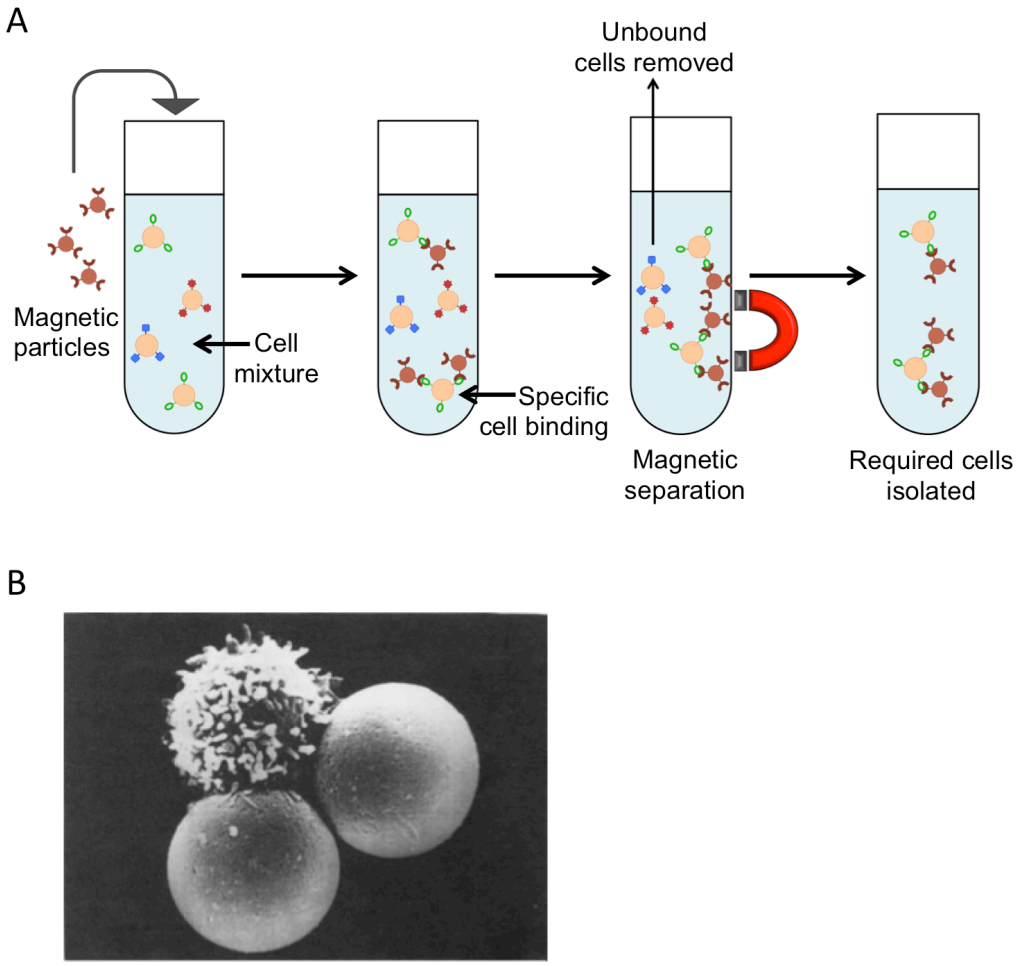

Figure 1.6. Immunomagnetic cell separation. A. Antibody-coupled magnetic particles are added to a cell mixture. Binding of the particles to specific cell-types allows the separation of magnetic particle-bound cells from the unbound cells, in the presence of a magnetic field. The isolated cells can be released by removing the magnetic field. B. An electron micrograph showing a T-lymphocyte bound to two magnetic beads (Dynabeads M-450) (from Safarík and Safaríková, 1999. Permission obtained).

1.3 Challenges and limitations of isolating circulating tumour cells (CTCs)

1.3.1 Metastasis

Metastasis is the process by which cancer spreads from one part of the body to another. As a malignant tumour develops, it will typically sheds cells into the neighbouring blood vessels. These tumour cells circulating in peripheral blood are termed circulating tumour cells (CTCs) and can travel to distant tissues where they may start metastatic tumours. Cells in a metastatic tumour have similar characteristics as the original tissue of the primary tumour. For instance, a metastatic tumour in the

lungs of a breast cancer patient will resemble breast cancer cells. Most human cancer deaths are caused due to metastatic tumours rather than primary tumours (Pantel et al., 2008).

In the field of cancer research, there are two major metastasis paradigms (Klein, 2009). In the classical linear model, metastasis is considered as the last step in tumour evolution. Accumulation of genetic and epigenetic alterations are accompanied with selection of most fit cells that can proliferate relatively autonomously and leave the primary site to seed secondary growths (Klein, 2009). This Darwinian sequence supports that invasive behaviour and tumour dissemination occur late in tumour evolution, and that secondary tumours can only develop once the primary tumour has reached a certain growth stage (Cairns, 1975). However, this model fails to account for two major observations; 1.) metastatic tumours are sometimes detected in patients with no detectable primary tumour (Klein, 2009) and 2.) metastatic lesions can appear years after the surgical removal of a primary tumour that did not have metastasis at diagnosis. Indeed, more than 75% patients who underwent resection of small pancreatic tumours and showed no evidence of metastasis at the time, died from metastatic cancer within 5 years (Neoptolemos et al., 2004).

An alternative model, which supports parallel, independent progression of metastasis has now been proposed (Weigelt et al., 2005; Klein, 2009). Recent studies have shown that tumour cells can disseminate systemically in the pre-malignant phase of murine breast cancer (Hüsemann et al., 2008). Studying pancreatic cancer in the mouse model, it was shown that even cells in pre-malignant lesions underwent epithelial-mesenchymal transition (EMT), invaded the bloodstream and had tumour initiating properties (Rhim et al., 2012). Furthermore, DNA microarrays show that metastasis is an inherent feature of a tumour and is not necessarily dependent on the tumour development stage (Weigelt et al., 2005). Therefore, the model supporting seeding of metastatic tumours in parallel to tumour progression at the primary site is now widely accepted and has led scientists and clinicians to reconsider current diagnostic and therapeutic routines.

1.3.2 Circulating tumour cells

During malignant progression, carcinoma cells acquire the ability to extravasate into the surrounding tissue, by degrading the basement membrane and extracellular matrix. Growing tumours can shed anywhere from 10^5 – 10^6 CTCs/day/g malignant tissue (Butler and Gullino, 1975), but only a small percentage of such CTCs form distant lesions. Fortunately, the metastatic process is highly inefficient due to the failure of CTCs to initiate growth and the failure of early micrometastasis to develop into macroscopic tumours (Luzzi et al., 1998). Most CTCs are either cleared by the immune system, destroyed by haemodynamic forces, become lodged in the lymph nodes or remain in circulation as dormant solitary cancer cells (no proliferation or apoptosis) (Luzzi et al., 1998). Furthermore, many CTCs may not necessarily seed metastatic tumours in distant organs, but self-seed back into the original tumour.

However, even small numbers of CTCs present in the peripheral blood of patients form an important prognostic marker of disease progression and overall survival rate. The correlation between CTC enumeration and disease progression has been shown in a number of cancers, including breast, prostate, colorectal, lung, bladder, renal, gastric and liver cancer (Sun et al., 2011). In breast cancer, pre-treatment CTC counts above 5 CTCs per 7.5 mL of blood were associated with shorter progression-free survival and shorter overall survival (Cristofanilli, 2006). CTC count can also be used to monitor therapy and adapt drug dosage to individual patient responses, as CTC count can reflect tumour volume, vascularity and invasiveness.

One of the biggest challenges in studying CTCs has been the identification of markers that distinguish CTCs from blood cells. Usually, this is done by looking for epithelial markers normally over expressed in cancer but not on blood cells, such as EpCAM (Antolovic et al., 2010). However, recent data suggests that carcinoma cells undergo an epithelial-to-mesenchymal transition during which they lose their epithelial characteristics, and acquire invasive stem cell-like properties, along with the expression of mesenchymal markers (Rhim et al., 2012). Therefore, current CTC detection technologies, which rely heavily on cellular expression of epithelial markers, are inefficient and may give false negatives.

1.3.3 Methods for CTC detection and isolation

The correlation between CTC number and cancer prognosis has led to a need for accurate, reliable and reproducible CTC detection and isolation devices. However, even in highly advanced cancer patients, CTCs are extremely rare, vastly outnumbered by normal blood cells, sometimes at a frequency of 1-100 CTCs per 10^9 mononuclear blood cells (Allard et al., 2004). Therefore, a number of CTC isolation devices have been developed, which sometimes combine CTC enumeration with genetic and molecular characterization of the captured CTCs.

CellSearch™ (Veridex, LLC) is currently the only FDA-approved device for CTC enumeration in a clinical setting for breast, prostate and colorectal cancers and has been widely used in the last decade (Fig. 1.7A). CellSearch™ is an automated device, which counts the number of CTCs from a 7.5 mL peripheral blood sample, by fractionating the blood and mixing the leukocyte- and CTC-containing layer with a colloidal ferrofluid composed of magnetic nanoparticles coated with anti-EpCAM antibodies. After immunomagnetically enriching the cancer cells, cells are fixed, permeabilized and labelled with a cocktail of antibodies for cytokeratins 8, 18 and 19, markers characteristic of epithelial cells. In a study conducted at three independent laboratories, CellSearch™ detected CTCs in ~70% of metastatic breast cancer patients (Riethdorf et al., 2007). Although recovery from spiked samples was 80-82%, it should be noted that only cell-lines expressing high EpCAM were used for spiking and therefore the experiment does not validate the detection efficiency of CTCs that have undergone EMT. Similarly, in another study, CellSearch™ did not detect CTCs in ~30% metastatic breast cancer patients (Allard et al., 2004). The purity of CTCs after CellSearch™ enrichment is still low, with 800 contaminating leukocytes present per 1 CTC (Sieuwerts et al., 2009). Therefore, there is much scope for improvement in sensitivity and specificity of CellSearch™, especially with regard to reducing its dependence on high-expressing epithelial markers.

Alternative microfluidic devices used for CTC isolation are the CTC-chip (Fig. 1.7B and C) and the herringbone-chip, which have high sensitivity but low purity of 0.1 - 50% (also reviewed in Section 1.2.3) (Nagrath et al., 2007; Stott et al., 2010). The CTC-chip isolated CTCs from patients suffering from metastatic lung, prostate, pancreatic, breast and colon cancer in 99% of advanced cancer patient samples

(Nagrath et al., 2007). The advantages of the CTC-chip over CellSearch™ include its ability to sort cells directly from blood without fractionation, thereby avoiding loss of CTCs, and isolating live CTCs without fixing or permeabilizing them (Nagrath et al., 2007; Stott et al., 2010). The disadvantages of the CTC-chip are that when high EpCAM-expressing NCI-H1650 cells (>500,000 surface antigens) were spiked into human blood, only ~60% cells were recovered and that this device is not yet mass produced or optimized for high-throughput.

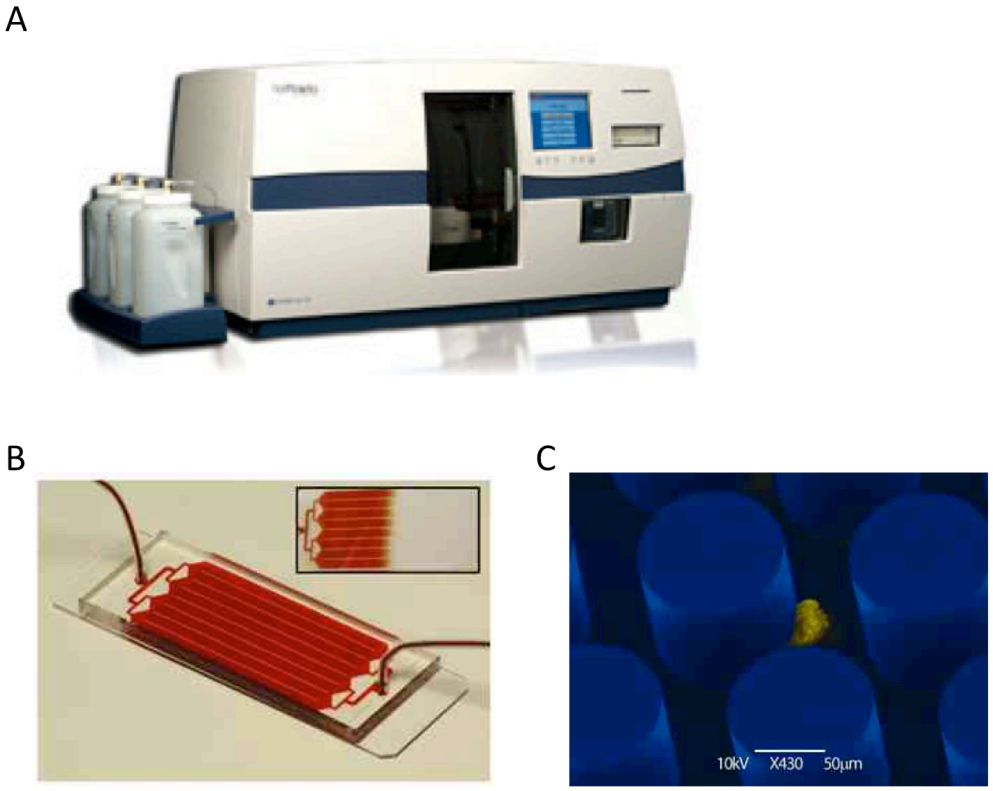

Figure 1.7. CTC isolation technology. A. Automated CTC isolation device, CellSearch (Veridex LLC). B. Herringbone-chip technology can isolate CTCs directly from whole blood (Stott et al., 2010. Permission obtained). C. An isolated CTC bound to a micropost on CTC-chip.

The archetypal CTC isolation approach is FACS, which is now considered inefficient for rare cell isolation (reviewed in section 1.2.2). The recent development of a microfluidic chip-based micro-Hall detector combines microfluidics and magnets, to simultaneously detect CTCs based on three epithelial markers, EpCAM, HER2 and Epidermal Growth Factor Receptor (EGFR) (Issadore et al., 2012). Also, in an

interesting *in vivo* application of immunomagnetic targeting in tumour-bearing mice, CTCs were captured by magnetic nanoparticles in the bloodstream, followed by their rapid photoacoustic detection using gold-plated carbon nanotubes conjugated with folic acid (Galanzha et al., 2009). Magnetic nanoparticles functionalized to target tumour cell markers in the bloodstream of mice were used to bind and capture CTCs under a magnet (Galanzha et al., 2009). The captured cells were then further detected with gold-plated carbon nanotubes coated with folic acid, to target folate receptors on cancer cells. The gold-plated nanotubes thereby acted as a second contrasting agent for photoacoustic imaging, in which non-ionizing laser pulses were delivered to the captured cells and the emitted ultrasonic waves were processed by ultrasonic transducers to form images of the captured cells (Galanzha et al., 2009).

Such techniques have the potential for early diagnosis of metastasis in cancer. However, in the absence of a "gold standard" with which to measure the exact CTC counts in cancer patients, defining the efficiency and sensitivity of the various CTC isolation devices remains a challenge. Assays targeting epithelial cancer cells in blood are susceptible to missing the most invasive tumour cells, those that have undergone EMT. Implementation of isolation based on other cancer biomarkers such as HER2, EGFR and Insulin-like growth factor-1 receptor (IGF1R) could reduce the dependence on EpCAM to some degree, but are challenged by the heterogeneity in tumour cells. An ideal CTC isolation device should be highly robust and specific, have high throughput, reduced dependence on surface expressed biomarkers and yield CTCs in a form that is compatible with their further molecular and cellular characterization and propagation in cell culture.

1.3.4 Applications of CTC isolation

With the renewed metastatic model, supporting early progression of metastasis independent of tumour growth (section 1.3.1), it has become increasingly important to detect CTCs, not only as a prognostic marker to detect recurrence after the resection of a tumour, but also as a primary diagnostic marker to detect cancer in susceptible patients. Apart from CTC enumeration, molecular and genetic characterization of isolated CTCs acts as a non-invasive liquid biopsy in cancer patients and gives a wealth of information about the nature and evolution of the primary tumour. CTC characterization can also be used to predict drug sensitivities in patients and help

design more effective therapies, as CTCs provide real-time information on the biomarker status of the primary tumour.

Isolated CTCs have been used for a number of downstream applications (Fig. 1.8), such as immunostaining for specific cell markers and fluorescence in situ hybridization (FISH) to examine genomic amplification and translocation (Yu et al., 2011). DNA and RNA can be extracted from CTCs and subjected to sequencing, quantitative reverse transcription PCR and microarrays to study genetic mutations and expression profiles (Yu et al., 2011). Viable CTCs can also be propagated in cell culture for further molecular characterization and screening drugs to meet the individual needs of the cancer patients.

In breast cancer patients, captured CTCs have been used for biomarker analyses such as HER2 status, qRT-PCR for breast cancer subtype markers, KRAS mutation detection and EGFR staining by immunofluorescence (Punnoose et al., 2010). The HER2 status of CTCs was shown to concur with the HER2 status of the primary tumour in 89% of cases (Punnoose et al., 2010). In non-small cell lung cancer patients, EGFR mutations in CTCs have been directly related back to the primary tumour (Maheswaran et al., 2008). The detection of the T790M mutation in EGFR (conferring tyrosine kinase inhibitor drug resistance) in CTCs was correlated with reduced progression-free survival of lung cancer patients; serial analysis of CTCs showed that increase in CTC number was directly associated with tumour progression (Maheswaran et al., 2008). Multi-gene expression profiling by qRT-PCR of CTCs in metastatic breast, prostate and colorectal cancers has been used to distinguish cancer patients from healthy donors, while CTC-specific expression of selected genes could differentiate between the three types of cancers (Smirnov et al., 2005). In metastatic carcinoma, patients with high CTC counts expressed IGF1R on CTCs, supporting the correlation between IGF1R expression and more aggressive disease progression (de Bono et al., 2007).

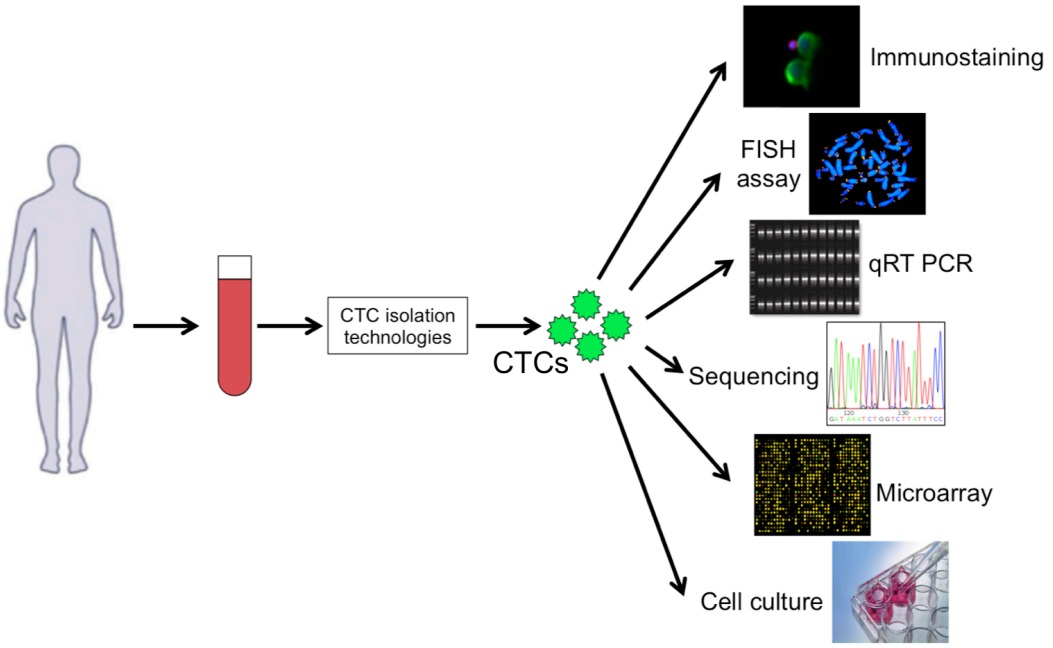

Figure 1.8. Illustration of CTC applications. Peripheral blood from a cancer patient can be used to isolate CTCs, which can be then analysed using a battery of genomic and proteomic techniques (Figure adapted from Yu et al., 2011).

Therefore, CTCs can be representative of primary tumours and can be used to genetically fingerprint tumours. In the near future, CTCs can be regularly used to detect cancer in susceptible populations with genetic predispositions, as surrogate markers for response to therapy, to identify patients in need of adjuvant therapy and to survey for a relapse of the disease. However, CTCs are heterogeneous, and it is important to consider this when evaluating their significance in the disease.

1.4 Overview of the HER2-4D5 interaction

1.4.1 HER2 biology and significance

HER2 (ErbB2/Neu/p185) or Human Epidermal growth factor Receptor 2 is a 185 kDa tyrosine kinase receptor that belongs to the ErbB family of epidermal growth factor receptors, which include EGFR, HER2, HER3 and HER4 (Rubin and Yarden, 2001). ErbB receptors generally consist of an extracellular ligand binding domain, an α-helical transmembrane domain and a cytoplasmic protein tyrosine kinase domain. On ligand activation, ErbB receptors undergo a conformational rearrangement and

dimerize, initiating cross-phosphorylation and transactivation of their intracellular kinase domains and downstream cell signalling (Rubin and Yarden, 2001).

HER2 does not have an identified ligand. HER2 exists in a constitutive "open" conformation, blocking self-association but rendering HER2 available for heterodimerization with other activated ErbB receptors (Rubin and Yarden, 2001). On activation of other ErbB receptors with ligands such as Epidermal Growth Factor (EGF) or neuregulins, HER2 is the preferred binding partner for EGFR, HER2 and HER4 proteins, leading to the formation of heterodimers. Dimers containing HER2 have higher ligand binding and signalling potency as compared to homodimers and heterodimers without HER2 (Rubin and Yarden, 2001). ErbB receptor activation leads to the activation of mitogen-activated protein kinase (MAPK), phosphoinositide 3-kinase (PI3K/Akt) and protein kinase C (PKC)-mediated pathways among many others, eventually translating into different transcriptional programmes in the nucleus and changes in cell growth, migration, adhesion, differentiation and sensitivity to apoptosis (Yarden and Sliwkowski, 2001).

Receptor deactivation by phosphatase activity or temporary downregulation of the cell surface receptors via endocytosis before receptor recycling, eventually directs the termination of the HER2 signal (Yarden and Sliwkowski, 2001). HER2 internalization has been shown to occur in a clathrin- and tyrosine kinase-independent pathway in geldanamycin-treated human breast cancer cells (Barr et al., 2008). In such cells, HER2 internalization follows the glycosylphosphatidylinositol (GPI)-anchored protein-enriched early endosomal compartment (GEEC) pathway, and HER2 is eventually transported through early and late endosomes for degradation in lysosomes (Barr et al., 2008).

In cancer, high surface expression of HER2 results in closely spaced HER2 receptors, and a higher probability of their spontaneous dimerization and transactivation of kinase domains (Slamon et al., 1987). A Val to Glu point mutation in the transmembrane domain of HER2 could also lead to ligand-independent activation of HER2, thereby resulting in hyperactivation of downstream pathways and misregulated cell growth (Bargmann et al., 1986). The HER2 gene is amplified from 2- to >20-fold in 30% of breast cancer tumours; in patients with >5 copies of HER2, the overall survival probability of the patient is reduced to less than 50% after 3 years

(Slamon et al., 1987). Measurements of serum HER2 extra-cellular domain have also been used to determine HER2 status in metastatic breast cancer patients (Tse et al., 2005), indicating that HER2 overexpression is associated with aggressive tumour growth and metastatic activity. HER2 has been detected on the CTCs of metastatic breast cancer patients, independent of the HER2 status of the primary tumour and therefore HER2-targeted therapy could still be useful in preventing metastasis in HER2-negative patients (Ignatiadis et al., 2011). Apart from breast cancer, HER2 overexpression also plays a role in prostate, pancreatic, bladder, lung, colorectal, ovarian, gastric, head and neck cancers (Menard et al., 2001; Rubin and Yarden, 2001; Minner et al., 2010).

1.4.2 Antibodies against HER2

Following the discovery of HER2 amplification in cancer, HER2 became an attractive target for monoclonal antibody-based therapies. Antibodies can inhibit cell growth by various mechanisms, such as direct inhibition of receptor signalling via ligand competition, obstruction of receptor dimerization, immune cell recruitment and delivery of toxins. A number of antibodies against HER2 have now been developed for use in research, diagnosis and therapy.

Herceptin (trastuzumab) and Pertuzumab are currently the only FDA-approved antibodies against HER2 and are widely used in breast cancer treatment. Herceptin is the humanized version of murine monoclonal 4D5 and the complete IgG binds HER2 with a K_d = 0.1 nM (Carter et al., 1992). Herceptin works as an anti-cancer agent by inhibiting cell growth and by inducing antibody-dependent cellular cytotoxicity (ADCC response) (Carter et al., 1992). Furthermore, Herceptin has also been shown to inhibit the proteolytic cleavage of HER2 N-terminal domain, which otherwise produces a truncated HER2 protein in its activated conformation with phosphorylation and increased kinase activity (Molina et al., 2001).

Pertuzumab (2C4), another monoclonal antibody against HER2, binds to domain II of HER2 extracellular region with a K_d=2.2 nM. Pertuzumab sterically inhibits the heterodimerization of HER2 with other ErbB receptors such as EGFR and HER3, thereby preventing receptor phosphorylation and some of the most potent downstream signalling (Baselga and Swain, 2009). Ertumaxomab, a member of the Bi-specific T-

cell engager (BiTE) class, is a bispecific antibody, which can simultaneously bind CD3 on an immune cell and HER2 on a cancer cell, subsequently bringing the immune cell close to the HER2-overexpressing tumour cell for immunological destruction of the tumour cell (Baselga and Swain, 2009). Antibody-drug conjugates such as trastuzumab-DM1 (T-DM1), which links trastuzumab to microtubule polymerization inhibitor DM1 are also being evaluated for their therapeutic efficiency (Stopeck et al., 2012).

Five novel antibodies binding the extracellular domain of HER2 have recently been produced and shown to inhibit growth of HER2-overexpressing cancer cell-lines in culture (Ceran et al., 2012). The use of anti-HER2 antibodies in pairs, comprising an antibody against the HER2 dimerization site and another antibody binding to a different HER2 epitope, inhibits cell growth more efficiently than individual antibodies (Friedman et al., 2005; Ben-Kasus et al., 2009). This synergistic effect is hypothesized to be a result of better HER2 endocytosis when targeted with more than one antibody (Ben-Kasus et al., 2009). However, the efficacy of this combination still needs to be tested in a clinical setting.

1.4.3 Binding kinetics of humanized 4D5 (hu4D5)

The murine monoclonal antibody mumAb4D5 against HER2 was first synthesized and characterized by Genentech in order to study the structure and function of HER2 (Fendly et al., 1990). mumAb4D5 was later humanized into huAb4D5-8 (referred to as hu4D5 in my work) and commercialized as Herceptin (Carter et al., 1992). The Fab fragment of hu4D5 has a k_{on}= 1.0 × 10^6 $M^{-1}s^{-1}$ and a k_{off} = 3.5 × 10^{-4} s^{-1} giving a dissociation constant of K_D= 0.35 ± 0.05 nM at 37°C in PBS when measured by surface plasmon resonance (Gerstner et al., 2002).

The crystal structure of hu4D5 Fab bound to HER2 revealed that the Fab bound to HER2 at the C-terminal portion of domain IV of the HER2 extracellular region (Fig. 1.9) (Cho et al., 2003). The steric block imposed by hu4D5 binding to the juxtamembrane region of HER2 may be the cause of Herceptin's inhibition of proteolytic cleavage of HER2's extracellular domain (Molina et al., 2001). The HER2-hu4D5 interaction site covers a surface area of 1350 $Å^2$ over a long groove and consists of three HER2 loops interacting with the CDR regions of hu4D5 Fab. Two

loops are primarily involved in electrostatic interactions, whereas the third HER2 loop makes hydrophobic contacts with the CDR3 loop in the Fab (Cho et al., 2003).

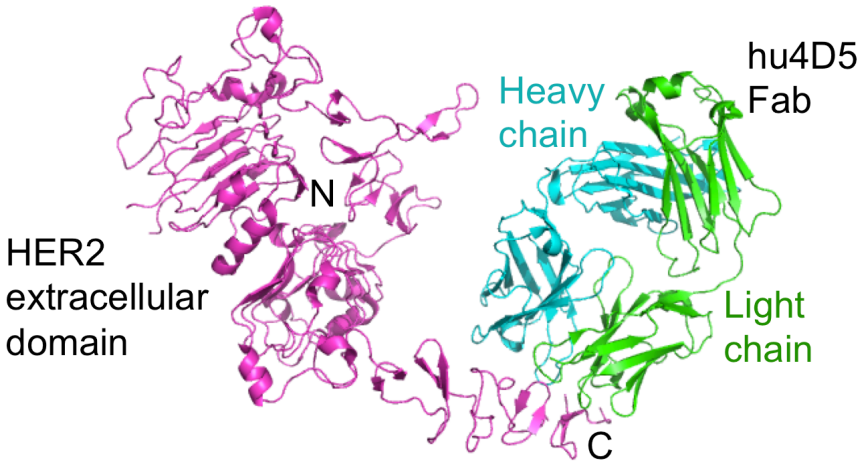

Figure 1.9. HER2-hu4D5 complex. An X-ray crystallographic image of HER2 extracellular domain in complex with the hu4D5 Fab (adapted from PDB 1N8Z).

1.5 Engineering interlocked antigen-antibody complexes

From the above discussion on CTC isolation, the downregulation of tumour cell biomarkers and the current antibodies used to target cancer cells (sections 1.3 and 1.4), it is evident that there exists a need for very high affinity antibodies engineered specifically for isolating cells with low antigen levels. One way of making highly stable antigen-antibody complexes, resistant to the pulling forces applied during cell separation, is to mechanically lock the antigen-antibody complex. Engineering such a tool might overcome the dependence on high antigen expression levels during affinity-based cell separation techniques (section 1.2.3 and 1.2.4).

1.5.1 Mechanically interlocked molecules: Rotaxanes

The field of mechanically interlocked molecules is a fascinating research area for many organic chemists and biochemists. Mechanical molecular locks are those in which two or more molecules are linked together mechanically, and the individual components cannot be separated unless a covalent or metal coordination bond is broken within the components (Haussmann and Stoddart, 2009). Such systems can be employed to form various components of molecular switches, motors and other molecular machinery.

Various kinds of locking scaffolds have been explored. The simplest type of interlocked architecture is a catenane, which is made up of interlocked rings that can rotate with respect to each other (Fig. 1.10A) (Haussmann and Stoddart, 2009). A widely used mechanical lock model is a rotaxane, a dumbbell-shaped construct consisting of a rod encircled by a ring (Fig. 1.10B) (Haussmann and Stoddart, 2009). The ends of the rod have bulky components that are larger than the inner diameter of the ring, preventing the ring dissociating from the rod (Fig. 1.10B). A number of other more complex mechanically interlocked scaffolds such as suitanes (Williams et al., 2006), Borromean rings (Chichak et al., 2004) and cysteine knots (Dietrich-Buchecker et al., 2003) have also been studied in organic chemistry.

The rotaxane model has been widely applied to a number of DNA and protein constructs. The rotaxane model has been used to thread a linear p53 thioester peptide through a cyclic p53 peptide to form a topologically linked p53 heterodimer (Blankenship and Dawson, 2007). An artificial small-molecule machine that can synthesize peptides in a sequence-specific manner has recently been designed based on rotaxane modeling (Lewandowski et al., 2013). Double-stranded DNA molecules have also been used to assemble the dumbbell-shaped construct and the encircling ring, thereby demonstrating the possible use of this technique in synthetic biology (Ackermann et al., 2010). Perhaps the most exciting use of mechanical interlocking for biomolecules has been devised by Williams et al. (Williams et al., 2008). This group genetically modified a DNA polymerase to insert two biotinylated peptide legs at the positions flanking the DNA binding cleft. Once the engineered polymerase bound the DNA template, tetravalent streptavidin was used to bind each of the two biotinylated legs, trapping the DNA template in the cleft and orienting the complex towards a biotinylated surface (Williams et al., 2008). This assembly allowed single molecule DNA sequencing of templates consisting of thousands of nucleotides, with a great enhancement of processivity (Williams et al., 2008).

However, to my knowledge, the use of such interlocking scaffolds in order to lock antibodies onto their antigens has not yet been explored. Many antibodies are raised against peptide fragments of the antigenic protein and the linear peptides could potentially be used as a dumbbell in the rotaxane model, around which the antibody

can be clamped. If the antibody is encircled around the peptide, the peptide-antibody complex would not dissociate easily, due to the mechanical locking of the complex.

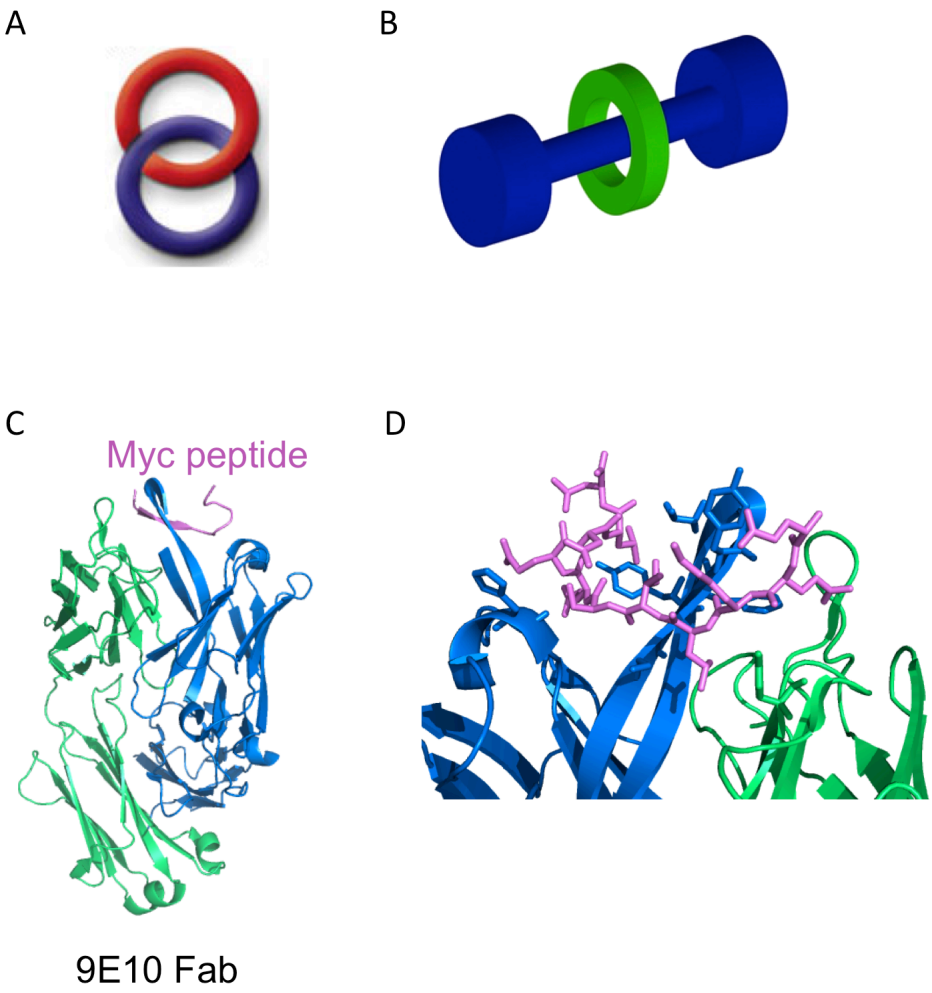

Figure 1.10. Molecular locks and myc-9E10 interaction. A. Cartoon representation of a catenane. B. Cartoon representation of a rotaxane. C. The heavy (blue) and light chain (green) of the 9E10 Fab in complex with myc peptide (pink) (based on PDB 2OR9). D. Myc peptide binding to residues in the CDR regions of 9E10 Fab via hydrogen bonding and van der Waals interactions (based on Krauß et al., 2008).

1.5.2 Antibodies against peptide tags

In order to explore the possibility of engineering a rotaxane-based clamp onto anti-peptide antibodies, it is important to first review some basic features of peptide-antibody interactions. Antibodies for research are often raised against peptides, as peptides are small, simple structures that can be synthesized in an automated fashion. Peptides are most commonly used to tag proteins of interest, which can then be

detected or purified using the available antibodies against the peptide tag (Lobbestael et al., 2010). Peptides are easier to use as epitope tags, compared to larger globular proteins, which can block important surfaces for the required protein function and whose folding and solubility can be unpredictable and challenging (Vincentelli et al., 2004). A number of peptides such as the myc tag, FLAG-tag and Strep-tag have been widely used as affinity tags to detect recombinant proteins of interest (Terpe, 2003).

However, anti-peptide antibodies have moderate affinities and fast dissociation rates, due to the decreased surface area available for interaction with the antibody (Houk et al., 2003). Peptides varying from 7-12 residues and lacking structural rigidity have an average buried surface area of around 480 $Å^2$ when present in a complex with an antibody (Wilson et al., 1994). This is considerably lower than the average buried surface area of 700-900 $Å^2$ in a protein-antibody complex (Wilson et al., 1994). Therefore, the interactions between peptides and their binding partners are limited and antibodies bind their peptide antigens with lower affinity. Thus there exists considerable scope for improvement in peptide-antibody binding.

1.5.3 9E10-myc interaction

9E10 is an antibody against the widely used myc peptide tag and the 9E10-myc interaction has many conventional features of a peptide-antibody complex, including a β-turn (in myc peptide) that helps the peptide interact with the CDR regions on the 9E10 antibody heavy chain (Wilson et al., 1994; Krauß et al., 2008). 9E10 is an IgG1/κ murine monoclonal antibody against the synthetic peptide immunogen myc, derived from the C-terminal region of the human c-myc proto-oncoprotein (Evan et al., 1985). The c-myc gene product is mainly localized in the nucleus of the cell and c-myc expression levels are deregulated in many types of cancers such as multiple myeloma (Greil et al., 1991; Skopelitou et al., 1993). The myc tag is a powerful tool used in protein localization, immunochemistry, ELISA and protein purification. 9E10 Fab fragments have been expressed and purified from bacterial strains (Schiweck et al., 1997) and the myc-9E10 Fab complex has been studied by X-ray crystallography (Fig. 1.10C) (Krauß et al., 2008).

In cancer research, 9E10 has been used to detect and study the distribution of the c-myc oncogene product by immunohistochemistry (Skopelitou et al., 1993; Feller et

al., 2012). In cell biology, the myc tag has been used to study the expression patterns of endogenous proteins *in vivo* (Lobbestael et al., 2010). In protein engineering, 9E10 is widely used as a detection and purification tool for recombinant proteins fused to myc at their C-termini as an affinity tag in expression systems such as yeast, bacteria or insect cells (Weidner et al., 2010). Proteins labelled with the myc tag can be purified in a single-step procedure using affinity columns coupled with 9E10 antibody.

However, the affinity of 9E10 for the myc peptide, although higher than most other peptide-antibody interactions, is relatively low as compared to average protein–antibody interactions. The original myc1 tag (EQKLISEEDLN) binds 9E10 antibody with an affinity of $K_d \sim 5 \times 10^{-7}$ M (Hilpert et al., 2001), whereas most optimized antibodies have an affinity in the range of 10^{-8}-10^{-10} M (Foote and Eisen, 1995). The myc peptide forms a short anti-parallel β-strand, fitting into the groove between the 9E10 heavy and light chains and interacting with the CDR regions of 9E10 via hydrophobic interactions, hydrogen bonding and electrostatic interactions (Krauß et al., 2008). The apparent affinity of 9E10 might be enhanced compared to the actual monomeric affinity, since two 9E10 molecules can bind one myc tag (Krauß et al., 2008). In cases where such dual binding cannot occur, the peptide-antibody affinity would be even lower.

1.6 Objectives of this work

Through the efforts described in my thesis, I intended to achieve three main goals -

1.) Identify the important protein-protein interactions between a cell and a magnetic bead and quantify the extent to which each one affects cell isolation in immunomagnetic cell separation. These protein interaction variables included the expression levels of the targeted antigen, antibody affinity and the secondary linkage of the antibody to the bead. Using the cancer biomarker HER2, the anti-HER2 antibody fragment hu4D5 Fab and streptavidin-coated magnetic dynabeads, I studied each variable individually. Although massive efforts have been taken to invent and optimize devices for cell separation, extensive research on the optimization of the molecular aspects of the synapse between the cell and the solid-phase capture surface is still needed. My work on understanding these aspects has been detailed in Chapter 3 and could provide useful insights and considerations for current affinity-based cell separation techniques.

2.) Improve isolation of cancer cells and reduce dependence of immunomagnetic cell isolation on antigen expression levels. Using the information from chapter 3, I aimed to increase the isolation of cancer cells by immunomagnetic cell isolation, specifically of cells that express lower amounts of the biomarker. With the increasing need for isolating CTCs in cancer therapy, and the recent evidence of CTCs undergoing EMT (Yu et al., 2013), this investigation could provide valuable information on how to increase the efficiency of current CTC isolation technology, as well as for the development of novel tumour cell isolation devices.

3.) Devising an alternative approach to increase antigen-antibody stability by mechanical clamping of the interaction. In order to increase the mechanical strength of an antigen-antibody interaction, such that the interaction can sustain the physical pull exerted by a magnetic bead or the flow of solution in a microfluidic device, I aimed to develop a generic clamp that could trap the antigen within its binding site on the antibody, as described in Chapter 5.

Chapter 2: Methods

Chapter 2: Methods

2.1 Cloning strategies: gene synthesis, point mutants, AP insertions

2.1.1 General cloning procedures

All Polymerase Chain Reactions (PCRs) were performed with KOD Hot Start DNA polymerase (Merck), following the protocol recommended by the manufacturer, in a C1000^{TM} Thermal Cycler (Bio-Rad). Site-directed mutations and overlap extensions were made using the QuikChange® (Stratagene) protocol but with the KOD polymerase. All DNA primers were designed and ordered from Life Technologies. All reagents were purchased from Fisher unless stated otherwise.

A typical 50 µL PCR reaction mixture was made in MilliQ H_2O containing 1× KOD Hot Start DNA Polymerase buffer, 1.5 mM $MgSO_4$, 0.4 mM dNTPs, 0.4 µM forward primer, 0.4 µM reverse primer, ~20-50 ng DNA template and 1 µL KOD polymerase. In general, the thermal cycling conditions were as follows: 3 min at 95°C, then 20 cycles of 20 s at 95°C, 30 s at 55°C and 1 min at 68°C, followed by 10 min at 68°C and a final incubation at 10°C. In two-step PCR reactions used for the insertion of AP tags, the DNA template was first amplified using one forward and one reverse primer, and the PCR product was then used as the template for a second PCR reaction with the second forward primer and the same reverse primer (Chiu et al., 2004). For site-directed mutagenesis of the myc constructs, the cycling conditions were the same as above, except the elongation period was 4 min at 68°C (instead of 1 min). Each PCR reaction was optimized for annealing temperature according to the primers in use. PCR products were analysed for size and purity by running 5 µL of the amplified reaction on an agarose gel (0.7-2% w/v, depending on the size of the DNA fragment) containing 0.01% (v/v) ethidium bromide (Sigma), in an Owl electrophoresis system (Thermo Scientific) for 30-40 min at 130 V. The DNA fragments were visualized in a Gel Imager Universal Hood II (Bio-Rad).

QuikChange products were digested with DpnI (New England Biolabs Inc.) at 37°C for 1 hr to digest the methylated plasmid template. For cloning, PCR products and required vectors were digested with the appropriate restriction enzyme (New England

Biolabs Inc.) according to the manufacturer's instructions, typically for 4 hr at 37°C. The digested products were then run on an agarose gel and gel-purified using the QIAquick Gel Extraction Kit (Qiagen).

For a typical ligation experiment, digested PCR product and vector were mixed in 9:1, 3:1, 1:1 and 1:3 ratios of insert:vector in a 10 μL reaction mixture along with 1× T4 DNA ligase buffer, 1 μL T4 DNA ligase (New England Biolabs Inc.) and MilliQ H_2O. The reaction was incubated at 25°C for 1 hr or at 16°C overnight. 4 μL of the ligated samples were then transformed into 50 μL heat-competent or electrocompetent *Escherichia coli* DH5α (Life Technologies) or XL-1 blue (Stratagene) cells.

The transformed cells were plated onto Luria-Bertani (LB) plates containing 1.5% agar and the appropriate antibiotic for selection of transformed clones. After overnight incubation at 37°C, individual colonies were picked and inoculated into 12 mL LB containing the respective antibiotic and grown at 37°C for 16 hr in a shaking incubator. Cells were harvested by centrifugation at 4,000 g for 5 min and DNA was extracted using GeneJET™ Plasmid Miniprep Kit (Fisher). For mammalian transfections, endotoxin-free DNA was prepared using a 300 mL bacterial culture and Nucleobond Maxi plus kit (Fisher Scientific) according to the manufacturer's recommendations. The kit uses silica-based anion exchange resin to selectively purify plasmid DNA that after purification is expected to contain < 0.05 endotoxin units/μg. DNA concentration was measured using a 2 μL sample on NanoDrop ND-1000 Spectrophotometer (Thermo Scientific) at 260 nm. All constructs made in this study were verified by DNA sequencing (Source BioScience Lifesciences).

2.1.2. Cloning of hu4D5 constructs

Humanized 4D5 Fab, hu4D5, which binds the extracellular domain of HER2 (Cho et al., 2003) was generated with an additional Lys-Ser-Cys at the C-terminus of the light chain and a His_6 tag at the C-terminus of the heavy chain. Acceptor peptide tags (GLNDIFEAQKIEWHE) (Beckett et al., 1999) were inserted at the C-termini of both the chains. The assembled protein sequence was used to generate the gene sequence using DNAworks gene synthesis (Hoover and Lubkowski, 2002), which involves the use of multiple primers to stitch together the required gene by PCR. The PCR products were digested with KpnI and DraIII (for V_H) and KpnI and PmeI (for V_L).

The heavy chain was inserted into pOPINVH and the light chain into pOPINVL (kind gifts of Ray Owens, University of Oxford) (Nettleship et al., 2008) for expression in the mammalian system. Primers 5'-GATCGGTACCGGAGAGGTGCAGCTGGTAGAGTCCGGAGGCGGCCTCGTGC-3' and 5'-GATCCACTTAGTGTTATTAATGATGATGGTGGTGATGCTCATGC-3' were used for the heavy chain insertion and 5'-GATCGGTACCGGA GACATCCAGATGACCCAGAGTCCCTCTT-3' and 5'-GATCGTTTAAACTTATTACTCGTGCCATTCGATCTTCTGCG-3' for light chain insertion. Starting from the N-terminus, the heavy chain construct contained a signal sequence (cleavable in the endoplasmic reticulum), V_H domain, C_{H1} domain, $(Gly\text{-}Ser\text{-}Gly)_3$ linker, AP tag and a His_6 tag. The light chain consisted of the signal sequence, V_L domain, Cκ domain (with the extra Lys-Ser-Cys), $(Gly\text{-}Ser\text{-}Gly)_3$ linker and an AP tag. Both these chains were used to produce the wildtype hu4D5 Fab with the two biotinylated AP tags, termed Fab0.35.

To generate point mutants of hu4D5 with AP tags, overlap extension PCR was carried out using primers 5'-CCGATGGGGCGGATGGGGCTTCTATGCCATG-3' and 5'-CATGGCATAGAAGCCCCATCCGCCCCATCGG-3' for D102W to make Fab0.11, 5'-GGAGACGGCTTCTTTGCCATGGACTACTGGG-3' and 5'-CCCAGTAGTCCATGGCAAAGAAGCCGTCTCC-3' for Y105F to make Fab1.4, 5'-CTGCCAACAGCACGCCACCACCCCCCCTAC-3' and 5'-GTAGGGGGGGTGGTGGCGTGCTGTTGGCAG-3' for Y92A to make Fab2.7; and 5'-CTACTGCCAACAGGCCTACACCACCCCCCC-3' and 5'-GGGGGGGTGGTGTAGGCCTGTTGGCAGTAG-3' for H91A to make Fab55 (Kelley and Connell, 1993; Gerstner et al., 2002). The same forward and reverse primers were used for the mutants as for the wildtype. D102W and Y105F mutations were in the heavy chain and Y92A and H91A were in the light chain. Digestion and insertion of the mutants into pOPINVH and pOPINVL plasmids was also similar to the wildtype.

All hu4D5 Fab constructs were bis-biotinylated unless otherwise indicated. The non-biotinylated Fabs had the same protein sequence as the bis-biotinylated, but had not been incubated with BirA. Mono-biotinylated Fabs had the AP tag on either the heavy or the light chain. Primer 5'-

GATCGCGGCCGCCTATTAGCACTCGCCCCTGTTGAAGCTC-3' was used as the reverse primer to generate the light chain without the AP tag, and produce mono-biotinylated Fab0.35 used in quantitative flow cytometry. To generate the heavy chain without the AP tag, primer 5'-GATCCACTTAGTGCTATTAGTGGTGGTGATGATGGTGGCAAGACTTGGGC TCTACCTTC-3' was used as the reverse primer. Mono-biotinylated Fab0.11, used in quantitative flow cytometry and immunomagnetic cell isolation, was made by transfecting heavy chain D102W mutant containing the AP tag and wildtype light chain without the AP tag.

2.1.3. Cloning of mouse 4D5 constructs

GATCGGTACCGGACAGGTGCAACTGCAGCAGTCTGGCCCCGAACTGG-3' and 5'-CTTAGGCGCCAGAGCTCACGGTCACACTGGCTCCCTGTCCC-3' were used for heavy chain insertion. Primers 5'-GATCGGTACCGGAGACATCGTGATGACCCAGAGCCATAAGTTCATGAGC-3' and 5'-CGATGAGCTCCCTTGATCTCCACTTTGGTCCCACCCCCAAATGTTGGAGGG -3' were used for light chain insertion. The PCR products were inserted into pOPINVH and pOPINVL via restriction sites *KpnI* and *SfoI* (for V_H) and *KpnI* and *SacI* (for V_L) for expression in the mammalian system. As the pOPIN plasmids already contain the C_{H1} and Cκ mouse domains, only the variable domains of the mouse 4D5 were synthesized using DNAworks.

AP tags were inserted at the N-termini of the heavy and light chains of 4D5 with a two-step PCR reaction using primers 5'-GATCGGTACCGGAGGCCTGAACGACATCTTCGAGGCCCAGAAGATCGAGT GGCACGAGGGCAGCGGC-3', 5-CGAGTGGCACGAGGGCAGCGGCGGCAGCGGCGGCAGCGGCCAGGTGCAA CTGCAGCAGTCTGG-3' and reverse primer 5'-CTTAGGCGCCAGAGCTCACGGTCACACTGGCTCCCTGTCCC-3' for the heavy chain; and 5'-GATCGGTACCGGAGGCCTGAACGACATCTTCGAGGCCCAGAAGATCGAGT GGCACGAGGGCAGCGGC-3', 5'-CGAGTGGCACGAGGGCAGCGGCGGCAGCGGCGGCAGCGGCGACATCGTG

ATGACCCAGAGCC-3' and reverse primer 5'-CGAT GAGCTCCCTTGATCTCCACTTTGGTCCCACCCCCAAATGTTGGAGGG-3' for the light chain. PCR products were digested and inserted into pOPIN vectors as for 4D5 Fab. The 4D5 Fab with the AP tags at the N-termini of the light "L" and heavy "H" chains was termed 4D5-APLH. Starting from the N-terminus, the heavy chain construct of 4D5-APLH contained a signal sequence (cleavable in the endoplasmic reticulum), AP tag, $(Gly\text{-}Ser\text{-}Gly)_3$ linker, V_H domain, C_{H1} domain and a His_6 tag. The light chain consisted of the signal sequence, AP tag, $(Gly\text{-}Ser\text{-}Gly)_3$ linker, V_L domain and Cκ domain. Both these chains were used to produce the wildtype mouse 4D5 Fab with the two biotinylated AP tags, termed 4D5-APLH (AP tags at the N-termini).

To generate the control with AP tags at the C-termini of the 4D5 chains, a 2-step PCR reaction was done on 4D5 Fab. Forward primer 5'-GATCGGTACCGGACAGGTGCAACTGCAGCAGTCTGGCCCCGAACTGG-3' and reverse primers 5'-GATCCACTTAGTGATGGTGATGGTGATGCTCGTGCCACTCGATCTTCTGGG CCTCGAAGATGTCGTTCAG-3' and 5'-GCCTCGAAGATGTCGTTCAGGCCGCCGCTGCCGCCGCTGCCGCCGCTGCC TTTACCACAATCCCTGGGC-3' were used for the heavy chain. For AP insertion in the light chain C-terminus, forward primer 5'-GATCGGTACCGGAGACATCGTGATGACCCAGAGCCATAAGTTCATGAGC-3 and reverse primers 5'-GATCGTTTAAACTGGTCTTTACTCGTGCCACTCGATCTTCTGGGCCTCGAA GATGTCGTTCAGGCCGC-3' and 5'-GAAGATGTCGTTCAGGCCGCCGCTGCCGCCGCTGCCGCCGCTGCCACACT CATTCCTGTTGAAGC-3' were used. PCR products were digested with KpnI and DraIII for heavy chain insertion into pOPINVH and with KpnI and PmeI for light chain insertion into pOPINVL. Going from the N-terminus, the heavy chain contained a signal sequence, V_H domain, mouse C_{H1} domain, $(Gly\text{-}Ser\text{-}Gly)_3$ linker, AP tag and a His_6 tag. The light chain consisted of the signal sequence, V_L domain, mouse Cκ domain, $(Gly\text{-}Ser\text{-}Gly)_3$ linker and AP tag. Both these chains were used to produce the wildtype mouse 4D5 Fab with the two biotinylated AP tags, termed 4D5-LHAP (AP tags at the C-termini).

2.1.4. Cloning of 9E10-APLH constructs

9E10 Fab, which binds to the myc peptide (EQKLISEEDLN) derived from the c-myc proto-oncogene product was present in the pASK88-9E10a vector (a kind gift from Prof. Arne Skerra, Munich) (Evan et al., 1985). Both the heavy chain and the light chain were present on the same plasmid in the following sequence, starting from the N-terminal; signal peptide OmpA, heavy chain variable region, human C_{H1} domain, His_6 tag, stop codon, ribosome binding sequence, signal peptide PhoA, light chain variable region, human Cκ domain, stop codon.

To insert AP tags at the N-termini of the heavy and light chains, a stepwise PCR protocol was followed and primers were designed based on Site-directed Ligase-Independent Mutagenesis (SLIM) technology (Chiu et al., 2004). First the AP tag was inserted in the heavy chain using primers 5'-CGCAGAAAATTGAATGGCATGAAGGCAGCGGCGGAAGTGGAGAAGTAG ATCTGGTTGAG-3' and 5'-GCCATTCAATTTTCTGCGCTTCAAAAATATCGTTCAGGCCCTCGGCCTGC GCTACGGTAGCG-3'. Once the insertion was confirmed, AP tag was inserted into the light chain using primers 5'-GCACAAAAGATCGAGTGGCACGAGGGTTCAGGAGGCTCCGGCGACATC GTACTCACACAG-3' and 5'-CCACTCGATCTTTTGTGCCTCGAAGATGTCATTAAGACCATCGGCTTTTGT CACAGGGG-3'. This construct with AP tags at the N-termini of the heavy and light 9E10 chains was termed 9E10-APLH.

To delete the leader sequences in 9E10-APLH (to be expressed in *E. coli* cytoplasm), the QuikChange protocol was followed using primer 5'-GATAACGAGGGCAAAAAATGGCCGAGGGCCTGAACG-3' and its reverse complement 5'-CGTTCAGGCCCTCGGCCATTTTTTGCCCTCGTTATC-3' to first delete the heavy chain leader; and 5'-GGAGAAAATAAAATGGCCGATGGTCTTAATGAC-3' with its reverse complement 5'-GTCATTAAGACCATCGGCCATTTTATTTTCTCC-3' to subsequently delete the light chain leader peptide in the same plasmid.

To insert 9E10-APLH into pOPIN plasmids for mammalian expression, the variable domains of the heavy and light chains containing the AP tags and $(Gly\text{-}Ser\text{-}Gly)_2$ linker were amplified from the bacterial plasmid using primers 5'-GATCGGTACCGGAGGCCTGAACGATATTTTTGAAGCG-3'and 5'-TGAGGAGACGGTGACCG-3' for the heavy chain, and primers 5'-GATCGGTACCGGAGGTCTTAATGACATCTTC-3' and 5'-CGATGAGCTCCTTTGATCTCGAGCTTGGTGC-3' for the light chain. The heavy chain was inserted using the *KpnI* and *SfoI* restriction sites into pOPINVH, and the light chain was inserted using *KpnI* and *SacI* into pOPINVL. The murine constant domains present in the pOPIN plasmids were different from the human constant domains present in the bacterial pASK88 plasmid.

To change the $(Gly\text{-}Ser\text{-}Gly)_2$ linker, connecting the AP tags and the 9E10 variable domains, to a longer linker $(Gly\text{-}Ser\text{-}Gly)_3$, a two-step PCR was used to amplify the Fab chains. Forward primers 5'-GATCGGTACCGGAGGCCTGAACGATATTTTTGAAGCGCAGAAAATTGAATGGCATGAAGGCAGCGGC-3' and 5'-GAATGGCATGAAGGCAGCGGCGGAAGTGGAGGTTCAGGGGAAGTAGATCTGGTTGAGTC-3' were used for the heavy chain, and 5'-GATCGGTACCGGAGGTCTTAATGACATCTTCGAGGCACAAAA GATCGAGTGGCACGAGGGTTC-3' and 5'-GATCGAGTGGCACGAGGGTTCAGGAGGCTCCGGCGGTTCAGGGGACATCGTACTCACACAGTC-3' were used for the light chain. The same reverse primers were used as for 9E10-APLH with $(Gly\text{-}Ser\text{-}Gly)_2$ linker. The PCR products were inserted into the pOPIN plasmids using restriction sites *KpnI* and *SfoI* (heavy chain) and *KpnI* and *SacI* (light chain).

To change the $(Gly\text{-}Ser\text{-}Gly)_2$ linker to a helical linker $Ala\text{-}(Glu\text{-}Ala\text{-}Ala\text{-}Ala\text{-}Lys)_2\text{-}Ala$ (Arai et al., 2001), the 9E10 variable chains were amplified using a two-step PCR reaction with forward primers 5'-GATCGGTACCGGAGGCCTGAACGATATTTTTGAAGCGCAGAAAATTGAA TGGCATGAAGCCGAGGC-3' and 5'-GAATGGCATGAAGCCGAGGCTGCAGCGAAAGAAGCTGCAGCGAAGGCT GAAGTAGATCTGGTTGAGTC-3' for the heavy chain; and 5'-GATCGGTACCGGAGGTCTTAATGACATCTTCGAGGCACAAAAGATCGAGT

GGCACGAGGCCGAGGCTGCAGC-3' and 5'-GGCACGAGGCCGAGGCTGCAGCGAAAGAAGCTGCAGCGAAGGCTGACATCGTACTCACACAGTC-3' for the light chain. The same reverse primers and restriction sites were used as for 9E10-APLH to insert into pOPIN plasmids.

To insert the BirA substrate peptide, BSP, (LHHILDAQKMVWNHR) (Jia et al., 2007) via a $(Gly\text{-}Ser\text{-}Gly)_3$ linker into the N-termini of the 9E10 Fab chains, a two-step PCR amplification process was employed. Forward primers 5'-GATCGGTACCGGACTGCACCACATCCTGGACGCCCAGAAGATGGTGTGGAACCACAGGGGCAGC-3' and 5'-GGTGTGGAACCACAGGGGCAGCGGCGGCAGCGGCGGCAGCGGCGAAGTAGATCTGGTTGAGTC-3' were used for the heavy chain; and 5'-GATCGGTACCGGACTGCACCACATCCTGGACGCCCAGAAGATGGTGTGGAACCACAGG GGCAGC-3' (same as heavy chain) and 5'-GGTGTGGAACCACAGGGGCAGCGGCGGCAGCGGCGGCAGCGGCGACATCGTACTCACACAGTC-3' were used for the light chain. The reverse primer and restriction sites for the heavy chain were the same as for 9E10-APLH, for insertion into pOPINVH. For the light chain, reverse primer 5'-TTTGATCTCGAGCTTGGTGCCAGC-3' was used. This light chain construct did not have the extra Gly-Ala between the light chain variable and constant domains (present in all other 9E10-APLH constructs in pOPIN). This was achieved by digesting pOPINVL with *SacI*, cleaving off the *SacI* overhang with DNA polymerase II, gel purifying the plasmid and then digesting with *KpnI*. The light chain PCR product was digested with *KpnI* and inserted into the digested pOPINVL.

2.1.5. Cloning of myc constructs

Three versions of the myc peptide were used in this study; myc1 (EQKLISEEDLN) is the original 11 amino acids long peptide tag, which binds 9E10 with high affinity; myc2 (KLISEEDLN) is 9 amino acids long and binds 9E10 with reduced affinity; and mycK is a point mutant of myc1 (EQKLISKEDLN) and does not bind 9E10 (Hilpert et al., 2001; Krauß et al., 2008).

To generate MBP-myc1, MBP was amplified from a previously constructed MBP-ZSPA (Holm et al., 2009) and myc1 was inserted at its C-terminus using primers 5'-CAAGCATATGAAAATCGAAGAAG-3' and 5'-

CAAGCTCGAGTTAGTTCAGATCTTCTTCGCTAATCAGTTTCTGTTCGCCG CTTTCGCCCGAACCCGAGCTCGAATT-3'. After digestion with NdeI and XhoI, the construct was cloned into pET21 using standard cloning techniques. For MBP-myc1-CFP, MBP-myc1 was first amplified using primers 5'-CAAGCATATGAAAATCGAAGAAG-3' 5'-GTTCAGATCTTCTTCGCTAATCAGTTTCTGTTCGCCGCTTTCGCCCGAAC CCGAGCTCGAATT-3'. CFP was amplified from AP-CFP-TM (Chen et al., 2005) using primers 5'-GCGAAGAAGATCTGAACGGTAGTGGCGAGTCGGGGATGGTGAGCAAGG GCGAG-3' and 5'-CAAGCTCGAGTTACTTGTACAGCTCGTCCAT-3'. Overlap extension PCR was used to link MBP-myc1 and CFP, and the resulting MBP-myc1-CFP construct was digested with NdeI and XhoI and cloned into pET21.

MBP-myc2 and MBP-myc2-CFP were derived from MBP-myc1 and MBP-myc1-CFP respectively, by site-directed mutagenesis, using primers 5'-GGGCGAAAGCGGCAAACTGATTAGCG-3' and 5'-CGCTAATCAGTTTGCCGCTTTCGCCC-3'. MBP-mycK and MBP-mycK-CFP were derived in a similar fashion using primers 5'-CGGCGAACAGAAACTGATTAGCAAAGAAGATCTGAAC-3' and 5'-GTTCAGATCTTCTTTGCTAATCAGTTTCTGTTCGCCG-3'.

For mammalian expression of myc1 in HeLa cells, the CFP-myc-TM used is the same as the CB-CFP-TM construct previously described (Zakeri and Howarth, 2010). The myc tag is present on a spacer between Cyan Fluorescent Protein (CFP) and transmembrane helix (TM), which targets the construct to the mammalian cell surface.

2.2 Protein expression, purification and biotinylation: Mammalian and bacterial

2.2.1 Protein expression in HEK-293T cells

Human fibroblast cell-line HEK-293T, expressing T-antigen (SV40 transformed), was a kind gift from Dr. Chris Scanlan, University of Oxford. All Fab expression was carried out in HEK-293T cells.

For Fab expression, cells were grown in three T-175 flasks (Corning) at 37°C with 5% CO_2 in a cell culture incubator until the cells reached a confluency of 95%. The cell media (D10) contained DMEM (Sigma) with 10% foetal calf serum (PAA labs), 50 U/mL penicillin and 50 μg/mL streptomycin (Sigma). Cells were then transferred into a roller bottle (Greiner) with 250 mL D10 and grown for three days or until they reached ~80% confluency. For transfection, 1.15 mg polyethyleneimine (branched, 25 kDa, Sigma) and 320 μg endotoxin-free DNA (160 μg each Fab chain plasmid) was incubated with 50 mL DMEM, 50 U/mL penicillin and 50 μg/mL streptomycin (D0) for 30 min at 25°C (Aricescu et al., 2006). The cell media in the roller bottles was then replaced with the transfection mixture, 200 mL additional D0, 25 mM 4-(2-hydroxyethyl)piperazine-1-ethanesulfonic acid (HEPES) (Sigma), 3.8 mM valproic acid (Sigma) and 4 mM glutamine (Life Technologies) (Backliwal et al., 2008). The Fab fragments were secreted from the cells. Four days after transfection, the cell supernatant was harvested and used to purify Fab (section *2.2.3.1*).

As the heavy and light chains were on separate vectors, the combination of heavy and light chain was adjusted according to the required Fab. To produce bis-biotinylated Fabs, both chains containing AP tags were co-transfected. To produce mono-biotinylated Fabs, one chain containing the AP tag and the other without the AP tag were co-transfected.

2.2.2 Protein expression in *E. coli*

2.2.2.1 Periplasmic expression of 9E10-APLH in C43 cells

9E10-APLH was expressed in the periplasm of *E. coli* C43 (DE3), a kind gift of Prof. Anthony Watts, University of Oxford. C43 cells, derived from the BL21 cell strain, have the F-ATPase subunit genes and are effective in expressing toxic proteins (Miroux and Walker, 1996; Attrill et al., 2009). Heat-competent C43 cells were transformed with the 9E10-APLH plasmid and plated on LB plates containing 1.5% agar and 100 μg/mL ampicillin (LB-amp). The plates were incubated overnight at 30°C, and individual colonies were picked and inoculated into 10 mL LB containing 1% glucose and 100 μg/mL ampicillin. Cells were grown at 25°C for 16 hr in a shaking incubator, then diluted 100-fold and grown further at 25°C for ~5 hr or until they reached A_{600}= 0.5. The cultures were induced with 100 μg/mL (0.4 mM)

Isopropyl-β-D-Thiogalactopyranoside (IPTG) (Melford labs) and 200 μg/mL anhydrotetracycline (Fisher Scientific) and further incubated at 22°C for ~20 hr in a shaking incubator, after which the cells were harvested by centrifugation at 7,000 rpm (7,500 g) for 15 min. Cell pellets were stored at -80°C until required for purification.

2.2.2.2 Cytoplasmic expression of 9E10-APLH in Rosetta Gami cells

Plasmid pASK88 containing 9E10-APLH without leader sequences was transformed into heat-competent *Rosetta Gami 2* (DE3) cells (Novagen). The *Rosetta Gami* cell strain has an oxidizing environment that favours disulfide bond formation in the bacterial cytoplasm (Bessette et al., 1999). Transformed cells were plated onto LB-Amp plates, which were incubated overnight at 30°C. Individual grown colonies were picked and inoculated into 12 mL LB containing 0.8% glucose and 100 μg/mL ampicillin. These starter cultures were grown overnight at 30°C and then diluted 1:100 into large-scale cultures containing 800 mL LB with 0.8% glucose and 100 μg/mL ampicillin. The cultures were grown at 30°C until they reached A_{600} = 0.6, and were then induced with 100 μg/mL IPTG and 200 μg/mL anhydrotetracycline. Cells were further incubated overnight at 25°C in a shaking incubator, after which cells were harvested by centrifugation and cell pellets were stored as described above.

2.2.2.3 Cytoplasmic expression of myc constructs in RIPL cells

The cloned myc constructs in pET21 plasmids were transformed into heat competent *E. coli* BL21 CodonPlus RIPL (DE3) cells (Stratagene), which have extra copies of specific tRNAs to aid in efficient protein translation. Transformed cells were plated onto LB-Amp plates and incubated overnight at 37°C. Individual colonies were picked and inoculated into 8 mL LB containing 0.8% glucose and 100 μg/mL ampicillin. These starter cultures were incubated overnight at 37°C in a shaking incubator and then diluted 1:100 into 800 mL LB containing 0.8% glucose and 100 μg/mL ampicillin. The large scale cultures were grown at 37°C for ~3 hr or until their optical density reached A_{600} = 0.5. The cultures were then cooled to 25°C for 2 min, and induced with 100 μg/mL IPTG. Cells were further incubated at 30°C for 4 hr, after which they were harvested and stored as described in section *2.2.2.1*.

2.2.3 Protein Purification

All protein purifications were carried out at 4°C, unless stated otherwise, to minimise degradation of the protein. In general, all proteins were dialyzed thrice against 1× Phosphate Buffered Saline (PBS; 137 mM NaCl, 2.7 mM KCl, 8.1 mM $Na_2HPO_4.2H_2O$, 1.8 mM KH_2PO_4 pH 7.4) for ~3 hr each time at 4°C, after every purification. Dialyzed protein was collected in a 1.5 mL microcentrifuge tube and centrifuged at 13,000 rpm (table top centrifuge, Thermo) for 10 min to remove aggregates. The supernatant containing purified protein was collected in a fresh tube and stored at -80°C. All protein concentrations were calculated using A_{280} measurements (NanoDrop) and extinction coefficients (as predicted by ExPASy ProtParam). Protein purity was checked by Sodium Dodecyl Sulfate- Polyacrylamide Gel Electrophoresis (SDS-PAGE) and AP-tagged Fabs were further processed for biotinylation.

2.2.3.1 Ni-NTA purification from mammalian cells

Four days after Fab transfection into HEK-293T cells, the cell supernatant was harvested by centrifuging the media at 2,000 rpm for 15 min on a Beckman Coulter centrifuge (J2-HS), and filtering the supernatant through a paper towel (Cherwell Packaging) to remove cell debris. 25 mL 10× PBS and 100 μM $MgCl_2$ final concentration were added to 225 mL filtered supernatant to equilibrate the supernatant and the His_6-tagged Fab was purified using Nickel affinity chromatography.

For purification, the processed cell supernatant was aliquoted into six 50 mL centrifuge tubes. 0.6 mL packed Ni-NTA superflow resin (Qiagen) was equilibrated with 1× PBS and 100 μL was added to the cell media in each 50 mL centrifuge tube, and incubated overnight with end-over-end rotation on an electric rotator (Stuart Equipment) at 4°C. Thereafter, the samples were always kept on ice or at 4°C. The samples were centrifuged at 1,500 rpm for 5 min (ALC multispeed refrigerated centrifuge) to collect the resin pellets, which were then pooled together and washed once with 15 mL binding buffer (50 mM Tris base, 300 mM NaCl, pH 7.8), once with 10 mL wash buffer (binding buffer with 10 mM Imidazole, pH 7.8), resuspended in 1 mL binding buffer and then transferred to a 15 mL Poly-prep chromatography column (Bio-Rad). The resin was washed further with 1 mL binding buffer containing 30 mM

imidazole, pH 7.8, and after the buffer had drained, His_6 tagged Fab fragments were eluted using 2 mL binding buffer containing 100 mM imidazole, pH 7.8. The elution was collected in four fractions, 0.5 mL each, which were analysed for protein concentration by measuring A_{280} on a spectrophotometer (NanoDrop). Fractions containing the highest protein concentration were pooled together and dialyzed 3× into PBS for up to 24 hr at 4°C.

2.2.3.2 Periplasmic purification of 9E10-APLH from C43 cells

Periplasmic purification of 9E10-APLH from C43 cells was carried out by resuspending the frozen bacterial pellet in 8 mL periplasmic buffer containing 100 mM Tris-HCl, 0.5 M sucrose, 1 mM Ethylenediaminetetraacetic acid (EDTA), pH 8.0 and adding 1 mM Phenylmethylsulfonyl Fluoride (PMSF) and 1× protease mixed inhibitor cocktail (Roche). After incubation on ice for 1 hr, the resuspension was centrifuged at 18,000 rpm for 20 min. 40 µL of 1 M $MgCl_2$ was added to saturate EDTA in the supernatant, before nickel affinity chromatography. Typically, 0.5 mL packed Ni-NTA resin was added to the 8 mL supernatant and incubated on a rotor at 4°C for 40 min. The resin was then centrifuged at 1,300 rpm for 2 min, washed twice with 5 mL binding buffer containing 10 mM imidazole, resuspended in 1 mL binding buffer and transferred to a 15 mL poly-prep column. After the buffer had drained, the resin was washed further with 0.5 mL binding buffer containing 30 mM imidazole, and finally eluted with 2 mL binding buffer containing 100 mM imidazole. 0.5 mL fractions were collected and assessed for protein content by measuring A_{280}. The highest protein-containing fractions were dialyzed 3× into PBS for up to 24 hr at 4°C.

2.2.3.3 Cytoplasmic purification of 9E10-APLH from Rosetta Gami cells

9E10-APLH Fab without leader sequences, expressed cytoplasmically in *Rosetta Gami* cells was purified using Protein G affinity chromatography. The frozen cell pellet was thawed on ice and resuspended in 8 mL Binding buffer (50 mM Tris base, 300 mM NaCl, pH 7.8), 1 mM PMSF and 1× protease mixed inhibitor cocktail. The resuspended bacteria were then sonicated 4 times, 1 min each at 40% pulse, on ice in an Ultrasonic Processor (Sonics Vibra-Cell sonicator). Cell lysate was centrifuged at 13,000 rpm for 10 min in a microcentrifuge at 4°C, and the supernatant was added to 0.2 mL Protein G agarose beads (Sigma), which had previously been washed once

with 10 mL MilliQ and equilibrated with 5mL binding buffer. The mixture was incubated at 4°C for 1 hr on a rotator (Stuart) and then centrifuged at 1,500 rpm for 2 min to collect the resin. The beads were washed twice with 5 mL binding buffer (each wash for 2 min), resuspended in 1 mL binding buffer and then transferred to a Poly-prep column. After the buffer had drained, bound protein was eluted using 0.8 mL Glycine-HCl buffer (100 mM Glycine-HCl, pH 2.7) as 0.2 mL elution fractions, which were collected in 1.5 mL centrifuge tubes containing 9 µL 1 M Tris-base, pH 8.5 (to neutralize the fractions). Elutions were checked for protein content by measuring A_{280} on a spectrophotometer. Fractions were collected from each stage of the purification process and run on SDS-PAGE to analyse the efficiency of the process.

2.2.3.4 Cytoplasmic purification of myc constructs from RIPL cells

MBP-myc and MBP-myc-CFP constructs were expressed in the cytoplasm of RIPL cells and purified on an amylose-agarose column. Frozen cell pellets were thawed on ice and resuspended in 4 mL column buffer (50 mM Tris HCl, 300 mM NaCl, 1 mM EDTA, pH 7.8), 1 mM PMSF and 1× protease mixed inhibitor cocktail. The samples were sonicated 6 times, 30 s each at 40% pulse, on ice. Cell lysate was centrifuged at 13,000 rpm for 10 min in a microcentrifuge at 4°C, and the supernatant was added to 0.4 mL packed amylose resin (New England Biolabs), which had previously been washed and equilibrated with 2 mL column buffer. The mixture was incubated on a rotator for 30 min at 4°C and then centrifuged at 2,000 rpm for 2 min. After discarding the supernatant, the resin was washed twice with 10 mL column buffer, resuspended in 1 mL column buffer and then transferred to a Poly-prep column. Protein was eluted using 2 mL elution buffer (column buffer with 10 mM maltose) and collected as 1 mL fractions. After checking for protein content by A_{280}, the purified protein was dialyzed 3× into PBS for up to 24 hr at 4°C. Dialyzed protein was centrifuged and stored in 100 µL aliquots at -80°C. SDS-PAGE was performed to check the purity and uniformity of the myc constructs.

2.2.4 *In vitro* biotinylation of Fab constructs

2.2.4.1 Synthesis of BirA

Biotin ligase BirA with a His_6 tag was expressed in *E. coli* RIPL (DE3) cells and purified on Ni-NTA column as described previously (Howarth and Ting, 2008). The plasmid for glutathione-S-transferase linked to BirA (BirA-GST) was a kind gift from Christopher O' Callaghan (University of Oxford) and was expressed in *E. coli* and purified using glutathione agarose (Sigma) (O'Callaghan et al., 1999). Briefly, the BirA-GST construct in pGEX-2T plasmid was transformed into heat competent *E. coli* BL21 RIPL (DE3) cells (Stratagene), plated onto LB-Amp plates and incubated overnight at 37°C. Individual colonies were picked and expressed in large scale cultures as described for myc proteins in Section *2.2.2.3* and cell pellets were stored at -80°C.

For purification, cell pellet was resuspended in 5 mL bacterial lysis buffer (25 mM Hepes, 0.15 M NaCl, 1.5 mM $MgCl_2$, 0.2 mM EDTA, 0.05% Triton X-100, pH 7.7) that also contained 1 mM PMSF, 1× protease mixed inhibitor cocktail (Roche), 10.5 mg solid NaF (Sigma) and 5 µL 1 M Dithiothreitol (DTT) (Fisher Scientific). Cells were then sonicated 6 times, 30 s each at 40% pulse, on ice in an Ultrasonic Processor (Sonics Vibra-Cell sonicator). Cell lysate was centrifuged at 13,000 rpm for 10 min in a microcentrifuge at 4°C, and the supernatant was added to 0.6 mL glutathione superflow resin (Qiagen) that had previously been washed 4× with 1 mL PBST (PBS with 0.05% Triton X-100). The mixture was incubated on a rotator for 30 min at 4°C and then centrifuged at 2,000 rpm for 2 min. After discarding the supernatant, the resin was washed thrice with 1 mL binding buffer (20 mM Hepes, 50 mM NaCl, 2.5 mM $MgCl_2$, 0.1 mM EDTA, 0.05% Triton X-100, pH 7.7), resuspended in 1 mL binding buffer and transferred to a Poly-prep column. BirA-GST was eluted using 2 mL elution buffer (50 mM Tris, 6.14 mg/mL reduced glutathione, pH 7.7) and collected as 0.5 mL fractions. Protein content was checked by measuring A_{280} and was ensured to be ≤60 µM as BirA-GST has a tendency to aggregate at higher concentrations. The purified protein was dialyzed into PBS, centrifuged to discard aggregates, and 10 µL aliquots of the supernatant containing purified BirA-GST were stored at -80°C.

2.2.4.2 Enzymatic biotinylation of AP-tagged constructs

Purified Fab fragments containing the AP tags were biotinylated *in vitro* by incubating the Fab (0.1 – 0.4 mg/mL) in PBS with 5 mM $MgCl_2$, 1 mM ATP, 50 μM biotin and 1-2 μM BirA or BirA-GST for 2 hr at 25°C.

BirA was removed by purifying the Fab using 100 μL Protein G agarose beads and eluting thrice with 150 μL Glycine-HCl buffer pH 2.6, before neutralizing with 6.75 μL 1 M Tris-base pH 8.5 (Protein G purification described in section *2.2.3.3*).

BirA-GST was removed by incubating the biotinylation mixture with 150 μL packed glutathione superflow resin (Qiagen), previously equilibrated with 1× PBS, in a 1.5 mL microcentrifuge tube for 45 min on a rotator. After centrifuging for 10 s on a mini-centrifuge (Bio-Rad), to separate the resin-bound BirA-GST, the supernatant containing biotinylated Fab was pipetted out and incubated again with fresh 150 μL glutathione resin for 45 min, to completely eliminate traces of BirA-GST. After spinning the mixture, the supernatant was collected and dialyzed 3× into PBS for up to 24 hr at 4°C to remove excess biotin. The concentration of the dialyzed purified Fab was determined using A_{280} measurements and the extinction coefficient predicted by ExPASy ProtParam. All constructs were checked for biotinylation using a SDS-PAGE gel-shift assay (section 2.3) and aliquots were stored for long-term use at -80°C.

2.2.4.3 Chemical biotinylation of Fab0.35

Non-biotinylated Fab0.35 (without AP tags) was chemically biotinylated by mixing 400 μL of 21.4 μM Fab with 40 μL 1 M $NaHCO_3$ pH 8.3 and adding the mixture quickly to a microcentrifuge tube containing 4 μL biotinamidohexanoic acid N-hydroxysuccinimide ester (10 mg/mL in DMSO, Sigma). The reaction was incubated at 25°C for 4 hr to allow for the biotinylation of reactive surface amines on the Fab. The biotinylated Fab was then separated from excess small molecule forms of biotin by gel filtration with Sephadex G-25 beads (Sigma) (section *2.2.5.2*) and dialyzing three times into PBS. The purified protein was checked for biotinylation on SDS-PAGE (section 2.3), aliquoted and stored at -80°C.

2.2.5 Streptavidin constructs

2.2.5.1 Synthesis of streptavidin constructs

Core tetravalent streptavidin (wild-type), divalent streptavidin (dSA) and monovalent streptavidin (mSA), were kindly produced by Dr. Michael Fairhead (Howarth laboratory), who expressed them in *E. coli* as inclusion bodies and after refolding *in vitro*, purified on a Ni-NTA column, as described previously (Howarth et al., 2006; Howarth and Ting, 2008). All streptavidin concentrations mentioned in this work refer to the concentration of the tetramer.

2.2.5.2 Dye labelling of SA constructs

To conjugate core tetravalent streptavidin to AlexaFluor488, 200 µL of 14 µM core streptavidin was mixed with 20 µL 1 M $NaHCO_3$ pH 8.3 and the mixture was quickly added to a microcentrifuge tube containing 7.5 µL AlexaFluor488 succinimidyl ester (10 mg/mL in DMSO, Life Technologies). After incubation in the dark for 4 hr at 25°C, excess dye was removed by purifying the protein using Sephadex G-25 beads (Sigma). 1 g Sephadex G-25 beads were left to swell in 10 mL PBS for 4 hr at °C, washed once with 1 mL PBS and transferred to a Poly-prep column. The protein-dye mixture was added to the column and the flowthrough was discarded. The SA-488 conjugate was eluted using 1 mL PBS and 0.2 mL fractions were collected in microcentrifuge tubes. Fractions with the highest A_{280} absorbance were pooled together, dialyzed 3× into PBS for up to 24 hr at 4°C and stored at -80ºC.

To prepare mSA-488, 300 µL of 35 µM mSA was mixed with 30 µL 1 M $NaHCO_3$ pH 8.3 and added to 6 µL AlexaFluor488 succinimidyl ester (10 mg/mL in DMSO, Life Technologies). The mixture was incubated in the dark for 4 hr at 25°C. Free dye was removed by gel filtration using Sephadex G-25 (Sigma) and dialyzing into PBS as described above.

To calculate the concentration of the conjugated protein, absorbance of SA-488 or mSA-488 was measured at A_{280} and A_{495}. The contribution of the dye to the protein absorbance was then accounted for in the following way –

$$A_{protein} = A_{280} - (A_{495} \times \text{correlation factor})$$

Where, correlation factor = $A_{280\ free\ dye}/A_{495\ free\ dye}$ and equals 0.11 for AlexaFluor488.

Using information that 0.1 mg/mL SA gives A_{280}=0.355,

the concentration of SA-488 or mSA-488 = [($A_{protein}$× 0.1)/0.355] mg/mL

The number of dye molecules conjugated per streptavidin molecule were calculated in the following way –

Degree of dye labelling = (A_{495} × molecular weight)/(protein concentration × ε_{dye}),

Where molecular weight of streptavidin was 54,000, protein concentration is in mg/mL and $\varepsilon_{AlexaFluor\ 488}$ = 71,000.

2.3 SDS-PAGE

Proteins were separated and analysed by Sodium Dodecyl Sulfate- Polyacrylamide Gel Electrophoresis (SDS-PAGE). Polyacrylamide gels, consisting of a 5% (v/v) acrylamide (Sigma) stacking layer and 12-14% (v/v) acrylamide separation layer, were prepared in disposable plastic gel cassettes (Life Technologies). SDS-PAGE was performed in a Tris-Glycine running buffer with 0.1% (w/v) SDS, using an XCell SureLock® Mini-Cell (Life Technologies) at 200 V for 1 hr.

Protein samples (1-2 μg/lane) were mixed in 6:1 ratio with 6× SDS-PAGE loading buffer (0.23 M Tris-HCl pH 6.8, 24% v/v glycerol, 120 μM bromophenol blue, 0.23 M SDS) and heated at 95°C for 3 min in a C1000™ Thermal Cycler (Bio-Rad) to break all non-covalent interactions, before loading onto a polyacrylamide gel. For the reduction of disulfide bonds, 5% (v/v) 2-mercaptoethanol (2-ME, BDH) was added to the 6× SDS-PAGE loading buffer before heating with the samples. In order to estimate the molecular weight of the protein bands, 3 μL PageRuler™ Prestained Protein Ladder (Fermentas) was also loaded onto the gel adjacent to the samples.

For gel shift assays, 1 μg Fab was boiled with SDS loading dye, cooled to 25°C for 1 min, and then 1.6 μg tetravalent streptavidin was added to the samples. The Fab-SA mixture was incubated at 25°C for 2 min to allow streptavidin to bind biotin conjugates, and then loaded onto the gel without any further heating.

After running, gels were Coomassie-stained with either Coomassie Brilliant Blue solution (1.25 g Coomassie Brilliant Blue R250 in 225 mL methanol, 225 mL MilliQ

H_2O and 50 mL glacial acetic acid) for 1 hr followed by overnight destaining (in 6:3:1 v/v mixture of MilliQ water: methanol: glacial acetic acid) or stained for 30 min with Instant blue solution (Triple Red). The resolved proteins could then be visualized and the gels were imaged using Gel DocXR+ Imaging System (Bio-Rad) and Image Lab™ 3.0 software (Bio-Rad).

2.4 ELISA

The efficiency of 9E10-APLHb to clamp myc peptide was tested using an Enzyme-Linked Immunosorbent Assay (ELISA). To check for 9E10-APLHb binding to the various myc constructs, 1 μM of the indicated myc construct in 100 μL PBS was added to wells (samples in duplicate) in a 96-well microtitre plate (Costar 9018 high capacity binding EIA/RIA polystyrene plates) and incubated overnight at 4°C.

All subsequent incubations were done on a rocker (MODEL R100 Rotatest Shaker Luckham) at 25°C. All wash steps were carried out for 2 min each. After overnight antigen coating, plates were washed 3× with 150 μL PBS containing 0.05% Tween (PBS-T), before blocking with 200 μL 1% BSA in PBS (w/v, Sigma) for 2 hr. Wells were then washed 4× with 200 μL PBS-T, before 100 μL of the indicated Fab was added at a concentration of 10 μg/mL (~0.2 μM) in PBS with 1% BSA, and incubated for 45 min. For clamping, Fab was removed from the wells, and 100 μL of 0.1 μM core streptavidin (in PBS with 1% BSA) was added to the wells for 15 min. To the control samples, 100 μL of PBS with 1% BSA was added to the wells. The wells were then washed 4× with 200 μL PBS-T, treated with 100 μL of 16.1 μg/mL goat anti-human IgG-Peroxidase antibody (Sigma) in PBS with 1% BSA, and further incubated for 1 hr. After washing the wells 4 times, 5 min each, with 200 μL PBS-T, the wells were developed in the following way: 2 mg o-phenylene diamine (OPD) was added to 5 mL phosphate-citrate buffer (103 mM dibasic sodium phosphate with 48.6 mM citric acid, pH 5.0) to a final concentration of OPD of 0.4 mg/mL. 2 μL H_2O_2 was added to the 5 mL OPD solution and immediately afterwards, 100 μL of this solution was added to each well on the ELISA plate. The plate was incubated in the dark on the rotor for ~30 min, after which the A_{450} of the wells was measured using a Spectramax M5 plate-reader (Molecular Devices Ltd).

For the myc titration experiments, the wells were coated with the indicated concentration (1000, 100, 10, 1, 0.1 or 0 nM) of the respective myc construct in triplicate for the overnight incubation at 4°C. 0.1 μM monovalent streptavidin (with only one active biotin-binding site) (Howarth et al., 2006) was used instead of tetravalent streptavidin, as a control to test clamping.

2.5 Mammalian cell culture

2.5.1 Cell-lines

MCF-7 (breast cancer cell-line), BT474 (breast cancer cell-line from invasive ductal carcinoma) and A431 (epidermoid carcinoma cell-line) were from Cancer Research UK, Lincoln's Inn Fields (CR-UK), validated using short tandem repeat profiling. MDA-MB-453 (breast cancer cell-line from metastatic carcinoma) and MDA-MB-468 (breast cancer cell-line) were from American Type Culture Collection (ATCC, Manassas, VA), validated using short tandem repeat profiling. HEK-293T (human fibroblast), a weakly adherent cell-line, was a kind gift from Chris Scanlan's laboratory. HeLa (epithelial cells from cervix adenocarcinoma) were purchased from ATCC. All cell-lines were adherent.

2.5.2 Cell culture conditions

All cell-lines were grown in D10 media containing Dulbecco's Modified Eagle Medium (DMEM, Sigma) with 10% Foetal Calf Serum (FCS, PAA labs), 50 U/mL penicillin and 50 μg/mL streptomycin (Sigma). 5 μg/mL Insulin (Sigma) was added to BT474 cells to supplement their growth (Gijsen et al., 2010). Cell-lines were grown in a monolayer in T-25, T-75 or T-175 flasks (Corning) at 37°C with 5% atmospheric CO_2 in a humidified cell culture incubator (Borolabs). For large-scale Fab production, HEK-293T cells were grown in roller bottles (Greiner) with 250 mL D10 and incubated on roller shelves (Wheaton roller apparatus) in a 37°C room.

Cells were typically passaged every 4-7 days, or whenever they reached 80-100% confluency. To split cells, the D10 media was first removed from the flask, and pre-warmed Trypsin-EDTA 0.05% (Life Technologies) was added to cells. After incubation at 37°C for 5-15 min (depending on cell-line), the flask was tapped slightly

to detach the cells, which were then pipetted into a 15 mL centrifuge tube and spun at 1,300 rpm for 2 min. The supernatant was discarded and the cell pellet was resuspended in 5 mL D10 media. Fast growing cells were split in a 1: 10 ratio; 0.5 mL of resuspended cells were plated in a new flask, fresh D10 media was added and cells were kept back in the incubator. Slow growing cells were usually split in a 1:2 ratio. All cell-lines were passaged for less than 6 months. Confluency of cells was regularly checked under an inverted phase contrast microscope (Leitz Diavert) and cell count was done using Trypan Blue solution (Sigma) on a haemocytometer (Neubauer-Improved).

Mycoplasma testing was done along with the positive control from EZ-PCR Mycoplasma Test Kit (Biological industries). 1 mL supernatant from adherent cells was collected and centrifuged at 200 *g* for 1 min at 25°C to pellet cellular debris. The supernatant was transferred to another tube and used as the template for PCR reaction. A 50 µL PCR reaction mixture was made in MilliQ H_2O containing 1× PCR buffer, 0.2 mM dNTPs, 2 µM forward primer, 2 µM reverse primer, 1 µL supernatant template (or the positive control) and 1 µL Taq polymerase (New England Biolabs). 1 µL cell culture medium was also added to the positive control to ensure that the cell media was not inhibiting the PCR reaction. The thermal cycling conditions were as follows: 5 min at 95°C, then 40 cycles of 30 s at 94°C, 30 s at 55°C and 1 min at 72°C, followed by 10 min at 72°C and a final incubation at 10°C. Primers used were MGSO (5′-TGCACCATCTGTCACTCTGTTAACCTC-3′) and GPO-3 (5′-GGGAGCAAACAGGATTAGATACCCT-3′). The PCR product was tested using agarose gel electrophoresis (section 2.1.1). A band at 270 basepairs indicated cell contamination. Cells in each case were found to be mycoplasma-negative.

2.6 Imaging experiments

2.6.1 Binding of hu4D5 Fab mutants to cell surface expressed HER2

BT474 cells were plated on 0.1 mm thick glass coverslips (VWR) in a 48 well plate (Greiner) at a concentration of 50,000 cells/well in 0.5 mL D10 and grown for 24 hr. D10 media was pipetted out and cells were washed once with 0.5 mL PBS with 5 mM $MgCl_2$ (PBS-Mg). Cells were then treated with 100 µL of 50 µg/mL of the indicated Fab in PBS-Mg containing 1% BSA (w/v) for 10 min on ice. After washing the cells

thrice with 0.4 mL PBS-Mg to remove unbound Fab, 100 μL of 27 nM core streptavidin-AlexaFluor488 in PBS-Mg with 1% BSA was added to cells for 10 min on ice. Cells were again washed thrice with 0.5 mL PBS-Mg and imaged live on a DeltaVision Core fluorescent microscope (Applied Precision).

To check for non-specific binding of the Fab, cell surface HER2 on plated BT474 cells was pre-blocked by incubating the cells with 100 μL of 10 μg/mL Herceptin (a kind gift from Genentech, dialyzed into PBS) in PBS-Mg with 1% BSA for 10 min on ice. Cells were washed thrice with 0.4 mL PBS-Mg and labelled with the indicated Fab as described above, before live cell imaging.

2.6.2 Cell-magnetic bead imaging

To visualize the various stages in immunomagnetic cell isolation by microscopy, trypsinized BT474 cells were labelled with 0.1 μg/mL biotinylated Fab0.35 and immunomagnetically isolated using streptavidin-coated magnetic beads (section *2.8.1*). Cells in the cell-bead mixture, flowthrough and recovery were then diluted 1:1 with 10 μL Trypan blue, loaded onto a haemocytometer with a 0.15 mm coverslip (VWR), and imaged using the brightfield channel on the DeltaVision Core fluorescent microscope.

To image the bead-cell synapse, BT474 cells were labelled with 0.01 μg/mL biotinylated Fab0.11 and immunomagnetically isolated using SA-beads (section *2.8.1*). To prepare the cell membrane staining solution, 2 μL Vybrant DiD cell labelling solution (1 mM, Life Technologies) was added to 300 μL D1 in a 1.5 mL microcentrifuge tube and vortexed thrice, for 15 s each. Immunomagnetically recovered cells were centrifuged in a mini-centrifuge (Bio-Rad) for 5 s, the supernatant pipetted out, and the cell pellet was resuspended in the DiD staining solution. Cells were incubated at 37°C for 30 min, after which cells were centrifuged for 5 s and washed twice with 400 μL D1. Cells were finally resuspended in 10 μL D1 and 5 μL of the resuspended cells was plated on a microscope glass slide (Fisher) and spread and covered with a 0.1 mm glass coverslip (VWR). Cells were imaged using the Cy5 and brightfield channels and a 100× oil-immersion lens on the DeltaVision Core fluorescent microscope (section *2.6.5*).

2.6.3 Binding of 9E10-APLHb Fab to surface-expressed myc

HeLa cells were plated on 0.1 mm glass coverslips (VWR) in a 48 well plate in 0.5 mL D10 and grown for 24 hr so they reached ~80% confluency. D10 media was pipetted out and 0.25 mL D0 was added per well to cells. Transfection mixture for each well was prepared by incubating 25 μL D0 with 1 μL Lipofectamine™ 2000 (Life Technologies) for 5 min at 25°C and then adding the mixture to 25 μL D0 containing 0.5 μg of CFP-myc-TM plasmid DNA. After incubating at 25°C for 20 min, 50 μL transfection mixture was added to cells which were then incubated at 37°C for 4 hr. Transfection mixture was pipetted out, fresh 0.5 mL D10 was added to each well, and cells were kept in the cell culture incubator.

One day after transfection, D10 media was pipetted out and cells were washed once with 0.5 mL PBS-Mg. Cells were then treated with 100 μL of 50 μg/mL of the indicated Fab in PBS-Mg containing 1% BSA for 20 min at 25°C. Cells were washed thrice with 0.4 mL PBS-Mg and labelled with 100 μL of 10 μg/mL AlexaFluor555 goat anti-human IgG (Life Technologies) in PBS-Mg with 1% BSA for 10 min on ice. Cells were again washed thrice with 0.5 mL PBS-Mg and imaged live.

2.6.4 Testing 4D5-APLHb clamping on cell surface expressed HER2

2.6.4.1 Acid wash experiments

BT474 cells were plated on glass coverslips in a 48 well plate and grown for 18-24 hr as above. Cells were washed once with 0.5 mL PBS-Mg and then labelled with 100 μL of 10 μg/mL of the indicated Fab in PBS-Mg containing 1% BSA for 10 min at 37°C. To prepare 4D5-APLHb prebound to SA, 100 μL of 10 μg/mL 4D5-APLHb was incubated with 0.2 μM tetravalent core streptavidin in PBS-Mg with 1% BSA for 5 min at 25°C, and then added to cells. After incubation, excess Fab was pipetted out, and 100 μL of 0.2 μM SA in PBS-Mg with 1% BSA was added to cells for 5 min at 25°C. Control samples were treated without SA, but with 100 μL PBS-Mg containing 1% BSA. Cells were then washed thrice with 0.4 mL PBS-Mg.

For acid stripping, cells were treated with acid stripping buffer (131 mM Sodium citrate, 66 mM Na_2HPO_4 pH 3.0) for 2 min at 25°C (Sugawara et al., 1987) and then quickly neutralized with 1 mL PBS-Mg. Control samples were treated with 0.2 mL PBS-Mg instead of acid stripping buffer. Cells were washed thrice with 0.5 mL PBS-

Mg on ice and bound Fab was labelled using 150 µL of 10 µg/mL AlexaFluor555 goat anti-mouse IgG (Life Technologies) in PBS-Mg with 1% BSA for 10 min on ice. Excess antibody was washed off using 0.5 mL PBS-Mg thrice, and cells were imaged live.

To check clamping with various SA constructs, BT474 cells were labelled with 4D5-APLHb as described above, and then incubated with 100 µL of 0.2 µM core tetravalent SA, 0. 2 µM divalent streptavidin or 0. 2 µM monovalent streptavidin, in PBS-Mg with 1% BSA for 5 min at 25°C. Cells were then washed, treated with acid stripping buffer and labelled with AlexaFluor555 goat anti-mouse IgG as described above.

To compare effects of 4D5-APLHb and 4D5-LHAPb, plated BT474 cells were labelled with 100 µL of 10 µg/mL of the indicated Fab, and then 0.2 µM divalent SA was added. Cells were then processed for acid wash and secondary antibody labelling as described above.

2.6.4.2 Time course experiments to test SA blocking on BT474 cells

BT474 cells, plated on glass coverslips in a 48 well plate as before, were washed once with 0.5 mL PBS-Mg and labelled with 100 µL of 15 µg/mL 4D5-APLHb in PBS-Mg containing 1% BSA for 10 min at 37°C. After pipetting out the Fab, 100 µL of 0.38 µM core streptavidin in PBS-Mg with 1% BSA was added to cells for 5 min at 25°C. Control samples were incubated without SA in 100 µL PBS-Mg containing 1% BSA. Cells were washed once with 0.5 mL PBS-Mg and then 0.5 mL D10 was added to cells. Cells were then incubated for 0, 1, 3, 6 or 21 hr in the cell culture incubator. After the indicated incubation time-period was over, the respective coverslips were transferred to another plate, and washed once with 0.5 mL PBS-Mg. Bound Fab was detected with 200 µL of 10 µg/mL AlexaFluor555 goat anti-mouse IgG as described in section *2.6.4.1* and imaged live.

2.6.5 Microscopy

Live cell imaging was carried out on a wide-field DeltaVision Core fluorescent microscope (Applied Precision), typically using a 40× oil-immersion lens, unless stated otherwise. The various channels used to capture dye labelled cells were – FITC/AlexaFluor488 (470DF40 excitation, 520DF50 emission, Chroma 84100bs

polychroic), ECFP (436DF20 excitation, 480DF40 emission, Chroma 86002v1 dichroic), AlexaFluor555 (540DF40 excitation, 600DF50 emission, Chroma 84100bs polychroic) and Cy5 (640DF20 excitation, 685DF40 emission, Chroma 84100bs polychroic). Brightfield images were collected for all samples. Images were collected and analysed using softWoRx 3.6.2 software (Applied Precision). Typical exposure time for fluorescence images was 0.4-0.8 s and for brightfield images was 0.1 – 0.5 s. All fluorescence images were background-corrected. Different samples in the same experiment were prepared, imaged and analysed under identical conditions.

2.7 Flow cytometry and receptor quantification

2.7.1 Cell labelling and flow cytometry

Flow cytometry was used to estimate the amount of Fab mutants bound to HER2 expressing cells at various Fab concentrations and on different cell-lines.

To label cells with Fab, BT474 cells were grown in D10 until they reached 80% confluency, and then trypsinized, washed once in D1, centrifuged and resupended in D1 at a concentration of 2.5×10^6 cells/mL. Triplicate samples of 125,000 cells in 50 μL D1 were incubated with each of the following concentrations: 10, 1, 0.1, 0.01, 0.001 or 0 μg/mL of the indicated mono-biotinylated Fab for 10 min at 25°C. The cells were spun at 1,700 *g* for 2 min and the supernatant was discarded to remove excess unbound Fab. Cell pellets were resuspended in 50 μL of 0.5 μM mSA-488 in FACS-A solution (PBS with 1% BSA, 0.1% NaN_3) and incubated on ice for 15 min. Cells were centrifuged, washed twice with 100 μL FACS-A and resuspended in 0.4 mL FACS-A. Cells were kept on ice throughout the process, until their analysis on the flow cytometer.

For quantification of Fab bound to different cell-types, cells were trypsinized, washed once with D1, and resuspended in D1 at a concentration of 2.5×10^6 cells/mL. Triplicate cell samples (125,000 cells in 50 μL D1) were labelled with 10 μg/mL mono-biotinylated Fab0.35 or no Fab control for 10 min at 25°C. Excess Fab was removed by centrifugation and cells were further labelled with mSA-488 as described above.

Labelled cells were analysed on a FACScalibur flow cytometer with CellQuest Pro version 5.2.1 (Becton Dickinson). The 488 signal from 20,000 cells, gated according to their size on the forward scatter (FSC) and side scatter (SSC) channels, was recorded on the FL1 channel (488 nm excitation with 530±15 nm emission), which had been adjusted for gain according to 488-MESF beads (section *2.7.2*), and plotted using CellQuest Pro.

2.7.2 Quantification of bound Fab

To quantitate the amount of Fab bound per cell, Quantum AlexaFluor488 MESF (Molecules of Equivalent Soluble Fluorochrome) beads (Bangs Laboratories) were used. The kit contained five different 488-MESF beads with various levels of MESF (0, 3507, 32348, 196948, 941222), which were analysed according to the manufacturer's instructions. Briefly, two drops (~100 μL) of each kind of bead was added to separate FACS tubes containing 0.8 mL FACS-A solution. The beads were then analysed on FACScalibur in triplicate and the 488 signal from 5,000 beads, gated according to their size on the FCS and SSC channels, was recorded on the FL1 channel. The gain of the FL1 channel was set so that the lowest fluorescence beads (MESF = 0) were between 10^0 and 10^1 on the FL1 scale. As this same FL1 setting was used while analysing cells, the cell autofluorescence rendered the background signal from unlabelled cells to lie between 10^1 and 10^2 on the FL1 scale.

The FL1 geometric mean from triplicate bead samples was used to calculate the average FL1 geometric mean and the background from blank beads was subtracted from the fluorescent beads, before plotting the average FL1 geometric mean against the respective MESF values of the beads using Microsoft Excel. A best-fit line was then generated, passing through (0,0) and its equation and R^2 values were calculated. This plot and equation were then used to back-calculate the MESF values for cells.

First, the FL1 geometric mean of background cells (labelled with 0 μg/mL Fab) was subtracted from the FL1 geometric mean of Fab labelled cells (10 – 0.001 μg/mL Fab). The resulting value was then placed in the equation generated above and the MESF for cells was calculated. The obtained MESF value was then divided by the number of 488 dye molecules conjugated per mSA molecule (see section *2.2.5.2*), to give the final number of mSA molecules bound to cells at various Fab concentrations.

As mSA binds mono-biotinylated Fab in a 1:1 ratio, the number of bound Fab molecules could be estimated to be the same as the number of bound mSA molecules. As the samples were in triplicate, the average and standard deviation for each Fab concentration was calculated.

To calculate the exact number of Fab molecules needed to bind to a cell for it to be immunomagnetically isolated, the FL1 plot obtained from binding 0.01 μg/mL mono-biotinylated Fab0.35 (a concentration which gives partial immunomagnetic cell isolation), was further analysed. As the plot is a distribution of cells with slightly varying levels of bound Fab, the highest labelled cells with maximum fluorescence were bracketed off (to include the same percentage of cells as those recruited from immunomagnetic cell isolation). The FL1 value at the position of the lower bracket was then used further (after subtracting cell autofluorescence) to calculate the amount of Fab bound to cells at that level of cell fluorescence, based on the 488-MESF bead plot as described above.

Quantitation of bound Fab on different cell-types was done in the same way as described above, using a standard curve plotted using 488-MESF beads. The FL1 geometric mean of unlabelled cells (0 μg/mL Fab) was subtracted from the FL1 geometric mean of labelled cells (10 μg/mL Fab), before calculating the MESF values for cell samples using the 488-bead standard curve.

2.7.3 Changes in Fab binding on cholesterol treatment

To understand how cholesterol treatment changes Fab binding to cells, BT474 cells were trypsinized, washed once with D1, and resuspended at a concentration of 2.5 × 10^6 cells/mL. Triplicate samples of 125,000 cells in 50 μL D1 were incubated with 250 μg/mL cholesterol (containing 7× molar excess of methyl β-cyclodextrin to make cholesterol water-soluble, Sigma), 10 mM methyl β-cyclodextrin (Sigma) or water control, for 1 hr at 25°C. 0 or 0.01 μg/mL of mono-biotinylated Fab0.11 was then added to cells and incubated further for 10 min at 25°C. Cells were centrifuged to remove excess Fab, resuspended in 50 μL of 0.41 μM streptavidin conjugated to R-phycoerythrin (R-PE, Life Technologies) in FACS-A and incubated on ice for 15 min. Cells were centrifuged, washed twice with 100 μL FACS-A, resuspended in 0.4 mL FACS-A and stored on ice until their analysis on the flow cytometer. Labelled cells

were analysed on FACScalibur flow cytometer with CellQuest Pro version 5.2.1. Signal from 20,000 gated cells was recorded on the FL2 channel (488 nm excitation with 585±15 nm emission), which had been adjusted for gain so that unlabelled cells (0 μg/mL Fab) were between 10^0 and 10^1 on the FL2 scale.

2.8 Immunomagnetic cell isolation

2.8.1 General procedure

Immunomagnetic cell isolation was carried out using various cancer cell-lines. In general, cells were grown in D10 in T-175 flasks until they reached ~80% confluency. Cells were then harvested by trypsinizing for 5-15 min at 37°C, centrifuging at 1,300 rpm for 3 min, washing once in D1 and resuspending the cell pellet at a concentration of 2.5×10^6 cells/mL in D1. Triplicate samples, each containing 250,000 cells in 100 μL D1 were used for each condition, unless stated otherwise.

For Fab titration experiments, cells were incubated with the indicated Fab at concentrations ranging from 10 – 0.001 μg/mL or 0 μg/mL for 10 min at 25°C. Cells were then centrifuged at 1,700 *g* for 2 min to remove excess Fab, and resuspended in 0.5 mL D1. 25 μL streptavidin-beads (Dynabeads® Biotin Binder, 2.8 μm diameter, superparamagnetic polystyrene beads coupled to recombinant streptavidin, 4×10^8 beads/mL, Life Technologies) had previously been washed twice with 50 μL PBS and once with 25 μL D1 using a magnetic rack (MagRack 6, GE Healthcare). Cells were added to the beads and incubated in a 1.5 mL microcentrifuge tube at 25°C for 30 min with end-over-end rotation on an electric rotator (Stuart Equipment).

100 μL of the cell-bead mixture was pipetted out for counting the total number of cells in the cell-bead mixture. The remaining cells were placed on the magnetic rack for 2 min, after which the bead-bound cells collected in a pellet towards the magnet and the unbound cells were pipetted out for counting of the flowthrough cells. The cells that bound the magnetic beads were washed once with 100 μL D1, and the recovered cells were finally resuspended in 100 μL D1.

Cells in the bead-cell mixture and cells recovered from magnetic bead binding were counted on a Coulter Counter (CASY® Model TT, Innovatis) using a 150 μm

measuring capillary, 400 µL sample volume and evaluation cursor between 7.5 – 50 µm. 50 µL cell sample was diluted in 10 mL CASYton buffer (Roche) and the dilution factor on Coulter counter was adjusted to 200× before making measurements. Cell recovery was calculated as a percentage of the total number of cells in the bead-cell mixture using the following formula: 100×(number of recovered cells/number of cells in the original bead-cell mixture). All calculations and graphs were made using Microsoft Excel and the statistical analyses were carried out as two-tailed unpaired t-tests using GraphPad Software QuickCalcs.

2.8.2 Using hu4D5 mutants with varying affinities

To assess the effect of antibody affinity on immunomagnetic cell isolation, a series of hu4D5 Fab mutants with varying affinities for HER2 were used. BT474 cells, which express high surface HER2, were harvested and diluted to a concentration of 2.5×10^6 cells/mL in D1 as described above.

Bis-biotinylated Fab constructs (with two AP tags each) with the following mutations were used: wild-type hu4D5 Fab (Fab0.35), D102W in the heavy chain (Fab0.11), Y105F in the heavy chain (Fab1.4), Y92A in the light chain (Fab2.7) and H91A in the light chain (Fab55). Each Fab was termed according to its K_d for HER2. Cells were incubated with varying concentrations of the indicated Fab in triplicate, and immunomagnetic cell isolation was carried out using streptavidin-coated beads as described in section *2.8.1*.

2.8.3 Using various cell-bead linkages

To test the efficiency of various protein linkages between the cell and magnetic bead on immunomagnetic cell isolation, three kinds of linkages were tested on BT474 cells.

For the direct biotin-streptavidin linkage, BT474 cells were incubated with the indicated concentration of bis-biotinylated Fab0.11 and isolated using streptavidin-coated beads as described in section *2.8.1*.

For the secondary antibody linkage, streptavidin beads were washed twice with 50 µL PBS and then coated with 3 µg goat anti-human kappa chain, biotin conjugate (Thermo) per 25 µL streptavidin beads in 10 µL PBS, for 10 min at 25°C on a

microcentrifuge tube thermomixer (Eppendorf). The coated beads were again washed twice with 50 µL PBS and once with 25 µL D1. Harvested BT474 cells (250,000 cells in 100 µL D1) were incubated with the indicated concentration of non-biotinylated Fab0.11 in triplicate for 10 min at 25°C, before proceeding with immunomagnetic isolation using the above made secondary Ab-coated beads and the process described in section *2.8.1*.

For Protein L linkage, streptavidin beads were washed twice with 50 µL PBS and then coated with 3 µg Protein L, biotin conjugate (Thermo) per 25 µL streptavidin beads in 10 µL PBS, for 10 min at 25°C on a microcentrifuge tube thermomixer (Eppendorf). The coated beads were again washed twice with 50 µL PBS and once with 25 µL D1. Coated beads were then used to isolate BT474 cells treated with the indicated concentration of non-biotinylated Fab0.11 and processed in the same way as described above.

2.8.4 Chemical vs. site-directed biotinylation

BT474 cells were harvested and triplicate samples, each containing 250,000 cells in 100 µL D1, were incubated with the indicated concentration of chemically biotinylated Fab0.35 (Fab0.35-chemB, no AP tags) or with bis-biotinylated Fab0.35 (both AP tags) for 10 min at 25°C. Cells were processed using streptavidin-beads as described in section *2.8.1*.

2.8.5 One vs. two AP tags

BT474 cells were harvested and incubated with the indicated concentration of mono-biotinylated Fab0.11 (AP tag only on heavy chain) or with bis-biotinylated Fab0.11 (AP tags on both chains) for 10 min at 25°C in triplicate and further processed using streptavidin beads as described in section *2.8.1*.

2.8.6 Effect of small molecules

To test the effect of small molecules on immunomagnetic cell isolation, BT474 cells were harvested as in section *2.8.1*. Triplicate samples of 250,000 cells in 100 µL D1 were incubated with the respective small molecule for 1 hr at 25°C using the following concentrations: 50 µM cytochalasin D (Sigma) (4 mM stock prepared in DMSO), 16.5 µM nocodazole (Sigma) (16.5 mM stock in DMSO), 10 mM methyl β-

cyclodextrin (Sigma) (10 mM stock in D1), 250 μg/mL cholesterol (Sigma) (10 mg/mL stock in H_2O), 1 mM sodium azide (Merck) (100 mM stock in H_2O) or 10 μM AG825 (Merck) (10 mM stock in DMSO). For each treatment, a corresponding control sample was treated with the respective amount of either DMSO or H_2O. The cholesterol used was water-soluble as it contained a 1:7 molar ratio of cholesterol to methyl-β-cyclodextrin.

After drug treatment, 0.01 μg/mL of bis-biotinylated Fab0.11 was added to cells for 10 min at 25°C. Beading was carried out as described in section *2.8.1* but the same concentration of each inhibitor was present in D1 throughout the process. Cell viability was checked under the microscope using Trypan Blue (Sigma).

2.8.7 Cell panel testing

Immunomagnetic cell isolation was carried out on a panel of five cell-lines (BT474, MDA-MB-453, MCF-7, A431 and MDA-MB-468) to compare the efficiencies of standard conditions and enhanced conditions. Cell-lines were grown in D10 and harvested by trypsinization as described in section *2.8.1* and samples of 250,000 cells in 100 μL D1 were processed in triplicate.

Under the enhanced conditions, cells were treated with 250 μg/mL cholesterol for 1 hr at 25°C, and then incubated with 1 μg/mL bis-biotinylated Fab0.11. Cells were isolated using streptavidin beads as described in section *2.8.1*, but with 250 μg/mL cholesterol present in D1 throughout the process.

Under the standard conditions, cells were treated with 1 μg/mL non-biotinylated Fab0.35 for 10 min at 25°C and then isolated using secondary coated beads as described in section *2.8.3*.

To assess the effects of the individual enhancements of Fab affinity (*2.8.2)*, bead linkage (*2.8.3)* and cholesterol treatment (*2.8.6*) on the cell panel, the respective protocols were applied on the different cell-lines instead of just using BT474, using the indicated Fab mutant concentration.

2.8.8 4D5-APLHb vs. 4D5-LHAPb

To compare the isolation efficiencies of 4D5-APLHb and 4D5-LHAPb, BT474 cells were harvested as above and resuspended at a concentration of 3×10^6 cells/mL in

D1. Duplicate samples consisting of 300,00 cells in 100 µL were incubated with either 1 µg/mL or 0.1 µg/mL of the indicated Fab construct, for 10 min at 25°C. Cells were then processed and isolated using streptavidin beads as described in section *2.8.1*.

2.9. Spiking and recovery from rabbit blood

To assess the efficiency of the enhanced immunomagnetic cell isolation approach, it was used to isolate spiked cancer cells from rabbit blood. Cells from culture were harvested by trypsinizing for 5-15 min, washed once with PBS with 1% FCS (PBS-1) and resuspended at a concentration of 10^6 cells/mL in PBS-1. Cell tracer Carboxyfluorescein Succinimidyl Ester (CFSE, Life Technologies) was added to cells at a concentration of 10 µM (5 mM stock in DMSO) and incubated at 37°C for 15 min. Cells were then centrifuged at 1,300 rpm for 2 min, resuspended in fresh PBS-1 at 10^6 cells/mL, and incubated further for 30 min at 37°C, after which excess CFSE was discarded by centrifuging the cells and resuspending them in D1. Cells were counted on a haemocytometer (Neubauer-Improved) using Trypan blue and 100,000 CFSE-labelled cells were spiked in triplicate into 1 mL of rabbit blood (in Alsever's solution, TCS Biosciences). The spiked rabbit blood was then processed to remove red blood cells by incubating 1 mL of the whole-blood sample with 25 mL lysis buffer (154 mM NH_4Cl, 10 mM $KHCO_3$, 0.1 mM EDTA, pH 7.2) in a 50 mL centrifuge tube. After incubating at 25°C for 5 min and inverting the tube multiple times to ensure complete red blood cell lysis, the cells were spun down at 1,500 rpm for 6 min. Supernatant was discarded, the cell pellet was washed once with 1 mL D1, and the cell pellet was resuspended finally in 100 µL D1.

Cells were then immunomagnetically isolated under either the enhanced conditions or the standard conditions as described in section *2.8.7*. The final recovered cells were resuspended in 50 µL D1, counted on a haemocytometer under the DeltaVision microscope and checked for CFSE labelling in the FITC channel.

2.10. Figure presentation

All figures containing 3D molecular structures of antigen-Fab complexes were rendered in the PyMOL molecular visualization system (DeLano Scientific) and cartoon structures of cells with Fab and magnetic beads were made in Microsoft Powerpoint 2011. Chemical structures were drawn using ChemBioDraw 13.0 software. All graphs were plotted using Microsoft Excel 2011 and statistical analysis was done on Microsoft Excel 2011 and GraphPad QuickCalcs online software.

Chapter 3: Immunomagnetic Cell Isolation

Investigating the protein interactions between a cell and a magnetic particle

Chapter 3: Immunomagnetic Cell Isolation

Investigating the protein interactions between a cell and a magnetic particle

3.1 Introduction

Various areas of biology, including microbiology, immunology and stem cell research, require the isolation of specific kinds of cells from complex mixtures (Safarik et al., 1995; Grützkau and Radbruch, 2010) . Classically, cell separation was carried out by density gradient centrifugation (He et al., 2008), physical filtration based on cell size, or by flow cytometry (fluorescence-activated cell sorting) (Herzenberg et al., 2002). However, in recent years affinity-based capture of cells on a solid-phase has also gained popularity (Dainiak et al., 2007). Of these, magnetic separation of cells using immunomagnetic beads has increasingly grown in importance due to its ease of use, high throughput, low cost and reduced shear stress on cells (Thiel et al., 1998). Cells are first coated with an antibody against a specific cell membrane marker and then linked to micro- or nano-sized magnetic particles. Application of a magnetic field then allows for the enrichment or depletion of the cells bound to the magnetic particles, giving more than 20,000-30,000 fold enrichment rate (Thiel et al., 1998).

Immunomagnetic cell sorting is not only used in research, but is also employed in clinical work for enriching haematopoietic stem cells for bone marrow transplants (Powles et al., 2000), assisted reproduction (Said et al., 2008) and for isolation of cells for cancer immunotherapy (Stift et al., 2003). With the advancement in our knowledge about the presence and importance of circulating tumour cells (CTCs) in the bloodstream (Yu et al., 2011), immunomagnetic cell sorting is becoming a significant tool in cancer prognosis. CTCs have been shown to be present in the bloodstream well before metastatic tumours are established and even before a tumour is characterised as being malignant (Hüsemann et al., 2008). Isolating CTCs presents a powerful new approach for determining cancer prognosis and evolution, monitoring response to therapy, and evaluating signalling, proliferation and apoptosis in tumours (Yu et al., 2011). The effectiveness of studying CTCs led to the United States Food and Drug Administration approval of the immunomagnetic cell isolation method

CellSearch for CTC isolation in colorectal, prostate and breast cancer (Yu et al., 2011). Isolated CTCs may then be analysed via microscopic, genetic or proteomic techniques to understand their origin and behaviour (Leary et al., 2010; Dharmasiri et al., 2011)

Despite its widespread use in cell separation, the factors affecting immunomagnetic isolation are surprisingly under-studied. McCloskey et al. (McCloskey et al., 2003b) defined magnetophoretic mobility as the velocity of a magnetically tagged cell in the presence of a magnetic field. They then developed mathematical models defining parameters that affect magnetophoretic mobility of a cell, including the antibody binding capacity of the cell, secondary antibody amplification, cell diameter and magnetic particle size (McCloskey et al., 2000, 2001, 2003a). Various blood fractionation methods have also been assessed for optimal pre-enrichment of cancer cells from blood (He et al., 2008). However, many fundamental questions about the sensitivity of immunomagnetic cell isolation have still not been clearly answered. For instance, how many target antigens need to be present on a cell for the cell to be immunomagnetically isolated? How strongly does the antibody have to bind for the interaction to survive the pull between the cell and the magnetic particle? What is the most efficient form of protein linkage between the cell and the bead? Reducing dependence on target antigen expression level for immunomagnetic cell recovery was described as a major challenge for the field (Dharmasiri et al., 2010). With the recent data on epithelial-mesenchymal transition of blood vessel-invading tumour cells (Rhim et al., 2012), it has become even more important to be able isolate cancer cells that have down-regulated epithelial markers.

To explore and extend the limitations posed in magnetic cell separation, we test here a clinically relevant antibody fragment (hu4D5 Fab) against HER2 on breast cancer cells (Carter et al., 1992). We quantitate the amount of primary antibody required to bind a cell for it to be magnetically isolated and assess the importance of antibody affinity and antibody linkage to the bead in isolating cells with low numbers of target antigen.

3.2 Designing the cell-magnetic bead synapse using hu4D5 Fab and AP tags

In order to explore the variables affecting the cell-bead synapse, anti-HER2 hu4D5 Fab was used to bind HER2 present on breast cancer cell-lines. hu4D5 Fab consists of variable and constant domains of the heavy and light chain (V_H, C_{H1},V_L and C_L) of the hu4D5 antibody and binds with high affinity (K_d = 0.35 nM) (Gerstner et al., 2002) to the extracellular domain of HER2 (Fig. 3.1A) (Cho et al., 2003).

Acceptor peptide tags, also called AviTag, (15 amino acid peptide - GLNDIFEAQKIEWHE) (Beckett et al., 1999) were genetically inserted into the C-terminus of the light and heavy chains of the hu4D5 Fab and the recombinant Fab was expressed extracellularly using HEK-293T cells. After purification, the Fab was incubated with biotin ligase, *E. coli* BirA, to site-specifically biotinylate the AP tag at its lysine side chain and the doubly biotinylated hu4D5 Fab was termed Fab0.35 (based on its affinity in nM).

The purity and uniformity of Fab0.35 was checked on SDS-PAGE (Fig. 3.1B). Purified Fab0.35 gave a band at ~ 54 kDa and shifted slightly upwards on biotinylation, probably because of the change in overall charge. On reduction of the disulfide bonds, Fab0.35 dimer split into its constituent heavy and light chains (Fig. 3.1B). Complete biotinylation of both Fab chains was also verified by mixing the reduced Fabs with streptavidin and then running the sample on SDS-PAGE (Fig. 3.1B). Both chains showed streptavidin binding, as indicated by the shift in their bands. Due to its tetravalency, streptavidin can bind more than one Fab chain (Fig. 3.1B).

As the AP tags are away from the HER2-binding site (Fig. 3.1A), the biotinylated Fab0.35 could bind HER2 on the cell membrane and also streptavidin on the magnetic bead. The biotin-streptavidin binding is an extremely strong non-covalent interaction with a $K_d = 4 \times 10^{-14}$ M (off-rate at 37ºC ~ 4 hr) and an on-rate nearly at the diffusion limit (~10^7 M^{-1} s^{-1}) (Green 1990).

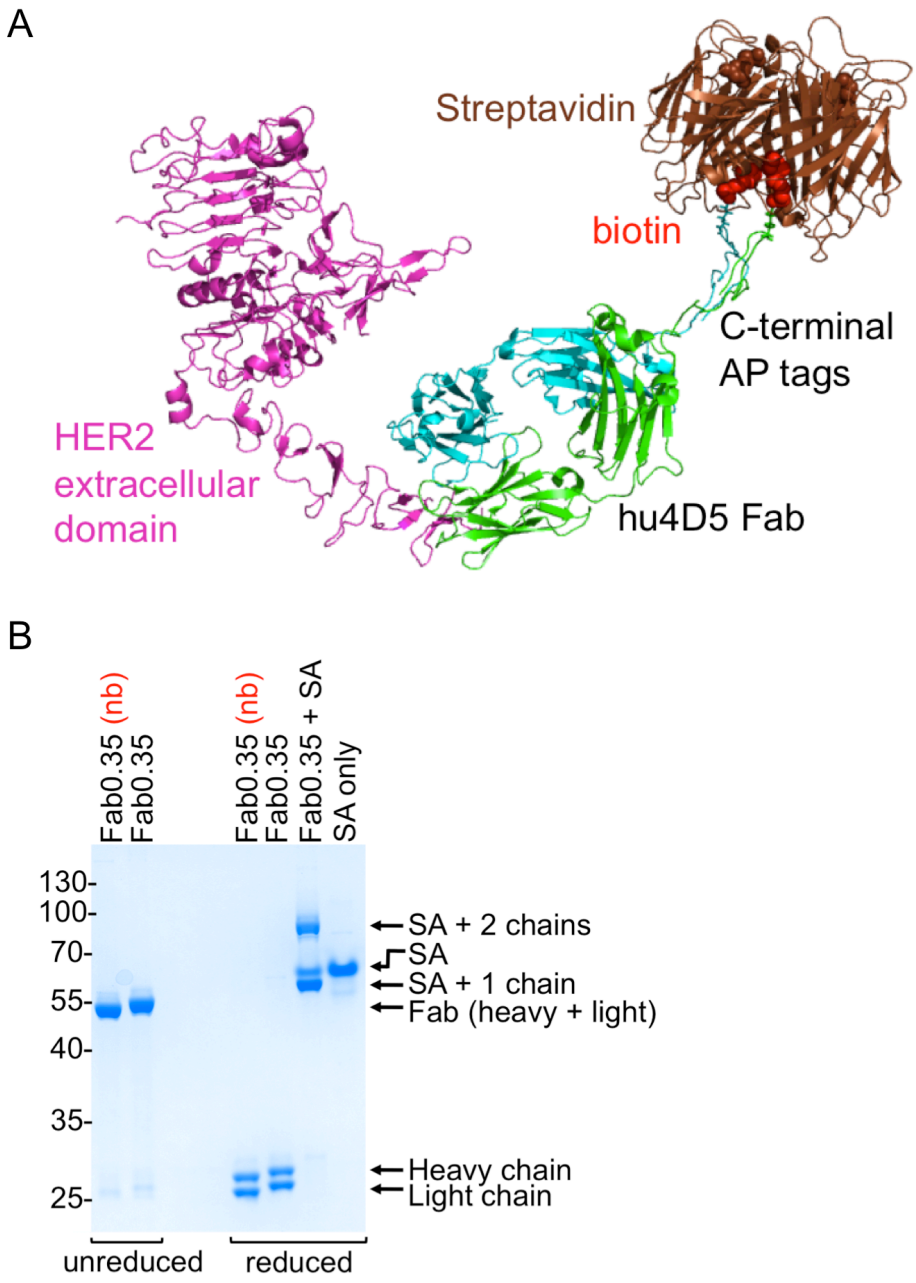

Figure 3.1. Engineering hu4D5 with AP tags for streptavidin binding. A. Cartoon of the protein interactions between cell and magnetic bead. The juxtamembrane extracellular region of HER2 is bound by humanized anti-HER2 4D5 Fab (based on PDB 1N8Z) bearing C-terminal AP tags on heavy and light chain. Site-specific biotinylation of the AP tags allows the Fab to bind to streptavidin (based on PDB 1SWE) present on magnetic beads. B. SDS-PAGE of AP-tagged hu4D5 termed Fab0.35 non-biotinylated (nb) and with biotinylation, stained with Coomassie blue. Reducing agent was used to break the disulfide bridges and test the individual heavy and light chains for biotinylation.

3.3 Immunomagnetic recovery depended on the amount of Fab bound to cells

For immunomagnetic isolation, I used BT474, a breast cancer cell-line (from invasive ductal carcinoma) that expresses high levels of surface HER2 (Gaborit et al., 2011). Cells were incubated with Fab0.35, excess antibody was washed away, and then cells were mixed with streptavidin-coated magnetic beads (2.8 μm diameter Dynabeads) at a ratio of 40 beads per cell. A magnetic field was then applied to this bead-cell mixture (Fig. 3.2A), and the bead-bound cells collected near the magnet. After pipetting out the unbound cells from the flowthrough (Fig. 3.2A), the bead-bound cells could be resuspended in fresh medium and recovered for cell counting.

The first variable I studied was the amount of Fab required to bind a cell for the cell to be immunomagnetically isolated. My approach was based on incubating BT474 cells with varying levels of Fab0.35 as a surrogate for cells expressing different levels of HER2 (Fig. 3.2B). Low amounts of bound Fab would give the streptavidin-beads limited number of binding sites, similar to a cell with few surface HER2 molecules. This enabled me to perform the experiment with only one variable, the Fab concentration, and avoid discrepancies arising due to cell size, shape, membrane fluidity, surface glycosylation and cell signalling, when different cell-types are compared.

My results indicated that at saturating Fab0.35 concentrations (≥ 1 μg/mL), 70-80% of BT474 cells could be isolated (Fig. 3.2C), However, lowering Fab0.35 concentration and thereby decreasing the number of HER2 receptors available for the magnetic bead to bind led to a decrease in the recovery of cells. In the negative control, with no Fab added to cells, very few cells were recovered, hence validating the low non-specific binding of streptavidin-magnetic particles to BT474 cells. A sharp drop in cell recovery between 0.1 and 0.01 μg/mL Fab (Fig. 3.2C) is consistent with the necessity for a minimum number of surface antigens to enable the cell to be isolated by magnetic separation.

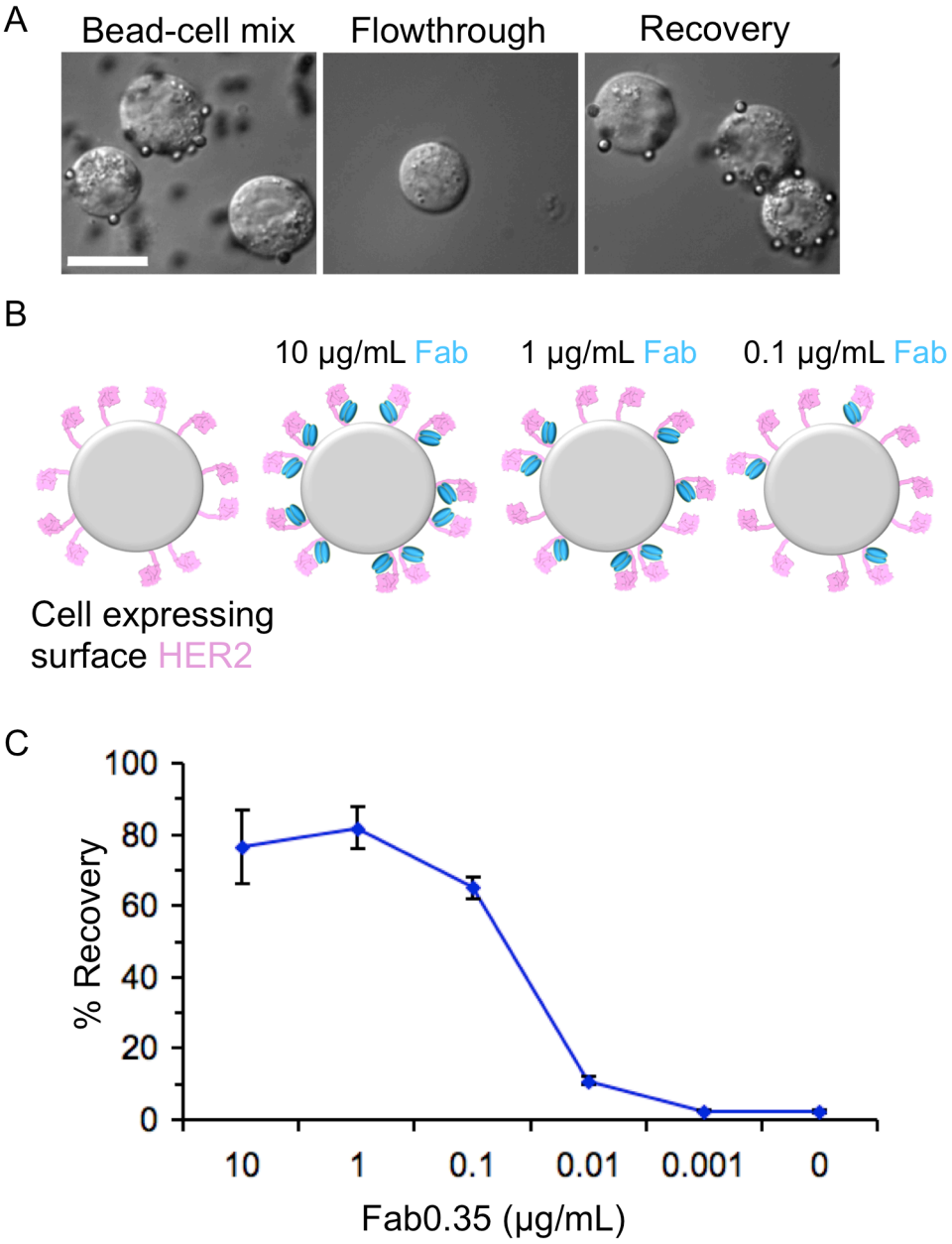

Figure 3.2. Immunomagnetic recovery depended on the amount of Fab bound to cells. A. Brightfield microscopy of BT474 cells at various stages during the isolation procedure. From left to right: initial incubation of cells with streptavidin-magnetic beads after labelling with 0.1 µg/mL Fab0.35; flowthrough of cells not attracted to the magnet; cells recovered after magnetic separation. Scale bar: 20 µm. B. Schematic representation of HER2-expressing cells incubated with varying concentrations of primary Fab, as a controlled proxy for cells expressing various levels of HER2. C. Plot showing dependence of cell recovery on Fab concentration. BT474 cells were labelled with the indicated concentration of Fab0.35 and isolated with SA-beads. Recovered cells were quantified on a Coulter counter and calculated as a percentage of the number of cells in the cell-bead mixture (mean of triplicate ± 1 s.d.).

To calculate this limit, I engineered Fab0.35 with AP tag inserted in only one chain, the mono-biotinylated Fab0.35. On the gel shift assay, only the chain with the biotinylated AP tag, either heavy or light chain, shifted upwards upon addition of streptavidin (Fig. 3.3A).

To quantitate the amount of Fab molecules bound to cells, I titrated Fab0.35-monobio (biotinylated only on heavy chain) onto BT474 cells and added excess monovalent streptavidin detection reagent (mSA-488) to detect cells by flow cytometry. This approach enabled a 1:1 ratio of HER2 to mSA-488 and so avoided underestimation of bound Fab numbers due to multivalency of core streptavidin or bivalent secondary antibodies (Fig. 3.3B).

To establish a standard curve of fluorescence from the FL1 channel versus number of 488 dye molecules, I used microspheres containing known levels of 488 dye molecules, 488-MESF (Molecules of Equivalent Soluble Fluorochrome) beads. Each of these five beads was conjugated to a set level of 488 dye molecules, including a blank of beads lacking the dye (Fig. 3.3C).

After plotting the calibration curve using the geometric mean of FL1 peaks (Fig. 3.3C and D), I measured the fluorescence of cells labelled with different concentrations of Fab0.35-monobio (Fig. 3.4A). Using the equation from Fig. 3.3D and the number of 488 dye molecules conjugated per mSA, the number of Fab bound per cell at each Fab concentration could be quantitated (Fig. 3.4C) (Lenkei et al., 1998).

Comparing the bound Fab levels to immunomagnetic cell isolation efficiency showed that 26,500 receptors were required for efficient (> 50%) recovery (Fig. 3.2C and Fig. 3.4C). Cells expressing less than 4,000 receptors had a low probability (~10%) of being isolated (Fig. 3.2C and 3.4C).

Furthermore, I wanted to determine the minimum number of bound Fab molecules required for a cell to be isolated, at the given Fab affinity (0.35 nM). Since at 0.01 μg/mL, only 10% cells were isolated, I calculated the amount of Fab bound to cells expressing fluorescence in the 10^{th} percentile of the 0.01 μg/mL FL1 peak (Fig. 3.4B). It was thereby estimated, that for a cell to be immunomagnetically isolated using a Fab of affinity 0.35 nM, the cell needs to bind atleast 12,300 ± 370 Fab molecules.

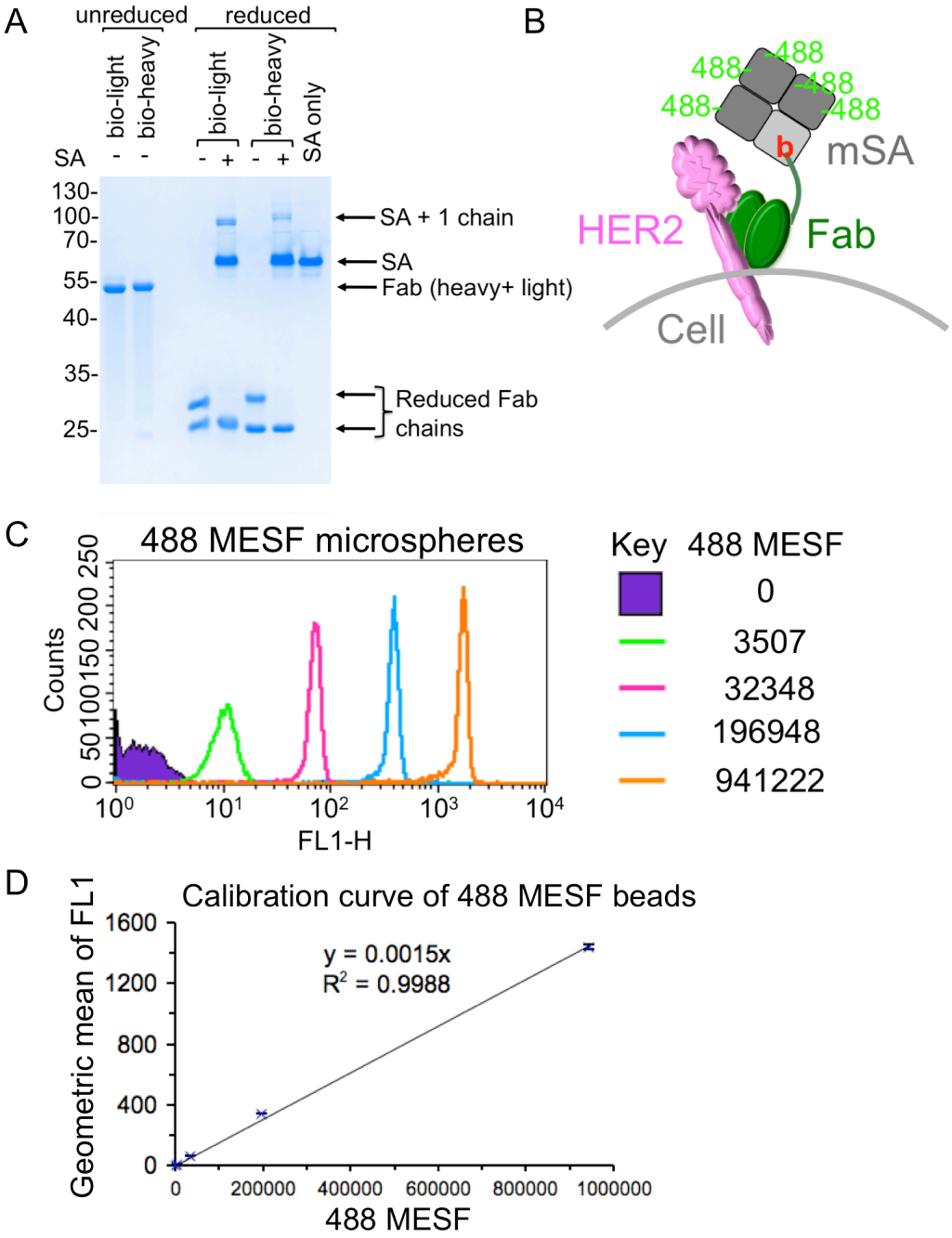

Figure 3.3. Quantitating Fab bound to cells using flow cytometry. A. SDS-PAGE of mono-biotinylated Fab0.35 with Coomassie staining. The AP tag was inserted and biotinylated only on the light (bio-light) or heavy (bio-heavy) chain. On reduction and addition of streptavidin, only the biotinylated Fab chain showed a band shift. B. Schematic of mono-biotinylated Fab (in green) being recognized by monovalent streptavidin (mSA) conjugated to multiple 488 dye molecules. Monovalent streptavidin (mSA) is a tetramer with three inactive subunits (dark grey) and one subunit that binds biotin (b) with wildtype-affinity (light grey). C. Flow cytometry of the various 488 MESF beads in the FL1 channel. D. The geometric means of the 488 MESF beads' FL1 peaks plotted against their MESF values (mean of triplicate ± 1 s.d.). Best-fit linear trendline added with y intercept = 0 and the correlation coefficient.

A

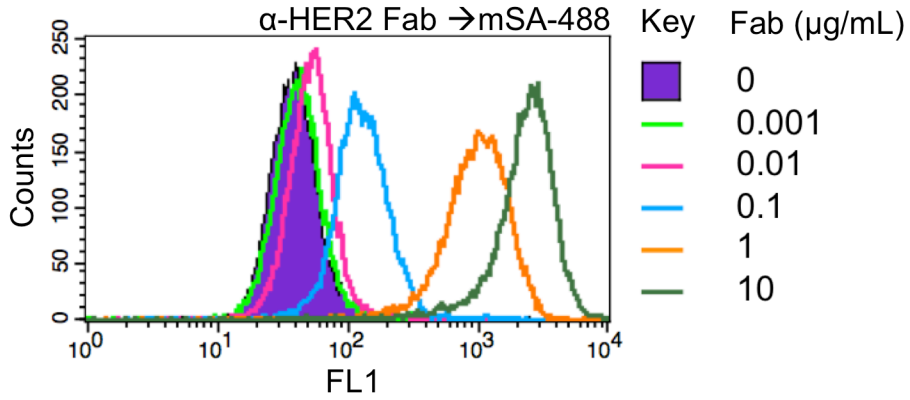

B

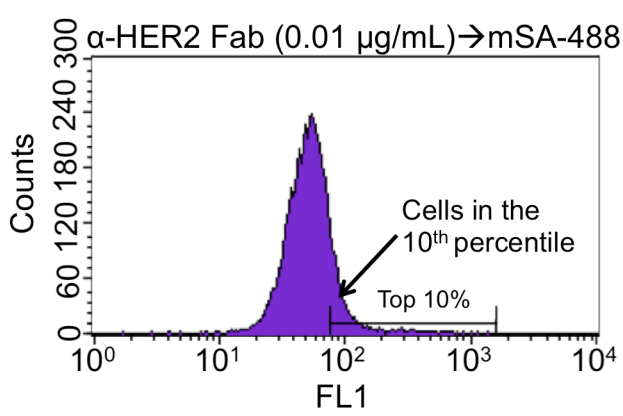

C

[Fab0.35] (μg/mL)	10	1	0.1	0.01	0.001	0
Fab0.35 bound per cell (mean ± 1 s.d., n = 3)	710,000 ± 14,000	284,000 ± 9,100	26,500 ± 2,660	3,810 ± 136	330 ± 220	0

Figure 3.4. Quantitating Fab bound to cells using flow cytometry. A. Flow cytometry of BT474 cells labelled with the indicated concentration of mono-biotinylated Fab0.35 and detected with mSA-488, for quantitating bound Fab number. B. Measuring the fluorescence of cells in the 10th percentile of the 0.01 μg/mL FL1 peak, to calculate the number of bound Fab0.35 at that level, which is then estimated to be 12,300 ± 370 Fab0.35 molecules. C. Relation between Fab0.35 concentration and number of Fab0.35 bound per cell.

3.4 Higher affinity antibodies increased immunomagnetic recovery of cells with low numbers of bound Fab

Beading efficiencies using different anti-EpCAM antibodies have previously been compared and shown to give heterogenous results in colorectal cancer patients (Antolovic et al., 2010). However, independent antibodies can differ in various properties, including the binding location on the target antigen and the antibody isotype. It is unusual to be able to study a system where binding affinity is the only major change in a series of antibodies. Such a system exists for hu4D5, where single-residue point mutants with differing binding strengths have been characterized for their kinetic properties: on-rates, off-rates, and dissociation constants (Kelley and O'Connell, 1993; Gerstner et al., 2002). We chose four hu4D5 mutants with affinities ranging over two orders of magnitude and named them according to their K_d in nM (Fig. 3.5B). All mutations were made in the HER2 binding pocket of hu4D5 (Fig. 3.5A). The heavy chain point mutant D102W (Fab0.11) had an affinity for HER2 that was three times stronger than the wildtype (Fab0.35), with a faster on-rate and a slower off-rate (Fig. 3.5B). Mutants Y105F (Fab1.4) and Y92A (Fab2.7) were made in the heavy and light chains respectively and had weaker affinities than the wildtype. H91A (Fab55) in the light chain had the fastest off-rate and the worst binding affinity for HER2.

A

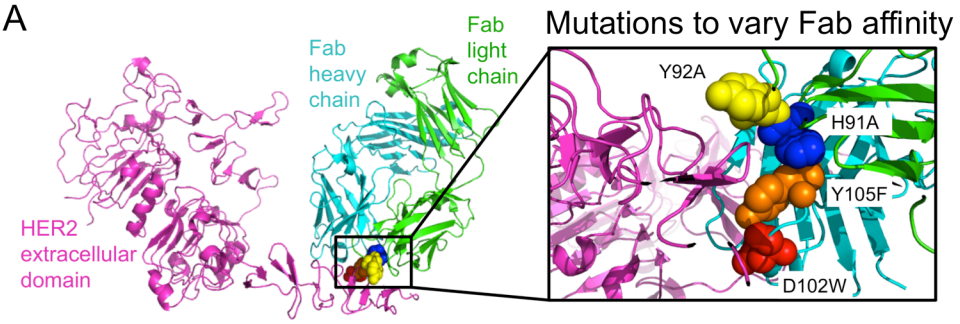

B

Fab	Mutant	$k_{on} \times 10^4$ ($M^{-1}s^{-1}$)	$k_{off} \times 10^{-5}$ (s^{-1})	K_d (nM)
Fab0.11	D102W V_H*	1.7 ± 0.45	0.19 ± 0.02	0.11 ± 0.04
Fab0.35	WT*(#)	1 ± 0.16 (6.4 ± 0.9)	0.35 ± 0.01 (1.7± 0.3)	0.35 ± 0.05 (0.27 ± 0.06)
Fab1.4	Y105F V_H*	0.9 ± 0.36	1.3 ± 0.02	1.4 ± 0.56
Fab2.7	Y92A V_L #	4.1	11	2.7
Fab55	H91A V_L #	3.2	170	55

Figure 3.5. hu4D5 point mutants. A. Crystal structure of the HER2 extracellular domain bound to hu4D5 Fab (PDB 1N8Z). Inset shows the binding interface, with residues subject to mutation in spacefill. H91A and Y92A mutations were made in the light chain, while D102W and Y105F were in the heavy chain. B. Fab mutants span a range of affinities. The table shows the on-rate (k_{on}), off-rate (k_{off}) and dissociation constant (K_d) of each mutant, from strongest to weakest. Data has been compiled from Gerstner et al., 2002 and Kelley and O'Connell., 1993.

Mutants were expressed with AP tags in their heavy and light chains in HEK-293T cells, purified and biotinylated. Fab dimers showed clear bands on SDS-PAGE (Fig. 3.6A). On reduction of disulfide bonds, the Fab dimers split into individual heavy and light chains, both of which showed streptavidin binding as indicated by the shift in their bands (Fig. 3.6B).

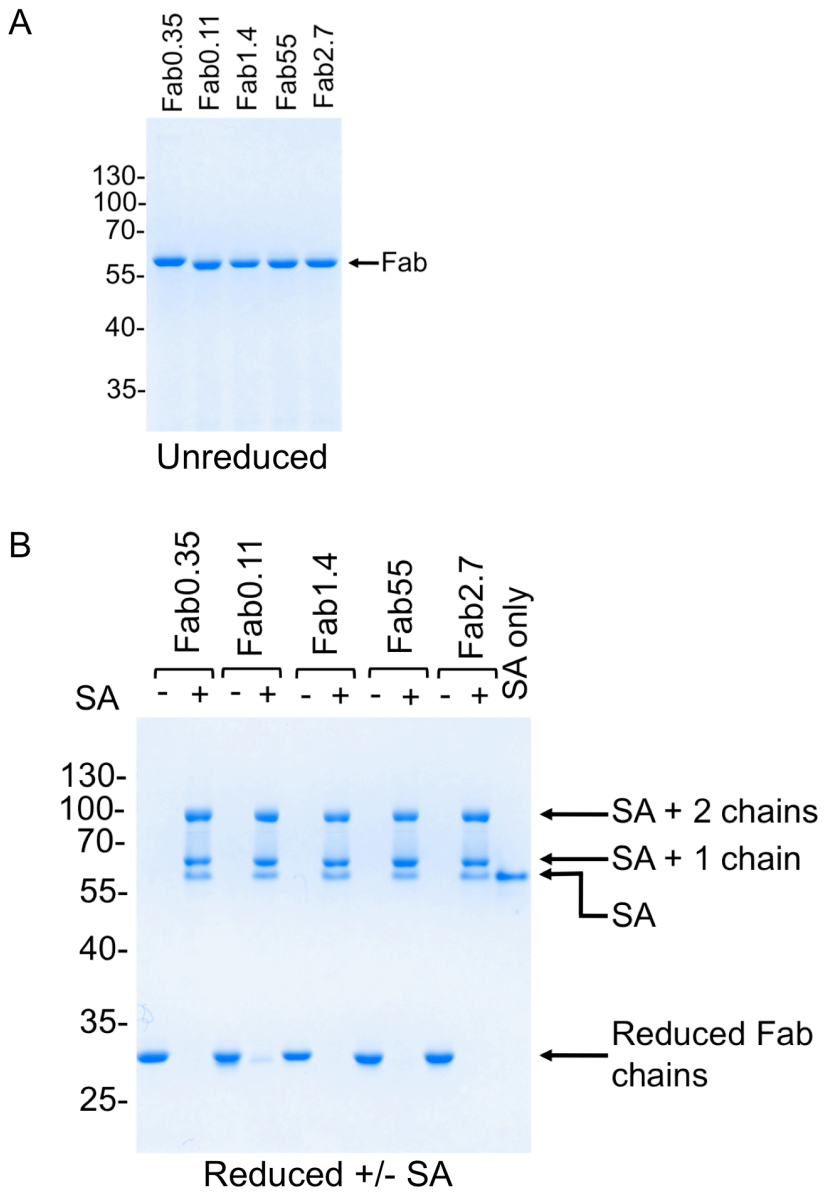

Figure 3.6. Purification and biotinylation of hu4D5 mutants. A. Each Fab variant (named according to its K_d in nM) with biotinylated AP tags and without reducing agent analysed by SDS-PAGE and stained with Coomassie blue. B. Testing biotinylation of both chains of each Fab variant, by adding 2-ME and running on SDS-PAGE before Coomassie staining. Heavy and light chains shifted uniformly on addition of streptavidin.

To check their functionality, mutant Fabs were used to bind to surface HER2 on BT474 and detected with streptavidin-conjugated to AlexaFluor488 dye (SA-488) using fluorescence microscopy (Fig. 3.7A). Fabs with affinities 0.11 nM to 2.7 nM gave strong cell staining and were readily detectable on the surface of cells, but Fab55 gave a much fainter signal (Fig. 3.7A). Mutation in Fabs did not damage the specificity of binding to HER2 on the cell surface, as verified by the loss in their binding ability when HER2 was pre-blocked with anti-HER2 IgG, Herceptin (Fig. 3.7B).

To compare the affinity series for immunomagnetic isolation, I titrated Fab mutants on BT474 cells (Fig. 3.7C). Again, the different antibody concentrations acted as a well-controlled proxy for cells expressing varying amounts of target antigens. Recovered cells were calculated as a percentage of the cells present in the bead-cell mix in order to avoid any underestimation due to loss of cells during processing. All mutants followed the same pattern as the wildtype Fab0.35, showing decreasing recovery with decreasing Fab concentration, representing decreasing antigen amount (Fig. 3.7C). When comparing different Fabs, it was seen that recovery of cells depended closely upon antibody affinity. The weakest Fab0.55 could only isolate 24.3 ± 8.2 % cells at the highest concentration of 10 μg/mL (Fig. 3.7C). As the affinity increased to 1.4 nM, the detection limit also improved to 0.1 μg/mL. The original Fab0.35 isolated 10.9 ± 1.2 % cells at 0.01 μg/mL. However, increasing affinity to 0.11 nM had a major effect and substantially improved isolation to 45.9 ± 6.3 % at 0.01 μg/mL Fab concentration (Fig. 3.7C, $P < 0.001$, $n=3$, two-tailed unpaired t-test). Fab0.35 is a highly optimized antibody refined by gene mutagenesis and molecular modelling (Carter et al., 1992) and has exceptionally high monovalent binding affinity compared to regular antibodies (Foote and Eisen, 1995). However, my results show that there is still need for improvement. Antibodies working well for immunostaining or Western blotting are not as strong as is optimal to withstand the physical pulling force applied by the magnetic field between the cell and microbead. Antibodies with affinities in the sub-nanomolar range should be engaged for efficient immunomagnetic cell sorting.

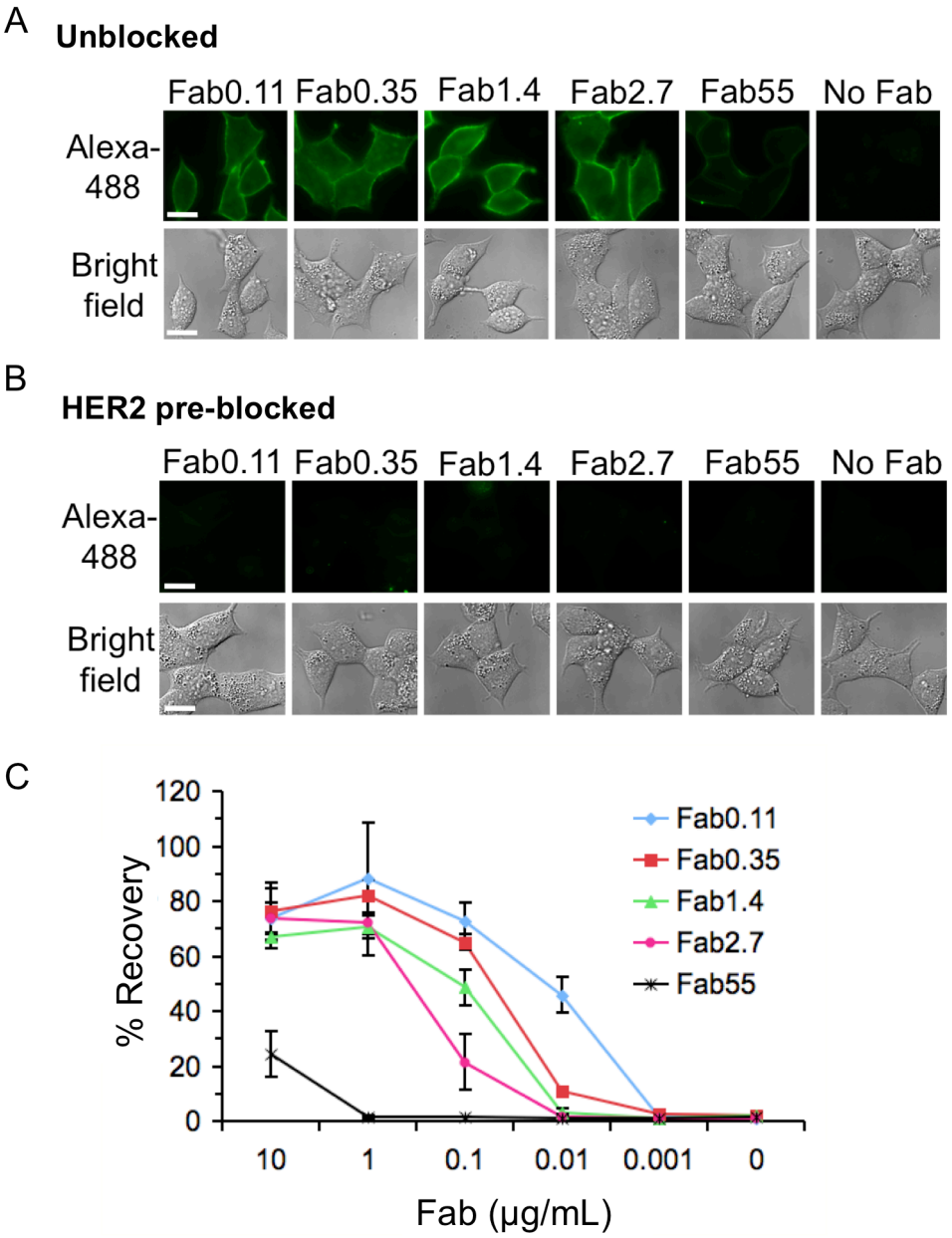

Figure 3.7. Fab variants were functional for cell labelling and could immunomagnetically isolate cells. A. Testing the functionality of Fab mutants by fluorescent microscopy. BT474 were incubated with the indicated Fab variant or with a no Fab control and detected using streptavidin-AlexaFluor488. The top panel shows streptavidin staining and the bottom panel shows the brightfield image of cells. Scale-bar: 30 µm. B. As a negative control to check for non-specific binding caused by the Fab mutations, BT474 were pre-blocked with anti-HER2 IgG and then incubated with the Fab variants as in A. C. BT474 were incubated with the indicated concentration of each Fab variant and isolated using SA-beads. Cell recovery is shown as a mean of triplicate ± 1 s.d.

For this purpose, it was important to assess whether the improvement in cell recovery by Fab0.11 was because Fab0.11 was binding cells in greater numbers at low concentrations (because of its lower K_d) or because Fab0.11 was able to resist the pull of the magnetic field more efficiently (lower force-induced off-rate). To test this, I designed Fab0.11 with only one AP tag, the mono-biotinylated Fab0.11 and checked its purity and biotinylation on SDS-PAGE (Fig. 3.10A). After titration on BT474 cells, bound Fab was detected using mSA-488 and cell fluorescence was measured by flow cytometry (Fig. 3.8A). The number of Fab0.11 molecules bound per cell, at each Fab concentration, was calculated on the basis of 488 MESF beads as before.

The number of Fab0.11 bound at each concentration (Fig. 3.8C) was slightly less than that seen for Fab0.35 (Fig. 3.4C), except for the highest concentration of 10 μg/mL, at which more Fab0.11 molecules bound than Fab0.35 (762,000 ± 14,000 for Fab0.11 versus 710,000 ± 14,000 for Fab0.35). Comparing these numbers to immunomagnetic cell recovery of the mutants (Fig. 3.7C), it can be seen that at 0.01 μg/mL, where Fab0.11 isolated 35% more cells than Fab0.35, fewer Fab0.11 molecules are bound to cells compared to Fab0.35 (2,460 ± 106 for Fab0.11 vs. 3,810 ± 136 for Fab0.35, $P < 0.0005$, $n=3$, two-tailed unpaired t-test). These results indicate that the increase in immunomagnetic recovery is not because more Fab0.11 molecules are binding to cells at each concentration, but it is more likely because the bound Fab0.11 resists the pull between the cell and the bead in the presence of a magnetic field more efficiently than Fab0.35.

Furthermore, calculating the number of bound Fab0.11 molecules to cells in the 45% percentile of the FL1 peak (at 0.01 μg/mL) suggests that for a cell to be immunomagnetically isolated using a Fab of affinity 0.11 nM, the cells needs to bind approximately 3,064 ± 220 Fab molecules (Fig. 3.8B). This value is strikingly lower than that of Fab0.35 (12,300 ± 370, Fig. 3.4B). This difference emphasizes the importance of a high affinity primary antibody that can strongly link the cell and magnetic particle and thereby isolate cells expressing low levels of antigen.

A

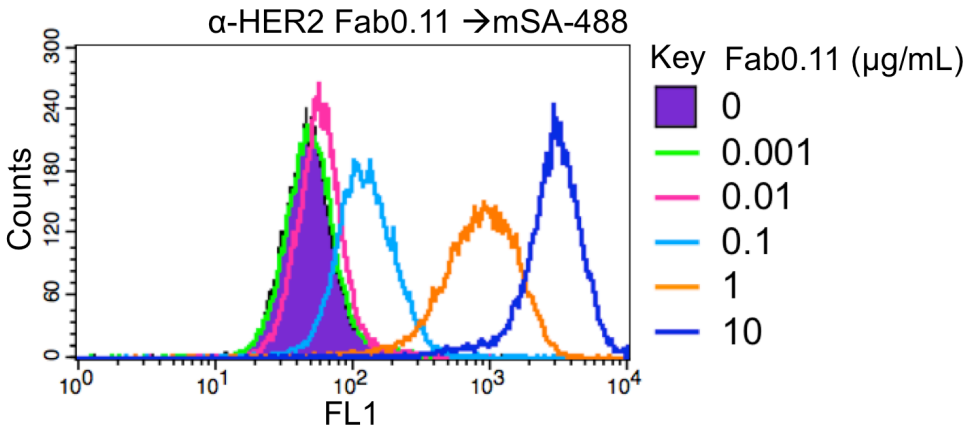

B

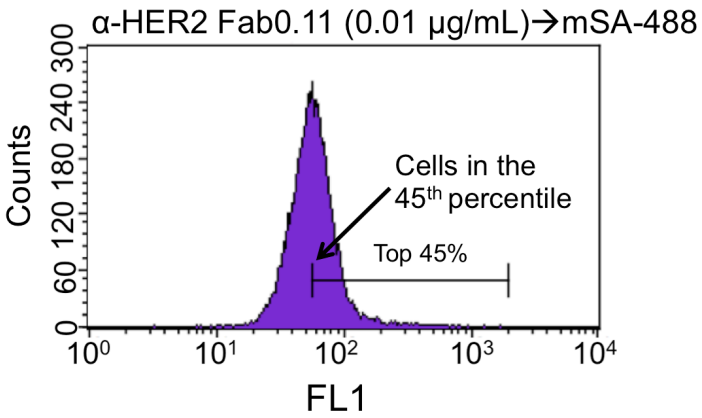

C

[Fab0.11] (µg/mL)	10	1	0.1	0.01	0.001	0
Fab0.11 bound per cell (mean ± 1 s.d., n = 3)	762,000 ± 14,000	218,000 ± 2,100	21,700 ± 530	2,460 ± 106	79 ± 170	0

Figure 3.8. Quantitating the amount of Fab0.11 bound to cells using flow cytometry. A. Flow cytometry of BT474 cells labelled with the indicated concentration of mono-biotinylated Fab0.11 and detected with mSA-488. B. Measuring the fluorescence of cells in the 45th percentile of the 0.01 µg/mL FL1 peak, to calculate the number of bound Fab0.11 at that level, which is then estimated to be 3,064 ± 220 Fab0.11 molecules. C. Relation between Fab0.11 concentration and number of Fab0.11 bound per cell.

3.5 Reducing the number of protein-protein links between the cell and magnetic particle improved cell recovery

After evaluating the significance of affinity between the primary antibody and target protein using the Fab affinity series, it was important to determine how the linkage

between the primary antibody and the magnetic bead influenced immunomagnetic isolation.

For this purpose, I compared the stability of two commonly-used linkages to my direct biotin-streptavidin link (Fig. 3.9A, B). Keeping the same primary antibody affinity (strongest binder Fab0.11, mutation D102W), and using the same streptavidin-coated beads in each case, we evaluated the efficiency of using intermediary links like secondary antibody and Protein L (Fig. 3.9A, B).

In the first condition, the direct biotin-streptavidin link was tested by labeling BT474 cells with biotinylated Fab0.11 and capturing the cells using streptavidin-coated magnetic beads. In the second condition, cells were labelled with non-biotinylated Fab0.11, and then mixed with streptavidin beads that had been coated with excess biotinylated anti-human secondary antibody. Using secondary antibodies to recognize the primary on cells is widely used in immunomagnetic isolation. For the third condition, cells were labelled with non-biotinylated Fab0.11 and mixed with streptavidin beads coated with excess biotinylated Protein L. Protein L is a 95 kDa surface protein from *Peptostreptococcus magnus* and is an immunoglobulin binding protein that binds with high affinity (K_d = 1.5 nM to human κ light chain) and specificity to mammalian light chain variable regions (Akerstrom and Bjorck, 1989). As the better known Protein A and Protein G do not have strong affinities for human Fabs (Tashiro and Montelione, 1995), Protein L was used to bind the κ light chain of our humanized Fab0.11.

Among the three conditions, the direct biotin-streptavidin linkage showed the best profile of cell recovery at all Fab concentrations (Fig. 3.9C). Even under saturating Fab conditions of 10 and 1 μg/mL, the direct biotin-streptavidin linkage gave better recovery than the indirect linkages. At the critical Fab concentration of 0.1 μg/mL, the biotin-streptavidin linkage recovered 20% more cells than secondary antibody linkage (Fig. 3.9C, $P < 0.05$, $n = 3$, unpaired t-test) and secondary antibody linkage recovered 40% more cells than Protein L linkage (Fig. 3.9C, $P < 0.001$, $n = 3$, unpaired t-test). The detection threshold also differed for the various linkages: to isolate >40% cells, Protein L linked beads required 1 μg/mL Fab, secondary Ab linked beads required 0.1 μg/mL, whereas direct biotin-streptavidin linked beads only required 0.01 μg/mL (Fig. 3.9C). Therefore, not only does the increase in the number of links between the

cell and bead lead to a decrease in immunomagnetic cell recovery, but the affinity of the secondary linking agent also has an effect on cell isolation. This effect is especially conspicuous when the number of bound Fab molecules (or similarly, the antigen expression on the cell surface) is low.

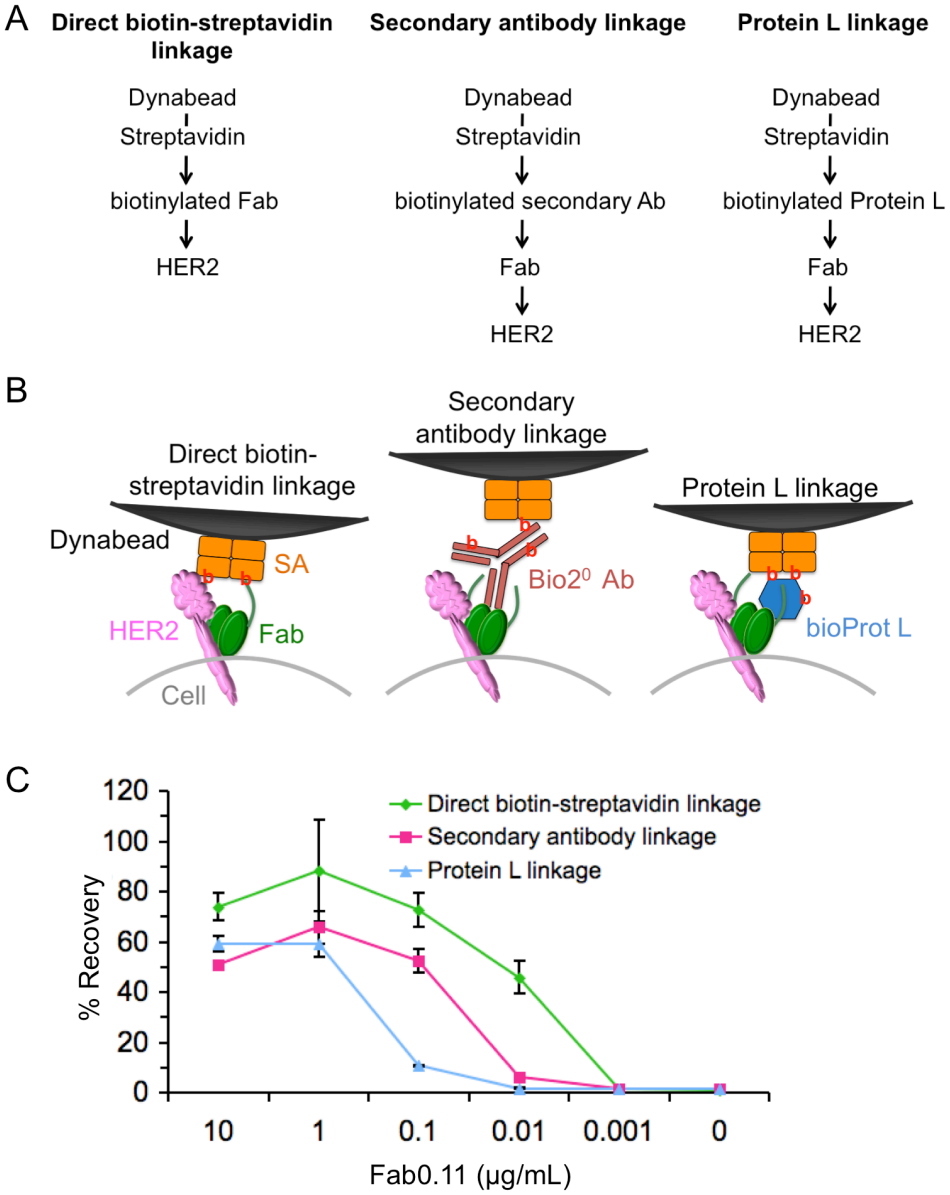

Figure 3.9. Dependence of cell recovery on cell-bead linkage. A. Flow diagram of the different linkages tested. From left to right: direct biotin-streptavidin linkage with biotinylated Fab0.11; Secondary antibody linkage with biotinylated secondary antibody binding non-biotinylated Fab0.11; Protein L linkage with biotinylated Protein L binding non-biotinylated Fab0.11. B. Pictorial representation of different linkages tested. In each case the same streptavidin-magnetic particles are used. C. Magnetic cell isolation efficiency using different linkages. BT474 were labelled with the indicated concentration of Fab0.11 and cell recoveries using the different linkages to the magnetic particle are shown (mean of triplicate ± 1 s.d.).

3.6 Decreasing the number of biotins per Fab fragment decreased immunomagnetic recovery

The final link to be tested was the biotin-streptavidin binding. Although the affinity of this interaction is extremely strong, the binding of biotin on the AP tags to streptavidin on the magnetic bead could be limited by the availability of biotins on the cell surface. Once the initial interaction between a few bound Fabs and the magnetic bead is made, more HER2 receptors with bound Fabs could be recruited to the cell-bead synapse, making the synaptic binding stronger. Based on this model, I wanted to test if reducing the number of AP tags from two to one on each Fab, while keeping the amount of Fab bound on cells the same, would reduce isolation efficiency.

We synthesized high affinity Fab0.11 with AP tag only on the heavy chain, termed Fab0.11-monobio, and confirmed complete biotinylation by SDS-PAGE (Fig. 3.10A). After Fab titration on BT474 cells, cells were isolated using streptavidin-beads and the recovery profiles of bis-biotinylated Fab0.11 and mono-biotinylated Fab0.11 were compared (Fig. 3.10B).

Mono-biotinylated Fab recovered fewer cells than bis-biotinylated Fab at all concentrations, although the difference was not significant at concentrations above 0.1 μg/mL (Fig. 3.10B, $P > 0.1$, $n = 3$, unpaired t-test), where both Fab types isolated more than 60% cells. The difference was maximum at 0.01 μg/mL, where mono-biotinylated Fab recovered 30% fewer cells than bis-biotinylated Fab. (Fig. 3.10B, $P < 0.001$, $n = 3$, unpaired t-test). Neither of the Fabs isolated cells at concentrations ≤ 0.001 μg/mL. Therefore, despite its high affinity, biotin binding to streptavidin may be a limiting factor, and needs to be further optimized for immunomagnetic cell isolation. There are now stronger binding streptavidin variants available and their use in immunomagnetic cell isolation might overcome such problems (Chivers et al., 2010).

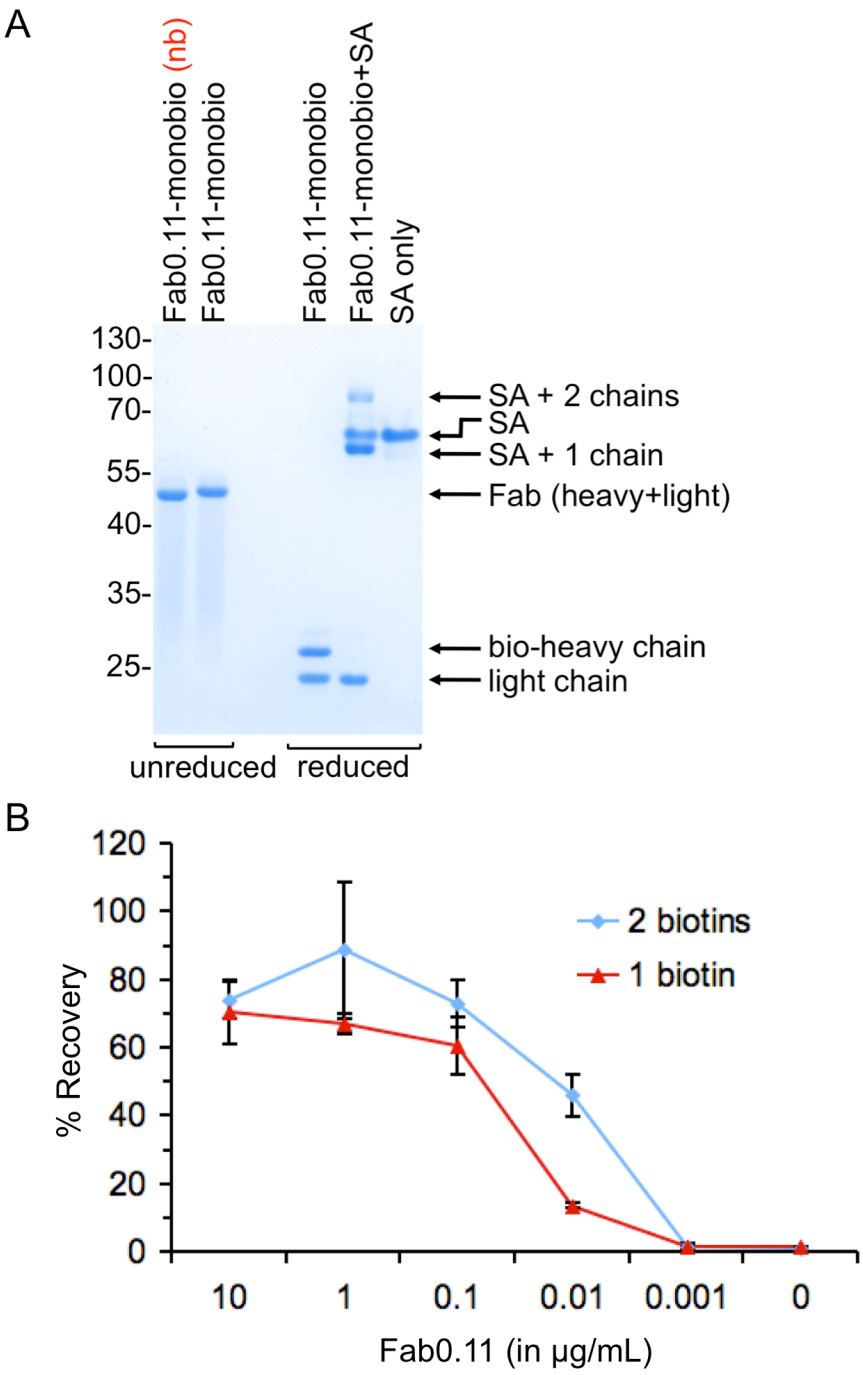

Figure 3.10. Dependence of cell recovery on the number of biotins per Fab. A. SDS-PAGE with Coomassie staining of mono-biotinylated Fab0.11. AP tag was inserted only in the heavy chain. On reduction and addition of streptavidin, only the biotinylated heavy chain showed a band-shift. B. BT474 were incubated with the indicated concentration of either bis-biotinylated Fab0.11 (2 AP tags) or mono-biotinylated Fab0.11 (1 AP tag) and recovered using SA-beads (mean of triplicate ± 1 s.d.).

3.7 Chemically biotinylated Fab0.35 recovered the same amount of cells as site-specifically biotinylated Fab0.35

Since genetically inserting the AP tag into Fabs and then expressing and purifying the modified Abs required knowing the Ab sequence and is time-consuming, it was essential to check if chemically biotinylated Fab is also efficient in immunomagnetic cell recovery. Most commercially available biotinylated antibodies (monoclonal and polyclonal IgG or antibody fragments) are generated by chemically modifying residues non-specifically to covalently bind biotin (Even-Desrumeaux and Chames, 2012). This is generally done by labeling primary amines such as lysines and N-terminal α-amines using biotin linked to N-hydroxysuccinimide esters (NHS-esters) (Fig. 3.11A). Sulfhydryl groups can also be targeted for biotinylation using sulfhydryl reactive groups such as maleimides, but these require disulfide bonds to be reduced and are therefore rarely used for biotin conjugation to complete antibodies, although it is a common way to conjugate biotin to Fabs.

To compare the immunomagnetic isolation efficiency of AP-tagged Fab versus chemically biotinylated Fab, I kept the affinity of the Fab constant (0.35 nM), and either biotinylated the Fab site-specifically by insertion of AP tags (termed Fab0.35 as before), or chemically by using biotin-NHS (termed Fab0.35-chemB) (Fig. 3.11A). Fab with the intermediate affinity of 0.35 nM was chosen so that any shift in cell recovery, higher or lower, could be easily detected. I had previously checked from the crystal structure that the HER2-hu4D5 binding interface did not contain any lysines (Cho et al., 2003), suggesting that NHS-mediated biotinylation of the Fab should not interfere with antigen binding.

The homogeneity and complete biotinylation of Fab0.35-chemB was checked on SDS-PAGE; as the Fab does not contain any AP tags, the band is seen at 45 kDa (Fig. 3.11B). Addition of streptavidin shifted the Fab0.35-chemB bands, both under non-reduced and reduced conditions, confirming biotinylation of both the heavy and light chains (Fig. 3.11B). As there are more than two biotins on each Fab, and there are four biotin-binding sites on streptavidin, multimers of Fab-streptavidin complexes can be seen in the gel shift assay (Fig. 3.11B).

For immunomagnetic isolation, site-specifically biotinylated Fab0.35 or Fab0.35-chemB was titrated onto BT474 cells, and streptavidin-beads were used to isolate the labelled cells. The recovery profile of Fab0.35-chemB was strikingly similar to that of site-specifically biotinylated Fab0.35 (Fig. 3.11C). Although Fab0.35-chemB gave slightly lower recovery at saturating Fab concentration of 1 μg/mL, the decrease was not significant (Fig. 3.11C, $P > 0.05$, $n = 3$, unpaired t-test). Both Fabs gave more than 50% recovery at Fab concentration of 10 μg/mL, 1 μg/mL and 0.1 μg/mL. More importantly, at the critical concentration of 0.01 μg/mL, both Fabs recovered ~10% cells. Chemically biotinylated primary antibodies with high affinities for their antigen can therefore in principle be used to immunomagnetically isolate cells with good efficiency.

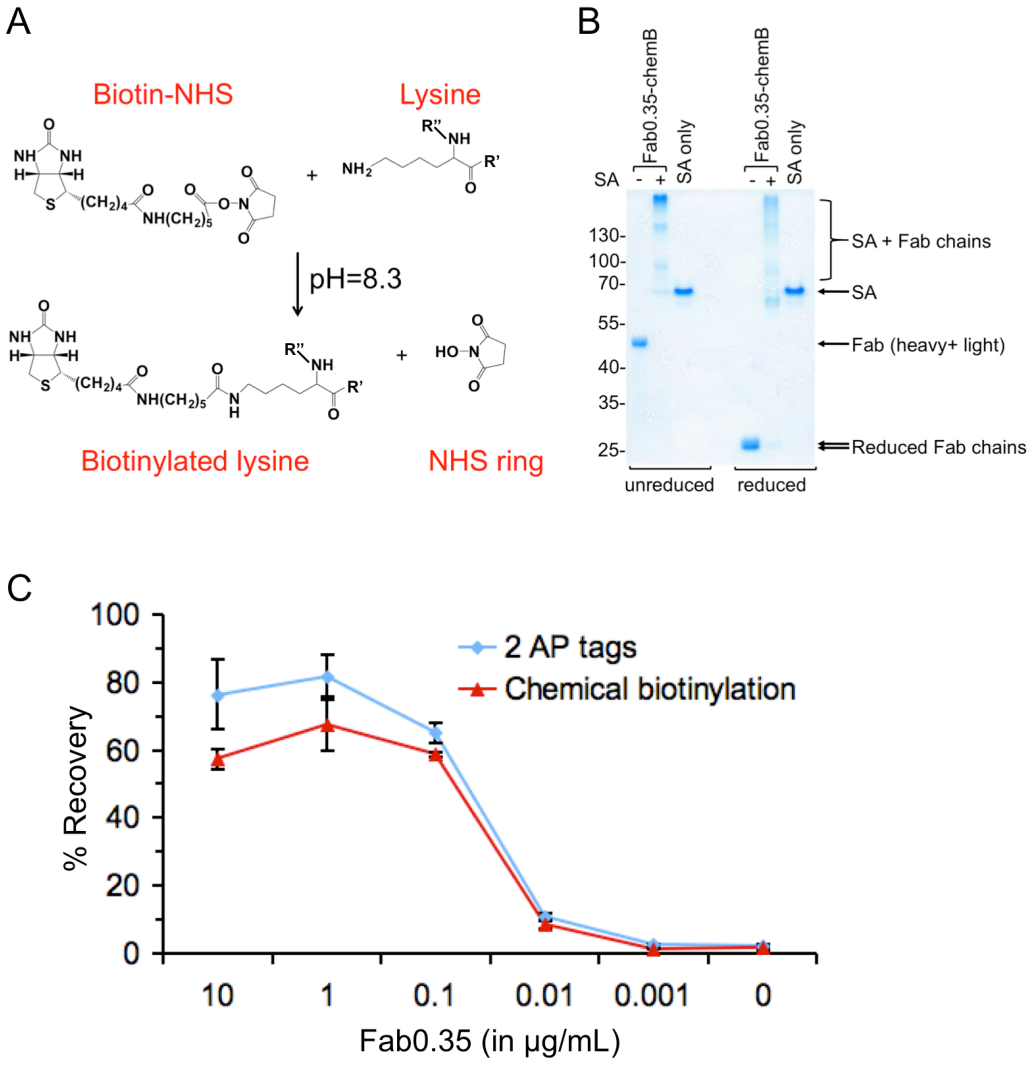

Figure 3.11. Isolating cells using chemically biotinylated Fab. A. Spontaneous amide bond formation between Biotin-NHS and lysine side chain. Biotin gets covalently attached to

lysine via the linker and NHS is a by-product. B. SDS-PAGE of chemically biotinylated Fab0.35 without or with reducing agent. Addition of streptavidin shifted both the Fab dimer and the individual Fab chains. C. BT474 were incubated with the indicated concentration of either the bis-biotinylated AP-tagged Fab0.35 or chemically biotinylated Fab0.35 before isolation with SA-beads. Cell recoveries are shown (mean of triplicate ± 1 s.d.).

3.8 Discussion

In this chapter, I first designed an anti-HER2 Fab that was site-specifically biotinylated and used it to isolate HER2 expressing cancer cells via streptavidin-coated magnetic beads. This model was then used to investigate how antigen number, antibody affinity, bead linkage, number of links and chemical biotinylation all have an effect on immunomagnetic cell isolation.

A clear dependence of antigen binding sites on cell isolation ability was established. From Figures 3.2-3.4 in this chapter, it is seen that by titrating in primary antibody with K_d= 0.35 nM, a minimum of 12,300 ± 370 connections needed to be made between a cell and magnetic bead for the cell to be isolated. This result can also be interpreted as the minimum number of HER2 molecules that need to be present on the cell; any cell expressing fewer than 12,300 receptors was beyond the isolation limit via Fab0.35. However, the Fab concentrations used in this experiment were 10-fold apart and therefore further characterization using more closely spaced Fab concentrations might give a more precise receptor value. The notion presented here, that of the necessity for a minimum number of connections for a cell to be isolated, has previously been explored in various other contexts. Cell surface receptor density has been suggested to act like a switch for particle capture, with a threshold value of >1,600 receptors per μm^2 of cell surface to isolate B cells using a 1 nM K_d biotinylated anti-CD19 antibody and streptavidin-magnetic beads (Sarda et al., 2004). Similarly, antibody binding capacity has also been shown to linearly affect the mobility of particle-bound cells in a magnetic field (McCloskey et al., 2000; Comella et al., 2001). Thus the number of antigens expressed on a cell is related to the cell's probability of being isolated in an affinity-based cell separation approach. This should be kept in mind when defining and quantitating various cell subtypes in cell isolation experiments. However, the limit posed by antigen density varies according to the affinity of the Fab used and, as seen in Fab affinity experiments, higher affinity Fabs can isolate cells expressing fewer antigens.

The second part of my data here suggests that antibody affinity is crucial in isolating low antigen-expressing cells. Monoclonal and polyclonal antibodies, produced in normal immune responses, have an affinity ceiling of around 10^{-10} M (Foote and Eisen, 1995). Figures 3.5–3.8 in this chapter describe the production and assessment of anti-HER2 Fab mutants with varying affinities. It is seen that immunomagnetic isolation increases with stronger affinity antibodies, but even a highly optimized Fab K_d = 0.35 nM is not enough. There have been enormous efforts to improve antigen-antibody affinity and other protein-protein interactions (reviewed in 1.1.5-1.1.8). However, such improvements in antibody affinity are not beneficial to targeting tumours for imaging or direct killing, as there is no improvement in sensitivity with antibody affinities beyond K_d=10 nM for such experiments (Wittrup et al., 2012). For simply delivering a dye or radioisotope to a tumour, there is minimal force favouring dissociation, and so antibody stability is less crucial. However, in cell isolation, the force between the ligand and its antibody must exceed the shear force between the cell and the magnetic bead, exercised by the flow of surrounding solution or the magnetic field (Dharmasiri et al., 2010). A sharp drop in antigen threshold from 12,300 ± 370 to 3,064 ± 220 can already be seen when using Fab0.11 instead on Fab0.35 for cell isolation (Fig. 3.4B and 3.8B). It is therefore important to assess antibody affinity when designing immunomagnetic cell isolation experiments and it will be valuable to consider the impact of recent antibody engineering techniques on cell isolation.

On investigating the other links between a cell and bead, it was found that apart from the primary antibody, any other weak interaction in the chain between target receptor and magnetic particle would also impair cell isolation. The direct and highly stable linkage between biotinylated primary Fab and streptavidin-coated beads, was much better at isolating cells bearing few primary Fabs. In comparison, the interaction between a primary monoclonal and secondary polyclonal antibody is much weaker ($K_d \approx$ 1-10 nM) (Foote and Eisen, 1995) than biotin-streptavidin interaction ($K_d = 4 \times 10^{-14}$ M) (Green 1990) and can therefore break more easily on induction of a magnetic field. A number of secondary antibody-coated magnetic particles are commercially available (Dynabeads by Invitrogen, MagnaBind by Thermo Fisher, MACS beads by Miltenyi Biotec.), but their affinities are rarely specified. Similarly, Protein L has a K_d=1.5 nM (Akerstrom and Bjorck, 1989), which is 100,000 times worse than the

biotin-streptavidin interaction. Secondary antibody-binding amplification in cell isolation has previously been investigated for its effects on magnetophoretic mobility of the cell, but not on isolation of low-expressing cells (McCloskey et al., 2001; Chosy et al., 2003). Introducing more proteins in the chain increases the number of points at which the chain can break, thereby reducing overall cell isolation efficiency. Thus the nature of linkage between the magnetic bead and the primary antibody has a dramatic effect on recovery of cells with low biomarker levels and should be optimized for increased cell isolation efficiency.

Although recombinant antibodies with site-specific enzymatic biotinylation were used in this project, regular monoclonal and polyclonal antibodies are generally functional after chemical biotinylation (Cho et al., 2007), and can therefore be used for streptavidin-based immunomagnetic capture of cells. To confirm the efficiency of chemical biotinylation, enzymatically biotinylated Fab0.35 was compared with chemically biotinylated Fab0.35-chemB and both were found to be equally efficient in immunomagnetic cell isolation. The AP tag projects 25 Å outwards, allowing for ample clearance from the Fab surface for the biotin to enter its binding site in streptavidin (Williams et al., 2008). Most chemically biotinylating reagents also consist of a long linker so that after conjugation to the protein, biotin is still easily accessible to its binding site in streptavidin. The use of biotin-streptavidin interaction is therefore advantageous for cell isolation and in future, it may also be interesting to explore antibody-bead interactions with even greater stability than streptavidin (Chivers et al., 2010; Haun et al., 2010; Zakeri et al., 2012).

Considering that the antibody affinity and bead type remain constant, the number of biotin molecules on the cell-surface could affect the number of beads bound to each cell and the strength of each cell-bead interaction. The number of biotin molecules on the cell-surface required for binding of streptavidin-coated beads has been determined using laser tweezers, but the force applied in this case is different from that of magnetic sorting and the biotin was chemically conjugated to surface proteins of live cells (Reichle et al., 2001). A recent study (Sarda et al., 2004) has also suggested that although several thousand receptors are involved in the cell particle contact at the end of the binding process, only eight bonds may be required for the initial capture of the particle. The dependence of cell-bead adhesion strength on individual bond numbers

in the contact area is assessed in Figure 3.10, where the same affinity Fab is inserted with 1 or 2 AP tags. Thus the number of Fab molecules per cell at each Fab concentration remains the same, but the number of biotins per cell is halved. It is seen that halving the number of biotins decreases the efficiency of immunomagnetic cell isolation. One explanation for this result could be that fewer biotins on cell surface make fewer initial contacts with the streptavidin bead, thereby leading to fewer bead cell interactions. However, it could also be hypothesized that fewer biotins leads to fewer individual contacts at each bead-cell synapse, thereby making the interaction weaker and prone to dissociation under magnetic force. However, further experiments need to be carried out to explore this mechanism.

The issues analysed in this chapter can also be applied to various other approaches where antibody recognition is used to attach cells to a solid-phase, such as cell isolation using antibody-coated pillars on a CTC-chip (Nagrath et al., 2007) or CTC trapping for detection within the bloodstream (Galanzha et al., 2009). Although HER2 and hu4D5 formed a good model to explore the cell-bead interaction because of the well-characterized Fab mutant series, it might be interesting to study other cancer related cell surface proteins such as EpCAM and EGFR, as they are also often used as target antigens to isolate cancer cells (Yu et al., 2011). Another major variable that should be kept in mind during cell isolation is the size of the magnetic bead. Here I used 2.8 μm Dynabeads, but a number of other magnetic particles with varying sizes are also available for various cell-sorting protocols (4.5 μm and 5 μm Dynabeads, Invitrogen; 50 nm MACS beads, Miltenyi Biotec). We used BT474 cells and titrated the Fab level as a proxy for cells with different levels of antigen expression. However, different cell-lines also differ in a number of other cell-related variables such as size, shape, membrane fluidity, cell signalling and these might also affect the way a bead binds to the cell. It is therefore important to study the cell-related aspects of immunomagnetic isolation, so that efficient capture of cells is possible independent of antigen down-regulation.

Chapter 4: Enhancing Immunomagnetic recovery of cells with low antigen expression levels

Exploring the cellular parameters affecting immunomagnetic cell isolation and
improving recovery of cancerous cells from blood

Chapter 4: Enhancing Immunomagnetic recovery of cells with low antigen expression levels

Exploring the cellular parameters affecting immunomagnetic cell isolation and improving recovery of cancerous cells from blood

4.1 Introduction

Exploring protein interactions between a cell and magnetic bead provided useful insights on how this interaction between a live cell and solid phase could be carefully optimized to ensure force-resistant and secure binding. Having investigated the antibody affinity and linking parameters, it was also important to explore how the structure and dynamics of the cell membrane affected receptor binding to the magnetic bead. An initial weak interaction between the cell and bead could be consolidated as new receptors are recruited to the cell-bead interface by diffusing through the membrane (Sarda et al., 2004). As this recruitment of receptors to the cell-bead synapse is controlled by various cytoarchitectural and membranal factors, I set out to research these factors by inhibiting certain cell processes and studying how they affected magnetic sorting.

HER2 was continued to be used as the cancer cell biomarker, as I had already constructed and characterized the antibody affinity series against it. Using the high affinity biotinylated Fab0.11 would allow a strong protein interaction between the cell and bead, while being able to alter and study cellular processes. The main aim of this work was to identify ways in which immunomagnetic recovery could be enhanced. Once the different ways in which immunomagnetic recovery of cells could be improved were established, the enhanced protocol could be tested on different cancer cell-lines, varying in HER2 expression levels, and used to isolate low HER2 expressing cells. Cancer cells circulating in the peripheral blood, or CTCs, are isolated from the blood of patients with metastatic disease, as cancer prognosis guide (O'Flaherty et al., 2012). Therefore, to demonstrate the advantage of my approach, the enhanced approach was applied to recover low HER2 expressing cells, which could not be isolated using the standard approach, from whole blood.

4.2 Effects of modifying cytoskeletal rigidity, cell membrane fluidity and HER2 activation status on immunomagnetic cell isolation

To assess the different ways in which cell membrane dynamics could affect immunomagnetic binding, I used a series of small molecules to modify membrane structure and fluidity.

4.2.1 Cytoskeletal modifications did not affect immunomagnetic cell isolation

According to the picket-fence model, the plasma membrane of a cell is a partitioned fluid with actin-based membrane-skeleton "fences" and anchored transmembrane protein "pickets", which together form compartment boundaries (Kusumi et al., 2005). Protein diffusion in the membrane is controlled by the actin-based cytoskeleton and its associated protein "pickets" through their partitioning and tethering effects (Kusumi et al., 2005).

To disrupt this network, thereby disturbing the movement of HER2 in the membrane, I incubated BT474 with actin inhibitor cytochalasin D for 1 hr, before immunomagnetically isolating the cells. Cytochalasin D is a fungal metabolite that sequesters actin monomers, binding and blocking the barbed ends of actin filaments, thereby inhibiting actin polymerization (Fenteany and Zhu, 2003). 0.01 μg/ml Fab0.11, which only partially recovers BT474 cells (Fig. 3.7C), was used so that even slight changes in cell-bead interaction could have a big effect on cell recovery. Fab-labelled cells were isolated using streptavidin-beads, and the recovery was calculated as the fold change compared to the DMSO control. Cytochalasin D slightly increased recovery, but its effect were not statistically significant (Fig. 4.1A, $P = 0.06$, $n = 3$, unpaired t-test).

Microtubules play a vital role in cell shape, cell movement through structures like cilia and flagella, intracellular transport of proteins and vesicles and also connect to actin dynamics (Fenteany and Zhu, 2003). To understand the role of microtubules in controlling the efficiency of magnetic bead binding, I added the microtubule destabilizer nocodazole. BT474 cells were incubated with the drug for 1 hr before labelling with 0.01 μg/ml Fab0.11 and isolating using streptavidin-beads (Fig. 4.1B). It was found that microtubule depolymerization did not affect cell isolation (Fig. 4.1B, $P = 0.4$, $n = 3$, unpaired t-test).

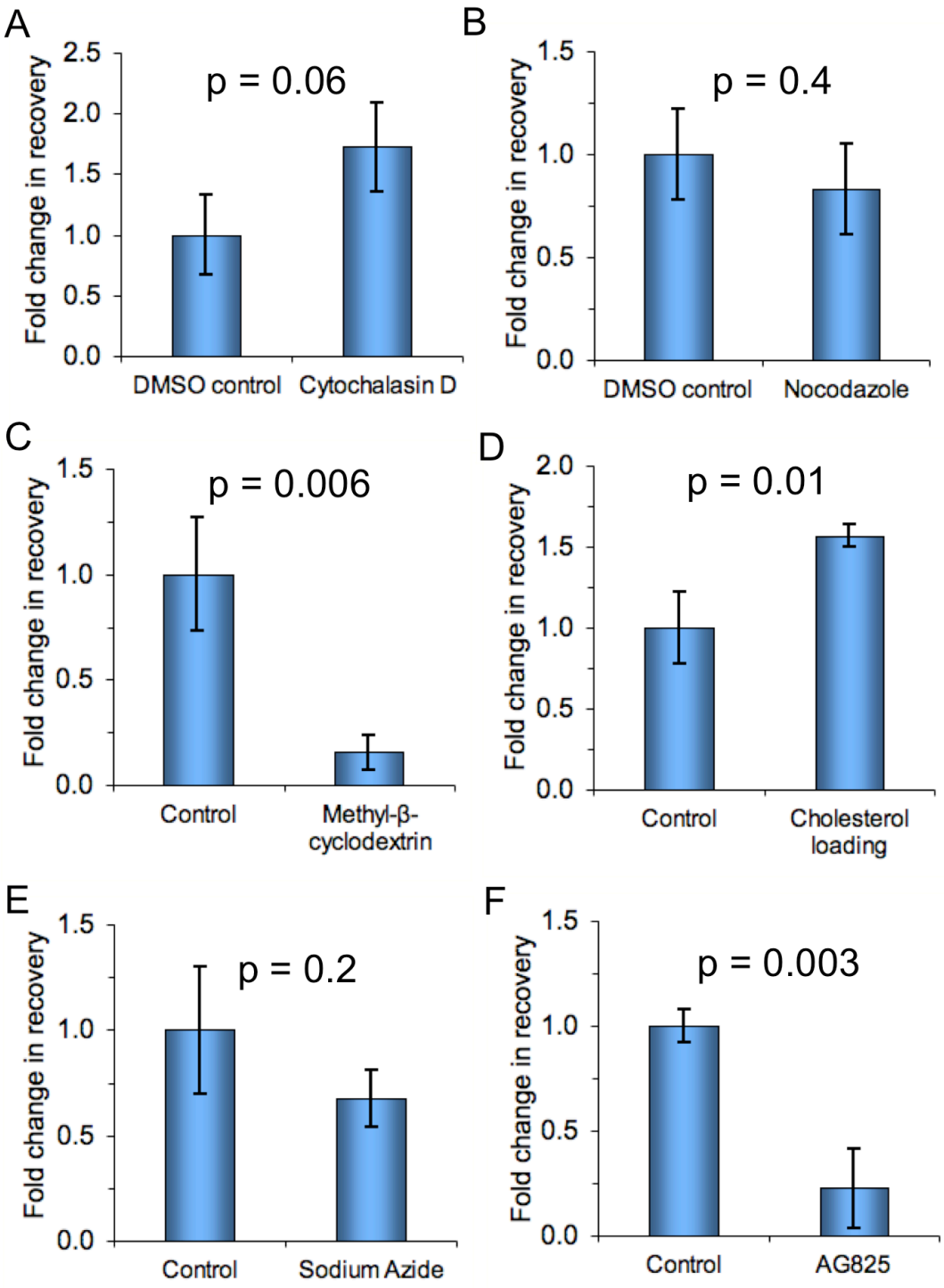

Figure 4.1. Effect of small molecules on immunomagnetic cell recovery. BT474 cells were incubated with the indicated drug or appropriate DMSO/water control for 1 hr before labelling with 0.01 μg/mL Fab0.11 and isolating with SA-beads. Results are represented as the fold change in recovery, with the control sample normalized to one (mean of triplicate ± 1 s.d.). A. 50 μM cytochalasin D. B. 16.5 μM nocodazole. C. 10 mM methyl-β-cyclodextrin. D. 250 μg/mL water-soluble cholesterol. E. 1 mM sodium azide. F. 10 μM AG825. *P* values were calculated using unpaired t-tests, $n = 3$.

4.2.2 Modifications to the cell membrane fluidity changed isolation efficiency

HER2 and other ErbB receptors are sometimes found to be associated with lipid rafts in the cell membrane (Nagy, 2002). According to the shell model, lipid rafts are membrane microdomains that are enriched in cholesterol and regulate membrane fluidity and interaction with surface proteins (Jacobson et al., 2007). Cholesterol has also been shown to control the movement of HER2 in the plane of the cell membrane (Orr et al., 2005).

Since cholesterol depletion confines receptor movement (Orr et al., 2005), I used methyl-β-cyclodextrin to decrease BT474 membrane cholesterol content. Methyl-β-cyclodextrin is a cyclic oligosaccharide with a hydrophilic exterior and a hydrophobic internal cavity (Christian et al., 1997) and has high affinity for sterols. This makes methyl-β-cyclodextrin effective as a cholesterol complexing agent and for modifying the cholesterol content of cells (Christian et al., 1997). Incubating BT474 cells with methyl-β–cyclodextrin for 1 hr, labelling with 0.01 μg/ml Fab0.11 and then isolating using SA-beads led to a striking decrease in cell recovery when compared to the untreated cells (Fig. 4.1C, $P < 0.01$, $n = 3$, unpaired t-test).

On further investigation, it was found that the converse is also true. I wanted to improve cell isolation, so I added excessive cholesterol to cells for 1 hr, in the presence of methyl-β–cyclodextrin. Methyl-β–cyclodextrin chelates cholesterol making it water soluble and so enables effective loading of cholesterol onto the cell membrane (Christian et al., 1997). Thereafter I labelled cells with 0.01 μg/ml Fab0.11 and isolated using SA-beads. Interestingly, cell isolation improved by more than 50% (Fig. 4.1D, $P < 0.05$, $n = 3$, unpaired t-test).

4.2.3 Receptor kinase activity but not cell metabolic activity decreased cell isolation

To investigate the contribution of the cell's metabolic activity to trafficking of HER2 to and from plasma membrane, and HER2-Fab binding, I inhibited cellular active processes using sodium azide. Sodium azide leads to rapid depletion of cellular ATP and is commonly used as a component of buffers for flow cytometry. Cell viability remained high over the period of measurement. Previously sodium azide has been shown to increase cell recovery by 15%, by increasing the number of magnetic particles bound to cells (Sarda et al., 2004). However, in my experiments, a small

decrease in recovery was observed with sodium azide treatment of BT474 cells, although the change did not reach significance (Fig. 4.1E, P =0.2, n = 3, unpaired t-test).

Activation of ErbB receptors increases their movement in the cell membrane and changes their clustering patterns (Abulrob et al., 2010; Nagy et al., 2010) . To evaluate the effect of inhibiting HER2 kinase activity, I used the small molecule tyrphostin AG825, which inhibits the HER2 tyrosine kinase domain by competing with ATP binding (Osherov et al., 1993) but may also have non-specific suppressive effects on certain signalling pathways such as gp130/STAT3 signalling (Lee et al., 2008). When incubated with AG825 for 1 hr before immunomagnetic isolation, cell recovery decreased dramatically (Fig. 4.1F, $P < 0.01$, n = 3, unpaired t- test), implying that HER2 kinase activity plays an important role in beading efficiency.

4.3 Further investigation of the role of cholesterol in increasing cell isolation

4.3.1 Addition of cholesterol did not affect surface HER2 expression level

Adding cholesterol to cells increased the efficiency of their immunomagnetic isolation (Fig. 4.1 D). However, the causation of this increase was not clear. There are a number of hypotheses that could explain this improvement in immunomagnetic cell isolation. Firstly, the HER2 surface expression could be modified by cholesterol content, either in terms of the total number of surface HER2 receptors or the way they are distributed in the cell membrane. An increase in receptor clustering could lead to stronger bead-cell synapses. Secondly, as cholesterol content affects the mechanical properties of the cell membrane and has been shown to influence the stiffness of membrane tethers (Khatibzadeh et al., 2012), addition of cholesterol could make the cell-bead synapse more mechanically flexible and less prone to tearing apart in the presence of the force from a magnetic field. Cholesterol content could also affect the activation status of HER2 and its endocytosis, as cholesterol influences downstream signalling in cells and has been associated with the migration, invasion and angiogenesis of breast cancer cells (Raghu et al., 2010). Unfortunately, due to time constraints and the limited scope of my project, it was not possible to test all of these hypotheses individually.

However, keeping in mind my bigger aim of increasing immunomagnetic isolation of lower antigen expressing cells, it was important to check if cholesterol content changed HER2 expression levels in cells. To test this hypothesis and to understand whether the change in cell recovery related to a change in the amount of Fab0.11 bound to cells, I detected bound Fab0.11 using flow cytometry (Fig. 4.2A and B). BT474 cells were treated with methyl-β–cyclodextrin or cholesterol loading and allowed to bind 0.01 μg/ml Fab0.11. The bound Fab was detected using streptavidin conjugated to phycoerythrin (SA-PE). For each condition, there was a no Fab control to make sure that the background signal in the absence of Fab0.11 was the same in the three conditions. Overall, Fab binding did not change substantially with change in cholesterol content (Fig. 4.2A and B). Treating cells with methyl-β–cyclodextrin decreased Fab0.11 binding by 17% ($P < 0.001$, $n = 3$, unpaired t-test) and cholesterol loading increased Fab0.11 binding by only 9% ($P < 0.001$, $n = 3$, unpaired t-test).

4.3.2 Increasing incubation time with cholesterol further improved cell isolation

I also wanted to check if loading the cells for more time with cholesterol would further increase isolation efficiency. Therefore, I added the same amount of methyl-β –cyclodextrin and cholesterol (as in Fig. 4.1C and 4.1D) but incubated for 3 hr (as compared to 1 hr in Fig. 4.1). Again, depleting cholesterol decreased recovery by 5-fold (Fig. 4.2C, $P < 0.01$, $n = 3$, unpaired t- test), and adding cholesterol led to an 80% increase in recovery ((Fig. 4.2C, $P < 0.05$, $n = 3$, unpaired t- test). This increase was higher than when cells were incubated for 1 hr (50% increase in isolation efficiency). Therefore, incubating cells with cholesterol for a longer period of time slightly increased the isolation efficiency.

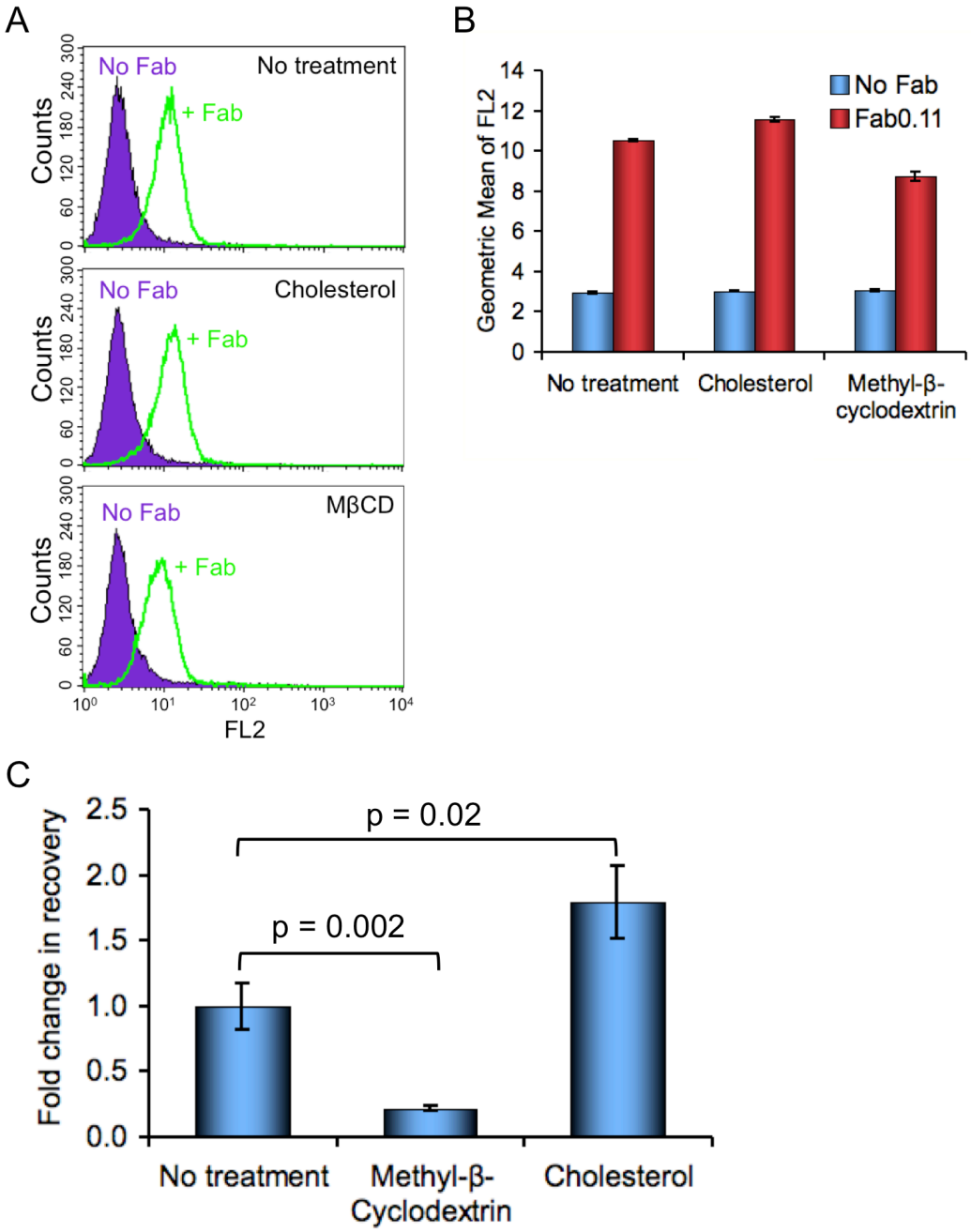

Figure 4.2. Investigating the role of cholesterol in increasing cell recovery. A. Change in HER2 staining with cholesterol loading or depletion. Flow cytometry of BT474 cells untreated, loaded with 250 µg/mL cholesterol or depleted of cholesterol with 10 mM methyl-β-cyclodextrin for 1 hr at room temperature, before labelling surface HER2 with 0.01 µg/mL mono-biotinylated Fab0.11 and staining with 0.41 µM streptavidin-phycoerythrin (in green). Each condition had a control in which no Fab was added (in purple). B. Graph of the geometric mean fluorescence of samples from A (mean of triplicate ± 1 s.d.). C. Change in cell recovery with cholesterol loading or depletion. BT474 cells were treated with 10 mM methyl-β-cyclodextrin or 250 µg/mL cholesterol for 3 hr, before labelling with 0.01 µg/mL Fab0.11 and isolating with SA-beads. Results are represented as the fold change in recovery, with the control sample normalized to one (mean of triplicate ± 1 s.d.). *P* values were calculated using unpaired t-tests, $n = 3$.

4.4 Assembling a cell-line panel with varying levels of HER2

Having investigated the different parameters affecting cell-bead interaction and from the data presented in the previous chapter, I found that cell isolation efficiency could be enhanced by the following three steps: 1.) Using a high affinity biotinylated Fab, with K_d in the sub-nanomolar range, 2.) Decreasing the number of links between the cell and bead by using the direct high-affinity biotin-streptavidin binding, and 3.) loading cells with cholesterol.

To test if these enhanced conditions could help isolate cancer cells expressing lower levels of antigen, I assembled a panel of various human cancer cell-lines, spanning a wide range of HER2 expression (Fig. 4.3). BT474 cells, with their high HER2 expression, were used as the standard positive. MDA-MB-453 cells derived from the pericardial effusion of a breast cancer patient, express medium levels of HER2 (Brinkley et al., 1980; McCabe et al., 2005; Rusnak et al., 2007). MCF-7 is also a breast cancer cell-line, expressing very low levels of surface HER2 (McCabe et al., 2005; Rusnak et al., 2007), such that the HER2 expression is often not detected on Western blots and by immunocytochemistry (Bayraktar et al., 2011; Ignatiadis et al., 2011). A431 is an epidermoid carcinoma cell-line also expressing low levels of HER2 (Rusnak et al., 2007; Larson et al., 2010). I used MDA-MB-468 as the HER2-negative cell-line (Brinkley et al., 1980; Rusnak et al., 2007).

To confirm HER2 expression levels of the cell-line panel, I labelled cell surface HER2 with mono-biotinylated Fab0.35, and detected the binding using mSA-488 by flow cytometry. mSA-488 is monovalent streptavidin that binds in a 1:1 ratio with the mono-biotinylated Fab0.35 (Fig. 3.3B). As both Fab0.11 and Fab0.35 bind cells equally well (Fig. 3.4C and Fig. 3.8C), either of these two could be used for quantification. The flow cytometry representation in Fig. 4.4A allowed us to compare HER2 levels and it was seen that HER2 levels decreased in the following descending order: BT474, MDA-MB-453, MCF-7, A431 and MDA-MB-468. It should also be noted that the autofluorescence (no Fab control) in each cell-line differed, and was therefore deducted individually for each cell-type. I further quantified the absolute number of HER2 binding sites on the cancer cells using MESF-488 beads (as done previously in Fig. 3.4): BT474 cell had 735,000 ± 17,000 anti-HER2 antibody binding sites per cell (Fig. 4.4B). MDA-MB-453 had 6.5 times fewer HER2 binding sites.

MCF-7 and A431 had only 15,300 ± 160 and 12,300 ± 36 bound Fab/cell respectively, and the level of Fab0.35 bound to MDA-MB-468 cells was not significantly different from zero, thereby confirming their HER2-negative status (Fig. 4.4B).

I then used this cell panel, spanning a few orders of magnitude of HER2 expression, to assess the efficiency of the enhanced immunomagnetic cell isolation approach on isolating low-expressing cells. The different cell-lines also allowed me to evaluate the protocol's efficiency across various cell-types which may differ in shape, size and cellular dynamics.

Cell type	Origin	HER2 level
BT474	Breast cancer cell line from invasive ductal carcinoma	High
MDA-MB-453	Metastatic breast carcinoma cell line	Medium
MCF-7	Breast adenocarcinoma cell line	Low
A431	Epidermoid carcinoma cell line	Low
MDA-MB-468	Metastatic breast adenocarcinoma cell line	Negative

Figure 4.3. Panel of human cancer cell-lines used in this study. Details of cancer cell-lines with their origin and surface HER2 expression level.

A

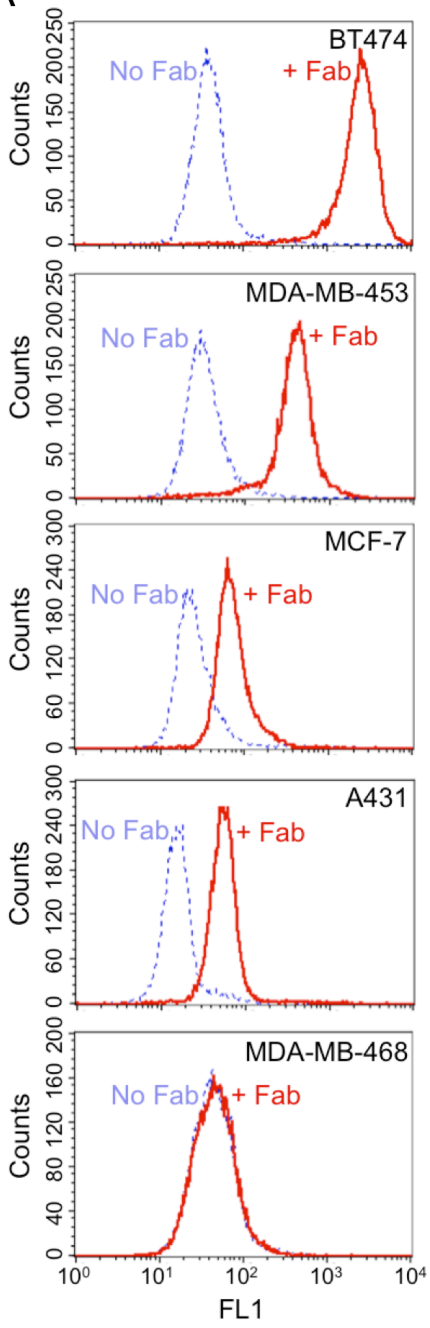

B

Cell-type	Fab bound per cell (mean ± 1 s.d., *n* = 3)
BT474	735,000 ± 17,000
MDA-MB-453	112,000 ± 1,900
MCF-7	15,300 ± 160
A431	12,300 ± 36
MDA-MB-468	19 ± 27

Figure 4.4. Quantifying surface HER2 expression on different cell-types. A. Indicated cells were labelled with or without 10 μg/mL mono-biotinylated Fab0.35, and detected with mSA-488, for quantitating surface HER2 by flow cytometry. 488 MESF beads were used to calibrate fluorescence units versus 488 dye numbers. B. Relation between cell-type and the calculated number of anti-HER2 binding sites per cell.

4.5 Using enhanced conditions to immunomagnetically recover cell-types with varying antigen expression levels

The standard approach of isolating cells based on affinity capture generally uses a primary antibody against the target antigen and then detects the binding using a secondary antibody that is either conjugated directly to the solid phase or via a strong protein interaction such as biotin-streptavidin (McCloskey et al., 2001; Antolovic et al., 2010; Mikolajczyk et al., 2011).

To mimic these existing standard approaches for cancer cell isolation, I used the high affinity Fab0.35 and anti-human biotinylated secondary antibody linked to streptavidin-coated magnetic beads. For the enhanced condition, I used the higher affinity Fab0.11 that was directly biotinylated, linkage through streptavidin on magnetic beads, and cholesterol loading on cells. I used the high Fab concentration of 1 μg/ml so that all HER2 binding sites were saturated.

For the high HER2-expressing BT474 cells, both the standard and enhanced protocols gave equally high recovery (Fig. 4.5). For the moderate HER2-expressing MDA-MB-453 cells, enhanced conditions gave a 20% higher recovery than standard conditions (Fig. 4.5, $P < 0.01$, $n = 3$, unpaired t-test). However, with the low expressing MCF-7 cells, the improvement with enhanced conditions was even higher as it doubled the percentage of cells recovered (Fig. 4.5, $P < 0.001$, $n = 3$, unpaired t-test). Finally for the very low HER2 expressing A431 cells, the standard approach isolated only 3% of cells, whereas the enhanced approached gave a more than 8-fold higher isolation efficiency (Fig. 4.5, $P < 0.001$, $n = 3$, unpaired t-test), making A431 cells easily differentiable from the HER2 negative MDA-MB-468 cells. Both protocols isolated less than 2% of the MDA-MB-468 cells, thereby confirming their specificity for HER2 (Fig. 4.5).

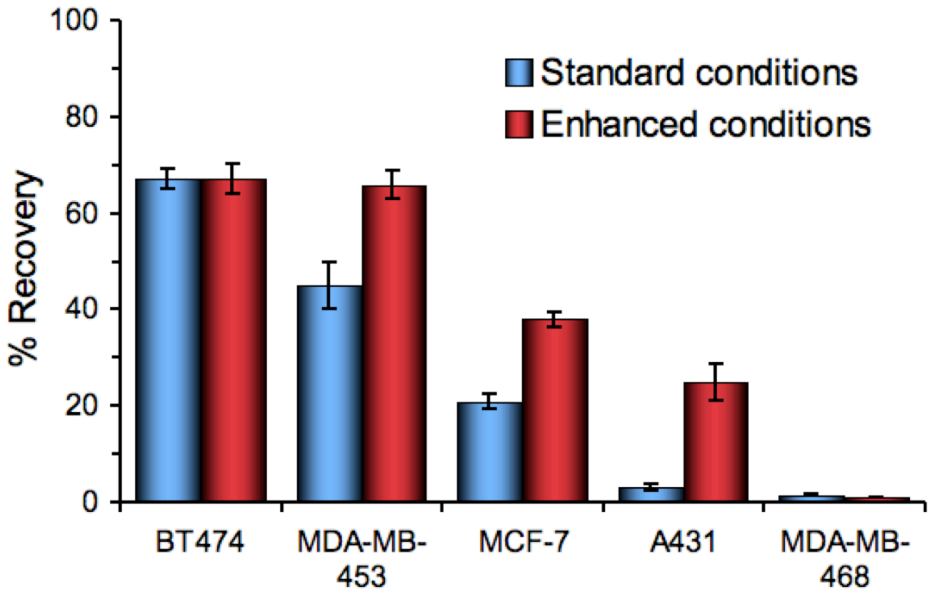

Figure 4.5. Comparing standard and enhanced conditions to immunomagnetically isolate various cell-types. Under the standard conditions, cells were labelled with 1 μg/mL non-biotinylated Fab0.35, and recovered using streptavidin magnetic beads coated with biotinylated secondary antibody. For the enhanced conditions, cells were loaded with cholesterol for 1 hr, labelled with 1 μg/mL biotinylated Fab0.11 and isolated using streptavidin-beads. Cell recovery is shown as the mean of triplicate ± 1 s.d.

To break down the contribution of each enhancement and to check how each of the three improvements affected the high, medium and low HER2 expressing cells, the enhanced parameters were changed independently. In Fig. 4.6A, using the same amount of biotinylated Fab, comparing Fab0.35 or Fab0.11, the various cell-types were isolated with SA-beads (by laboratory member Gianluca Veggiani, 2012). The improvement in affinity increased the recovery of A431 cells by 30% (Fig. 4.6A, $P < 0.01$, $n = 2$, unpaired t-test), but did not affect the recovery of other cells. Next, keeping the same affinity Fab0.11, either the direct linkage with biotinylated Fab0.11 and SA-beads, or secondary antibody linkage with non-biotinylated Fab0.11 and biotinylated secondary antibody linked to SA-beads, was used (by laboratory member Gianluca Veggiani, 2012) (Fig. 4.6B). The direct linkage enhanced the recovery of MCF-7 by 20% (Fig. 4.6B, $P < 0.05$, $n = 2$, unpaired t-test) and A431 by 30% (Fig. 4.6B, $P < 0.01$, $n = 2$, unpaired t-test). Finally, using biotinylated Fab0.11 and SA-beads, I loaded cells with cholesterol and compared to unloaded cells (Fig. 4.6C). Cholesterol loading increased A431 recovery by more than 2-fold (Fig. 4.6C, $P < 0.05$, $n = 3$, unpaired t-test). Thus, all three changes made to the beading protocol

enhanced the recovery of low HER2-expressing cells. None of the enhancements increased the recovery of MDA-MB-468 cells, thus verifying that the improvements did not increase non-specific background recovery.

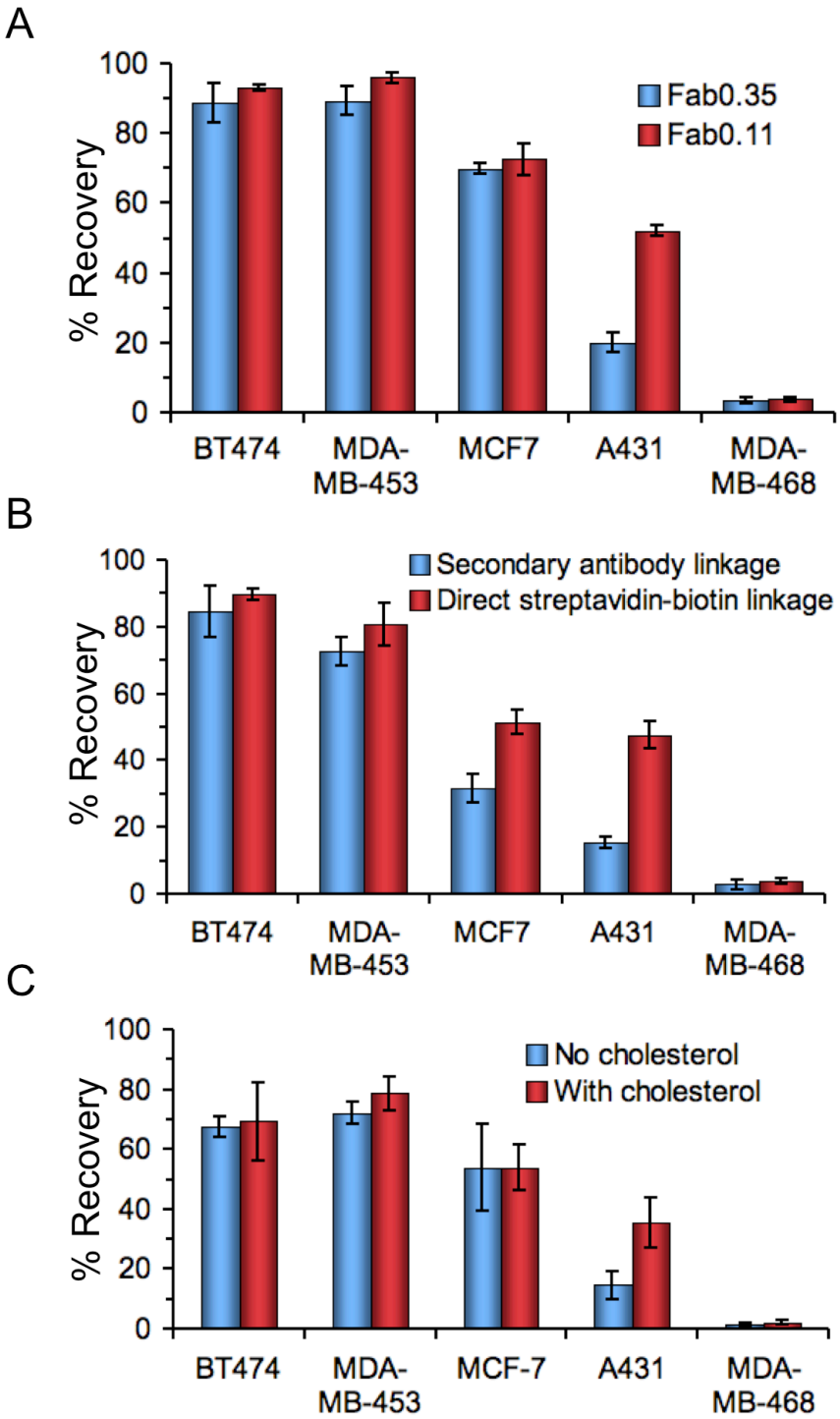

Figure 4.6. Effect of individual modifications on recovery of different cell-lines. A. Cells were incubated with 1 μg/mL biotinylated Fab0.35 or Fab0.11 and recovered using streptavidin-beads (mean of duplicate measurements ± 1 s.d.) (Data from G. Veggiani). B. For secondary antibody linkage, cells were labelled with 1 μg/mL non-biotinylated Fab0.11

and isolated using streptavidin beads coated with secondary antibody. For direct linkage, cells were labelled with biotinylated Fab0.11 and isolated with streptavidin beads. % Recovery is shown as the mean from duplicate measurements ± 1 s.d. (Data from G. Veggiani). C. Cells were incubated with or without 250 μg/mL cholesterol for 1 hr at room temperature before labelling with 1 μg/mL biotinylated Fab0.11 and magnetic isolation using streptavidin-magnetic particles (mean from triplicate measurements ± 1 s.d.).

4.6 Using the enhanced immunomagnetic approach to recover cancerous cells from rabbit blood

Once the improvement in cell recovery under enhanced conditions was confirmed, it was important to check the efficiency of the enhanced approach in isolating cancerous cells from blood. Circulating tumour cells are typically isolated from a 10 mL sample of patient blood using CellSearch or microfluidic chambers (Kling, 2012). Since the concentration of CTCs in peripheral circulation can be extremely low (one CTC in 10^6-10^7 mononuclear cells), highly sensitive isolation approaches are desired (Sun et al., 2011). To validate the enhanced protocol for isolating cells from blood, I performed cell spiking experiments in rabbit blood.

Cancer cell-lines were first labelled with carboxyfluorescein diacetate, succinimidyl ester (CFSE) to make them easily traceable and then spiked into rabbit whole blood (Fig. 4.7). The sample was then treated like a patient blood sample; the red blood cells were lysed and removed and the remaining cell mixture containing cancer cells, white blood cells and a few unlysed red blood cells was resuspended in DMEM (Fig. 4.7). Cancer cells from the cell mixture were then immunomagnetically isolated under either the standard or enhanced condition, counted and their identity confirmed on the basis of CFSE labelling by microscopy.

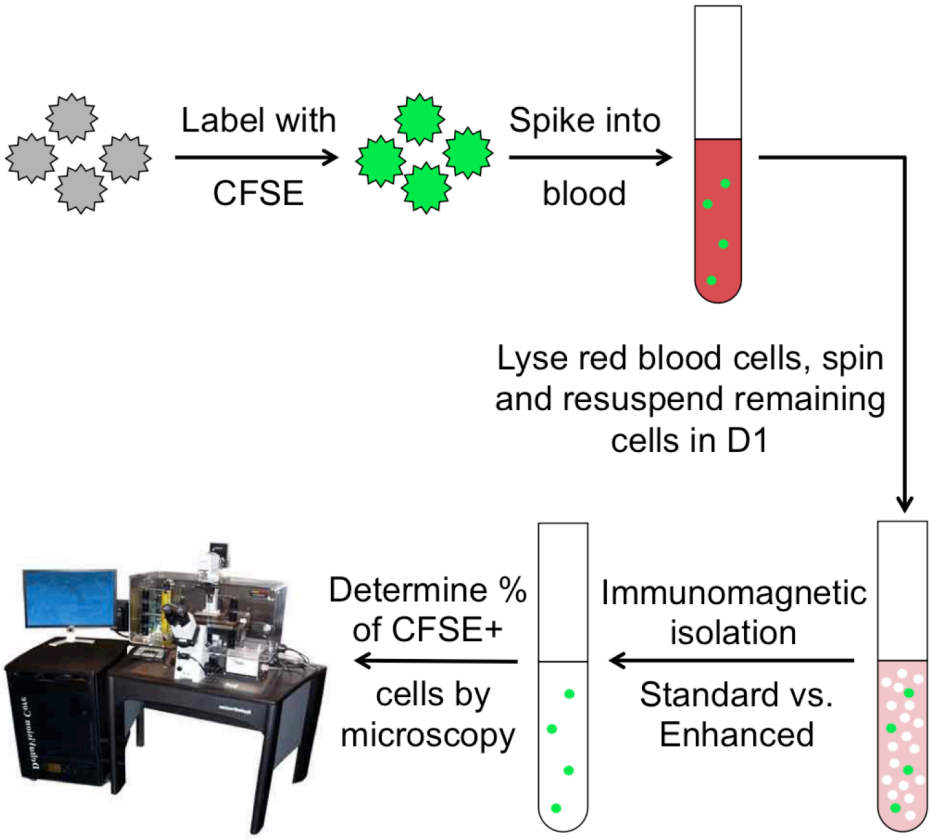

Figure 4.7. A schematic representation of cell spiking into blood. To mimic CTC isolation, cancer cells were spiked and recovered from blood. Cells were labelled with tracer dye CFSE, before spiking into 1 mL rabbit whole blood. Red blood cells were lysed using a hypotonic solution, discarded after centrifugation and the remaining cell mix containing the labelled cancer cells (green) and remaining white blood cells (white) was resuspended in DMEM with 1% FCS (D1). Cancer cells were then recovered from the blood cell mixture using the standard or enhanced immunomagnetic isolation protocol. Recovered cells were checked for CFSE labelling by fluorescence microscopy.

BT474, MCF-7 and A431 cells were spiked and recovered from rabbit blood (Fig. 4.8A). The standard protocol recovered >70% of high HER2 expressing BT474 cells, but recovered less than 5% of low HER2 expressing MCF-7 and A431 cells (Fig. 4.8A). On the other hand, under enhanced conditions, more than >70% of all three cancer cell-types were recovered from rabbit blood, regardless of the variation in their HER2 expression. This increase (Fig. 4.8A, MCF-7 $P < 0.0001$, A431 $P < 0.001$, $n = 3$, unpaired t-test) in recovery using enhanced conditions was more prominent in isolation from blood than in isolation from cell media, where some MCF-7 and A431 cells could be recovered even under standard conditions (Fig. 4.5). To ensure that the recovery was not due to non-specific binding of the magnetic beads in blood, I applied enhanced conditions to isolate cancerous cells from rabbit blood, in the

absence of Fab0.11 (Fig. 4.8B). No cells were recovered, consistent with HER2 specificity of the protocol. On checking the CFSE status of the recovered cells by microscopy, it was found that almost all recovered cells were CFSE-positive (BT474 98.3 ± 1.6%, n = 3; MCF-7 98.9 ± 1.9%, n = 3; A431 99.2 ± 1.4%, n = 3). The conditions gave minimal isolation endogenous blood cells, thereby allowing a high purity of recovery of the spiked cancer cells.

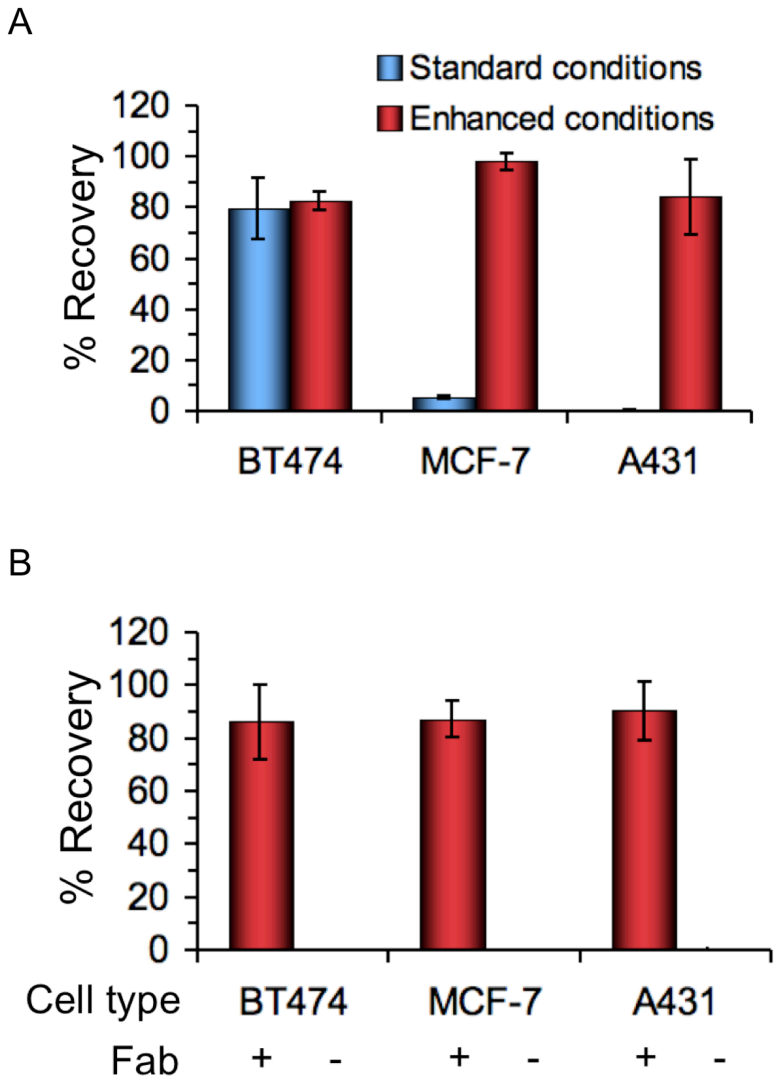

Figure 4.8. Cancer cell isolation from rabbit blood. Rabbit blood was spiked with the different cell-types varying in HER2 expression level. A. Cells were isolated using either the standard or enhanced approach, as described in Fig. 4.5. % Recovery is shown as the mean from triplicate measurements ± 1 s.d. B. To check the specificity of the enhanced approach, cell-lines were spiked into rabbit blood and recovered under enhanced conditions, with or without the biotinylated Fab0.11. No cells were recovered in the absence of Fab0.11 (mean from triplicate measurements ± 1 s.d.).

4.7 Using enhanced immunomagnetic approach to recover low HER2 expressing cells from human blood

The enhanced conditions were further used to isolate cancerous cells from human blood. MCF-7, A431 and HER2-negative MDA-MB-468 cells were spiked into human blood and the recoveries of cells using standard or enhanced protocols were compared (Fig. 4.9A) (by laboratory member Gianluca Veggiani, 2012). Again, the enhanced conditions gave a higher recovery of MCF-7 cells (Fig. 4.9A, $P < 0.01$, $n = 2$, unpaired t-test) and A431 cells ($P < 0.01$, $n = 2$, unpaired t-test) compared to the standard approach. No MDA-MB-468 cells were isolated, thereby confirming that the magnetic beads specifically bound cells via anti-HER2 Fab0.11 (Fig. 4.9A). The CFSE status of the counted cells is shown in Fig. 4.9B. Recovered A431 and MCF-7 cells were positive for CFSE and negative for the leucocyte marker CD45, authenticating the high purity of recovered cell-lines (Fig. 4.9B). The whole blood sample, following hypotonic lysis, had many CD45-positive cells (Fig. 4.9B).

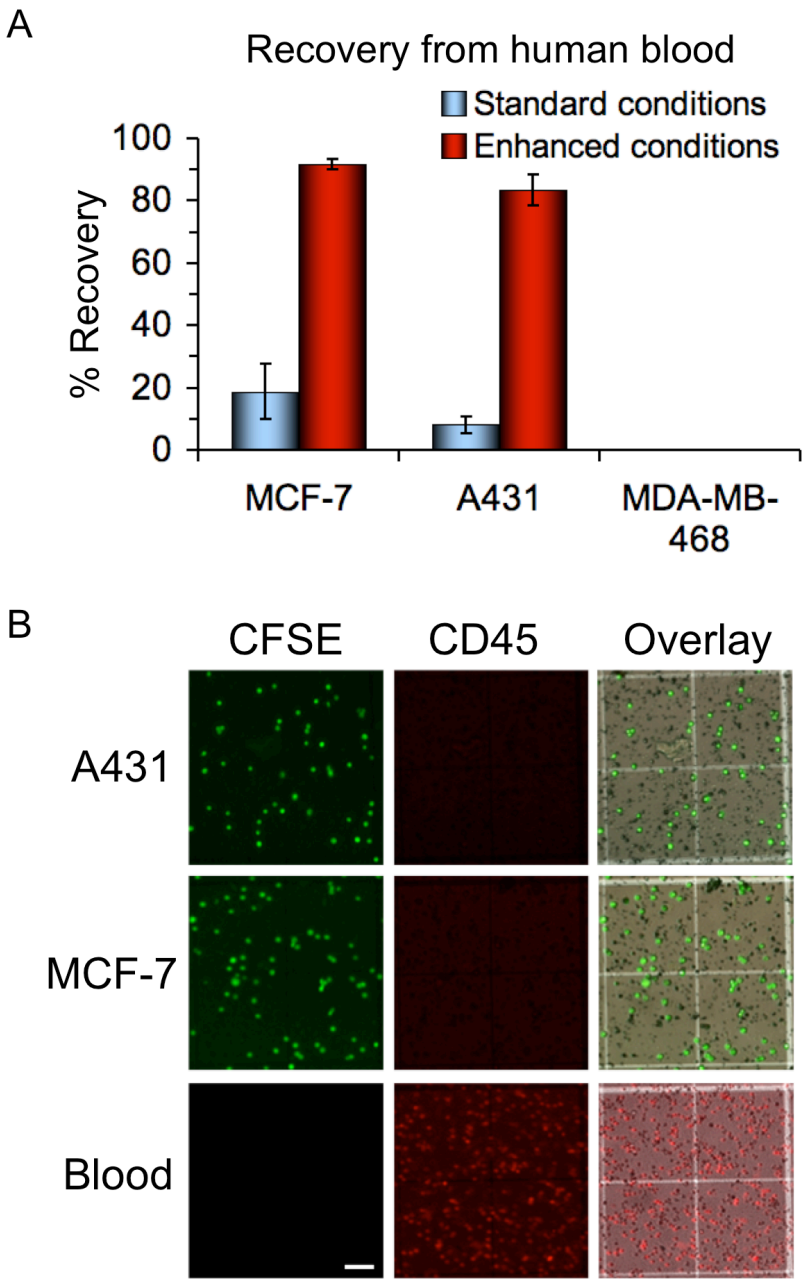

Figure 4.9. Evaluating enhanced approach to isolate cancer cells from human blood. A. Low HER2 expressing cell-lines were labelled with CFSE and spiked into human blood. After red blood cell lysis, cancer cells were recovered using the standard or enhanced approach. For standard conditions, cells were incubated with 10 μg/mL non-biotinylated Fab0.35, and isolated using SA-beads coated with biotinylated secondary antibody. Under enhanced conditions, cells were loaded with cholesterol, labelled with 10 μg/mL biotinylated Fab0.11, and isolated using SA-beads (mean from duplicate measurements ± 1 s.d.) (Data from G. Veggiani). B. Recovered cells were analysed by fluorescent microscopy for CFSE labelling. A431 (top row) and MCF-7 (middle row) were stained with CFSE, spiked into human blood and isolated by the enhanced approach. Left column shows CFSE labelling, middle column shows anti-CD45-PE staining and right column represents the overlay (CFSE: green, anti-CD45-PE: red, brightfield: grey). As a positive control for CD45 staining, whole human blood was lysed and stained with anti-CD45-PE (bottom row) (Data from G. Veggiani). Scale bar 50 μm.

4.8 Imaging the cell-bead synapse

An interesting parameter to explore was how elastic and malleable the cell membrane is around the cell-bead synapse. In T cells bound to anti-CD4 coated beads, cell polarization and reorganization of adhesion molecules, chemokine receptors and lipid rafts have been observed (Nguyen et al., 2005). During immuno-isolation, once the bead attaches to the cell membrane and strengthens its interaction via multiple antigen-antibody binding, the bead may then exert pull or push forces on the cell membrane, as the bead drags the cell through the fluid towards the magnet. On the application of a magnetic field, the magnetic beads exert a unidirectional pull force on the cell. Assuming that the protein interaction between the cell and the bead resists breaking apart, if the membrane is not malleable enough, the force may lead to the magnetic bead pulling out a part of the membrane from the cell (Rubbi et al., 1993). Similarly, if the cell lies between the magnet and the bead, the bead then exerts a unidirectional push force on the cell, and this might lead to the cell membrane wrapping around the bead (Costa et al., 2012).

To investigate this phenomenon and visualize the cell-bead synapse, I used cell tracer DiD, a lipophilic carbocyanine dye that is incorporated into the cell membrane (Honig and Hume, 1986). BT474 cells that had been isolated using biotinylated Fab0.11 and SA-beads (Fig. 3.11C) were stained with DiD and then visualized by fluorescent microscopy (Fig. 4.10). Two fields of view showing two different cells from the same sample are presented; both cells had magnetic beads attached to them. The attached beads had a ring of DiD staining around them, suggesting the presence of cell membrane. Magnetic beads in the same plane that were not attached to the cell (indicated by the red arrows in the brightfield image) did not show any DiD signal. Thus, the beads did not bind DiD non-specifically. Only the beads attached to the cell showed DiD staining.

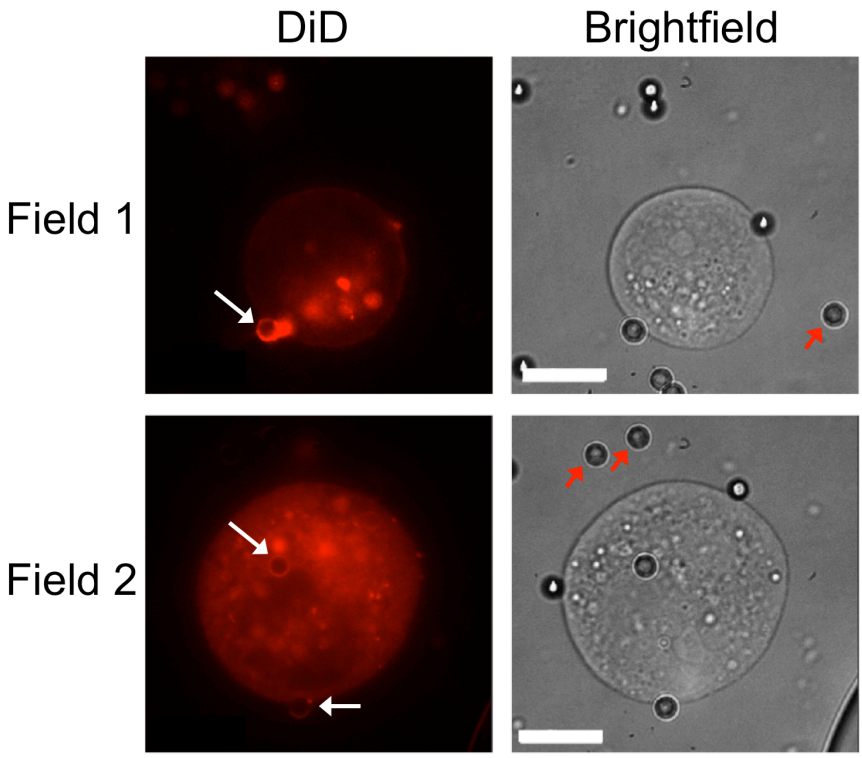

Figure 4.10. Imaging the cell-bead synapse. BT474 cells were labelled with 0.01 μg/mL biotinylated Fab0.11 and isolated using SA-beads. Recovered cells were stained with DiD and analysed by fluorescent microscopy. Left column shows DiD staining and right column shows the brightfield image. Two fields of view from the same sample are shown. White arrows indicate magnetic beads bound to cells; the red halos around the beads suggest the cell membrane has wrapped around the beads. Red arrows indicate magnetic beads not bound to the cell, but present in the same plane as the cell. Scale bar 30 μm.

4.9 Discussion

In this chapter, I explored how changes to the target-cell affected immunomagnetic sorting and devised an enhanced approach to improve cell isolation. The improved efficiency of this approach in isolating low HER2 expressing cells from rabbit and human whole blood was shown.

The use of small molecules to inhibit various cellular components is generally fraught with problems of non-specificity and often interferes with various non-targeted functions of the cell. However, the drugs' widespread use, thorough characterization, easy availability and cost-effectiveness made them suitable for the general aims of my project. Inhibiting cytoskeletal components, such as actin and microtubule polymers, did not affect the amount of cancer cells that could be immunomagnetically recovered.

Actin and microtubule depolymerization has been shown to cause rounding up of adherent cells, as they lose their stress fibers (Spector et al., 1989). However, the cells used for magnetic sorting in my experiments were trypsinized and in suspension before drug treatment. Since trypsin also disrupts microfilaments and microtubules in the cell and causes changes to the cell morphology ((Furcht and Wendelschafer-Crabb, 1978), the action of the added actin and microtubule inhibitors was probably redundant and therefore did not affect immunomagnetic cell recovery.

Actin has been shown to associate with HER2 after addition of Transforming Growth Factor-β (TGF-β) (Wang et al., 2009b). TGF-β induces focal-adhesion kinase dependent clustering of HER2 in HER2 over-expressing epithelial cells without altering the surface expression level of HER2. TGF-β thereby integrates HER2 receptors and F-actin at cell protrusions to induce cell migration and survival in breast cancer (Wang et al., 2009b). Therefore, in future experiments, it might be interesting to see if TGF-β stimulation induced actin reorganization leads to larger HER2 clusters, thereby strengthening the bead-cell synapse and improving cell isolation recovery.

Modifying cholesterol content in the cell membrane led to the most exciting change in magnetic recovery. Cholesterol depletion results in the disorganization of lipid rafts in plasma membrane and dissociation of the proteins bound to the lipid rafts (Barman and Nayak, 2007). Quantitative fluorescence microscopy has also shown that lipid rafts facilitate the formation of large HER2 clusters involving 100-1,000 molecules in SKBR-3 cells, and disintegration of such rafts leads to the dissociation of HER2 clusters (Nagy, 2002), which would thereby lead to lower immunomagnetic recovery consistent with my results. Since cholesterol modification does not change the amount of Fab bound to cells by a large degree, it is more likely the distribution of HER2 clusters that affect bead binding and immunomagnetic recovery. Furthermore, single-molecule fluorescence tracking of receptors has shown that cholesterol depletion confines HER2 receptors by restricting their mobility in the plasma membrane (Orr et al., 2005) and would therefore inhibit the recruitment of new HER2 to stabilize an initial cell-bead interaction. On the other hand, cholesterol enrichment facilitates receptor diffusion (Orr et al., 2005), leading to easy formation of HER2 clusters at the bead-cell synapse and increasing immunomagnetic recovery. Cholesterol levels of cells can be easily modified externally by applying a water-soluble form of

cholesterol and so this approach should be easy and practical for isolation of CTCs from patient blood samples.

From my work, sodium azide seems safe to be used for cell preservation during immunomagnetic isolation, as sodium azide does not significantly affect cell recovery. Inhibiting HER2 kinase activity using AG825 dramatically decreased cell recovery. HER2 receptors are present in pre-formed aggregates of 5-15 molecules in the cell membrane of high HER2 expressing cells (Nagy et al., 2010). It has previously been shown that a tyrosine kinase inhibitor, AG1478, causes partial dispersal of EGFR clusters in A431 cells (Clayton et al., 2007) and decreases the fraction of EGFR receptors colocalising with lipid rafts in HeLa cells (Abulrob et al., 2010). As EGFR and HER2 belong to the same ErbB family and HER2 molecules have also been shown to be present in preformed clusters, it could be postulated that the HER2 clusters behave similar to EGFR clusters and are dispersed on treatment with AG825 in BT474 cells. This would explain why the cell-magnetic bead synapse weakens and reduces immunomagnetic recovery of BT474 cells treated with AG825. However, variable results in different cell-lines may arise due to differences in HER2 expression level and the diversity in the cells' steady-state. Therefore, further experiments involving single molecule tracking and FRET analyses of HER2 clusters on treatment with AG825 in various cell-lines should be carried out in subsequent studies.

My preliminary experiments studying the cell-bead synapse by microscopy suggested that the cell-bound magnetic beads were covered with plasma membrane. A recent study on detecting cancer cells with magnetic nanoparticles employed scanning electron microscopy and visualized finger-like cell membrane protrusions surrounding a magnetic bead attached to the cell (Costa et al., 2012). Such physical structures comprising the cell-bead synapse are important to study, since uprooting of antigens from the cell membrane by an attached magnetic bead would not only damage the cell but also lower the cell's chances of being recovered. For instance, a fraction of Daudi cells that were incubated overnight with anti-CD19 coated Dynabeads, showed depletion of surface antigen and did not bind the magnetic beads even in the second round of immunomagnetic incubation (Rubbi et al., 1993). In my experiment I incubated the cell-bead mixture for 30 min and although the cell-bound beads were covered with cell membrane, the free beads did not have any cell

membrane on them and therefore antigen detachment of the cell had not occurred. This shows the importance of optimizing cell mixing techniques and incubation times during the isolation. Very long incubation and harsh mixing conditions could lead to more cells getting depleted of their antigens (Rubbi et al., 1993). Furthermore, comparing the cell-bead interface to a more dynamic cell-cell synapse can give us valuable insights on membrane curvature, stretching and force resistance of protein-protein links at the point of contact. Immunological synapses are also often accompanied by the transfer of membranous structures and cell surface proteins (Williams et al., 2007). In future experiments, it would also be interesting to see how cholesterol modulates the membranous structures around the beads and if cholesterol can be used to prevent shearing tearing of cell membranes during CTC isolation.

Having assessed cellular parameters that affect cell-bead interaction and from observations about antibody links in the previous chapter, I identified three ways in which immunomagnetic isolation could be improved. First, load cells with cholesterol, then use the highest affinity biotinylated primary antibody available, and finally capture cells using a direct linkage to the magnetic surface via covalently-bound streptavidin. Together, I termed these three conditions the "enhanced approach" and validated its efficiency on a panel of cell-lines.

I ensured that I included a wide range of HER2 expressing cell-lines in the test panel, so that I could quantify the improvement in cell recovery in high as well as low HER2 expressing cells. There is much variability in the published number of HER2 receptors expressed on the surface of various cell-types. For example, BT474 cells have been reported to have 478,000±75,800 (Gaborit et al., 2011), 499,795.2 (Larson et al., 2010) and 1,706,601 (McDonagh et al., 2012) receptors/cell. I therefore decided to quantify surface HER2 using the mono-biotinylated Fab0.35 and monovalent-streptavidin-488 on flow cytometry, avoiding any misinterpretation due to bivalent binding by whole IgGs or multivalent binding by tetravalent streptavidin. Relative HER2 levels in the cell panel were as expected, although the absolute receptor numbers were different from previous studies (Gaborit et al., 2011). Apart from cell passage numbers, antibodies and detection techniques, this variation could also have arisen due to the kind of calibration beads used to map the standard curve of fluorescence units vs. dye molecules. The monovalent binding approach using a 1:1:1

ratio of HER2:Fab:mSA described here can also be useful for biological assays that are otherwise hampered by the clustering of receptors after divalent IgG binding.

The cell-line panel was used to compare a standard immunomagnetic sorting approach and the enhanced approach I had devised based on the factors identified as important for this process. The conventional protocol involving the use of a standard antibody and linking to beads via a secondary antibody, gave good cell recovery for high HER2 expressing cells, but did not isolate low HER2 expressing cells. On the other hand, the enhanced approach isolated low HER2 expressing cells much more efficiently, greatly improving the detection limit of immunomagnetic sorting. With the recent data on how low-level HER2 overexpression in prostate cancer is associated with rapid tumour cell proliferation and poor prognosis (Minner et al., 2010), the enhanced approach would be even more useful in diagnosing and monitoring CTCs in such cases. Applying each of the three enhancements individually on the cell-line panel showed that all three were beneficial for recovery of low expressing cells and so can be independently applied wherever possible.

The impact of the enhanced approach in isolating low HER2 expressing cells was even greater on isolation of cancer cells from blood. From both rabbit and human blood, low expressing cells could not be recovered even in low percentages when isolated under the standard conditions. This is probably because when isolating from blood, cancer cells have to travel through a denser mixture of contaminating cells and debris, and therefore a stronger bead-cell synapse is required to resist the drag forces of the solution. However, the enhanced approach still captured the low HER2 expressing cells as efficiently as the highest HER2 expressing cell-line.

The work presented in this chapter made affinity-based capture of cells less dependent on the antigen expression level of cells. Due to the heterogenous expression of antigen levels on CTCs in breast cancer (Braun et al., 1999), such an enhancement in recovery would be particularly advantageous. With the downregulation of EpCAM in invading metastatic cells (Rhim et al., 2012), using alternate tumour markers such as HER2 to isolate CTCs would also be useful. The enhanced approach described here has also recently shown success in isolating low EpCAM-expressing cells, thereby confirming its validity on a second antigen-antibody interaction (see attached manuscript).

The issues discussed in this chapter can also be applied to other cell isolation techniques, used for sorting of immune or stem cells. The existing cancer cell detection and isolation techniques rely heavily on high expression of antigens, and reducing this dependence by understanding antigen detection limits is especially important. Efficient cell capture will make the use of existing biomarkers less vulnerable to antigen-down regulation and also increase the possibility of using novel low-expressed biomarkers for detecting and isolating cancer cells.

Chapter 5: Towards antibody clamping

Exploring an approach to surround the antibody-antigen complex, to increase the stability of antibody interactions

Chapter 5: Towards antibody clamping

Exploring an approach to surround the antibody-antigen complex, to increase the stability of antibody interactions

5.1 Introduction

In previous chapters, we saw how an antibody with improved affinity could significantly improve the sensitivity of immunomagnetic cell isolation, a diagnostic method of great potential in cancer. Antibody affinities are indeed the limiting factor in a number of research, diagnostic and therapeutic approaches. Antibodies with exceptional affinities in the 10^{-9}-10^{-11} M range are sometimes insufficient to neutralize lethal agents like botulinum neurotoxins and have to be used in combinations of two or more antibodies (Nowakowski et al., 2002). Antibody constructs with picomolar affinities are often needed for the visualization of tumour markers *in vivo* (Orlova et al., 2006). Antibody affinity can also be a limiting factor in live cell imaging, as antibody off-rates are on the order of minutes (Foote and Eisen, 1995; Houk et al., 2003), whereas certain cell surface proteins have lifetimes of a few days (Bruneau et al., 2005).

In the mammalian immune system, the various possible gene segments and affinity maturation produce mature antibodies with affinities typically in the range K_d=10^{-7}-10^{-9} M (Houk et al., 2003). However, the inability of B cells to discriminate between antibody dissociation kinetics and intrinsic B-cell receptor internalization rates during affinity maturation create an affinity ceiling of 10^{-9}-10^{-10}M (Foote and Eisen, 1995). Furthermore, antibody fragments, such as Fabs and scFvs, which are often favoured over intact antibodies because of the fragments' smaller size and higher tumour penetration, display reduced binding stability because of their reduced avidity and faster off-rates (Batra et al., 2002). The on-rate for an antibody to bind its antigen is approximately 10^{5}-10^{6} $M^{-1}s^{-1}$, and is limited by the diffusion coefficient of the reactant molecules (Foote and Eisen, 1995; Caoili, 2012). As detection of protein biomarkers with antibody-based affinity assays is the basis of molecular diagnostics in clinical practice today, enormous efforts have been taken to artificially generate antibodies with slower dissociation rates.

As discussed in Chapter 1 (sections 1.1.5-1.1.8), some approaches to increase antigen-antibody binding include selection from large libraries (containing > 10^9 clones), generated from technologies like phage display, mRNA display and ribosome display (Lipovsek and Pluckthun, 2004; Dufner et al., 2006). However, generating libraries for each antigen-antibody combination can be painstaking, time consuming and expensive. Irreversibly binding antibodies, such as metalloantibodies (Trisler et al., 2007) and electrophilic affibodies (Holm et al., 2009) need various accessory groups in the active site and may promote non-specific binding of the antibody. Binding proteins based on non-immunoglobulin domains also require each construct to be individually optimized to increase its affinity (Binz et al., 2005).

In this chapter, I work towards an alternative idea on increasing antigen-antibody stability. The ideal Ab engineering approach should be able to 1.) dramatically decrease the off-rate of the antibody 2.) not affect the specificity of the antibody, and 3.) be a generic technique that could be applied to different antibodies and antibody fragments. To fulfill these aims, it is necessary to keep the antigen-antibody interaction site unmodified. I therefore introduce a third player, a clamp, which is engineered to bind the Fab after the Fab has bound its antigen and block the Fab's dissociation from the antigen. I made use of the high affinity and tetravalency of the biotin-streptavidin interaction (Green, 1990), to try to engineer a clamp that could surround the antigen–Fab complex and physically block the antigen from leaving the binding site (Fig. 5.1). I used Fab instead of intact IgG, as Fab fragments are easier to express and avoid problems related to bivalency of IgG. As antigen-binding sites are often like clefts or grooves with the heavy and light chain variable domains on each side, I aimed to exploit this characteristic to clamp the antigen into the binding site from both directions, to form a loop around the antigen (Fig. 5.2).

A similar approach has been used to generate an artificial clamp around a DNA polymerase to increase its processivity in single strand DNA sequencing (Williams et al., 2008). Bringing a surface directly above a binding protein, and trapping the interaction between two surfaces has also shown to decrease dissociation and has been used in eukaryotic transcription factor arrays (Maerkl and Quake, 2007). Such interactions where the target is surrounded and locked from dissociating out, as in

rotaxanes and pseudorotaxanes, is also a feature of growing importance in supramolecular chemistry (Haussmann and Stoddart, 2009).

Initially basing the clamping model on a rotaxane (section 1.5.1), I used a peptide-binding Fab, 9E10. 9E10 is an IgG1/κ murine monoclonal antibody raised against myc1, a synthetic peptide immunogen derived from human c-myc proto-oncoprotein (Evan et al., 1985). 9E10 is commonly used as a detection and purification tool for proteins that are fused with myc1 as an affinity tag (Lobbestael et al., 2010; Weidner et al., 2010). As interactions between a peptide and its antibody are limited due to the decreased surface area available for interaction and lack of structural rigidity (Wilson et al., 1994; Houk et al., 2003), anti-peptide antibodies generally have low affinities, and there exists considerable scope for improvement. I also applied the clamp blocking strategy to HER2-binding mouse monoclonal 4D5 Fab, to test clamping of a protein domain (Cho et al., 2003) and to assess the generality of the clamping approach.

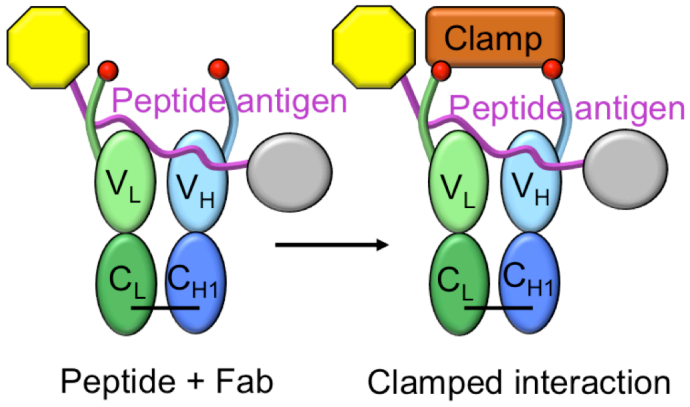

Figure 5.1. Cartoon representation of antibody clamping. Recombinant Fab fragment, consisting of four immunoglobulin domains (heavy chain:blue; light chain:green), in complex with a peptide antigen (pink) fused to globular domains at each end (yellow, grey). Each oval represents an immunoglobulin domain; lighter shades represent variable domains (V_L, V_H) and darker shades represent constant domains (C_L, C_{H1}). Disulfide bonds (—) hold the two chains together. The engineered clamp will trap the peptide in the binding site.

5.2 9E10-APLH generation and clamp development

9E10 Fab had previously been generated by linking the variable domains of mouse 9E10 with human IgG C_H1 and Cκ domains in a bacterial expression vector (Schiweck et al., 1997). To engineer the recombinant 9E10 Fab, I genetically inserted an acceptor peptide (AP) into the N-termini of the heavy and light chains of the 9E10 Fab, and termed the resultant Fab 9E10-APLH. The N-termini of the heavy and light chains of 9E10 are on either side of the myc-binding pocket, allowing the AP tags to extend out on each side of the binding pocket. To help the AP tag to be flexible, I inserted glycine-serine linkers between the AP tags and the N-termini. As myc1 is a very small peptide (11 amino acids), I expressed myc1 fused to the C-terminus of Maltose Binding Protein (MBP) (Fig. 5.2A). The AP tags can be specifically biotinylated at their lysine side chain using *E. coli* biotin ligase, BirA, allowing the AP tags to strongly and non-covalently interact with streptavidin (Beckett et al., 1999). As streptavidin is a tetramer with four equal affinity binding sites, it was hypothesized that streptavidin could bind to both AP tags on each side of the myc binding groove in the Fab, and thus clamp the myc1-9E10 interaction (Fig. 5.2A).

The bacterial cytoplasm has a reducing environment and is therefore inappropriate for the expression of Fab fragments, which rely on disulfide bonds for structure stability (Martin et al., 2006). Therefore, both chains in 9E10 Fab contained leader sequences, so that 9E10-APLH could be expressed in the periplasm of *E. coli* strain C43 (DE3). This process required a highly optimized environment with low temperature (18-25ºC) to control cotranslation and secretion, addition of glucose to avoid leaky Fab expression that could otherwise be toxic, and occasional addition of sucrose to assist in correct Fab folding (Bannister et al., 2006). Even under these conditions, I found that bacterial cells would often grow up to a certain density and then undergo lysis, before reaching the required optical density for protein induction.

When the cells did survive up to the optimal density, a 6-His tag on the C-terminus of the heavy chain allowed the Fab to be purified on a Ni-NTA column. After biotinylation with BirA, biotinylated 9E10-APLH, termed 9E10-APLHb, was further purified on a Protein G column to remove BirA and other impurities. To check for Fab purity and biotinylation, 9E10-APLHb was mixed with streptavidin and run on a SDS-PAGE (Fig. 5.2B). Biotinylated Fab gave a band at around 56 kDa, and shifted

upwards to 120 kDa in the presence of streptavidin. However, there was some degradation of 9E10-APLHb, as indicated by the presence of a smear between 30–40 kDa (Fig. 5.2B). On reduction of the disulfide bonds, 9E10-APLHb split into its constituent heavy and light chains, giving bands at ~30 kDa (Fig. 5.2B). Both light and heavy chains formed complexes with streptavidin, confirming complete biotinylation of both AP tags. There was also a faint band at around 28 kDa below the reduced Fab chains (Fig. 5.2B). Its smaller size and inability to bind streptavidin on SDS-PAGE, indicated the presence of Fab chains whose AP tags had been cleaved during the purification and biotinylation process. As 9E10-APLH induction in bacterial periplasm was not very strong and some protein would be lost during processing, the overall yield of the final 9E10-APLHb was very low, ranging from 0.05 – 0.10 mg from a 750 mL bacterial culture. Although the obtained yield and purity of 9E10-APLHb were not ideal, in the interest of time we decided to use this antibody stock for some preliminary tests, while I continued optimising the expression and purification of 9E10-APLH (section 5.6 and appendices 1 and 2).

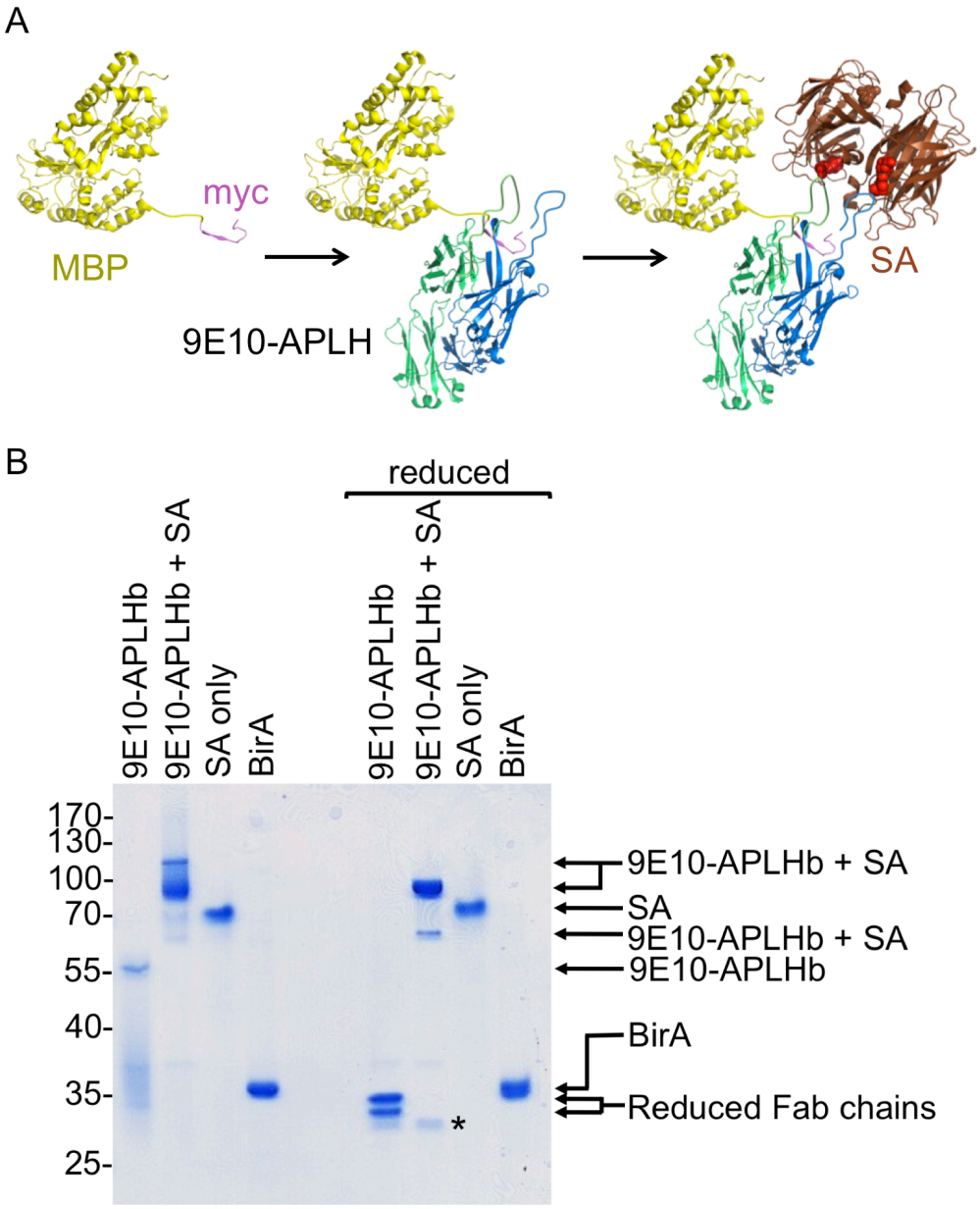

Figure 5.2. 9E10-APLHb synthesis and clamp development. A. Schematic representation of clamping with streptavidin. Myc tag is expressed on the C-terminus of Maltose Binding Protein (MBP, based on PDB 2KLF). 9E10 (based on PDB 2OR9) expressed with AP tags on the N-termini, and biotinylated *in vitro*, binds to myc. Tetravalent streptavidin (PDB 1SWE) binds biotin on both AP tags and locks the peptide in the binding site. B. 9E10-APLHb purification and biotinylation analysed using SDS-PAGE and Coomassie staining. On reduction with 2-ME and addition of streptavidin, both biotinylated Fab chains show a band shift. The faint band at ~28 kDa (denoted by *) is probably representative of the Fab chains in which an AP tag has been cleaved.

5.3 Generation of the myc series

To test the functionality of the recombinant 9E10-APLHb, a series of myc mutants was constructed (Fig. 5.3). As the efficiency of clamping could depend upon the size of the folded domain on either side of the part recognized by the antibody, it was important to test clamping efficiency using the myc peptide in different positions. I therefore engineered the myc peptide attached to either one or two globular proteins. In the MBP-myc series, myc was expressed at the C-terminus of Maltose Binding Protein, giving the Fab easy access to the peptide (Fig. 5.3). In the MBP-myc-CFP series, Cyan Fluorescent Protein was attached to the C-terminus of MBP-myc, forming a dumbbell shaped protein with myc tag in the centre (Fig. 5.3). This would also allow us to assess if the clamp worked better on the rotaxane model, with the two globular domains inhibiting the "slipping off" of the Fab-SA clamp from the myc peptide. Glycine-serine linkers were inserted between the different domains to provide flexibility to the tag. To test the clamping efficiency on different affinity interactions, three variants of myc tag were used (Fig. 5.3). Myc1 is the original myc tag composed of 11 amino acids (Glu-Gln-Lys-Leu-Ile-Ser-Glu-Glu-Asp-Leu-Asn) and binds 9E10 with a $K_d = 5 \times 10^{-7}$ M in PBS (Krauß et al., 2008). Myc2 is a shorter myc tag, comprising 9 amino acids (Lys-Leu-Ile-Ser-Glu-Glu-Asp-Leu-Asn) and has a lower affinity for 9E10, $K_d = 2.5 \times 10^{-6}$ M in PBS (Krauß et al., 2008). MycK (Glu-Gln-Lys-Leu-Ile-Ser-Lys-Glu-Asp-Leu-Asn) is a point mutant that does not bind 9E10 and was therefore used as a negative control in experiments (Hilpert et al., 2001).

The various myc constructs were cloned and expressed in the cytoplasm of *E. coli* strain RIPL (DE3) and purified on an amylose-agarose column. To check for protein purity and uniformity, the myc proteins were analysed by SDS-PAGE (Fig. 5.4). MBP-myc constructs gave single bands at ~40kDa. MBP-myc-CFP constructs appeared at ~70kDa, with some degradation in MBP-myc1-CFP and MBP-mycK-CFP.

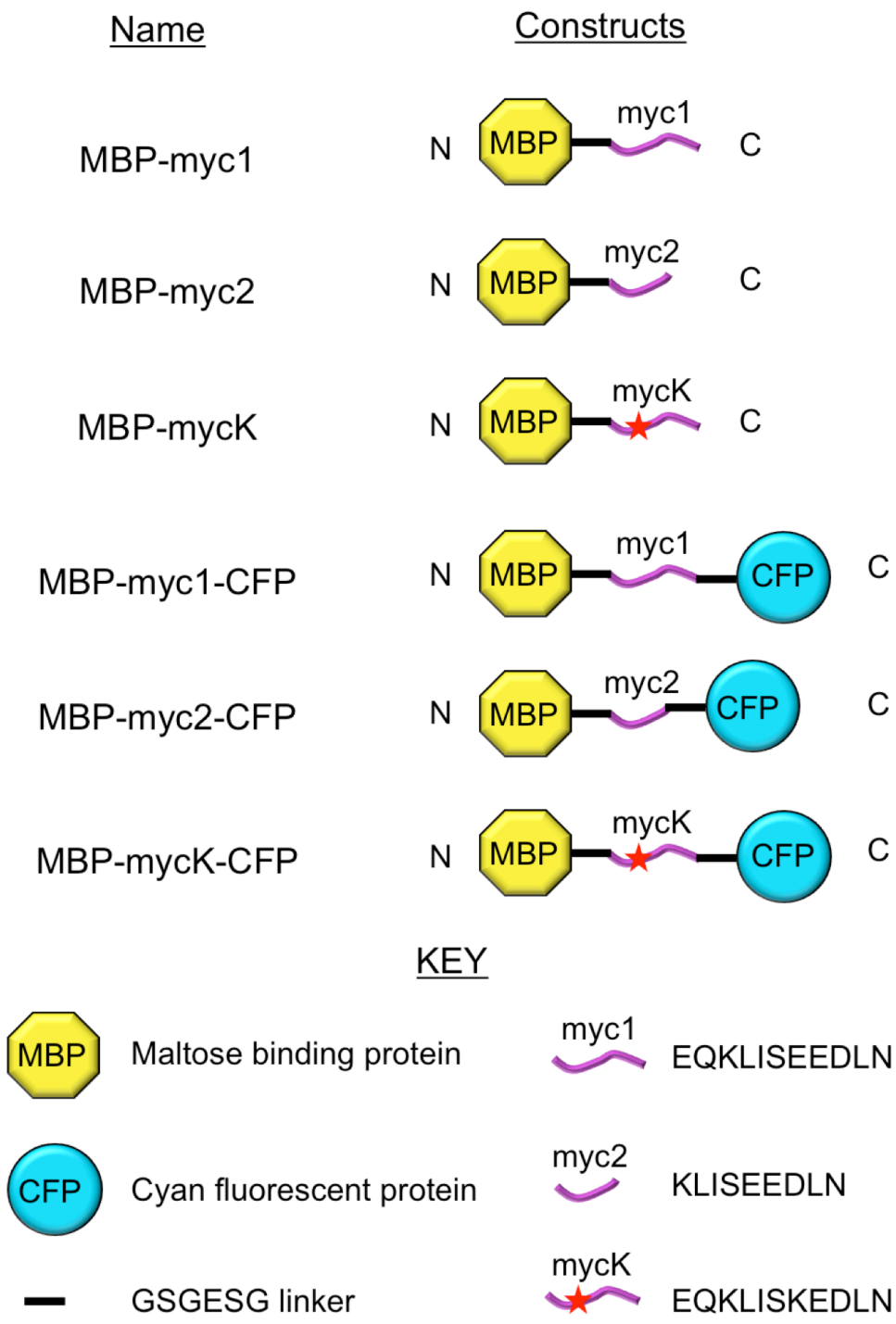

Figure 5.3. A list of the myc constructs used to test 9E10-APLH clamp. Myc mutants were attached to either MBP only, or to MBP and CFP. Myc1 has high affinity for 9E10, myc2 has lower affinity and mycK does not bind 9E10.

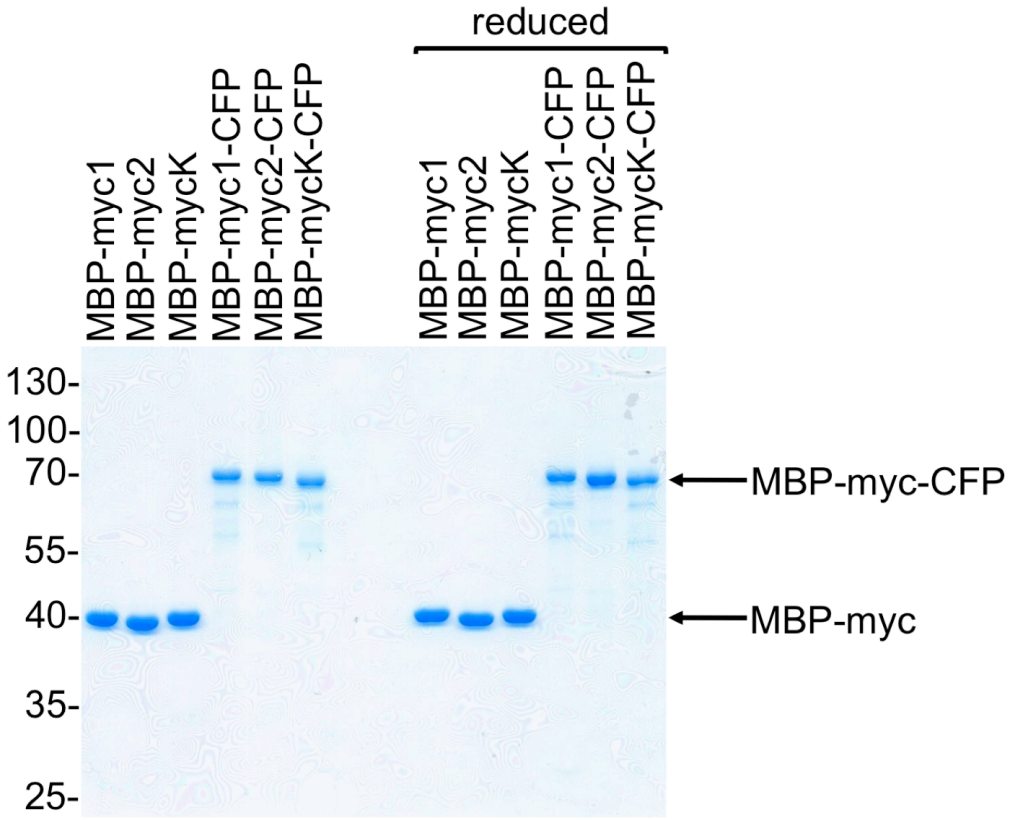

Figure 5.4. Expression of the myc series. SDS-PAGE, stained with Coomassie dye, showing purified myc constructs under non-reducing and reducing conditions. The MBP-myc series is 40 kDa and the MBP-myc-CFP series is 70 kDa. No disulfide bonds are present in these constructs.

5.4 ELISA showed improved myc : 9E10-APLHb binding with SA block

9E10-APLHb was tested for its binding to the different myc constructs by ELISA. 1 μM of each myc construct was coated overnight onto wells in an ELISA plate. 10 μg/mL 9E10-APLHb was then allowed to bind to the myc construct, and excess Fab was washed off. Fab binding to the myc construct was detected using an anti-human IgG-HRP secondary antibody. As expected, 9E10-APLHb showed strongest binding to myc1 (Fig. 5.5A, $P < 0.01$, $n = 2$, unpaired t- test, comparing MBP-myc1 and MBP-myc2; $P < 0.001$, $n = 2$, unpaired t- test, comparing MBP-myc1-CFP and MBP-myc2-CFP). Binding to myc2 was much lower and mycK binding was negligible, comparable to the PBS control (Fig. 5.5A, $P > 0.4$, $n = 2$, unpaired t- test, comparing MBP-mycK and PBS). Thus the 9E10-APLHb binding pattern was similar to that expected from 9E10, and the insertion of AP tags had not affected the specificity of myc-9E10 interaction. Overall, binding to the MBP-myc-CFP constructs showed

higher absorbance compared to the MBP-myc constructs. One explanation for this difference could be that the presence of the second globular domain in MBP-myc-CFP constructs limits the myc peptide into a conformation that favours Fab binding. As CFP absorbs at 450 nm, its presence might also contribute to the higher absorption observed for MBP-myc-CFP and 9E10-APLHb binding in ELISA.

To test for clamping, I first used 9E10-APLH or 9E10-APLHb as a primary antibody to bind to 1 μM MBP-myc1 on ELISA, and then treated the wells with or without streptavidin, before detecting Fab binding with the secondary antibody (Fig. 5.5B). As hypothesized, treating with streptavidin increased the signal from the myc-9E10-APLHb binding, but not myc-9E10-APLH, confirming that SA was specifically binding to the biotins on the AP tags (Fig. 5.5B). The absorbance for 9E10-APLHb binding increased 2.5-fold in the presence of streptavidin, greatly stabilising the interaction (Fig. 5.5B, $P < 0.01$, $n = 2$, unpaired t- test). However, it was also noted that the initial binding of 9E10-APLHb to myc was worse than that of 9E10-APLH (Fig. 5.5B, $P < 0.01$, $n = 2$, unpaired t- test), suggesting that the presence of biotins was somehow inhibiting 9E10-APLHb binding to myc. Therefore, the improvement by clamping was just a restoration to the level of the original 9E10-APLH binding (Fig. 5.5B). One reason for the difference in 9E10-APLH and 9E10-APLHb binding to myc could be the uncertainty about their purity and concentration. The biotinylation of the AP tag could also inhibit binding to myc, either by direct steric hindrance or by altering the way that the AP tags interacted with the CDRs. As the Fab I purified degraded easily, it was difficult to measure the exact concentrations of well-folded Fab constructs in use. There could be small amounts of BirA present in the 9E10-APLHb sample and removing this BirA would require another cycle of purification that would further lower 9E10-APLHb yield. Therefore the unavailability of a pure, uniform, high yielding Fab construct was a major deterrent in further exploring the reasons for lower 9E10-APLHb binding to myc. However, the SA blocking did show initial promise as once 9E10-APLHb had bound myc1, adding SA greatly enhanced the signal.

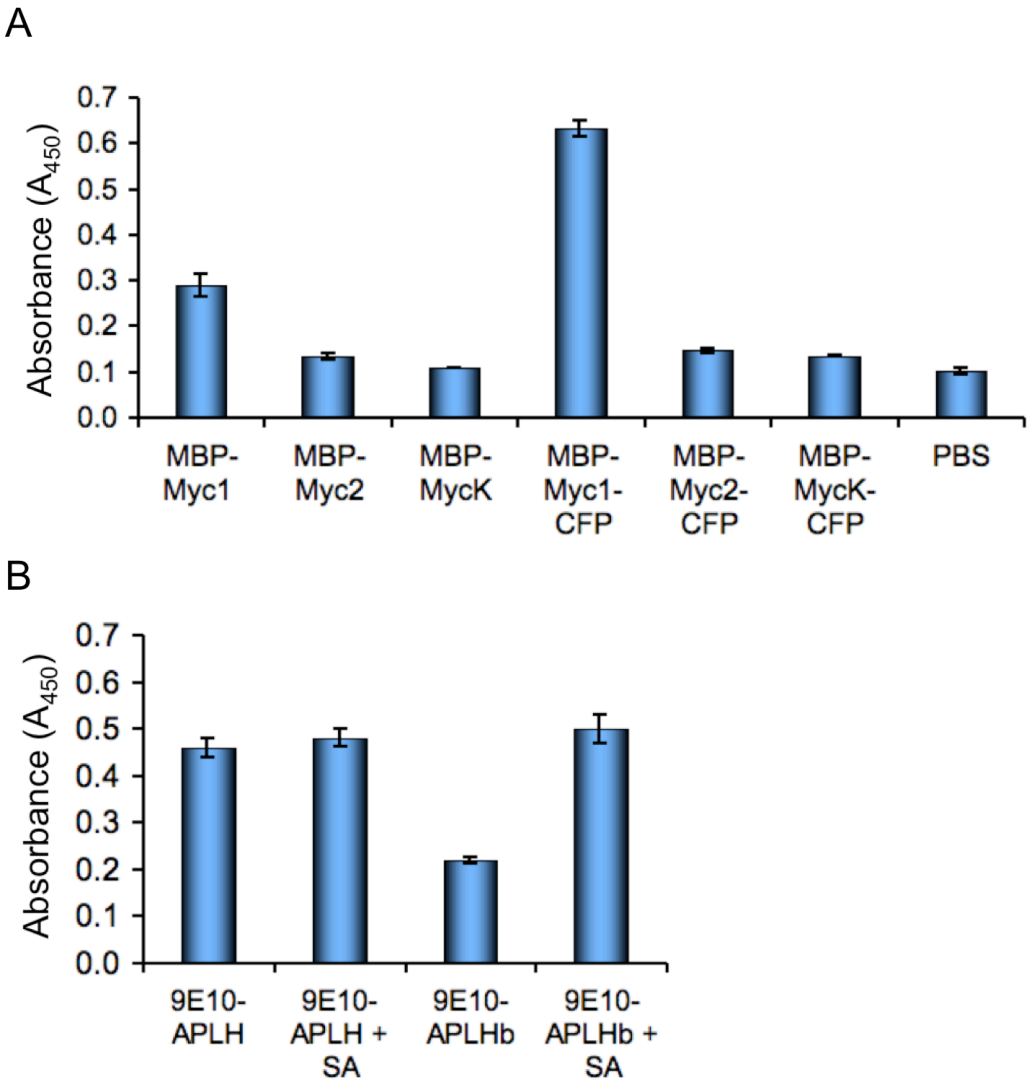

Figure 5.5. ELISA to test 9E10-APLHb binding. A. Microtitre plate wells were coated with 1 μM of the indicated myc protein construct and 10 μg/mL 9E10-APLHb was used as the primary antibody. Anti-human IgG-HRP was used as secondary Ab to detect binding and A_{450} was measured. Binding levels to the different myc constructs are shown (mean of duplicate ± 1 s.d.). B. ELISA to compare 9E10-APLH and 9E10-APLHb binding. 10 μg/mL 9E10-APLH or 9E10-APLHb was used as primary Ab against 1 μM MBP-myc1. SA binding improved binding with 9E10-APLHb but not 9E10-APLH (mean of duplicate ± 1 s.d.).

To further investigate how clamping efficiency varied with a change in myc concentration and if the SA blocking improved myc detection limit, MBP-myc1 was titrated onto an ELISA plate and 9E10-APLHb was used as the primary antibody, with or without the SA clamp (Fig. 5.6A). Overall, blocking dissociation with SA showed greater absorbance than the unblocked antibody. At the highest MBP-myc1

concentration of 1 μM, adding SA gave a ~2.5-fold increase in absorbance (Fig. 5.6A, $P < 0.01$, $n = 3$, unpaired t- test), and this increase was consistent until 10 nM concentration of MBP-myc1 (Fig. 5.6A, $P < 0.0001$, $n = 3$, unpaired t- test). When MBP-myc1 concentration was below 1 nM, 9E10-APLHb did not bind the antigen, and there was no improvement with the SA block (Fig. 5.6A, $P > 0.2$, $n = 3$, unpaired t- test). This suggests that the SA clamp does not increase the original binding of the Fab to the antigen, but rather stabilizes the interaction once 9E10-APLHb has bound to myc1, by inhibiting dissociation. It was also important to check if the increase in myc-Fab stability was due to SA locking and clamping the myc peptide in the antigen-binding groove, or due to the mere presence of the bulky SA molecule. When monovalent streptavidin (mSA) with only one biotin-binding site (Howarth et al., 2006) was used to block 9E10-APLHb, instead of the regular tetravalent SA, there was a small but significant increase in absorbance (Fig. 5.6A, $P < 0.01$, $n = 3$, unpaired t- test). This is consistent with the design of the clamp, as each mSA would bind only one of the two AP tags, thereby leaving the antibody:antigen complex unlocked, but the mere presence of the bulky mSA would still provide a physical block and hinder the dissociation of myc to a slight extent.

A similar titration was done using MBP-myc1-CFP, which gave a comparable binding pattern (Fig. 5.6B). As the initial binding of 9E10-APLHb for MBP-myc1-CFP is stronger, the increase in absorbance with SA clamp was only ~2-fold (Fig. 5.6B, $P < 0.01$, $n = 3$, unpaired t- test). Again, there was no increase in absorbance for MBP-myc1-CFP concentrations lower than 1 nM (Fig. 5.6B, $P > 0.3$, $n = 3$, unpaired t- test), consistent with the design of the clamp that is engineered to maintain binding for longer periods of time rather than to increase the intrinsic affinity of the Fab (Fig. 5.6A and B). Thus, although the SA clamp stabilized the myc-9E10 interaction consistently, SA did not improve the detection limit of the assay. No increase in absorbance was observed on applying the SA clamp to mycK constructs, confirming that the SA clamp did not interfere with Fab specificity (Fig. 5.6A, $P > 0.2$, $n = 3$, unpaired t- test; and Fig. 5.6B, $P > 0.2$, $n = 3$, unpaired t- test).

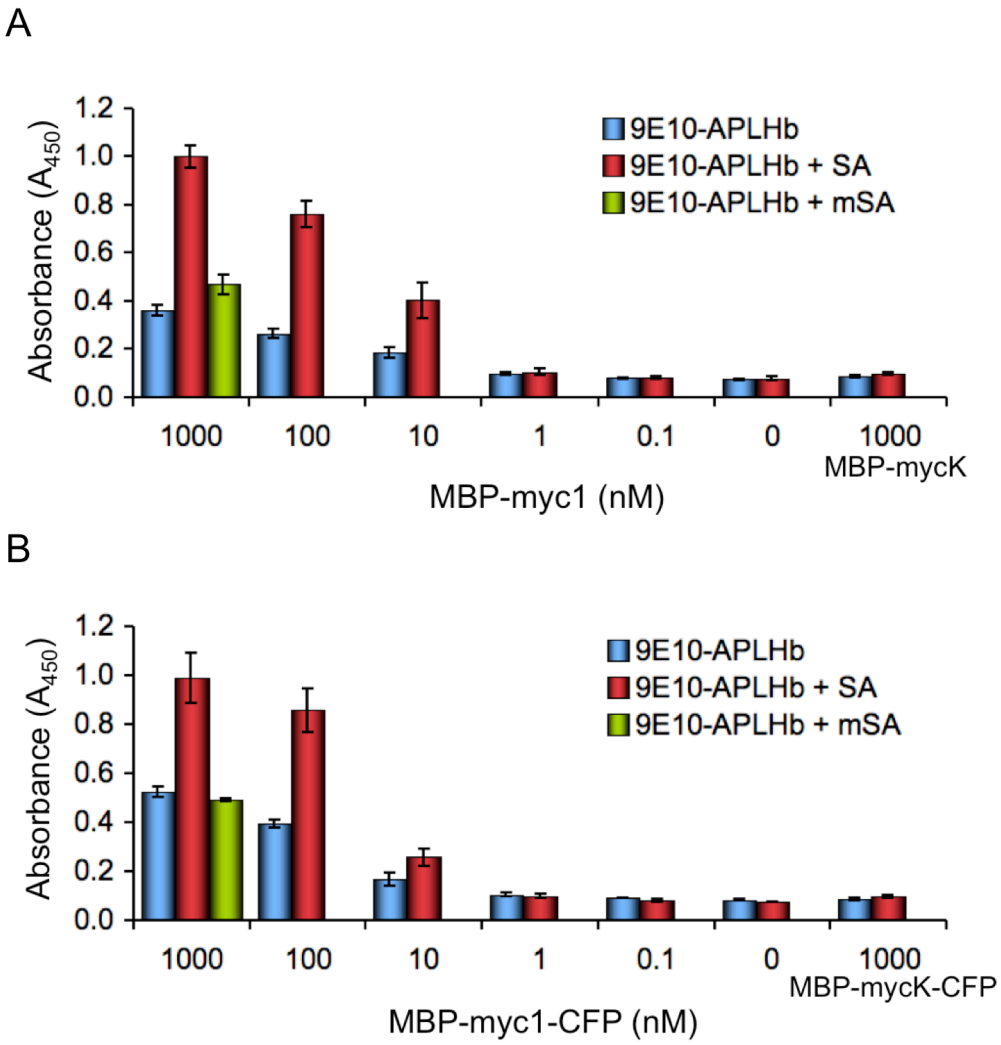

Figure 5.6. ELISA to test SA clamping on myc1. Clamping efficiency was analysed on a dilution series ranging from 0-1000 nM of A.) MBP-myc1 and B.) MBP-myc1-CFP. 9E10-APLHb was added to myc constructs, before treatment with or without SA. MBP-mycK and MBP-mycK-CFP were used as respective negative controls. Monovalent streptavidin (mSA) binds only one AP tag and is therefore inefficient in clamping the myc-Fab complex (mean of triplicate ± 1 s.d.).

5.5 9E10-APLHb recognition of myc expressed on the mammalian cell surface

As the clamp had been designed to be used on live cells and given its partial success in increasing antigen-antibody complex stability *in vitro*, it was important to test if 9E10-APLHb could bind to myc expressed on the cell surface. For this purpose, I used a gene construct with the myc1 tag between CFP and a transmembrane domain (TM), termed CFP-myc1-TM, and inserted the gene construct into a mammalian

expression vector. HeLa cells transfected with CFP-myc1-TM expressed myc1 on their cell surface and were easily recognizable as the CFP positive cells by fluorescent microscopy (Fig. 5.7). 9E10-APLH or 9E10-APLHb was used to label cell surface myc1 and binding was detected using anti-human IgG AlexaFluor555 (Fig. 5.7). 9E10-APLH showed clear binding to myc1, as represented by the co-localization of CFP and AlexaFuor555 signals, which form rings on the transfected cells' plasma membranes. However, very faint to no binding was observed with 9E10-APLHb (Fig. 5.7). The presence of biotins on the AP tags could obstruct the myc-binding site, thereby leading to weaker binding of 9E10-APLHb to cell surface myc1. Therefore, 9E10-APLHb was not ideal for clamping on cells, as further optimization of the Fab was required.

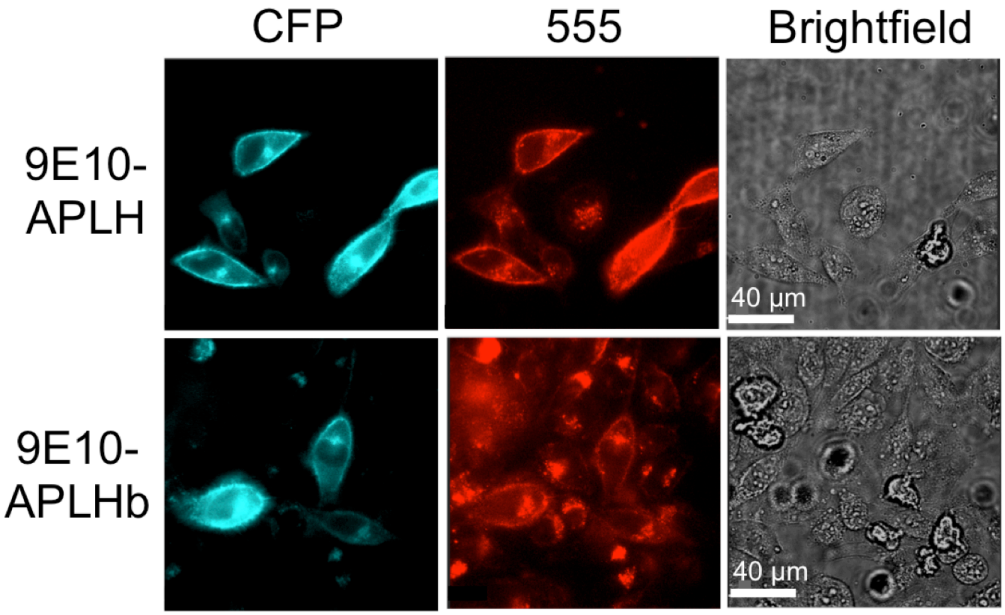

Figure 5.7. Live cell imaging to test 9E10-APLHb binding. Myc1 was cloned with CFP and a transmembrane domain (CFP-myc1-TM) and transfected into HeLa cells. Transfected cells display CFP and myc extracellularly on the plasma membrane and can be identified from the ring of CFP fluorescence. 9E10-APLH or 9E10-APLHb was used to bind surface-expressed myc; binding was detected using anti-human IgG AlexaFluor555 and analysed by fluorescent microscopy. 9E10-APLH, but not 9E10-APLHb, bound specifically to myc-expressing cells.

5.6 Efforts to improve 9E10-APLH expression and purity

In order to develop the clamp, it was important to first optimise 9E10-APLHb so that 1.) the Fab was easier to fold, express and purify and 2.) the reduced binding efficiency to myc compared to the original 9E10 was overcome. Both these targets were interdependent and multiple ways were tried to achieve these.

Expressing 9E10-APLH in the periplasm of bacterial cells required the Fab chains to be individually translated in the cytoplasm and translocated to the periplasm through the Sec-dependent pathway (Baneyx and Mujacic, 2004). However, protein overexpression in the periplasm can trigger oxidative stress or improper formation of disulfide bonds, leading to misfolding or aggregation of Fab fragments (Missiakas et al., 1996). This limits the amount of correctly folded Fab that can be produced in the bacterial periplasm. To overcome this issue, the *Rosetta Gami* bacterial strain favouring disulfide bond formation in the cytoplasm, by mutating thioredoxin reductase (*trxB*) and glutathione reductase (*gor*) genes, has been developed (Proba et al., 1995; Bessette et al., 1999; Levy et al., 2001). I deleted the leader sequences from the light and heavy chains of 9E10-APLH and expressed the constructs in *E. coli Rosetta Gami 2* (DE3) (Fig. 5.8A). No band of the appropriate size was detected for 9E10-APLH. Under reduced conditions, extremely faint Fab chains could be detected, but the presence of other impurities rendered this expression and purification process unsuccessful.

I then moved on to the mammalian system, which is more suited for the expression of recombinant eukaryotic proteins (Geisse and Henke, 2005; Backliwal et al., 2008). 9E10 Fab chains with the AP tags were inserted into mammalian expression vectors and targetted for extracellular secretion in HEK-293T cells (Durocher et al., 2002; Backliwal et al., 2008) (Fig. 5.8 B). Although faint Fab chains were detected on reduction, a clear Fab dimer was absent from the eluted samples (Fig. 5.8B). The presence of multiple impurities of various sizes also made this process undesirable.

I next went on to redesign the linkers between 9E10 Fab chains and the AP tags. Linkers confer structural flexibility to a multidomain protein and a bad linker can lead to poor product expression and function (Wriggers et al., 2005). The AP tag, attached via a $(Gly\text{-}Ser\text{-}Gly)_2$ linker at the N-terminus of the heavy and light chains, may have

been interrupting proper folding of 9E10-APLH. One way to overcome this issue was to modulate the length and flexibility of the linkers between the 9E10 Fab and AP tags, such that the AP tags stay clear of the myc binding site but are still close enough to be clamped by tetravalent streptavidin. I therefore modulated the $(Gly\text{-}Ser\text{-}Gly)_2$ linker in two ways. First, I elongated it to $(Gly\text{-}Ser\text{-}Gly)_3$. In a second version, I inserted a rigid helical linker, $Ala\text{-}(Glu\text{-}Ala\text{-}Ala\text{-}Ala\text{-}Lys)_2\text{-}Ala$, which controls distance to an estimated length of 51 Å, and could reduce interference between adjacent domains (Arai et al., 2001). I expressed both constructs in HEK-293T cells, isolated the Fab with Ni-NTA and ran purified fractions on SDS-PAGE (Fig. 5.8C). A strong band at 60 kDa represented BSA, which is present in high amounts in cell culture media. For 9E10-APLH with long linker, a Fab dimer was observed and the band split into two chains on reduction (Fig. 5.8C). However, the yield was less than 0.06 mg from a 250 mL cell culture. No Fab was isolated for the 9E10-APLH construct with the helical linker.

As all efforts to express 9E10 with AP tags had been ineffective, it was possible that the AP tags themselves were causing misfolding. I therefore replaced the AP tag with the BirA Substrate Peptide (BSP) (LHHILDAQKMVWNHR) that can also be biotinylated *in vitro* (Jia et al., 2007). The BSP tags were attached via $(Gly\text{-}Ser\text{-}Gly)_3$ linkers to the N-termini of heavy and light chains of 9E10 Fab. After expression in 293T cells, the purified fractions were run on SDS-PAGE (Fig. 5.8D). The 9E10-BSP dimer was observed at ~50 kDa, and its reduced Fab chains were present at ~25 kDa. The yield was still very low and impure: <0.2 mg 9E10-BSP from 250 mL cell culture.

After exploring further conditions, without substantial improvement in antibody expression (appendices 1 and 2), I focussed instead on testing clamping with anti-HER2.

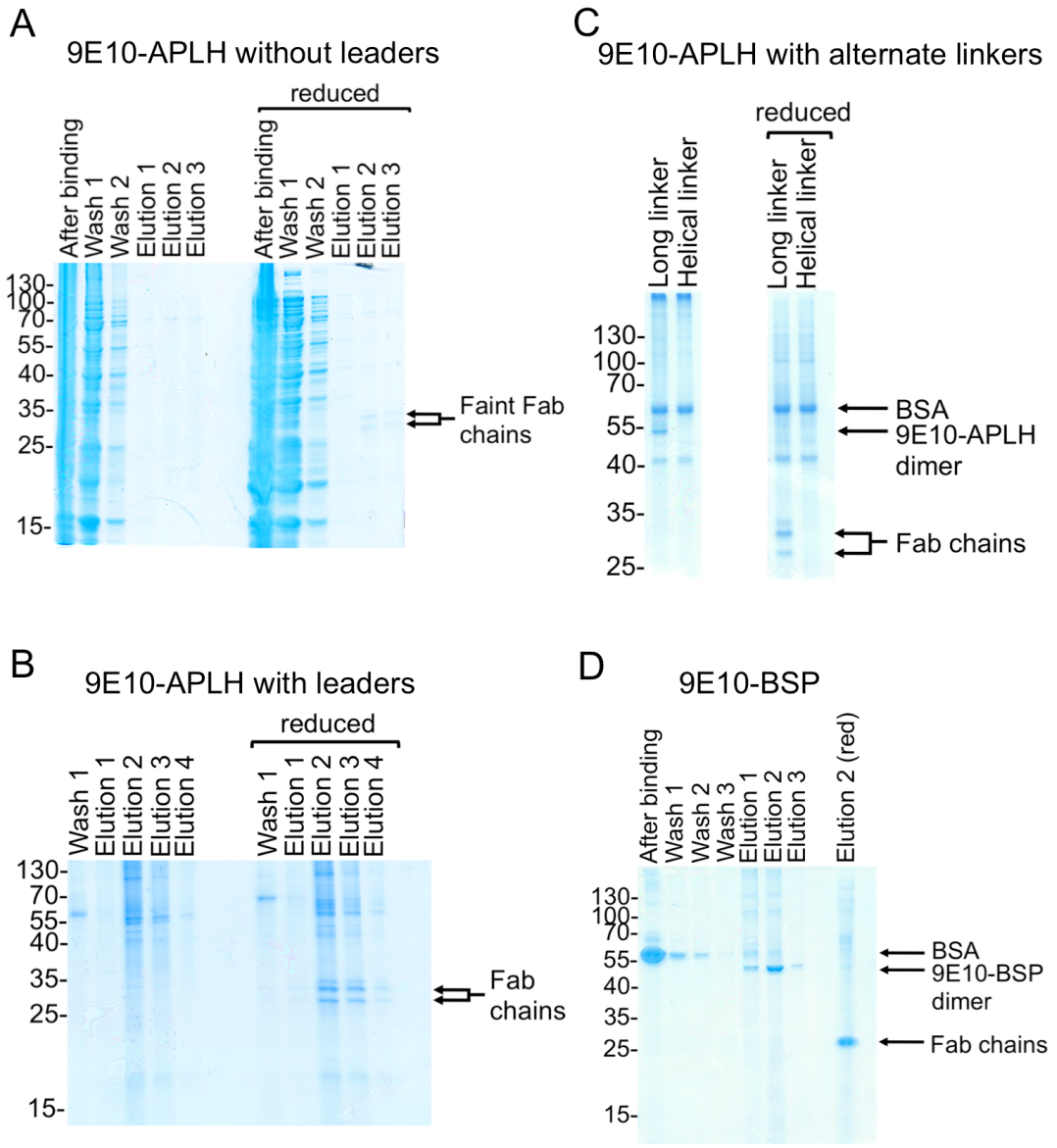

Figure 5.8. Efforts to improve 9E10-APLH expression. A. 9E10-APLH without leader sequences was expressed in the cytoplasm of *E. coli* strain *Rosetta Gami 2*. B. 9E10-APLH was expressed using HEK-293T cells and purified using Ni-NTA. C. 9E10-APLH, with long linker (GSG-GSG-GSG) or helical linker (A-EAAAK-EAAAK-A) between the AP tag and the N-termini of the Fab chains, was expressed extracellularly in HEK-293T cells. Fab was purified on Ni-NTA and run without or with reducing agent. D. 9E10, with BSP tag on the N-termini of heavy and light chains, was expressed in HEK-293T cells and purified on Ni-NTA.

5.7 Developing a clamp based on the HER2-4D5 interaction

As the expression of 9E10-APLHb was a major hindrance in obtaining robust and reliable results, it was important to test the clamping technique on an alternate antibody. 4D5, the mouse monoclonal precursor to hu4D5 and Herceptin, binds the HER2 receptor with high affinity (Carter et al., 1992) and is often used as a tool to detect HER2 on the cell surface. As 4D5 binds the β-sheets in domain IV of HER2 (Fig. 5.9A) (Cho et al., 2003), testing clamping using 4D5 would allow us to explore if the clamping approach was restricted to peptide antigens like myc, or if clamping could also be applied to clamp folded protein domains. Furthermore, as 4D5 binds HER2 with high affinity (K_d = 6 nM for mouse 4D5 IgG) (Shepard et al., 1991), it would be interesting to explore if clamping improved the binding characteristics of a protein interaction where binding was already strong.

For this purpose, I engineered to clamp 4D5 by genetically inserting the AP tags into the N-termini of the heavy and light chains of 4D5 Fab, attached via glycine-serine linkers, and termed the construct 4D5-APLH. As the N-termini are on either side of the HER2 binding interface, the AP tags were designed to extend out on both sides of the HER2 domain and be bridged by tetravalent streptavidin as previously outlined for myc-9E10 (Fig. 5.9A). 4D5-APLH was expressed in HEK-293T cells. After purification on Ni-NTA column, the AP tags on the Fab were biotinylated with BirA, and the doubly biotinylated 4D5-APLH was termed 4D5-APLHb. To check for purity, 4D5-APLH and 4D5-APLHb samples were run on SDS-PAGE (Fig. 5.9B). The Fab dimer showed a clear band at ~52 kDa, and a fainter band at ~53 kDa, which may result from glycosylation of a fraction of the Fab produced. On reduction, the Fab dimer split into its constituent heavy and light chains at ~26 kDa, both of which shifted upwards on the addition of streptavidin. Therefore, complete biotinylation of both Fab chains was achieved. The overall purity of the Fabs was not ideal, as faint bands of various sizes could be seen in each lane. Ideally, the Fab should be purified further under more stringent conditions to obtain a cleaner uniform band. However, as the 4D5-APLHb yield I obtained was low (0.15 mg-0.2 mg from 250 mL cell culture), additional purification cycles were not deemed feasible in the interest of time and resources.

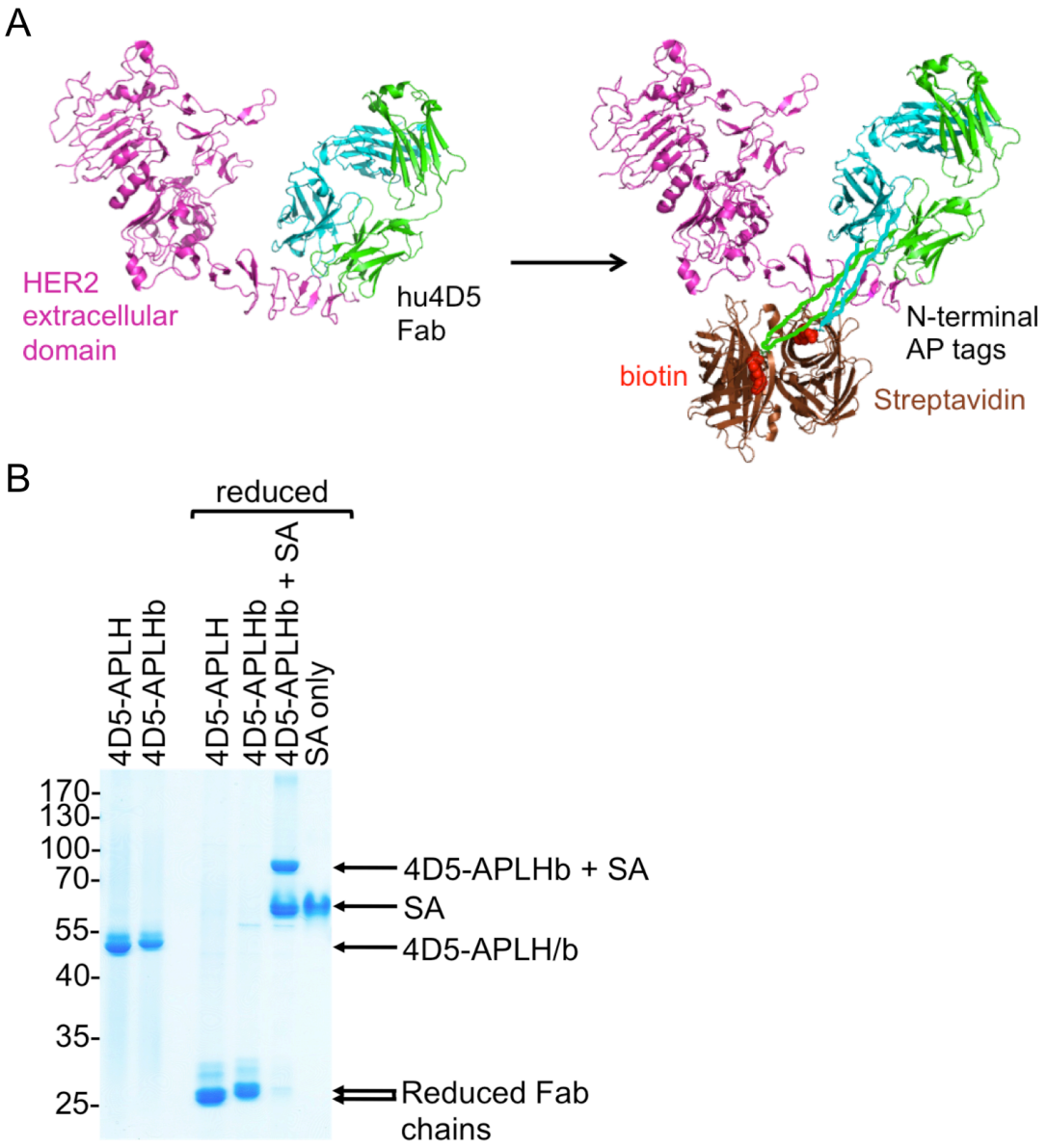

Figure 5.9. Designing the clamp on the HER2-4D5 interaction. A. Cartoon representation of HER2 extracellular domain in complex with hu4D5 (PDB 1N8Z). AP tags inserted on N-termini of light and heavy chains of mouse 4D5 can be biotinylated *in vitro* and bound by tetravalent streptavidin (PDB 1SWE), clamping the HER2 domain within the binding site. HER2-hu4D5 complex is used in this representation although the actual modifications were made on mouse 4D5 Fab. B. SDS-PAGE to analyse the purity and biotinylation of 4D5-APLHb, stained with Coomassie blue.

5.8 Improved stability of the SA-bound antibody on HER2-expressing cells

A sturdy protein lock should be able to survive multiple dissociation forces including chemical interference, physical pulling and time-dependent dissociation. To test the clamp for these features, I exposed the antibody complex to various stringent environments and then compared its binding to the original 4D5 Fab. Using an acidic buffer, I tested whether the antibody complex could maintain its non-covalent interaction in a low pH environment, which would otherwise strip off the antibody. I then proceeded to compare how much longer the clamp would remain bound to cells in a time-course experiment. Finally, I assessed the complex's resistance to physical pulling force on immunomagnetic cell isolation.

5.8.1 Stability of anti-HER2 antibody binding with streptavidin in acid wash

Firstly, to test the functionality of 4D5-APLHb, I used the Fab to bind surface HER2 on high HER2-expressing BT474 cells. Live BT474 cells were labelled with 4D5-APLHb as the primary antibody and then incubated with streptavidin, before detecting bound Fab using anti-mouse IgG conjugated to AlexaFluor555 (Fig. 5.10). As a positive control, I used the unmodified 4D5 Fab to bind BT474 cells. When analysed by fluorescent microscopy, both 4D5 Fab and 4D5-APLHb showed strong binding to the BT474 cell surface (Fig. 5.10, left panel). When 4D5-APLHb was pre-incubated with streptavidin, and then added to BT474 cells, very little to no binding to the cell surface was observed (Fig. 5.10). This is consistent with the clamp design, because incubating with streptavidin should bridge the AP tags and block the HER2 binding site in 4D5, inhibiting HER2 from entering its binding site on the Fab. However, if SA was binding AP tags on different Fab molecules, leading to multimerization of Fabs instead of clamping individual Fabs, the HER2 binding site would still be open and 4D5-APLHb prebound to SA would be able to bind HER2. The effectiveness of the clamp under chemically harsh conditions was assessed by subjecting labelled cells briefly to a pH 3 buffer. Acid wash disrupts weak non-covalent interactions and removes bound antibody, without impairing cell viability (Sugawara et al., 1987).

Cells labelled with primary Fab, with or without SA, were washed with the acid buffer and the bound Fab was detected using anti-mouse IgG-555 (Fig. 5.10, right

panel). Acid wash did not obviously damage cells, as they appeared healthy in the brightfield images (Fig. 5.10). None of the unmodified 4D5 Fab was detected on cells after acid wash, suggesting that 4D5 had dissociated on treatment with the acid (Fig. 5.10). However, almost all of the SA-bound antibody survived acid wash, showing strong binding to cells (Fig. 5.10). This was a promising result as it clearly demonstrated the improved stability of the recombinant antibody in the presence of streptavidin compared to the regular antibody.

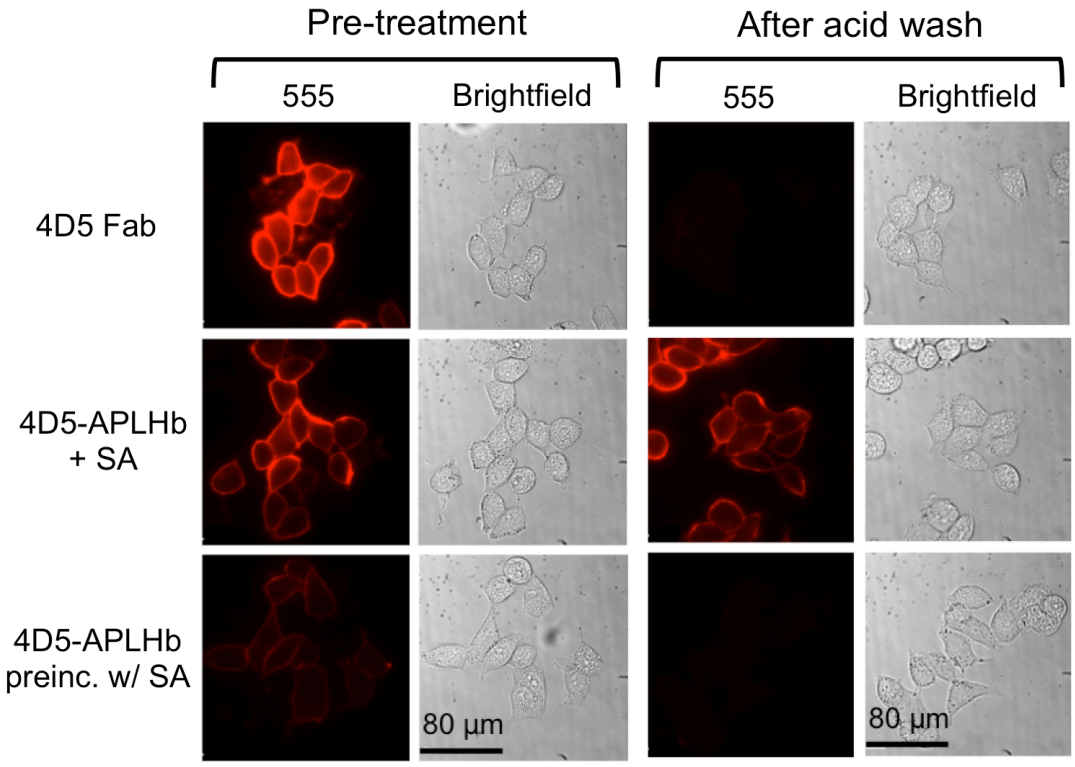

Figure 5.10. Acid wash to test 4D5 stability. BT474 cells were labelled with 10 µg/mL of the indicated 4D5 construct and binding to surface HER2 was detected with anti-mouse IgG AlexaFluor555 and fluorescent microscopy. Acid washing can strip bound 4D5 from the cells, but was unable to remove 4D5-APLHb when SA was added. 4D5-APLHb pre-incubated with SA (bottom row) resulted in weak staining of BT474.

5.8.2 Clamp stability with different SA constructs

As a further control, I tested clamping with various streptavidin constructs containing four (tetravalent SA, SA), two (divalent SA, dSA) or one (monovalent SA, mSA) biotin binding sites on the streptavidin tetramer (Howarth et al., 2006). After labelling with 4D5-APLHb, BT474 cells were incubated with the indicated SA construct, acid

washed as before and analysed by microscopy (Fig. 5.11). Tetravalent streptavidin clamped most efficiently and Fab stayed bound to the cells despite acid wash. As expected, mSA was incapable of bridging the two AP arms, and therefore behaved in a similar fashion as unclamped Fab; no 4D5-APLHb remained bound to cells after acid wash (Fig. 5.11). Interestingly, dSA also increased Fab stability, although it was less efficient than SA (Fig. 5.11).

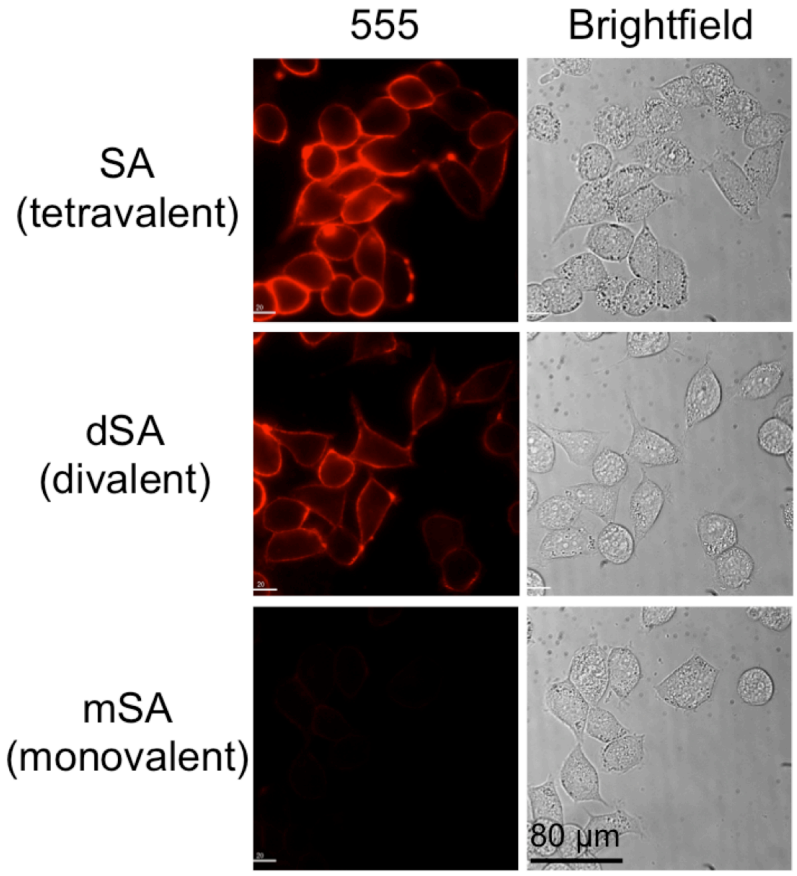

Figure 5.11. Acid wash to test clamping with various SA constructs. BT474 cells were labelled with 10 µg/mL 4D5-APLHb and then incubated with 0.2 µM of the indicated streptavidin construct. After acid wash, bound Fab was detected using anti-mouse IgG AlexaFluor555 and analysed by fluorescent microscopy.

5.8.3 Time-course experiments to assess clamp stability

In order to evaluate the dissociation rate of SA-bound Fab, time-course experiments were conducted. BT474 cells were labelled with 4D5-APLHb and then treated with or without SA. After removing excess Fab and SA, cells were incubated at 37°C for 0, 1, 3, 6 or 21 hr in a cell-culture incubator. The Fab that remained bound to cells after these time periods was detected with anti-mouse IgG-555 and analysed by microscopy (Fig. 5.12). At 0 hr, 4D5-APLHb showed strong binding to HER2 expressing cells, independent of the presence of SA. Within 1 hr, the 4D5-APLHb signal was much weaker compared to its original binding (Fig. 5.12). 4D5-APLHb sustained some binding on cells until 3 hr but had gave almost no signal after 6 hr. On the other hand, in the presence of SA, there was no decrease in the 4D5-APLHb signal at 1 hr: the signal remained high even after 3 hr, and still showed signal at 6 hr (Fig. 5.12). No Fab remained bound at the cell-surface after 21 hr under either condition. Thus SA blocking considerably prolonged the time for which 4D5 stayed bound to HER2 at the cell-surface, suggesting it might show promise as a tool for long-term imaging (Hayashi-Takanaka et al., 2009). As some decrease in the cell surface signal could also be due to endocytosis of the Fab or Fab-SA complex, longer signal on addition of SA could also mean that the SA binding to the Fab is inhibiting its endocytosis and retaining the HER2 on the cell surface.

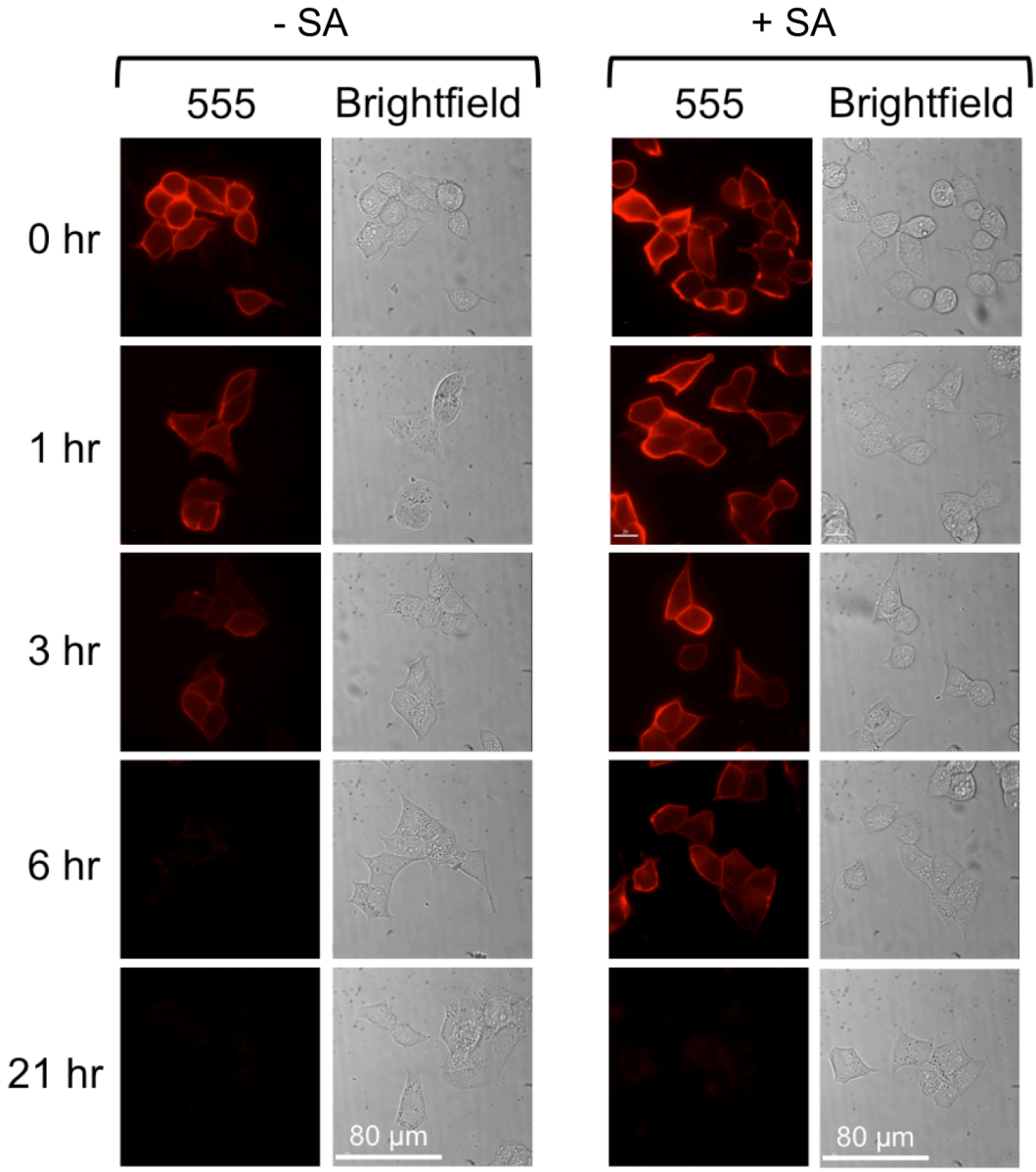

Figure 5.12. Time-course experiment to study clamping efficiency at the cell-surface. BT474 cells were labelled with 15 µg/mL 4D5-APLHb and incubated without or with tetravalent SA. Cells were washed and incubated in cell media for the indicated duration of time. Fab that remained bound at the cell-surface was detected with anti-mouse IgG 555 and imaged with fluorescent microscopy.

5.9 Clamping vs. multimerization

Although the anti-HER2 Fab had shown greater apparent stability in the presence of streptavidin, the mechanism by which SA was reducing Fab dissociation was not confirmed. Bridging two AP tags on the same Fab, thereby locking the antigen

domain, is one way of mechanically restraining dissociation. However, it is also conceivable that SA could bind two AP tags on adjacent Fab molecules. As tetravalent SA can bind up to four biotins, SA could easily crosslink multiple Fabs, forming multimers of 4D5-APLHb and SA (Fig. 5.13A). Therefore, increased Fab-SA stability could be due to multivalency and not protein locking. To test this hypothesis, I designed 4D5-LHAPb bearing AP tags on the *C-termini* of the heavy and light chains of 4D5 Fab. If Fab stability was mostly due to streptavidin's tendency to bind two AP tags on the same Fab, 4D5-LHAPb would not be able to lock HER2 and would behave similarly to unmodified 4D5 (Fig. 5.13B). However, if SA-enhanced stability was a result of multimerization, 4D5-LHAPb would be as stable as 4D5-APLHb (Fig. 5.13B).

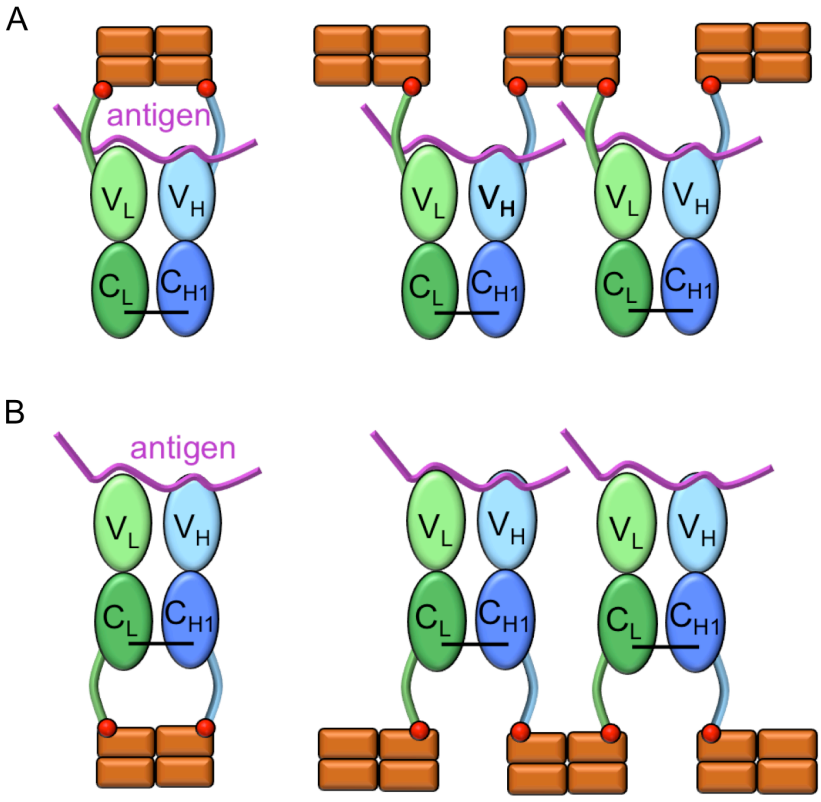

Figure 5.13. Schematic representation of clamping versus multimerization model. Tetravalent SA (orange) could bind AP tags on the Fab (blue, green) in two ways: - it could bind both AP tags on the same Fab, locking the antigen (pink) into the binding site, or it could bind AP tags on different Fabs, crosslinking multiple antigen-Fab interactions. As multimers dissociate slower than individual interactions, both clamping and multimerization can be associated with more stable Fab binding. A. The two models on N-terminally inserted AP tags, 4D5-APLHb. B. The two models on C-terminally inserted AP tags, 4D5-LHAPb. If the clamping model is dominant, 4D5-LHAPb will not be as stable as 4D5-APLHb.

4D5-LHAPb was expressed and purified and both AP tags were biotinylated with BirA. The Fab dimer gave a strong band at ~56 kDa on SDS-PAGE (Fig. 5.14). On reduction, the dimer split into individual Fab chains, which were ~28 kDa in size, and shifted in the presence of SA, suggesting complete biotinylation (Fig. 5.14). To check if 4D5-LHAPb was as resistant to chemical interference as 4D5-APLHb, I labelled BT474 cells with the two different Fabs and then incubated with dSA (Fig. 5.15A). After acid wash, the bound 4D5-LHAPb was detected with a secondary antibody and was found to have survived acid wash with the same intensity as 4D5-APLHb (Fig. 5.15A). Thus, both Fab constructs, with AP tags in opposite directions, sustained binding to HER2, when dSA was used to bind their AP tags. This result supports the multimerization mechanism over the clamping mechanism (Fig. 5.13): the enhanced antigen binding with streptavidin is most likely a result of crosslinking of multiple Fabs rather than due to individual Fab clamps.

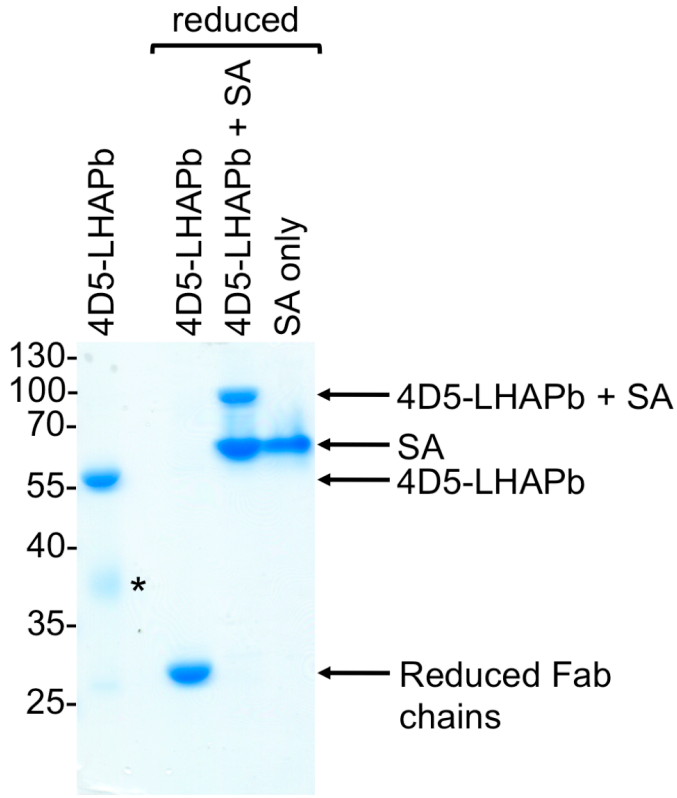

Figure 5.14. Purification and biotinylation of 4D5-LHAPb. SDS-PAGE of 4D5 with C-terminal AP tags (4D5-LHAPb) without or with reducing agent. Addition of streptavidin shifted both Fab chains. Smeared band between 35-40 kDa (*) is probably degraded Fab.

Furthermore, I compared the two constructs using immunomagnetic cell isolation. I coated BT474 cells with either 4D5-APLHb or 4D5-LHAPb at 1 μg/mL or 0.1 μg/mL and then isolated cells using SA-coated magnetic particles (Fig. 5.15B). In the presence of a magnetic field, a pulling force is applied on the magnetic bead. As SA is attached to the magnetic bead from one side and binds 4D5 from the other, SA will be pulled in a direction away from the Fab. In the case of 4D5-APLHb, this force should have less effect on the HER2-Fab interaction, as HER2 would be trapped between the Fab and SA. However, with 4D5-LHAPb, SA would be pulling the Fab away from HER2, and therefore the amount of cells recovered by immunomagnetic cell isolation should be lower. On the other hand, if multimerization was dominating over clamping, both constructs would form large networks of HER2-Fab-SA complexes, and 4D5-APLHb would not have an advantage over 4D5-LHAPb. When the immunomagnetically isolated cells were calculated as a percentage of total number of cells, 4D5-LHAPb recovered a higher number of cells than 4D5-APLHb (Fig. 5.15B). At 1 μg/mL, 4D5-LHAPb recovered 20% more cells than 4D5-APLHb (Fig. 5.15B, $P < 0.01$, $n = 2$, unpaired t- test). At 0.1 μg/mL, recovery from 4D5-APLHb was negligible, whereas 4D5-LHAPb recovered more than 70% cells (Fig. 5.15B, $P < 0.005$, $n = 2$, unpaired t- test). Therefore the antibody with the potential to clamp (4D5-APLHb) did not show any improvement over the antibody that could only multimerize (4D5-LHAPb) and in fact performed worse. This result is also inconsistent with the clamping model and consistent with the multimerization model.

Moreover, when the bis-biotinylated 4D5-APLHb was incubated with dSA in solution before running on SDS-PAGE, a bias towards 1Fab:2dSA was seen, and little 1Fab:1dSA complex was detected (Appendix 3, observed by laboratory member Dr. Denis Krndija, 2011). Higher molecular weight complexes denoting multimers of Fab-dSA complexes were also evident and were absent when 4D5-APLHb was incubated with mSA instead of dSA (Appendix 3, observed by laboratory member Dr. Denis Krndija, 2011).

It should however be noted that 4D5-LHAPb may not be the best control to compare to 4D5-APLHb, as the distance between the C-termini of 4D5 Fab (9.8 Å) differs from the distance between the two N-termini in 4D5 Fab (34.2 Å) (based on PDB 1N8Z). Furthermore, the movement of the extended AP tags might be restricted in

4D5-APLHb due to the presence of HER2 in the binding site, whereas the AP tags may move more freely when they are at the C-termini of the Fab chains, away from the binding site. This could also lead to a difference in the ratio of clamped vs. multimerized Fab when using the two constructs.

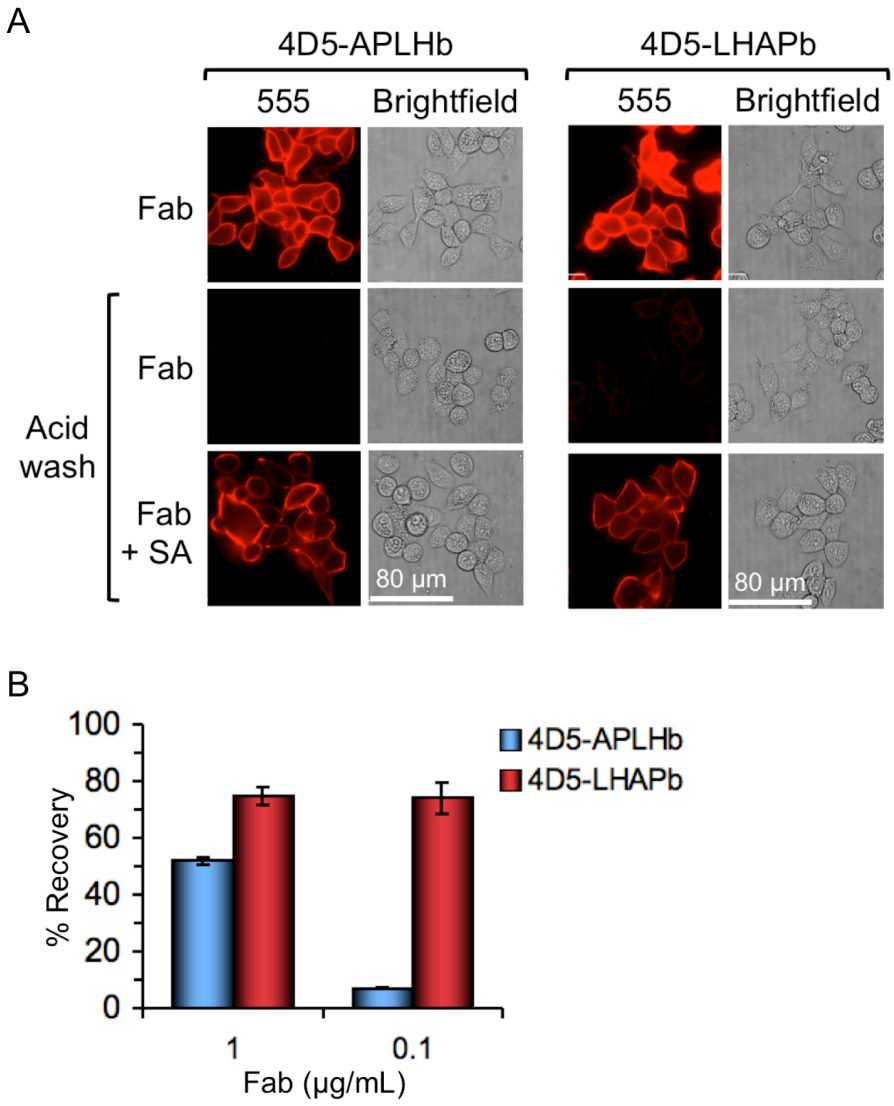

Figure 5.15. Comparing stability of 4D5-APLHb and 4D5-LHAPb on HER2 binding. A. BT474 cells were labelled with the indicated Fab and binding was detected with anti-mouse IgG-555 by fluorescent microscopy. B. BT474 cells were labelled with the indicated concentration of either 4D5-APLHb or 4D5-LHAPb and isolated with SA-coated magnetic beads. Recovered cells were quantified on a Coulter counter and calculated as a percentage of the total number of input cells (mean of duplicate ± 1 s.d.).

5.10 Discussion

Most antibodies associate with their ligands in a reversible manner to form complexes based on non-covalent interactions. A slow rate of dissociation is important for *in vivo* targetting applications when a therapeutic drug requires a longer period on target to be effective, as well as for immunoassays or live cell imaging. In this chapter, I describe efforts to develop an alternative way to achieve antigen-antibody complex stability, by not modifying the primary binding interaction but, once the antigen-antibody complex has formed, clamping the antigen in place in a way that is irrespective of the particular antibody-antigen complex. The design of the clamp was to allow an external SA molecule to bind to biotinylated AP tags on either side of the antigen binding group on the Fab, physically restricting the antigen from dissociating from the complex. The engineered clamp was tested on two Fabs, myc peptide-binding 9E10 and HER2-binding 4D5. The strategy showed some promise initially, as adding SA to the engineered Fabs increased binding on ELISA and cell imaging. However, it was difficult to demonstrate experimentally if the antibodies actually clamped as designed, or if the increased stability was a result of previously unanticipated antibody multimerization.

During the process of engineering the clamp, AP tags were chosen for clamping, as they are short peptide tags that can be easily inserted genetically into the Fab chains. After biotinylation, these tags bind SA with extremely high affinity, forming an almost irreversible interaction. Alternate SA-binding tags, such as Streptag (AWRHPQFGG, $K_d = 3.7 \times 10^{-5}$ M), Streptag II (WSHPQFEK, $K_d = 7.2 \times 10^{-5}$ M) and P25 (CWHPQAGC, where C residues are disulfide-bonded, $K_d = 1.3 \times 10^{-5}$ M) (Schmidt et al., 1996) can also be considered, especially as they are shorter than the AP tag and would not have to undergo the additional process of biotinylation. However, their affinity for SA is 10^9 fold worse than biotin-streptavidin, and would therefore not be ideal for clamping. BSP tags were also used as a replacement for AP tags, to try to reduce the impairment caused by AP tags on 9E10 Fab folding, but BSP-tagged 9E10 did not express substantially better in HEK-293T cells, and was therefore not explored further. The N-termini of the Fab chains were a convenient place to attach AP tags, but it might be possible to insert the AP tags into loops

surrounding the antigen binding site, as would be required to clamp single-chain Fv fragments, although this remains to be investigated.

For the clamp, tetravalent SA was chosen as it could bind both AP tags on a Fab with equal affinity. Divalent SA would have been preferable, as it would minimize the issue of multimerization. However, the two species of divalent SA, 1,2 dSA (adjacent active subunits) and 1,3 dSA (diagonally positioned active subunits), were difficult to differentiate and the restricted distances between the two biotin binding sites may have affected clamping the 2 AP tags.

It is now possible to isolate each dSA species separately (based on unpublished work by Dr. Michael Fairhead, Howarth laboratory) and the use of divalent SAs can be further explored in clamping (Appendix 4). A higher stability SA mutant, traptavidin, with 10-fold lower off-rate for biotin conjugates (Chivers et al., 2010) is also an interesting candidate to further optimize SA clamping.

The AP-tagged 9E10-APLHb showed binding to myc on ELISA (Fig. 5.5A). As it is imperative that the Fab first bind its antigen for the clamp to be effective, 9E10-APLHb clamping was tested on myc1 constructs; its binding to myc2 was negligible (Fig. 5.5A). On ELISA, > 2-fold increase in absorbance was observed when myc1 was clamped with 9E10-APLHb and SA (Fig. 5.6). This suggests that SA had successfully bound AP tags, stabilizing the complex and holding the myc peptide in place. This increase in absorbance was only observed at myc1 concentrations above 10 nM, and the clamp did not affect absorbance for lower myc1 concentrations (Fig. 5.6A and B), exposing an important limitation of the clamping technique. When there is no initial myc-9E10 binding at lower myc1 concentrations, there is nothing for SA to clamp and therefore there is no increase in absorbance. Thus clamping does not increase detection of lower concentrations of antigen. However, a resulting counter advantage of clamping is that it achieves higher Ag-Ab stability without losing specificity of the interaction. However, in light of the later results regarding multimerization of 4D5-APLHb by SA binding, the increase in 9E10-APLHb stability seen here could also be due to multimerization and not clamping. However, it would have been difficult to do all the careful experiments with ELISA, especially as the 9E10-APLH yield was so low and impure. Therefore, at this stage, it is difficult to

predict the possible use of the rotaxane model for antibody clamping, due to the problems posed by multimerization.

One major issue with 9E10-APLHb was its reduced intrinsic affinity to myc peptide. The absorbance on ELISA halved when 9E10-APLHb was used to bind myc instead of 9E10-APLH (Fig. 5.5B). The 9E10-myc interaction is an unusual one, as the antibody forms a ternary complex, with one 9E10 Fab molecule binding to myc, and a second 9E10 Fab binding to the peptide-Fab complex, sandwiching the myc peptide in between the two Fabs, giving rise to a 2 Fab:1 peptide complex (Krauß et al., 2008). This sandwich might increase the apparent affinity of 9E10 for myc, as binding of two Fabs amplifies the signal and therefore the absorbance on ELISA. The tags on 9E10-APLHb might lead to steric clash with the second Fab molecule, and therefore, only one Fab binds the myc peptide instead of two, thereby giving lower absorbance. Thus the tag may hinder the natural self-clamp in 9E10-myc, and this is restored in the presence of the artificial SA block. If anything, the SA clamp might work better on other peptide-Fab interactions, where self-clamping is not an issue. Fusion of the N-terminal AP tags could interfere with myc1 binding, and lower the Fab affinity, and such complications should be kept in mind when designing N-terminal peptide tags on antibodies.

Various methods were employed to improve the expression of 9E10-APLH and it was indeed the most challenging aspect of this study. To improve 9E10-APLH yield, I expressed the Fab in an oxidized bacterial cytoplasmic environment, in mammalian HEK-293T cells, inserted alternative linkers between the Fab and AP tags, used an alternative streptavidin binding BSP tag and a number of other techniques (Fig. 5.8 and appendices 1 and 2). However, none of these approaches were successful in expressing high amounts of 9E10-APLH. Furthermore, the His-tag used to isolate 9E10-APLH by Ni-NTA, was only present on the heavy chain, as the light chains have higher a tendency to homodimerize. The Ni-NTA purification could have still pulled down heavy chain dimers and multimers, contaminating the Fab fraction. One could also use Protein A, Protein G or Protein L columns to further purify 9E10-APLH, but this risks losing a lot of protein yield. Low Fab expression could also be due to premature termination of translation or the inhibition of translation by mRNA secondary structure and it might therefore be interesting to check if codon

optimization of the 9E10-APLH gene enhances its expression efficiency (Chattopadhaya et al., 2006). However, even with high Fab expression, the biotinylation process is itself inefficient and can lead to a 60% loss in protein yield (Saviranta et al., 1998).

As efforts to express 9E10-APLH did not yield positive results, the clamping approach was applied to HER2-binding 4D5 Fab. 4D5-APLH, with N-termini AP tags, was relatively easier to express and purify in workable yields. As HER2 domain IV (the antigen region for 4D5), is a much bigger domain than myc peptide, longer linkers were used to insert the AP tags. Conducting ELISA experiments were not deemed suitable for the HER2-4D5 interaction, as HER2 is a much larger protein than MBP-myc, and isolating and purifiying the HER2 domain, to be used as antigen on ELISA, would have posed an additional set of challenges. 4D5-APLHb was therefore directly tested on HER2-expressing cells and additions of SA helped sustain the HER2-Fab interaction for prolonged time and on treatment with acid buffer.

In order to differentiate between clamping of each antigen-Fab interaction and multimerization of multiple antigen-Fab interactions, a control was synthesized with AP tags at the C-termini of the 4D5-Fab, 4D5-LHAPb. 4D5-LHAPb also survived acid wash like 4D5-APLHb. Furthermore, when both constructs were tested on immunomagnetic cell isolation using HER2 expressing cells and SA-coated magnetic beads, 4D5-LHAPb recovered more cells than 4D5-APLHb at two different Fab concentrations (Fig. 5.15B). Both these results indicate that the increased Fab stability on cells in the presence of SA is due to multimerization and not necessarily due to clamping. However, it is difficult to directly make comparisons between 4D5-APLHb and 4D5-LHAPb, as the distance between the two AP tags is different in the two constructs. 4D5-LHAPb might be more prone to multimerization, and 4D5-APLHb might prefer clamping, based on the distance between the biotin binding sites in SA. Furthermore, when SA is attached to a rigid magnetic bead, SA molecules might have restricted movement, leading to a preference for multimerization instead of clamping in immunomagnetic cell isolation. However, in acid wash, both 4D5-APLHb and 4D5-LHAPb survive when incubated with SA. Therefore, if enhanced binding is required for live cell imaging and multimerization is not an issue, 4D5-APLHb or 4D5-LHAPb can still be used with SA for prolonged stabilization of antibody on cell

surface. Furthermore, in this study we had used BT474 cells, which have an extremely high expression of surface HER2 (Gaborit et al., 2011). In cases where the antigen is present sparsely (Kaplan and Smith, 2000), clamping might predominate over multimerization.

In conclusion, clamping showed some promise, but its advantages are limited and clamping was difficult to differentiate from multimerization as we could not find a straightforward approach to prove clamping. There may have been clamping of a fraction of the Fabs in some of the best assays; but even if it was occurring, it was masked by the reduced binding efficiencies of the AP-tagged Fab constructs and the increase in Fab stability due to multimerization. While engineering such a tool, it is imperative to consider not just the desired assembly, but all possible assemblies, their potential occurrence rate and effects; there is great scope in further exploring this strategy.

The final goal of clamping should be to clamp unmodified antibodies and binding proteins, so that problems with protein expression, affinity and specificity are avoided. Enhancing the stability of protein-protein interactions will go a long way in discovering and studying new biomarkers for the advancement of research and medicine.

Chapter 6: Summary and General discussion

Chapter 6: Summary and General discussion

6.1 Development of an enhanced approach to isolate cells

Antibodies are routinely used for a number of applications in cell separation. In the work presented here, I show how immunomagnetic cell separation can be made more efficient by optimizing the cell-magnetic bead interaction at the molecular level. These efforts enhanced immunomagnetic recovery, while still giving high purity and throughput of cells. In the light of the observations presented in Chapter 3, cell surface-expressed antigen number, antibody affinity, antibody linkage to the bead and membrane cholesterol levels all contribute to the ability to magnetically isolate cells. Through this work, it can also be seen how the recovery of cells expressing low levels of antigen can be enhanced by three steps: 1.) loading cells with cholesterol 2.) seeking the highest affinity biotinylated antibody available and 3.) capturing the biotinylated antibody with streptavidin conjugated to the solid phase, thereby avoiding any intermediary weak link. Together, these steps greatly increased the recovery of low HER2-expressing cancer cells from rabbit and human blood, and showed the potential for use of this approach in isolating CTCs from cancer patients. As each of these enhancements works independently, they can also be employed individually as required.

The enhancements described here apply to capture based on HER2 as well as EpCAM (see attached manuscript) and are therefore likely to be relevant to other cell-surface expressed antigen-antibody interactions. Although Fab affinity and secondary linkage enhancements should be independent of antigen type, membrane cholesterol content may affect different membrane receptors in a variable manner and its effect should therefore be checked before using on other receptors.

My work here was based on immunomagnetic separation, but the results from this thesis could be applied to other solid-phase affinity capture systems, such as CTC-Chip, CellSearch, MACS, chromatography columns or any system where antibody-based recognition of cells is required. These enhancements can be applied to the current affinity-based cell isolation appliances and do not require re-engineering of any machinery, such as capture material components or blood centrifugation/flow rate

settings, thereby making the enhanced approach immediately applicable in the research setting.

However, these enhancements face a number of challenges. A major deterrent in selecting high affinity antibodies for use is that data on antibody affinity is not readily available from commercial entities. Researchers have to select antibodies based on the information presented via Western blots and immunofluorescence assays. However, such data is not sufficient to predict the performance of the selected antibody in affinity-based cell capture. Affinity-based cell capture subjects the antigen-antibody interaction to high mechanical and physical pulling forces, created due to the drag of the cells and the friction generated by the flow of the solution (Chalmers et al., 1999). Therefore, antibodies that are otherwise efficient in detecting antigen in various immunoassays may not necessarily be suitable for affinity capture of cells.

Furthermore, antibodies produced for therapy are not always optimized for the highest affinity, as very high affinity can decrease effective tumour targeting (Carter, 2001). However, these antibodies with medium affinities are then continued to be used for research and diagnostic purposes due to their approved status and widespread popularity. Such antibodies often have a number of higher affinity mutants, (such as D102W for HER2 (Gerstner et al., 2002)) that are less well known but can be more effective in cell capture. This study further emphasizes the need for antibodies with very high affinities (sub-nanomolar range) and well-defined kinetics; although such antibodies have been engineered using a variety of different techniques (Chapter 1), extensive production and usage of such constructs is still lacking.

In CTC isolation, a cocktail of antibodies is sometimes preferred over the use of a single antibody ((Mikolajczyk et al., 2011). A single tumour marker, such as EpCAM, may be downregulated in CTCs and therefore a mixture of antibodies targetting various tumour markers imparts a higher probability of isolating CTCs based on alternate markers. In such cases, it might be difficult to obtain biotinylated high affinity versions of each antibody and using a secondary antibody that can target all the primary monoclonal antibodies might be preferred.

Furthermore, addition of cholesterol leads to variable increase in cell recovery depending on cell-type, as seen in Chapter 4. Such variability could be due to

differences in the endogenous cholesterol levels in the cell membrane. Some cell-types have very high basal cholesterol content (Awad et al., 2003) and therefore adding more cholesterol might not make substantial difference. However, addition of cholesterol is the easiest and most practical of the three enhancements. Keeping in mind that cholesterol can be added to blood after the blood has been drawn from the patient, addition of cholesterol might be used to increase CTC isolation from cancer patients.

The improvement of the enhanced approach over the standard approach was starker in isolation from blood than from cell media, probably because the magnetic beads had to pull through a denser mixture of cells and debris in blood and therefore the need for the bead:cell synapse to be stronger was higher when isolation was from blood. Preliminary results on cell-magnetic bead imaging showed that within just half an hour of incubating cells with beads, the cell membrane had wrapped around the bound beads. In future, it will be interesting to see how addition of cholesterol changes the membrane's flexibility and the pace with which the membrane envelops the bead. Incubation with immunomagnetic beads can lead to a cell membrane detachment phenomenon, which involves immunobead-induced removal of specific cell surface antigen, without killing the cells (Rubbi et al., 1993). Data on cholesterol's effects on such antigen uprooting by magnetic beads can also provide useful insights on why cholesterol addition increases immunomagnetic isolation efficiency.

In summary, I see this work having the potential to contribute to scientific research in three main ways:- 1.) gaining a better understanding of the interaction between a cell and the solid-phase from a molecular perspective 2.) using the enhanced isolation approach in various areas of cell separation techniques and 3.) using the enhanced isolation approach in isolating low antigen expressing CTCs from cancer patients. The worked described in this thesis may have implications on designing antibodies specifically for use in cell isolation, reconsidering the current dependence on high-expressing cell surface antigens and the discovery and use of alternative cancer biomarkers.

6.2 Physically blocking the dissociation of an antigen-antibody interaction

In the second part of my thesis, I worked towards developing a molecular clamp for the antigen-antibody interaction. As the major force induced on the cell-bead synapse during immunomagnetic cell isolation is the physical pulling by the bead and the friction presented by the flow of the solution, it seemed reasonable to decrease the chances of Fab dissociation from the antigen, by introducing a physical block. I used streptavidin to bind biotinylated peptide tags inserted on each side of the antigen binding site in the Fab and block the dissociation of the antigen. Although my efforts were successful in making the antigen-Fab interaction resistant to various chemical and physical forces, a number of challenges relating to recombinant Fab production and difficulties in testing clamping were faced and therefore my work was only partially fruitful.

However, my findings were preliminary and there are a number of other ways varying in size, stability, reversibility and genetic encodability that could be explored while engineering an antibody clamp. DNA and RNA aptamers that specifically bind to the protein region next to the antigen binding sites (Ellington and Szostak, 1990) could be used to encircle the antigen-antibody interaction. Such an approach would allow the clamping of unmodified antibodies, as secreted by hybridomas, thereby extending the scope and power of this approach. This approach is similar to sandwich immunoassays, which employ anti-metatypic antibodies raised against already existing antigen-antibody complexes, and have shown to increase the interactions' stability (Towbin et al., 1995). Another possibility could be chemical modification of the antibody so that the clamp can react with the antibody and lock the antigen in the binding site. Peptides that covalently bind their protein partners (Zakeri et al., 2012) could also be genetically inserted into the Fab to lead to covalent clamping. However, these ideas are theoretical and empirical testing will have to be carried out to investigate their efficacy.

A lot of work still needs to go into designing an antibody clamp. However, once developed, the clamp's use will not be limited to immunomagnetic cell isolation. Clamping could be useful for long-term imaging, for ELISA to detect low levels of antigen, and for purification of peptide-tagged proteins. Clamping could also allow the capture of transient interactions such as those of DNA-binding transcription

factors and histone-binding proteins. One major advantage of the clamping approach is that it does not change the intrinsic affinity of the antibody, but just blocks its dissociation after the antibody has bound. This could have potential use in tumour targeting and therapy, where very high affinity antibodies are adsorbed on the surface of the tumour and therefore do not penetrate deeper into the tumour (Peer et al., 2007). The clamping approach would allow the primary antibody to first enter the tumour and then clamp the bound antibodies to ensure that they produce the desired effect. This approach could also be applied to antibody fragments other than Fab such as scFvs or non-immunoglobulin scaffolds (Gebauer and Skerra, 2009) such as DARPins (Zahnd et al., 2010) and affibodies (Orlova et al., 2007).

References

Abulrob, A., Lu, Z., Baumann, E., Vobornik, D., Taylor, R., Stanimirovic, D., and Johnston, L.J. (2010). Nanoscale imaging of epidermal growth factor receptor clustering: effects of inhibitors. The Journal of Biological Chemistry 285, 3145–3156.

Ackerman, M., Levary, D., Tobon, G., Hackel, B., Orcutt, K.D., and Wittrup, K.D. (2009). Highly Avid Magnetic Bead Capture: An Efficient Selection Method for de novo Protein Engineering Utilizing Yeast Surface Display. Biotechnology Progress 25, 774–783.

Ackermann, D., Schmidt, T.L., Hannam, J.S., Purohit, C.S., Heckel, A., and Famulok, M. (2010). A double-stranded DNA rotaxane. Nature Nanotechnology 5, 436–442.

Ahmad, Z.A., Yeap, S.K., Ali, A.M., Ho, W.Y., Alitheen, N.B.M., and Hamid, M. (2012). scFv antibody: principles and clinical application. Clinical & Developmental Immunology 2012, 980250.

Aitken, R. (2009). Antibody Phage Display: Methods and Protocols.

Akerstrom, B., and Bjorck, L. (1989). Protein L□: An Immunoglobulin Light Chain-binding Bacterial Protein. The Journal of Biological Chemistry 264, 19740–19746.

Al-Lazikani, B., Lesk, a M., and Chothia, C. (1997). Standard conformations for the canonical structures of immunoglobulins. Journal of Molecular Biology 273, 927–948.

Allard, W.J., Matera, J., Miller, M.C., Repollet, M., Connelly, M.C., Rao, C., Tibbe, A.G.J., Uhr, J.W., and Terstappen, L.W.M.M. (2004). Tumor cells circulate in the peripheral blood of all major carcinomas but not in healthy subjects or patients with nonmalignant diseases. Clinical Cancer Research: an Official Journal of the American Association for Cancer Research 10, 6897–6904.

Allen, T.M. (2002). Ligand-targeted therapeutics in anticancer therapy. Nature Reviews. Cancer 2, 750–763.

Antolovic, D., Galindo, L., Carstens, A., Rahbari, N., Büchler, M.W., Weitz, J., and Koch, M. (2010). Heterogeneous detection of circulating tumor cells in patients with colorectal cancer by immunomagnetic enrichment using different EpCAM-specific antibodies. BMC Biotechnology 10, 35.

Arai, R., Ueda, H., Kitayama, a, Kamiya, N., and Nagamune, T. (2001). Design of the linkers which effectively separate domains of a bifunctional fusion protein. Protein Engineering 14, 529–532.

Aricescu, a R., Lu, W., and Jones, E.Y. (2006). A time- and cost-efficient system for high-level protein production in mammalian cells. Acta Crystallographica. Section D, Biological Crystallography 62, 1243–1250.

Attrill, H., Harding, P.J., Smith, E., Ross, S., and Watts, A. (2009). Improved yield of a ligand-binding GPCR expressed in E. coli for structural studies. Protein Expression and Purification 64, 32–38.

Autebert, J., Coudert, B., Bidard, F.-C., Pierga, J.-Y., Descroix, S., Malaquin, L., and Viovy, J.-L. (2012). Microfluidic: an innovative tool for efficient cell sorting. Methods (San Diego, Calif.) 57, 297–307.

Awad, A.B., Williams, H., and Fink, C.S. (2003). Effect of phytosterols on cholesterol metabolism and MAP kinase in MDA-MB-231 human breast cancer cells. The Journal of Nutritional Biochemistry 14, 111–119.

Backliwal, G., Hildinger, M., Chenuet, S., Wulhfard, S., De Jesus, M., and Wurm, F.M. (2008). Rational vector design and multi-pathway modulation of HEK 293E cells yield recombinant antibody titers exceeding 1 g/l by transient transfection under serum-free conditions. Nucleic Acids Research 36, e96.

Baneyx, F., and Mujacic, M. (2004). Recombinant protein folding and misfolding in Escherichia coli. Nature Biotechnology 22, 1399–1408.

Bannister, D., Wilson, A., Prowse, L., Walsh, M., Holgate, R., Jermutus, L., and Wilkinson, T. (2006). Parallel , High-Throughput Purification of Recombinant Antibodies for In Vivo Cell Assays. Biotechnology and Bioengineering 94, 932–937.

Barbas, C.F., Kang, a S., Lerner, R. a, and Benkovic, S.J. (1991). Assembly of combinatorial antibody libraries on phage surfaces: the gene III site. Proceedings of the National Academy of Sciences of the United States of America 88, 7978–7982.

Bargmann, C.I., Hung, M.C., and Weinberg, R. a (1986). Multiple independent activations of the neu oncogene by a point mutation altering the transmembrane domain of p185. Cell 45, 649–657.

Barman, S., and Nayak, D.P. (2007). Lipid raft disruption by cholesterol depletion enhances influenza A virus budding from MDCK cells. Journal of Virology 81, 12169–12178.

Barr, D.J., Ostermeyer-Fay, A.G., Matundan, R. a, and Brown, D. a (2008). Clathrin-independent endocytosis of ErbB2 in geldanamycin-treated human breast cancer cells. Journal of Cell Science 121, 3155–3166.

Baruah, K., Bowden, T. a, Krishna, B. a, Dwek, R. a, Crispin, M., and Scanlan, C.N. (2012). Selective deactivation of serum IgG: a general strategy for the enhancement of monoclonal antibody receptor interactions. Journal of Molecular Biology 420, 1–7.

Baselga, J., and Swain, S.M. (2009). Novel anticancer targets: revisiting ERBB2 and discovering ERBB3. Nature Reviews. Cancer 9, 463–475.

Basiji, D.A., Ortyn, W.E., Liang, L., Venkatachalam, V., and Morrissey, P. (2007). Cellular Image Analysis and Imaging by Flow cytometry. Journal of Laboratory and Clinical Medicine 27, 653.

Batra, S.K., Jain, M., Wittel, U.A., Chauhan, S.C., and Colcher, D. (2002). Pharmacokinetics and biodistribution of genetically engineered antibodies. Current Opinion in Biotechnology 13, 603–608.

Bayraktar, U.D., Kim, T.K., Drews-Elger, K., Benjamin, C., El-Ashry, D., Wieder, E., and Komanduri, K. V (2011). Simultaneous measurement of ERα, HER2, and phosphoERK1/2 in breast cancer cell lines by flow cytometry. Breast Cancer Research and Treatment 129, 623–628.

Bayry, J., Thirion, M., Misra, N., Thorenoor, N., Delignat, S., Lacroix-Desmazes, S., Bellon, B., Kaveri, S., and Kazatchkine, M.D. (2003). Mechanisms of action of intravenous immunoglobulin in autoimmune and inflammatory diseases. Neurological Sciences 24, S217–21.

Beckett, D., Kovaleva, E., and Schatz, P.J. (1999). A minimal peptide substrate in biotin holoenzyme synthetase-catalyzed biotinylation. Protein Science: a Publication of the Protein Society 8, 921–929.

Behring, E.A., and Kitasato, S. (1890). Uber das Zustandekommen der Diphtherie-Immunitat und der Tetanus-Immunitat bei Thieren. Deutsche Medicinische Wochenschrift 49, 1113–1114.

Belogurov, A., Smirnov, I., Ponomarenko, N., and Gabibov, A. (2012). Antibody-antigen pair probed by combinatorial approach and rational design: bringing together structural insights, directed evolution, and novel functionality. FEBS Letters 586, 2966–2973.

Ben-Kasus, T., Schechter, B., Lavi, S., Yarden, Y., and Sela, M. (2009). Persistent elimination of ErbB-2/HER2-overexpressing tumors using combinations of monoclonal antibodies: relevance of receptor endocytosis. Proceedings of the National Academy of Sciences of the United States of America 106, 3294–3299.

Berenson, R.J., Bensinger, W.I., and Kalamasz, D. (1986). Positive selection of viable cell populations using avidin-biotin immunoadsorption. Journal of Immunological Methods 91, 11–19.

Bessette, P.H., Aslund, F., Beckwith, J., and Georgiou, G. (1999). Efficient folding of proteins with multiple disulfide bonds in the Escherichia coli cytoplasm. Proceedings of the National Academy of Sciences of the United States of America 96, 13703–13708.

Binz, H.K., Amstutz, P., and Plückthun, A. (2005). Engineering novel binding proteins from nonimmunoglobulin domains. Nature Biotechnology 23, 1257–1268.

Blankenship, J.W., and Dawson, P.E. (2007). Threading a peptide through a peptide□: Protein loops , rotaxanes , and knots. Protein Science 16, 1249–1256.

Bonner, W. a. (1972). Fluorescence Activated Cell Sorting. Review of Scientific Instruments 43, 404.

de Bono, J.S., Attard, G., Adjei, A., Pollak, M.N., Fong, P.C., Haluska, P., Roberts, L., Melvin, C., Repollet, M., Chianese, D., et al. (2007). Potential applications for circulating tumor cells expressing the insulin-like growth factor-I receptor. Clinical Cancer Research: an Official Journal of the American Association for Cancer Research 13, 3611–3616.

Braun, S., Hepp, F., Sommer, H.L., and Pantel, K. (1999). Tumour-antigen heterogeneity of disseminated breast cancer cells: implications for immunotherapy of minimal residual disease. International Journal of Cancer (Pred. Oncol.) 84, 1–5.

Brinkley, B.R., Beall, P.T., Wible, L.J., Mace, M.L., Turner, D.S., and Cailleau, R.M. (1980). Variations in cell form and cytoskeleton in human breast carcinoma cells in vitro. Cancer Research 40, 3118–3129.

Bruneau, E., Sutter, D., Hume, R.I., and Akaaboune, M. (2005). Identification of nicotinic acetylcholine receptor recycling and its role in maintaining receptor density at the neuromuscular junction in vivo. The Journal of Neuroscience: the Official Journal of the Society for Neuroscience 25, 9949–9959.

Bryan, N., Lewis, F.C., Bond, D., Stanley, C., and Hunt, J. a (2013). Evaluation of a novel non-destructive catch and release technology for harvesting autologous adult stem cells. PloS One 8, e53933.

Butler, T.P., and Gullino, P.M. (1975). Quantitation of Cell Shedding into Efferent Blood of Mammary. Cancer Research 35, 512–516.

Cairns, J. (1975). Mutation selection and the natural history of cancer. Nature 255, 197–200.

Caoili, S.E.C. (2012). On the meaning of affinity limits in B-Cell epitope prediction for antipeptide antibody-mediated immunity. Advances in Bioinformatics 2012, 346765.

Carter, P. (2001). Improving the efficacy of antibody-based cancer therapies. Nature Reviews. Cancer 1, 118–129.

Carter, P., Presta, L., Gorman, C.M., Ridgway, J.B., Henner, D., Wong, W.L., Rowland, a M., Kotts, C., Carver, M.E., and Shepard, H.M. (1992). Humanization of an anti-p185HER2 antibody for human cancer therapy. Proceedings of the National Academy of Sciences of the United States of America 89, 4285–4289.

Ceran, C., Cokol, M., Cingoz, S., Tasan, I., Ozturk, M., and Yagci, T. (2012). Novel anti-HER2 monoclonal antibodies: synergy and antagonism with tumor necrosis factor-α. BMC Cancer 12, 450.

Chalmers, J.J., Haam, S., Zhao, Y., Mccloskey, K., Moore, L., Zborowski, M., and Williams, P.S. (1999). Quantification of Cellular Properties from External Fields and Resulting Induced Velocity: Magnetic Susceptibility. Biotechnology and Bioengineering 64, 519–526.

Chao, G., Lau, W.L., Hackel, B.J., Sazinsky, S.L., Lippow, S.M., and Wittrup, K.D. (2006). Isolating and engineering human antibodies using yeast surface display. Nature Protocols 1, 755–768.

Chattopadhaya, S., Tan, L.P., and Yao, S.Q. (2006). Strategies for site-specific protein biotinylation using in vitro, in vivo and cell-free systems: toward functional protein arrays. Nature Protocols 1, 2386–2398.

Chen, I., Howarth, M., Lin, W., and Ting, A.Y. (2005). Site-specific labeling of cell surface proteins with biophysical probes using biotin ligase. Nature Methods 2, 99–104.

Chichak, K.S., Cantrill, S.J., Pease, A.R., Chiu, S.-H., Cave, G.W. V, Atwood, J.L., and Stoddart, J.F. (2004). Molecular borromean rings. Science (New York, N.Y.) 304, 1308–1312.

Chiu, J., March, P.E., Lee, R., and Tillett, D. (2004). Site-directed, Ligase-Independent Mutagenesis (SLIM): a single-tube methodology approaching 100% efficiency in 4 h. Nucleic Acids Research 32, e174.

Chivers, C.E., Crozat, E., Chu, C., Moy, V.T., Sherratt, D.J., and Howarth, M. (2010). A streptavidin variant with slower biotin dissociation and increased mechanostability. Nature Methods 7, 391–396.

Cho, H., Mason, K., Ramyar, K.X., Stanley, A.M., Gabelli, S.B., Denney Jr, D.W., and Leahy, D.J. (2003). Structure of the extracellular region of HER2 alone and in complex with the Herceptin Fab. Nature 421, 756–760.

Cho, I., Paek, E., Lee, H., Yoon, J., Song, T., and Paek, S. (2007). Site-directed biotinylation of antibodies for controlled immobilization on solid surfaces. Analytical Biochemistry 365, 14–23.

Chosy, E., Nakamura, M., Melnik, K., Comella, K., Lasky, L.C., Zborowski, M., and Chalmers, J.J. (2003). Characterization of antibody binding to three cancer related antigens using flow cytometry and cell tracking velocimetry. Biotechnology and Bioengineering 82, 341–351.

Christian, A.E., Haynes, M.P., Phillips, M.C., and Rothblat, George, H. (1997). Use of cyclodextrins for manipulating cellular cholesterol content. Journal of Lipid Research 38, 2264–2272.

Clayton, A.H. a, Tavarnesi, M.L., and Johns, T.G. (2007). Unligated epidermal growth factor receptor forms higher order oligomers within microclusters on A431 cells that are sensitive to tyrosine kinase inhibitor binding. Biochemistry 46, 4589–4597.

Colinas, R.J., and Walsh, a C. (1998). Cell separation based on the reversible interaction between calmodulin and a calmodulin-binding peptide. Journal of Immunological Methods 212, 69–78.

Comella, K., Nakamura, M., Melnik, K., Chosy, J., Zborowski, M., Cooper, M.A., Fehniger, T.A., Caligiuri, M.A., and Chalmers, J.J. (2001). Effects of Antibody Concentration on the Separation of Human Natural Killer Cells in a Commercial Immunomagnetic Separation System. Cytometry 45, 285–293.

Costa, M.M., Escosura-Muniz, A. de la, Nogues, C., Barrios, L., Ibanez, E., and Merkoci, A. (2012). Simple Monitoring of Cancer Cells Using Nanoparticles. Nano Letters 12, 4164–4171.

Crispin, M., Bowden, T. a, Coles, C.H., Harlos, K., Aricescu, a R., Harvey, D.J., Stuart, D.I., and Jones, E.Y. (2009). Carbohydrate and domain architecture of an immature antibody glycoform exhibiting enhanced effector functions. Journal of Molecular Biology 387, 1061–1066.

Cristofanilli, M. (2006). Circulating tumor cells, disease progression, and survival in metastatic breast cancer. Seminars in Oncology 33, S9–14.

Curran, J.M., Pu, F., Chen, R., and Hunt, J. a (2011). The use of dynamic surface chemistries to control msc isolation and function. Biomaterials 32, 4753–4760.

Dainiak, M.B., Kumar, A., Galaev, I.Y., and Mattiasson, B. (2007). Methods in Cell Separations. Advances in Biochemical Engineering/Biotechnology 106, 1–18.

Desitter, I., Guerrouahen, B.S., Benali-Furet, N., Wechsler, J., Jänne, P. a, Kuang, Y., Yanagita, M., Wang, L., Berkowitz, J. a, Distel, R.J., et al. (2011). A new device for rapid isolation by size and characterization of rare circulating tumor cells. Anticancer Research 31, 427–441.

Dharmasiri, U., Njoroge, S.K., Witek, M. a, Adebiyi, M.G., Kamande, J.W., Hupert, M.L., Barany, F., and Soper, S. a (2011). High-throughput selection, enumeration, electrokinetic manipulation, and molecular profiling of low-abundance circulating tumor cells using a microfluidic system. Analytical Chemistry 83, 2301–2309.

Dharmasiri, U., Witek, M. a, Adams, A. a, and Soper, S. a (2010). Microsystems for the capture of low-abundance cells. Annual Review of Analytical Chemistry (Palo Alto, Calif.) 3, 409–431.

Dickson, M.N., Tsinberg, P., Tang, Z., Bischoff, F.Z., Wilson, T., and Leonard, E.F. (2011). Efficient capture of circulating tumor cells with a novel immunocytochemical microfluidic device. Biomicrofluidics 5, 34119–3411915.

Dietrich-Buchecker, C., Jimenez-Molero, M.C., Sartor, V., and Sauvage, J.-P. (2003). Rotaxanes and catenanes as prototypes of molecular machines and motors. Pure and Applied Chemistry 75, 1383–1393.

Dufner, P., Jermutus, L., and Minter, R.R. (2006). Harnessing phage and ribosome display for antibody optimisation. TRENDS in Biotechnology 24, 523–529.

Durocher, Y., Perret, S., and Kamen, A. (2002). High-level and high-throughput recombinant protein production by transient transfection of suspension-growing human 293-EBNA1 cells. Nucleic Acids Research 30, E9.

Ellington, A.D., and Szostak, J.W. (1990). In vitro selection of RNA molecules that bind specific ligands. Nature 346, 818–822.

Evan, G.I., Lewis, G.K., Ramsay, G., and Bishop, J.M. (1985). Isolation of Monoclonal Antibodies Specific for Human c-myc Proto-Oncogene Product. Molecular and Cellular Biology 5, 3610–3616.

Even-Desrumeaux, K., and Chames, P. (2012). Affinity Determination of Biotinylated Antibodies by Flow Cytometry. In Antibody Engineering: Methods and Protocols, Second Edition, Methods in Molecular Biology, pp. 443–449.

Feller, K., Yang, S., Tung, N., Lee, J., and Mahalingam, M. (2012). c-myc in Kaposi's sarcoma: analyses by fluorescent in situ hybridization and immunohistochemistry. Journal of the European Academy of Dermatology and Venereology: JEADV.

Fendly, B.M., Winget, M., Hudziak, R.M., Lipari, M.T., Napier, M.A., and Ullrich, A. (1990). Characterization of Murine Monoclonal Antibodies Reactive to Either the Human Epidermal Growth Factor Receptor or HER2/neu Gene Product. Cancer Research 50, 1550–1558.

Fenteany, G., and Zhu, S. (2003). Small-molecule inhibitors of actin dynamics and cell motility. Current Topics in Medicinal Chemistry 3, 593–616.

Foote, J., and Eisen, H.N. (1995). Kinetic and affinity limits on antibodies produced during immune responses. Proceedings of the National Academy of Sciences 92, 1254–1256.

Friedman, L.M., Rinon, A., Schechter, B., Lyass, L., Lavi, S., Bacus, S.S., Sela, M., and Yarden, Y. (2005). Synergistic down-regulation of receptor tyrosine kinases by combinations of mAbs: implications for cancer immunotherapy. Proceedings of the National Academy of Sciences of the United States of America 102, 1915–1920.

Furcht, L.T., and Wendelschafer-Crabb, G. (1978). Trypsin-induced coordinate alterations in cell shape, cytoskeleton and intrinsic membrane structure of contact-inhibited cells. Experimental Cell Research 114, 1–14.

Gaborit, N., Larbouret, C., Vallaghe, J., Peyrusson, F., Bascoul-Mollevi, C., Crapez, E., Azria, D., Chardès, T., Poul, M.-A., Mathis, G., et al. (2011). Time-resolved fluorescence resonance energy transfer (TR-FRET) to analyze the disruption of EGFR/HER2 dimers: a new method to evaluate the efficiency of targeted therapy using monoclonal antibodies. The Journal of Biological Chemistry 286, 11337–11345.

Gai, S.A., and Wittrup, K.D. (2007). Yeast surface display for protein engineering and characterization. Current Opinion in Structural Biology 17, 467–473.

Galanzha, E.I., Shashkov, E. V, Kelly, T., Kim, J.-W., Yang, L., and Zharov, V.P. (2009). In vivo magnetic enrichment and multiplex photoacoustic detection of circulating tumour cells. Nature Nanotechnology 4, 855–860.

Gebauer, M., and Skerra, A. (2009). Engineered protein scaffolds as next-generation antibody therapeutics. Current Opinion in Chemical Biology 13, 245–255.

Geens, M., Van de Velde, H., De Block, G., Goossens, E., Van Steirteghem, a, and Tournaye, H. (2007). The efficiency of magnetic-activated cell sorting and fluorescence-activated cell sorting in the decontamination of testicular cell suspensions in cancer patients. Human Reproduction (Oxford, England) 22, 733–742.

Geisse, S., and Henke, M. (2005). Large-scale transient transfection of mammalian cells: a newly emerging attractive option for recombinant protein production. Journal of Structural and Functional Genomics 6, 165–170.

Gerstner, R.B., Carter, P., and Lowman, H.B. (2002). Sequence Plasticity in the Antigen-binding Site of a Therapeutic Anti-HER2 Antibody. Journal of Molecular Biology 321, 851–862.

Gijsen, M., King, P., Perera, T., Parker, P.J., Harris, A.L., Larijani, B., and Kong, A. (2010). HER2 phosphorylation is maintained by a PKB negative feedback loop in response to anti-HER2 herceptin in breast cancer. PLoS Biology 8, e1000563.

Gram, H., Marconi, L. a, Barbas, C.F., Collet, T. a, Lerner, R. a, and Kang, a S. (1992). In vitro selection and affinity maturation of antibodies from a naive combinatorial immunoglobulin library. Proceedings of the National Academy of Sciences of the United States of America 89, 3576–3580.

Green, M.N. (1990). Avidin and Streptavidin. Methods in Enzymology 184, 51–67.

Greil, R., Fasching, B., Loidl, P., and Huber, H. (1991). Expression of the c-myc proto-oncogene in multiple myeloma and chronic lymphocytic leukemia: an in situ analysis. Blood 78, 180–191.

Grützkau, A., and Radbruch, A. (2010). Small but mighty: how the MACS-technology based on nanosized superparamagnetic particles has helped to analyze the immune system within the last 20 years. Cytometry. Part A: the Journal of the International Society for Analytical Cytology 77, 643–647.

Hanes, J., Schaffitzel, C., Knappik, a, and Plückthun, a (2000). Picomolar affinity antibodies from a fully synthetic naive library selected and evolved by ribosome display. Nature Biotechnology 18, 1287–1292.

Hankin, E.H. (1890). A cure for tetanus and diphtheria. Nature 43, 121–123.

Haun, J.B., Devaraj, N.K., Hilderbrand, S.A., and Lee, H. (2010). Bioorthogonal chemistry amplifies nanoparticle binding and enhances the sensitivity of cell detection. Nature Nanotechnology 5, 660–665.

Haurum, J.S. (2006). Recombinant polyclonal antibodies: the next generation of antibody therapeutics? Drug Discovery Today 11, 655–660.

Haussmann, P.C., and Stoddart, J.F. (2009). Synthesizing interlocked molecules dynamically. Chemical Record (New York, N.Y.) 9, 136–154.

Hawley, T.S., Herbert, D.J., Eaker, S.S., and Hawley, R.G. (2004). Multiparameter Flow cytometry of Fluorescent Protein Reporters. In Methods in Molecular Biology: Flow Cytometry Protocols, 2nd Ed, pp. 219–237.

Hayashi-Takanaka, Y., Yamagata, K., Nozaki, N., and Kimura, H. (2009). Visualizing histone modifications in living cells: spatiotemporal dynamics of H3 phosphorylation during interphase. The Journal of Cell Biology 187, 781–790.

He, W., Kularatne, S.A., Kalli, K.R., Prendergast, F.G., Robert, J., Klee, G.G., Hartmann, L.C., and Low, P.S. (2008). Quantitation of circulating tumour cells in blood samples from ovarian and prostate cancer patients using tumor-specific fluorescent ligands. International Journal of Cancer 123, 1968–1973.

Herzenberg, L. a, Parks, D., Sahaf, B., Perez, O., Roederer, M., and Herzenberg, L. a (2002). The history and future of the fluorescence activated cell sorter and flow cytometry: a view from Stanford. Clinical Chemistry 48, 1819–1827.

Herzenberg, L.A., Sweet, R.G., and Herzenberg, L.A. (1976). Fluorescence-activated Cell Sorting. Scientific American 234, 108–117.

Hilpert, K., Hansen, G., Wessner, H., Küttner, G., Welfle, K., Seifert, M., and Höhne, W. (2001). Anti-c-myc antibody 9E10: epitope key positions and variability characterized using peptide spot synthesis on cellulose. Protein Engineering 14, 803–806.

Holm, L., Moody, P., and Howarth, M. (2009). Electrophilic affibodies forming covalent bonds to protein targets. The Journal of Biological Chemistry 284, 32906–32913.

Honig, M.G., and Hume, R.I. (1986). Fluorescent Carbocyanine Dyes Allow Living Neurons of Identified Origin to Be Studied in Long-Term Cultures. The Journal of Cell Biology 103, 171–187.

Hoover, D.M., and Lubkowski, J. (2002). DNAWorks: an automated method for designing oligonucleotides for PCR-based gene synthesis. Nucleic Acids Research 30, e43.

Hou, H.W., Bhagat, A.A.S., Lee, W.C., Huang, S., Han, J., and Lim, C.T. (2011). Microfluidic Devices for Blood Fractionation. Micromachines 2, 319–343.

Hou, H.W., Warkiani, M.E., Khoo, B.L., Li, Z.R., Soo, R. a, Tan, D.S.-W., Lim, W.-T., Han, J., Bhagat, A.A.S., and Lim, C.T. (2013). Isolation and retrieval of circulating tumor cells using centrifugal forces. Scientific Reports 3, 1259.

Houk, K.N., Leach, A.G., Kim, S.P., and Zhang, X. (2003). Thermodynamic Organic Complexes: Binding Affinities of Host – Guest , Protein – Ligand , and Protein – Transition-State Complexes. Angewandte Chemie (International Ed. in English) 42, 4872–4897.

Howarth, M., Chinnapen, D.J., Gerrow, K., Dorrestein, P.C., Grandy, M.R., Kelleher, N.L., El-husseini, A., and Ting, A.Y. (2006). A monovalent streptavidin with a single femtomolar biotin binding site. Nature Methods 3, 267–273.

Howarth, M., and Ting, A.Y. (2008). Imaging proteins in live mammalian cells with biotin ligase and monovalent streptavidin. Nature Protocols 3, 534–545.

Hüsemann, Y., Geigl, J.B., Schubert, F., Musiani, P., Meyer, M., Burghart, E., Forni, G., Eils, R., Fehm, T., Riethmüller, G., et al. (2008). Systemic spread is an early step in breast cancer. Cancer Cell 13, 58–68.

Ibrahim, S.F., and van den Engh, G. (2003). High-speed cell sorting: fundamentals and recent advances. Current Opinion in Biotechnology 14, 5–12.

Ignatiadis, M., Rothé, F., Chaboteaux, C., Durbecq, V., Rouas, G., Criscitiello, C., Metallo, J., Kheddoumi, N., Singhal, S.K., Michiels, S., et al. (2011). HER2-positive circulating tumor cells in breast cancer. PloS One 6, e15624.

Issadore, D., Chung, J., Shao, H., Liong, M., Ghazani, A. a, Castro, C.M., Weissleder, R., and Lee, H. (2012). Ultrasensitive clinical enumeration of rare cells ex vivo using a micro-hall detector. Science Translational Medicine 4, 141ra92.

Jacobson, K., Mouritsen, O.G., and Anderson, R.G.W. (2007). Lipid rafts: at a crossroad between cell biology and physics. Nature Cell Biology 9, 7–14.

Jaye, D.L., Bray, R. a, Gebel, H.M., Harris, W. a C., and Waller, E.K. (2012). Translational applications of flow cytometry in clinical practice. Journal of Immunology (Baltimore, Md.□: 1950) 188, 4715–4719.

Jia, Q., Xu, L., Zha, Q., Chi, X., Li, F., and He, X. (2007). High level expression of HLA-A*0203-BSP fusion protein in Escherichia coli and construction of soluble HLA-A*0203 monomer and tetramer loaded with Epstein-Barr virus peptide. Cellular & Molecular Immunology 4, 301–308.

Kaplan, D., and Smith, D. (2000). Enzymatic amplification staining for flow cytometric analysis of cell surface molecules. Cytometry 40, 81–85.

Kelley, R.F., and Connell, M.P.O. (1993). Thermodynamic Analysis of an Antibody Functional Epitope. Biochemistry 32, 6828–6835.

Kelley, R.F., and O'Connell, M.P. (1993). Thermodynamic analysis of an antibody functional epitope. Biochemistry 32, 6828–6835.

Khatibzadeh, N., Gupta, S., Farrell, B., Brownell, W.E., and Anvari, B. (2012). Effects of cholesterol on nano-mechanical properties of the living cell plasma membrane. Soft Matter 8, 8350–8360.

Klein, C. a (2009). Parallel progression of primary tumours and metastases. Nature Reviews. Cancer 9, 302–312.

Kling, J. (2012). Beyond counting tumor cells. Nature Biotechnology 30, 578–580.

Kohler, G., and Milstein, C. (1975). Continuous cultures of fused cells secreting antibody of predefined specificity. Nature 256, 495–497.

Krauß, N., Wessner, H., Welfle, K., Welfle, H., Scholz, C., Seifert, M., Hahn, M., Scheerer, P., Skerra, A., Zubow, K., et al. (2008). The structure of the anti-c-myc antibody 9E10 Fab fragment/epitope peptide complex reveals a novel binding mode dominated by the heavy chain hypervariable loops. Proteins 73, 552–565.

Kuroda, D., Shirai, H., Jacobson, M.P., and Nakamura, H. (2012). Computer-aided antibody design. Protein Engineering, Design & Selection□: PEDS 25, 507–521.

Kusumi, A., Nakada, C., Ritchie, K., Murase, K., Suzuki, K., Murakoshi, H., Kasai, R.S., Kondo, J., and Fujiwara, T. (2005). Paradigm shift of the plasma membrane concept from the two-dimensional continuum fluid to the partitioned fluid: high-speed single-molecule tracking of membrane molecules. Annual Review of Biophysics and Biomolecular Structure 34, 351–378.

Larson, J.S., Goodman, L.J., Tan, Y., Defazio-Eli, L., Paquet, A.C., Cook, J.W., Rivera, A., Frankson, K., Bose, J., Chen, L., et al. (2010). Analytical Validation of a Highly Quantitative, Sensitive, Accurate, and Reproducible Assay (HERmark) for the Measurement of HER2 Total Protein and HER2 Homodimers in FFPE Breast Cancer Tumor Specimens. Pathology Research International 2010, 814176.

Leary, R.J., Kinde, I., Diehl, F., Schmidt, K., Clouser, C., Duncan, C., Antipova, A., Lee, C., McKernan, K., De La Vega, F.M., et al. (2010). Development of personalized tumor biomarkers using massively parallel sequencing. Science Translational Medicine 2, 20ra14.

Lee, H.K., Seo, I.A., Lee, S.H., Seo, S.-Y., Kim, K.S., and Park, H.T. (2008). Tyrphostin ErbB2 Inhibitors AG825 and AG879 Have Non-specific Suppressive Effects on gp130/ STAT3 Signaling. The Korean Journal of Physiology & Pharmacology 12, 281–286.

Lenkei, R., Gratama, J.W., Rothe, G., Schmitz, G., D'hautcourt, J.L., Arekrans, a, Mandy, F., and Marti, G. (1998). Performance of calibration standards for antigen quantitation with flow cytometry. Cytometry 33, 188–196.

Levy, R., Weiss, R., Chen, G., Iverson, B.L., and Georgiou, G. (2001). Production of correctly folded Fab antibody fragment in the cytoplasm of Escherichia coli trxB gor mutants via the coexpression of molecular chaperones. Protein Expression and Purification 23, 338–347.

Lewandowski, B., De Bo, G., Ward, J.W., Papmeyer, M., Kuschel, S., Aldegunde, M.J., Gramlich, P.M.E., Heckmann, D., Goldup, S.M., D'Souza, D.M., et al. (2013). Sequence-specific peptide synthesis by an artificial small-molecule machine. Science (New York, N.Y.) 339, 189–193.

Lindenmann, J. (1984). Origin of the terms "antibody" and "antigen". Scandinavian Journal of Immunology 19, 281–285.

Lipman, N.S., Jackson, L.R., Trudel, L.J., and Weis-Garcia, F. (2005). Monoclonal versus polyclonal antibodies: distinguishing characteristics, applications, and information resources. ILAR Journal 46, 258–268.

Lipovsek, D., and Pluckthun, A. (2004). In-vitro protein evolution by ribosome display and mRNA display. Journal of Immunological Methods 290, 51–67.

Llewelyn, M.B., Hawkins, R.E., and Russell, S.J. (1992). Monoclonal Antibodies in Medicine: Discovery of antibodies. BMJ 305, 1269–1272.

Lobbestael, E., Reumers, V., Ibrahimi, A., Paesen, K., Thiry, I., Gijsbers, R., Van den Haute, C., Debyser, Z., Baekelandt, V., and Taymans, J.M. (2010). Immunohistochemical detection of transgene expression in the brain using small epitope tags. BMC Biotechnology 10,.

Luzzi, K.J., MacDonald, I.C., Schmidt, E.E., Kerkvliet, N., Morris, V.L., Chambers, a F., and Groom, a C. (1998). Multistep nature of metastatic inefficiency: dormancy of solitary cells after successful extravasation and limited survival of early micrometastases. The American Journal of Pathology 153, 865–873.

Maerkl, S.J., and Quake, S.R. (2007). A systems approach to measuring the binding energy landscapes of transcription factors. Science (New York, N.Y.) 315, 233–237.

Maheswaran, S., Sequist, L., Nagrath, S., Ulkus, L., Brannigan, B., Collura, C., Inserra, E., Diederichs, S., Iafrate, A.J., Bell, D.W., et al. (2008). Detection of Mutations in EGFR in Circulating Lung Cancer cells. New England Journal of Medicine 359, 366–377.

Marks, J.D., Hoogenboom, H.R., Bonnert, T.P., McCafferty, J., Griffiths, a D., and Winter, G. (1991). By-passing immunization. Human antibodies from V-gene libraries displayed on phage. Journal of Molecular Biology 222, 581–597.

Martin, C.D., Rojas, G., Mitchell, J.N., Vincent, K.J., Wu, J., Mccafferty, J., and Schofield, D.J. (2006). A simple vector system to improve performance and utilisation of recombinant antibodies. BMC Biotechnology 6,.

Maynard, J., and Georgiou, G. (2000). Antibody Engineering. Annual Review of Biomedical Engineering 2, 339–376.

McCabe, A., Dolled-Filhart, M., Camp, R.L., and Rimm, D.L. (2005). Automated quantitative analysis (AQUA) of in situ protein expression, antibody concentration, and prognosis. Journal of the National Cancer Institute 97, 1808–1815.

McCloskey, K.E., Chalmers, J.J., and Zborowski, M. (2000). Magnetophoretic mobilities correlate to antibody binding capacities. Cytometry 40, 307–315.

McCloskey, K.E., Chalmers, J.J., and Zborowski, M. (2003a). Magnetic cell separation: characterization of magnetophoretic mobility. Analytical Chemistry 75, 6868–6874.

McCloskey, K.E., Comella, K., Chalmers, J.J., Margel, S., and Zborowski, M. (2001). Mobility Measurements of Immunomagnetically Labeled Cells Allow Quantitation of Secondary Antibody Binding Amplification. Biotechnology and Bioengineering 75, 642–655.

McCloskey, K.E., Moore, L.R., Hoyos, M., Rodriguez, A., Chalmers, J.J., and Zborowski, M. (2003b). Magnetophoretic cell sorting is a function of antibody binding capacity. Biotechnology Progress 19, 899–907.

McDonagh, C.F., Huhalov, A., Harms, B.D., Adams, S., Paragas, V., Oyama, S., Zhang, B., Luus, L., Overland, R., Nguyen, S., et al. (2012). Antitumor activity of a novel bispecific antibody that targets the ErbB2/ErbB3 oncogenic unit and inhibits heregulin-induced activation of ErbB3. Molecular Cancer Therapeutics 11, 582–593.

Menard, S., Casalini, P., Campiglio, M., Pupa, S., Agresti, R., and Tagliabue, E. (2001). HER2 overexpression in various tumor types, focussing on its relationship to the development of invasive breast cancer. Annals of Oncology 12, 15–19.

Merino, A.G. (2011). Monoclonal antibodies. Basic features. Neurología (Barcelona, Spain) 26, 301–306.

Mikolajczyk, S.D., Millar, L.S., Tsinberg, P., Coutts, S.M., Zomorrodi, M., Pham, T., Bischoff, F.Z., and Pircher, T.J. (2011). Detection of EpCAM-Negative and Cytokeratin-Negative Circulating Tumor Cells in Peripheral Blood. Journal of Oncology 2011, 252361.

Miller, K., Meng, G., Liu, J., Hurst, A., Wong, W., Ekert, R., Lawrence, D., Deforge, L., Gaudreault, J., Sliwkowski, M., et al. (2003). Design, Construction, and In Vitro Analyses of Multivalent Antibodies. The Journal of Immunology 170, 4854–4861.

Minner, S., Jessen, B., Stiedenroth, L., Burandt, E., Köllermann, J., Mirlacher, M., Erbersdobler, A., Eichelberg, C., Fisch, M., Brümmendorf, T.H., et al. (2010). Low level HER2 overexpression is associated with rapid tumor cell proliferation and poor prognosis in prostate cancer. Clinical Cancer Research□: an Official Journal of the American Association for Cancer Research 16, 1553–1560.

Miroux, B., and Walker, J.E. (1996). Over-production of proteins in Escherichia coli: mutant hosts that allow synthesis of some membrane proteins and globular proteins at high levels. Journal of Molecular Biology 260, 289–298.

Missiakas, D., Betton, J., and Raina, S. (1996). New components of protein folding in extracytoplasmic compartments of Escherichia coli SurA, FkpA and Skp/OmpH. Molecular Microbiology 21, 871–884.

Mohamed, H., Murray, M., Turner, J.N., and Caggana, M. (2009). Isolation of tumor cells using size and deformation. Journal of Chromatography. A 1216, 8289–8295.

Molina, M. a, Codony-Servat, J., Albanell, J., Rojo, F., Arribas, J., and Baselga, J. (2001). Trastuzumab (herceptin), a humanized anti-Her2 receptor monoclonal antibody, inhibits basal and activated Her2 ectodomain cleavage in breast cancer cells. Cancer Research 61, 4744–4749.

Nagrath, S., Sequist, L. V, Maheswaran, S., Bell, D.W., Irimia, D., Ulkus, L., Smith, M.R., Kwak, E.L., Digumarthy, S., Muzikansky, A., et al. (2007). Isolation of rare circulating tumour cells in cancer patients by microchip technology. Nature 450, 1235–1239.

Nagy, P. (2002). Lipid rafts and the local density of ErbB proteins influence the biological role of homo- and heteroassociations of ErbB2. Journal of Cell Science 115, 4251–4262.

Nagy, P., Claus, J., Jovin, T.M., and Arndt-Jovin, D.J. (2010). Distribution of resting and ligand-bound ErbB1 and ErbB2 receptor tyrosine kinases in living cells using number and brightness analysis. Proceedings of the National Academy of Sciences of the United States of America 107, 16524–16529.

Neoptolemos, J.P., Stocken, D.D., Friess, H., Bassi, C., Dunn, J. a, Hickey, H., Beger, H., Fernandez-Cruz, L., Dervenis, C., Lacaine, F., et al. (2004). A randomized trial of chemoradiotherapy and chemotherapy after resection of pancreatic cancer. The New England Journal of Medicine 350, 1200–1210.

Nettleship, J.E., Ren, J., Rahman, N., Berrow, N.S., Hatherley, D., Barclay, a N., and Owens, R.J. (2008). A pipeline for the production of antibody fragments for structural studies using transient expression in HEK 293T cells. Protein Expression and Purification 62, 83–89.

Nguyen, D.H., Giri, B., Collins, G., and Taub, D.D. (2005). Dynamic reorganization of chemokine receptors , cholesterol , lipid rafts , and adhesion molecules to sites of CD4 engagement. Experimental Cell Research 304, 559–569.

Nilsson, B., Moks, T., Jansson, B., Abrahmsén, L., Elmblad, A., Holmgren, E., Henrichson, C., Jones, T. a, and Uhlén, M. (1987). A synthetic IgG-binding domain based on staphylococcal protein A. Protein Engineering 1, 107–113.

Nishiyama, Y., Mitsuda, Y., Taguchi, H., Planque, S., Salas, M., Hanson, C. V, and Paul, S. (2007). Towards covalent vaccination: improved polyclonal HIV neutralizing antibody response induced by an electrophilic gp120 V3 peptide analog. The Journal of Biological Chemistry 282, 31250–31256.

Nowakowski, A., Wang, C., Powers, D.B., Amersdorfer, P., Smith, T.J., Montgomery, V.A., Sheridan, R., Blake, R., Smith, L.A., and Marks, J.D. (2002). Potent neutralization of botulinum neurotoxin by recombinant oligoclonal antibody. Proceedings of the National Academy of Sciences of the United States of America 99, 11346–11350.

Orlova, A., Magnusson, M., Eriksson, T.L.J., Nilsson, M., Larsson, B., Höidén-Guthenberg, I., Widström, C., Carlsson, J., Tolmachev, V., Ståhl, S., et al. (2006). Tumor imaging using a picomolar affinity HER2 binding affibody molecule. Cancer Research 66, 4339–4348.

Orlova, A., Tolmachev, V., Pehrson, R., Lindborg, M., Tran, T., Sandström, M., Nilsson, F.Y., Wennborg, A., Abrahmsén, L., and Feldwisch, J. (2007). Synthetic affibody molecules: a novel class of affinity ligands for molecular imaging of HER2-expressing malignant tumors. Cancer Research 67, 2178–2186.

Orr, G., Hu, D., Ozçelik, S., Opresko, L.K., Wiley, H.S., and Colson, S.D. (2005). Cholesterol dictates the freedom of EGF receptors and HER2 in the plane of the membrane. Biophysical Journal 89, 1362–1373.

Osherov, N., Gazit, a, Gilon, C., and Levitzki, a (1993). Selective inhibition of the epidermal growth factor and HER2/neu receptors by tyrphostins. The Journal of Biological Chemistry 268, 11134–11142.

O'Callaghan, C. a, Byford, M.F., Wyer, J.R., Willcox, B.E., Jakobsen, B.K., McMichael, a J., and Bell, J.I. (1999). BirA enzyme: production and application in the study of membrane receptor-ligand interactions by site-specific biotinylation. Analytical Biochemistry 266, 9–15.

O'Flaherty, J.D., Gray, S., Richard, D., Fennell, D., O'Leary, J.J., Blackhall, F.H., and O'Byrne, K.J. (2012). Circulating tumour cells, their role in metastasis and their clinical utility in lung cancer. Lung Cancer (Amsterdam, Netherlands) 76, 19–25.

Pancer, Z., Amemiya, C.T., Ehrhardt, G.R. a, Ceitlin, J., Gartland, G.L., and Cooper, M.D. (2004). Somatic diversification of variable lymphocyte receptors in the agnathan sea lamprey. Nature 430, 174–180.

Pantel, K., Brakenhoff, R.H., and Brandt, B. (2008). Detection, clinical relevance and specific biological properties of disseminating tumour cells. Nature Reviews. Cancer 8, 329–340.

Park, J.-M., Lee, J.-Y., Lee, J.-G., Jeong, H., Oh, J.-M., Kim, Y.J., Park, D., Kim, M.S., Lee, H.J., Oh, J.H., et al. (2012). Highly efficient assay of circulating tumor cells by selective sedimentation with a density gradient medium and microfiltration from whole blood. Analytical Chemistry 84, 7400–7407.

Pavlinkova, G., Colcher, D., Booth, B.J., Goel, a, Wittel, U. a, and Batra, S.K. (2001). Effects of humanization and gene shuffling on immunogenicity and antigen binding of anti-TAG-72 single-chain Fvs. International Journal of Cancer. Journal International Du Cancer 94, 717–726.

Peer, D., Karp, J.M., Hong, S., Farokhzad, O.C., Margalit, R., and Langer, R. (2007). Nanocarriers as an emerging platform for cancer therapy. Nature Nanotechnology 2, 751–760.

Powles, R., Mehta, J., Kulkarni, S., Treleaven, J., Millar, B., Marsden, J., Shepherd, V., Rowland, A., Sirohi, B., Tait, D., et al. (2000). Early report Allogeneic blood and bone-marrow stem-cell transplantation in haematological malignant diseases□: a randomised trial. The Lancet 355, 1231–1237.

Proba, K., Ge, L., and Plückthun, a (1995). Functional antibody single-chain fragments from the cytoplasm of Escherichia coli: influence of thioredoxin reductase (TrxB). Gene 159, 203–207.

Punnoose, E. a, Atwal, S.K., Spoerke, J.M., Savage, H., Pandita, A., Yeh, R.-F., Pirzkall, A., Fine, B.M., Amler, L.C., Chen, D.S., et al. (2010). Molecular biomarker analyses using circulating tumor cells. PloS One 5, e12517.

Raghu, H., Sodadasu, P.K., Malla, R.R., Gondi, C.S., Estes, N., and Rao, J.S. (2010). Localization of uPAR and MMP-9 in lipid rafts is critical for migration, invasion and angiogenesis in human breast cancer cells. BMC Cancer 10, 647.

Reichle, C., Sparbier, K., Müller, T., Schnelle, T., Walden, P., and Fuhr, G. (2001). Combined laser tweezers and dielectric field cage for the analysis of receptor-ligand interactions on single cells. Electrophoresis 22, 272–282.

Rhim, A.D., Mirek, E.T., Aiello, N.M., Maitra, A., Bailey, J.M., McAllister, F., Reichert, M., Beatty, G.L., Rustgi, A.K., Vonderheide, R.H., et al. (2012). EMT and dissemination precede pancreatic tumor formation. Cell 148, 349–361.

Riethdorf, S., Fritsche, H., Müller, V., Rau, T., Schindlbeck, C., Rack, B., Janni, W., Coith, C., Beck, K., Jänicke, F., et al. (2007). Detection of circulating tumor cells in peripheral blood of patients with metastatic breast cancer: a validation study of the CellSearch system. Clinical Cancer Research□: an Official Journal of the American Association for Cancer Research 13, 920–928.

Rubbi, C.P., Patel, D., and Rickwood, D. (1993). Evidence of surface antigen detachment during incubation of cells with immunomagnetic beads. Journal of Immunological Methods 166, 233–241.

Rubin, I., and Yarden, Y. (2001). The basic biology of HER2. Annals of Oncology 12, S3–S8.

Rusnak, D.W., Alligood, K.J., Mullin, R.J., Spehar, G.M., Arenas-Elliott, C., Martin, a-M., Degenhardt, Y., Rudolph, S.K., Haws, T.F., Hudson-Curtis, B.L., et al. (2007). Assessment of epidermal growth factor receptor (EGFR, ErbB1) and HER2 (ErbB2) protein expression levels and response to lapatinib (Tykerb, GW572016) in an expanded panel of human normal and tumour cell lines. Cell Proliferation 40, 580–594.

Safarik, I., Safarikova, M., and Forsythe, S.J. (1995). The application of magnetic separations in applied microbiology. Journal of Applied Bacteriology 78, 575–585.

Safarík, I., and Safaríková, M. (1999). Use of magnetic techniques for the isolation of cells. Journal of Chromatography. B, Biomedical Sciences and Applications 722, 33–53.

Said, T.M., Agarwal, A., Zborowski, M., Grunewald, S., Glander, H.-J., and Paasch, U. (2008). Utility of magnetic cell separation as a molecular sperm preparation technique. Journal of Andrology 29, 134–142.

Sarda, S., Pointu, D., Pincet, F., and Henry, N. (2004). Specific recognition of macroscopic objects by the cell surface: evidence for a receptor density threshold revealed by micrometric particle binding characteristics. Biophysical Journal 86, 3291–3303.

Saviranta, P., Haavisto, T., Rappu, P., Karp, M., and Lövgren, T. (1998). In vitro enzymatic biotinylation of recombinant fab fragments through a peptide acceptor tail. Bioconjugate Chemistry 9, 725–735.

Schiweck, W., Buxbaum, B., Schätzlein, C., Neiss, H.G., and Skerra, A. (1997). Sequence analysis and bacterial production of the anti-c-myc antibody 9E10: the VH domain has an extended CDR-H3 and exhibits unusual solubility. FEBS Letters 414, 33–38.

Schmidt, T.G., Koepke, J., Frank, R., and Skerra, a (1996). Molecular interaction between the Strep-tag affinity peptide and its cognate target, streptavidin. Journal of Molecular Biology 255, 753–766.

Shepard, H.M., Lewis, G.D., Sarup, J.C., Fendly, B.M., Maneval, D., Mordenti, J., Figari, I., Kotts, C.E., Palladino, M. a, and Ullrich, a (1991). Monoclonal antibody therapy of human cancer: taking the HER2 protooncogene to the clinic. Journal of Clinical Immunology 11, 117–127.

Sieuwerts, A.M., Kraan, J., Bolt-de Vries, J., van der Spoel, P., Mostert, B., Martens, J.W.M., Gratama, J.-W., Sleijfer, S., and Foekens, J. a (2009). Molecular characterization of circulating tumor cells in large quantities of contaminating leukocytes by a multiplex real-time PCR. Breast Cancer Research and Treatment 118, 455–468.

Skopelitou, A., Hadjiyannakis, M., Tsenga, A., Theocharis, S., Alexopoulou, V., Kittas, C., and Agnantis, N. (1993). Expression of c-myc p62 Oncoprotein in Multiple Myeloma: An Immunohistochemical Study of 180 cases. Anticancer Research 13, 1091–1096.

Slamon, D.J., Clark, G.M., Wong, S.G., Levin, W.J., Ullrich, A., and Mcguire, W.L. (1987). Human Breast Cancer: Correlation of Relapse and Survival with Amplification of the HER-2lneu Oncogene. Science 235, 177–182.

Smirnov, D. a, Zweitzig, D.R., Foulk, B.W., Miller, M.C., Doyle, G. V, Pienta, K.J., Meropol, N.J., Weiner, L.M., Cohen, S.J., Moreno, J.G., et al. (2005). Global gene expression profiling of circulating tumor cells. Cancer Research 65, 4993–4997.

Spector, I., Shochet, N.R., Blasberger, D., and Kashman, Y. (1989). Latrunculins-Novel Marine Macrolides That Disrupt Microfilament Organization and Affect Cell Growth□: I . Comparison With Cytochalasin D. Cell Motility and the Cytoskeleton 13, 127–144.

Stift, A., Friedl, J., Dubsky, P., Bachleitner-Hofmann, T., Schueller, G., Zontsich, T., Benkoe, T., Radelbauer, K., Brostjan, C., Jakesz, R., et al. (2003). Dendritic Cell-Based Vaccination in Solid Cancer. Journal of Clinical Oncology 21, 135–142.

Stopeck, A.T., Brown-Glaberman, U., Wong, H.Y., Park, B.H., Barnato, S.E., Gradishar, W.J., Hudis, C. a, and Rugo, H.S. (2012). The role of targeted therapy and biomarkers in breast cancer treatment. Clinical & Experimental Metastasis 29, 807–819.

Stott, S.L., Hsu, C., Tsukrov, D.I., Yu, M., Miyamoto, D.T., Waltman, B.A., Rothenberg, S.M., Shah, A.M., Smas, M.E., Korir, G.K., et al. (2010). Isolation of circulating tumor cells using a microvortex-generating herringbone-chip. Proceedings of the National Academy of Sciences 107, 18392–18397.

Sugawara, S., Abo, T., and Kumagai, K. (1987). A simple method to eliminate the antigenicity of surface class I MHC molecules from the membrane of viable cells by acid treatment at pH 3. Journal of Immunological Methods 100, 83–90.

Sun, Y.-F., Yang, X.-R., Zhou, J., Qiu, S.-J., Fan, J., and Xu, Y. (2011). Circulating tumor cells□: advances in detection methods , biological issues , and clinical relevance. Journal of Cancer Research and Clinical Oncology 137, 1151–1173.

Tamaskovic, R., Simon, M., Stefan, N., Schwill, M., and Plückthun, A. (2012). Designed ankyrin repeat proteins (DARPins): from research to therapy.

Tashiro, M., and Montelione, G.T. (1995). Structures of bacterial immunoglobulin-binding domains and their complexes with immunoglobulins. Current Opinion in Structural Biology 5, 471–481.

Teerinen, T., Valjakka, J., Rouvinen, J., and Takkinen, K. (2006). Structure-based stability engineering of the mouse IgG1 Fab fragment by modifying constant domains. Journal of Molecular Biology 361, 687–697.

Terpe, K. (2003). Overview of tag protein fusions: from molecular and biochemical fundamentals to commercial systems. Applied Microbiology and Biotechnology 60, 523–533.

Thiel, a, Schmitz, J., Miltenyi, S., and Radbruch, a (1997). CD45RA-expressing memory/effector Th cells committed to production of interferon-gamma lack expression of CD31. Immunology Letters 57, 189–192.

Thiel, A., Scheffold, A., and Radbruch, A. (1998). Immunomagnetic cell sorting--pushing the limits. Immunotechnology□: an International Journal of Immunological Engineering 4, 89–96.

Towbin, H., Motz, J., Oroszlan, P., and Zingel, O. (1995). Sandwich immunoassay for the hapten angiotensin II. A novel assay principle based on antibodies against immune complexes. Journal of Immunological Methods 181, 167–176.

Trisler, K., Looger, L.L., Sharma, V., Baker, M., Benson, D.E., Trauger, S., Schultz, P.G., and Smider, V. V (2007). A metalloantibody that irreversibly binds a protein antigen. The Journal of Biological Chemistry 282, 26344–26353.

Tse, C., Brault, D., Gligorov, J., Antoine, M., Neumann, R., Lotz, J.-P., and Capeau, J. (2005). Evaluation of the quantitative analytical methods real-time PCR for HER-2 gene quantification and ELISA of serum HER-2 protein and comparison with fluorescence in situ hybridization and immunohistochemistry for determining HER-2 status in breast cancer pa. Clinical Chemistry 51, 1093–1101.

Vincentelli, R., Canaan, S., Campanacci, V., Valencia, C., Maurin, D., Frassinetti, F., Scappucini-calvo, L., Bourne, Y., Cambillau, C., and Bignon, C. (2004). High-throughput automated refolding screening of inclusion bodies. Protein Science 13, 2782–2792.

Wang, S., Wang, H., Jiao, J., Chen, K.-J., Owens, G., Kamei, K., Sun, J., Sherman, D., Behrenbruch, C., Wu, H., et al. (2009a). Three-Dimensional Nanostructured Substrates toward Efficient Capture of Circulating Tumor Cells. Angewandte Chemie 121, 9132–9135.

Wang, S.E., Xiang, B., Zent, R., Quaranta, V., Pozzi, A., and Arteaga, C.L. (2009b). Transforming growth factor beta induces clustering of HER2 and integrins by activating Src-focal adhesion kinase and receptor association to the cytoskeleton. Cancer Research 69, 475–482.

Weidner, M., Taupp, M., and Hallam, S.J. (2010). Expression of recombinant proteins in the methylotrophic yeast Pichia pastoris. Journal of Visualized Experiments 36,.

Weigelt, B., Peterse, J.L., and van 't Veer, L.J. (2005). Breast cancer metastasis: markers and models. Nature Reviews. Cancer 5, 591–602.

Will, B., and Steidl, U. (2010). Multi-Parameter Fluorescence-Activated Cell Sorting and Analysis of Stem and Progenitor Cells in Myeloid Malignancies. Best Practice and Research Clinical Haematology 23, 391–401.

Williams, A.R., Northrop, B.H., Chang, T., Stoddart, J.F., White, A.J.P., and Williams, D.J. (2006). Suitanes. Angewandte Chemie (International Ed. in English) 45, 6665–6669.

Williams, G.S., Collinson, L.M., Brzostek, J., Eissmann, P., Almeida, C.R., Mccann, F.E., Burshtyn, D., and Davis, D.M. (2007). Membranous Structures Transfer Cell Surface Proteins Across NK Cell Immune Synapses. Traffic 8, 1190–1204.

Williams, J.G.K., Steffens, D.L., Anderson, J.P., Urlacher, T.M., Lamb, D.T., Grone, D.L., and Egelhoff, J.C. (2008). An artificial processivity clamp made with

streptavidin facilitates oriented attachment of polymerase-DNA complexes to surfaces. Nucleic Acids Research 36, e121.

Wilson, I.A., Ghiara, J.B., and Stanfield, R.L. (1994). Structure of anti-peptide antibody complexes. Research in Immunology 145, 73–78.

Wittrup, K.D., Thurber, G.M., Schmidt, M.M., and Rhoden, J.J. (2012). Practical theoretic guidance for the design of tumor-targeting agents. Methods in Enzymology 503, 255–268.

Wriggers, W., Chakravarty, S., and Jennings, P. a (2005). Control of protein functional dynamics by peptide linkers. Biopolymers 80, 736–746.

Yamada, T. (2011). Therapeutic monoclonal antibodies. The Keio Journal of Medicine 60, 37–46.

Yarden, Y., and Sliwkowski, M.X. (2001). Untangling the ErbB signalling network. Nature Reviews. Molecular Cell Biology 2, 127–137.

Yu, M., Bardia, A., Wittner, B.S., Stott, S.L., Smas, M.E., Ting, D.T., Isakoff, S.J., Ciciliano, J.C., Wells, M.N., Shah, A.M., et al. (2013). Circulating breast tumor cells exhibit dynamic changes in epithelial and mesenchymal composition. Science (New York, N.Y.) 339, 580–584.

Yu, M., Stott, S., Toner, M., Maheswaran, S., and Haber, D. a (2011). Circulating tumor cells: approaches to isolation and characterization. The Journal of Cell Biology 192, 373–382.

Zahnd, C., Kawe, M., Stumpp, M.T., Pasquale, C. De, Tamaskovic, R., Nagy-Davidescu, G., Dreier, B., Schibli, R., Binz, H.K., Waibel, R., et al. (2010). Efficient Tumor Targeting with High-Affinity Designed Ankyrin Repeat Proteins□: Effects of Affinity and Molecular Size. Cancer Research 70, 1595–1605.

Zakeri, B., Fierer, J.O., Celik, E., Chittock, E.C., Schwarz-Linek, U., Moy, V.T., and Howarth, M. (2012). Peptide tag forming a rapid covalent bond to a protein, through engineering a bacterial adhesin. Proceedings of the National Academy of Sciences 109, E690–E697.

Zakeri, B., and Howarth, M. (2010). Spontaneous intermolecular amide bond formation between side chains for irreversible peptide targeting. Journal of the American Chemical Society 132, 4526–4527.

Zider, A., and Drakeman, D.L. (2010). The future of monoclonal antibody technology. mAbs 2, 361–364.

Appendices

Appendix 1: Efforts to express 9E10 Fab in bacterial cells

Construct	Rationale	Expression	Yield
9E10	Express in RIPL at 22°C, 25°C or 37°C. Variable temperatures to optimise protein production and folding	At each temperature, some heavy chain expression	Not detectable
9E10	Express in BL21 (DE3) pLysS. Lacks proteases and good for toxic protein expression	Cells did not grow after plasmid transformation	Not detectable
9E10	Rosetta Blue (DE3)* to support enhanced expression of eukaryotic proteins	Overnight cultures did not grow	Not detectable
9E10	Rosetta Gami 2 (DE3)** for enhanced disulfide bond formation in the cytoplasm	Overnight cultures did not grow	Not detectable
9E10	B834 (DE3) pLysS for expression of toxic proteins. Express in LB or 2TY media	Addition of sucrose to support Fab folding. Some expression when induced at 22°C in LB	<0.1 mg from 750 mL culture
9E10-APLH	B834 (DE3) pLysS for expression of toxic proteins	Addition of sucrose to support Fab folding. Some expression when induced at 22°C	<0.05 mg from 750 mL culture
9E10-APLH	B834 (DE3) pLysS for expression of toxic proteins	Addition of 0.4M Arginine and 5mM Glutathione to enhance folding and disulfide bond shuffling in the periplasm.	<0.05 mg from 750 mL culture

*Rosetta blue cells express rare tRNAs facilitating expression of genes that encode rare *E. coli* codons.
**Rosetta Gami 2 cells express rare tRNAs facilitating expression of genes that encode rare *E. coli* codons. Also have trxB/gor mutations, which enhance cytoplasmic disulfide bond formation.

Construct	Rationale	Expression	Yield
9E10	Express in K-12 RV308 (ATCC) for expression of toxic proteins.	Some expression when induced at 22°C.	Not detectable
9E10-APLH	C41 (DE3) for expression of globular and membrane proteins	Some expression when induced at 25°C.	<0.1 mg/mL
9E10-APLH	C43 (DE3) for expression of membrane proteins	Some expression when induced at 25°C.	<0.1 mg/mL
9E10-APLH without leader sequences	Rosetta Gami 2 (DE3) for enhanced disulfide bond formation in the cytoplasm	Some expression when induced at 25°C	Impure protein and Fab chains not dimerized
9E10-APLH without leader sequences	Express in RIPL as inclusion bodies	Refold i*n vitro* in 100 mM Tris, 400 mM Arginine, 0.5 mM oxidized glutathione, 5 mM reduced glutathione, pH 8.0. Purify using Ni-NTA	Not detectable
9E10-APLH (without leaders) with MBP fused to C-termini of Fab chains	Express in RIPL or Rosetta Gami. MBP might help increase Fab solubility	Fab chains not dimerized	Not detectable
9E10-APLH without leaders	K12 Shuffle strain*** (New England Biolabs Inc.) to promote disulfide bond formation in cytoplasm. Carbenicillin (degrades slower) instead of Ampicllin	No expression	Not detectable

***K12 Shuffle strain has deletions for the gor/trxB genes that allow cytoplasmic disulfide bond formation. Also has mutation in the peroxiredoxin enzyme, suppressing the lethality of the gor/trxB gene deletions. Also expresses periplasmic disulfide bond isomerase DsbC without its signal sequence, retaining DsbC in the cytoplasm.

Appendix 2: Efforts to express 9E10 Fab in mammalian cells

Construct	Rationale	Expression	Yield
9E10-APLH	HEK-293T cells for improved Fab dimerization and production	Not detectable	Impure Fab. <0.1 mg from 250 mL cell culture
9E10-APLH with GSG-GSG-GSG linker	Longer linker might help distance the AP tags from the Fab, and cause less interference to Fab folding	Not detectable	Impure Fab. <0.1 mg from 250 mL cell culture
9E10-APLH with GS-PPP-PPP-GS linker	Stiff poly-proline linker might reduce interference of AP tags in Fab folding	Not detectable	Impure Fab. <0.1 mg from 250 mL cell culture
9E10-APLH with A-EAAAK-EAAAK-A linker	Linker known to cause less interference between adjoining domains	Not detectable	Impure Fab. <0.1 mg from 250 mL cell culture
9E10-BSP	BirA substrate peptide LHHILDAQKMVWNHR instead of AP tag to check for less interference	Not detectable	Impure Fab. <0.1 mg from 250 mL cell culture

Appendix 3: 4D5-APLHb binding to mSA and dSA on SDS-PAGE

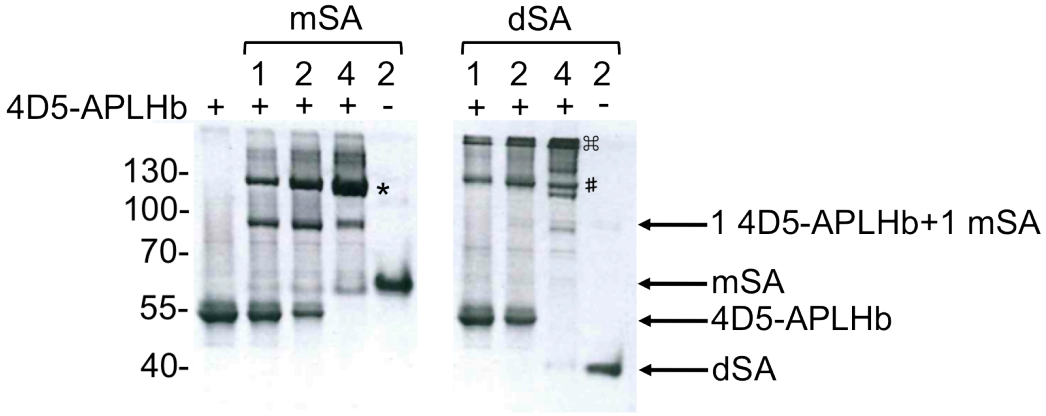

Appendix 3. 4D5-APLHb binding to mSA and dSA. 2 μg 4D5-APLHb was boiled with SDS loading buffer, cooled and mixed with 1, 2 or 4 μg of the indicated SA construct and analysed using SDS-PAGE and Coomassie staining. Addition of SA constructs shifted the Fab band. Increasing amounts of SA construct decreased the proportion of free 4D5-APLHb. Mixing with mSA, gives either 1 Fab:1 mSA complex (at ~95 kDa) or 1 Fab:2 mSA complex (denoted by * at ~120 kDa), which increases in intensity with increasing mSA concentration. Mixing with dSA gives a band at ~130 kDa (♯) probably representing 1Fab:2dSA. Higher complexes (⌘) are present in dSA bound Fab samples but not in mSA bound Fab samples. Data from Dr. D. Krndija, Howarth group.

Appendix 4: Different versions of divalent streptavidin

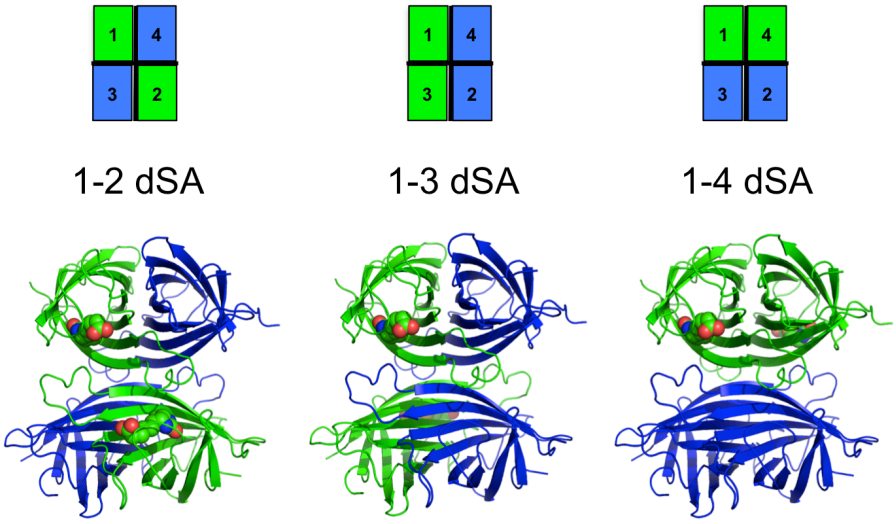

Appendix 4. Different versions of divalent streptavidin. Top row: Schematic representation of a divalent streptavidin tetramer composed of two active (green) and two dead (blue) subunits. Each square numbered 1, 2, 3 or 4 represents a monomeric subunit. The positioning of the two active subunits relative to each other can determine the distance between the two biotin-binding sites on a streptavidin molecule. The different versions are termed 1-2 dSA, 1-3 dSA or 1-4 dSA based on the positioning of the active subunits. Bottom row: Cartoon representations of the corresponding divalent streptavidins with active (green) and dead (blue) subunits. Bound biotin is shown in spacefill. Images produced by M. Fairhead, Howarth group.